Characterisation of the porcine corneal epithelial stem/progenitor cell niche

Thesis submitted to Cardiff University for the degree of Doctor of Philosophy

March 2021

Greg M. Hammond

Supervisors: Professor Andrew J. Quantock, Dr Robert D. Young and Professor Clare E. Hughes

Structural Biophysics Group

School of Optometry and Vision Sciences

College of Biomedical and Life Sciences

Cardiff University

Abstract

It is widely accepted that the surface epithelium of the cornea is maintained by a population of stem cells that resides in the corneoscleral limbus. However, the extracellular matrix and surrounding cells that maintain this stem cell population and constitute the niche of these cells are not fully understood.

The aim of this thesis was to further characterise the extracellular matrix, specifically the chondroitin sulphate/dermatan sulphate distribution, and cellular components of the limbal epithelial stem cell niche using a porcine model. This was done using immunohistochemistry, transmission electron microscopy, scanning electron microscopy and creating 3D tissue reconstructions via serial block-face scanning electron microscopy (SBFSEM) and X-ray micro-computed tomography (microCT).

This thesis was the first to investigate using microCT to image the limbal/corneal epithelium and found the porcine cornea has one or more continuous limbal troughs that span across all limbal quadrants, as opposed to small, discrete limbal crypts as found in humans. These elongated projections of the limbal epithelium into the stroma contain basal epithelial cells positive for the putative limbal stem cell markers cytokeratin 19 and ABCB5.

The stroma immediately subjacent to the limbal trough is rich in the chondroitin sulphate sulphation motifs recognised by antibodies 6C3 and 3B3(+), as well as hyaluronic acid. The distribution of sulphated proteoglycans varies between the stroma and epithelial basement membranes of the porcine central cornea versus the limbus.

SBFSEM reconstructions demonstrate direct cell-cell contact between stromal niche cells and limbal basal epithelial cells in the porcine cornea, the third mammalian species to show this.

This thesis has shown marked differences in the limbal stem cell niche of the porcine eye from the human, but also confirming some shared characteristics. The

newly identified limbal trough forms part of this niche, playing host to putative stem cells, where forms of chondroitin sulphate are in close proximity to these cells and stromal-epithelial cell interaction exists. These factors may play a role in stem cell maintenance *in vivo* in the porcine cornea and also could have uses in the culturing of limbal stem cells and future niche reconstruction.

Table of Contents

Acknowledgements

Firstly, I want to thank my supervisors Professor Andrew Quantock, Dr Rob Young, Professor Clare Hughes, and Professor Bruce Caterson. Their expertise and support have guided me through this extremely challenging, though highly rewarding, experience.

I would also like to thank all the members of the Structural Biophysics Group, who have all helped me at some point during my studies. In particular, I would like to thank Dr Eleanor Feneck for her help in grasping the biology that I was unfamiliar with, Sean Ashworth for his help refining the immunofluorescence experiments, and Dr Petar Markov for introducing me to image analysis techniques.

Thank you to Drs Julie Albon, Laura Paletto and the late Nick White for instructing me in the use of second harmonic generation microscopy. I would also like to thank Julie for acting as my advisor throughout my PhD and for her guidance and support. Thank you to Dr Duncan Muir for helping to acquire SEM images of Bowman's layer and for teaching me how to perform this technique. I am also very grateful to Dr David Williams for his huge amount of help with microCT experimentation and for carrying out these scans.

I am extremely grateful to collaborators at Kyoto Prefectural University of Medicine, Department of Ophthalmology and Baptist Eye Hospital in Kyoto for hosting me for several weeks during my PhD to carry out some experimentation. It was a great opportunity and I was very thankful to be able to visit the country once again.

Thank you to the staff at the Welsh Government's Department of Health and Social Care, Primary Care Division, Sensory Branch for hosting me during my professional internship placement. This was a refreshing break during my PhD that re-energised me and was a fantastic experience in itself. I thoroughly enjoyed every moment and it broadened my horizons to experiences I would never have had otherwise.

An enormous thank you to all of my friends in Cardiff, Taunton, and Wolverhampton for all of their support throughout my doctoral studies. This includes keeping me motivated and all the personal support during the many difficult times I have faced during this project. This thesis is as much a product of your unwavering support and friendship as it is my work.

Finally, a huge thank you to my family and my partner, Russell. None of this would be possible without your love and support. I can only hope that I have made you as proud of me as I am of every one of you. I would like to dedicate this thesis in memory of Ollie- someone whose love never wavered and who could always make me smile no matter how upset, exhausted, or demotivated I felt.

This work was supported by the Biotechnology and Biological Sciences Research Council-funded South West Biosciences Doctoral Training Partnership, Grant reference BB/M009122/1.

List of publications

Bains, K. K., Fukuoka, H., **Hammond, G. M.**, Sotozono, C. and Quantock, A. J. (2019) Recovering vision in corneal epithelial stem cell deficient eyes. *Contact Lens and Anterior Eye* 42(4), pp. 350-358.

Hammond, G. M., Young, R. D., Muir, D. D. and Quantock, A. J. (2020) The microanatomy of Bowman's layer in the cornea of the pig: Changes in collagen fibril architecture at the corneoscleral limbus. *European Journal of Anatomy* 24(5), pp. 399-406.

Ashworth, S., Harrington, J., **Hammond, G. M.**, Bains, K. K., Koudouna, E., Hayes, A. J., Ralphs, J. R., Regini, J. W., Young, R. D., Hayashi, R., Nishida, K., Hughes, C. E. and Quantock A. J. (2021) Chondroitin sulfate as a potential modulator of the stem cell niche in cornea. *Frontiers in Cell and Developmental Biology* 8, p. 567358.

List of Figures

List of Tables

List of Abbreviations

ABCB5- ATP-binding cassette subfamily B member 5

ABCG2- ATP-binding cassette subfamily G member 2

ALDH3A1- Aldehyde Dehydrogenase 3 Family Member A1

AQP1- aquaporin1

BCRP- breast cancer resistance protein (alternative name for ABCG2)

BDMA- benzyl dimethylamine

BSA- bovine serum albumin

CS- chondroitin sulphate

DAPI- 4',6-diamidino-2-phenylindole

DDSA- dodecenylsuccinic anhydride

DS- dermatan sulphate

ECM- extracellular matrix

EMT- epithelial-mesenchymal transition

FGF- fibroblast growth factor

FSP- focal stromal projection

FSP-1- fibroblast-specific protein-1

GAG- glycosaminoglycan

GalNAc- N-acetyl-galactosamine

GFP- green fluorescent protein

GlcA- glucuronic acid

GlcNAc- N-acetyl-glucosamine

HA- hyaluronic acid

Hep- heparin

HS- heparan sulphate

HMDS- hexamethyl-disilazane

IdUA- iduronic acid

Ig- immunoglobulin

iPS cell- induced pluripotent stem cell

K3- cytokeratin 3

K12- cytokeratin 12

K15- cytokeratin 15

K19- cytokeratin 19

KLF4- Krüppel-like factor 4

KS- keratan sulphate

LC- limbal crypt

LEC- limbal epithelial crypt

LEF-1- Lymphoid Enhancer Factor-1

LESC- limbal epithelial stem cell

LSCD- Limbal Stem Cell Deficiency

MSC- mesenchymal stem cell

N/T- nasal/temporal

OCT- optimal cutting temperature

PBS- phosphate buffered saline

PFA- paraformaldehyde

PG- proteoglycan

PTA- phosphotungstic acid

RAFT- Real Architecture for 3D Tissue

RNA- ribonucleic acid

S/I- superior/inferior

SBFSEM- serial block-face scanning electron microscope/microscopy

SEM- scanning electron microscope/microscopy

SLET- simple limbal epithelial transplant

SLRP- small leucine-rich proteoglycan

TAC- transient amplifying cell

TEM- transmission electron microscope/microscopy

UA- uranyl acetate

VE cadherin- vascular endothelial cadherin

VEGF- vascular endothelial growth factor

X-ray microCT- X-ray micro-computed tomography

Yap- Yes-associated protein

1 Introduction

The cornea is the anterior-most aspect of the eye-globe and is the primary refracting surface of the eye (Figure 1.1); it is essential to maintaining vision and the correct functioning of the eye (Remington 2012). The cornea, along with the sclera, also contributes to the tough outer tunic of the eye that provides structure and protection from external injury to the interior eye, as well providing a barrier to infection (Dawson *et al.* 2011; Di Girolamo 2011). Thus, any dysfunctions or diseases that affect the cornea need to be treated appropriately to ensure that ocular function is maintained, as corneal transparency and regularity are vital for this.

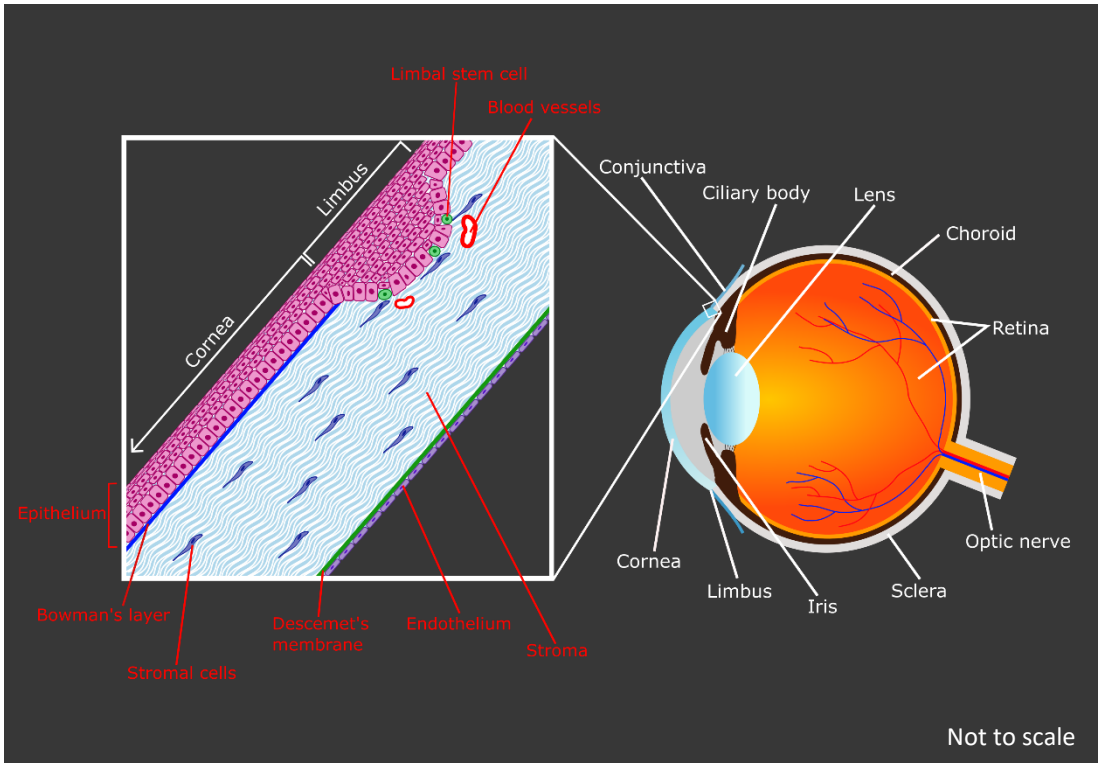

Figure 1.1- Diagram of the anatomy of the eye and cornea.
The cornea is situated at the anterior apex of the eyeball and is continuous with the conjunctiva and sclera.

The transparency of the cornea is, in part, due to its avascularity; except for at the transition zone between the cornea and the conjunctiva – the limbus (Figure 1.1) (Langley and Ledford 2008). An early thought on the cornea's transparency, which was found not to be the case, was that all the components of the cornea have equal

refractive indices (Smith 1969). Other theories then focused on light scattering through the cornea and the constructive and destructive interference of this scatter. It is thought that no sideways scattering of light occurs within the corneal stroma due to it being eliminated by destructive interference (Maurice 1957; Hart and Farrell 1969; Benedek 1971). The spacing of the collagen fibrils within the stroma is essential to this. However, the stroma does not form a perfectly regular lattice and this is most likely not required for corneal transparency (see below).

The thickness of the physiological human cornea ranges from 540-700 µm and it is composed of five layers, which each serve different functions, yet contribute to the main functions of the cornea (Dawson *et al.* 2011). These layers, from anterior to posterior, are: the epithelium, Bowman's layer, the stroma, Descemet's membrane and the endothelium.

1.1 Corneal anatomy

1.1.1 Epithelium

The corneal epithelium, the cornea's most anterior layer, consists of three cell types in 5-7 layers (Ramos *et al.* 2015). It is a stratified, non-keratinised, squamous epithelium and is itself comprised of three layers (Figure 1.2) (Langley and Ledford 2008; DelMonte and Kim 2011).

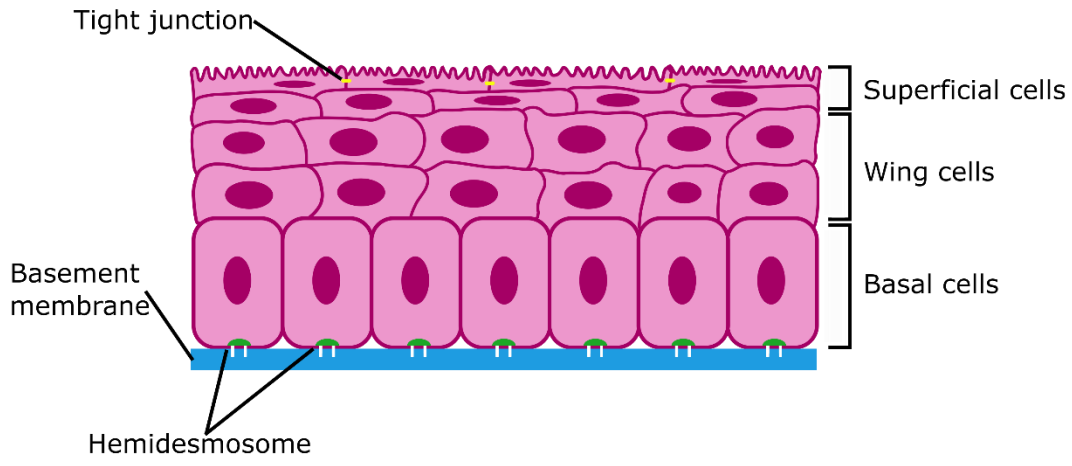

Figure 1.2- The cellular layers of the corneal epithelium.
The morphology of epithelial cells differs amongst the three layers, which are the superficial layer, the wing cell layer, and the basal cell layer, from anterior to posterior.

The superficial layer is 2-3 cells thick and consists of flattened cells with apical microvilli, which allow for an increased contact area with the tear film (DelMonte and Kim 2011). There are tight junctions between these superficial cells that create a very effective barrier to tear film components and also pathogens. Beneath this is a layer of several wing/suprabasal cells.

The basal layer is a single layer of columnar cells (Remington 2012). It is only these basal cells that undergo mitosis in the central cornea and they then migrate upwards, transforming into wing cells and, subsequently, into squamous cells. These cells are firmly adhered to their basement membrane by hemidesmosomes (DelMonte and Kim 2011).

Like other epithelia, the surface cells of the cornea are constantly being sloughed away. Thus, the epithelium maintains a population of slow-cycling stem cells to continually replenish the tissue, widely believed to be located at the corneoscleral transition zone, within the basal limbal epithelium (Cotsarelis *et al.* 1989). These basal cells migrate centripetally, giving rise to daughter cells that move towards the epithelial surface, becoming more differentiated and losing their proliferative potential as they do so (Beebe and Masters 1996). The X, Y, Z hypothesis, for maintenance of the corneal epithelium under normal conditions, was first proposed by Thoft and Friend (1983). The three components involved in epithelial maintenance are: the vertical proliferation of basal cells (X), the centripetal migration of limbal cells (Y) and the desquamation of superficial cells (Z). In order to sustain a normal, functional epithelium, the X and Y components combined must equal the Z component.

1.1.2 Bowman's layer

Bowman's layer is an acellular layer between the corneal epithelial basement membrane and the stroma, consisting of collagen fibrils in an interwoven, dense sheet (Wilson and Hong 2000; Birk 2001) (Figure 1.3). The fibrils are of uniform diameter, about 22 nm, and originate from the epithelium during development (Dawson *et al.* 2011). Bowman's layer is mostly comprised of collagen types I, III, V and VI (Marshall *et al.* 1991b,a). The thickness of this layer is 8-12 µm (Komai and Ushiki 1991).

The function of Bowman's layer is not entirely certain. Some have argued that it contributes to maintaining the corneal curvature, or that it protects the posterior cornea from the spread of infections originating in the epithelium by acting as an acellular barrier (Wilson and Hong 2000). Bowman's layer is non-regenerative and damage to it will often lead to the formation of scar tissue from the stroma or in-filling with epithelial cells (Remington 2012).

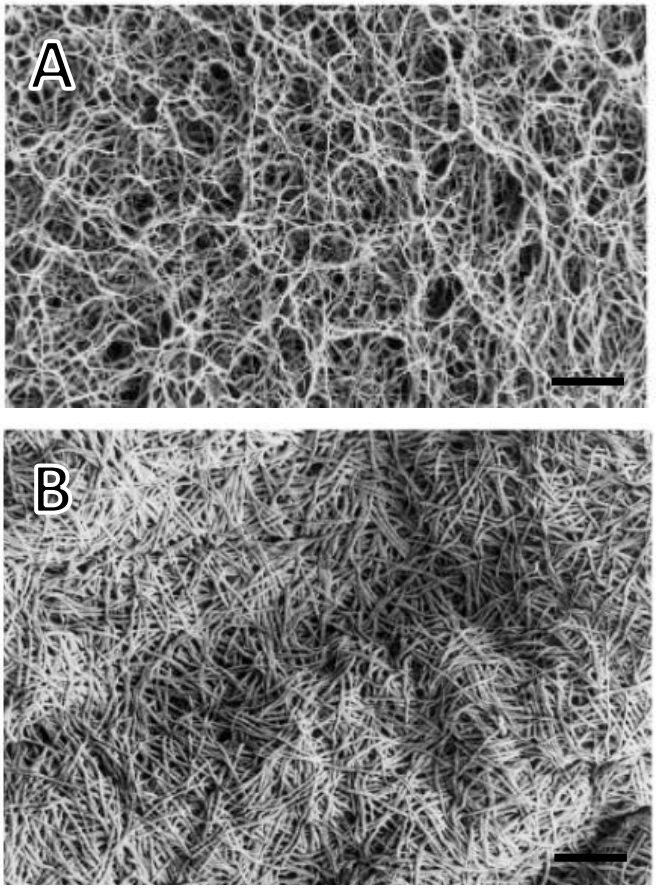

Figure 1.3- Scanning electron microscopy images of the epithelial surface of Bowman's layer.
Collagen fibrils form a dense, interwoven layer in both human (A) and rabbit (B) corneas. Scale bars = 1 µm. Adapted from Hayashi et al. (2002) with permission from the copyright holder.

1.1.3 Stroma

The stroma accounts for a large proportion of the total corneal thickness (approximately 90%) and the human cornea consists of 200-250 lamellae of collagen fibrils (Langley and Ledford 2008). The collagen fibrils are arranged parallel to each other within each lamella and run from limbus to limbus, spanning the entire width of the cornea (Remington 2012), with consistent diameters of 25-30

nm (Hassell and Birk 2010). The fibrils in each lamella have a different orientation to those in adjacent lamellae, with a preference for a superior-to-inferior or nasal-to-temporal orientation in the human central cornea (Meek *et al.* 1987). There are also thought to be collagen fibrils at the limbus/peripheral cornea that run circumferentially or tangentially to the limbus (Newton and Meek 1998; Meek and Boote 2004). The most prevalent type of collagen in the stroma is type I, with type V also associated with the fibrils (Birk *et al.* 1986).

The anterior stroma has a slightly different structure to the posterior, in that the lamellae are thinner – 0.2-1.2 μm compared to 0.2–2.5 μm – and some are interwoven (Komai and Ushiki 1991). In the posterior two-thirds of the stroma, lamellae do not interweave, which results in a less rigid structure. Komai and Ushiki also demonstrated keratocytes located between the lamellae. Flattened cells that join with each other via long pseudopodia, keratocytes produce collagen and components of the extracellular matrix (ECM) (Remington 2012). These cells are believed to contain corneal crystallins that cause them to have a similar refractive index to the surrounding matrix in order to contribute to corneal transparency (Jester 2008). The stromal ECM consists of many different substances and proteoglycans (PGs) are amongst some of the most important components (discussed in more detail below) (Hassell and Birk 2010). In brief, these molecules keep the collagen fibrils arranged in a specific structural and spatial arrangement. This is believed to be vital to the cornea's transparency, based on the theory that as long as the separation of the collagen fibrils is less than half the wavelength of visible light, then all sideways scattering of light will destructively interfere and only forward light will be transmitted, as reviewed by Meek and Knupp (2015).

Elastic fibres also form part of the human corneal stroma. These have been found in the posterior peripheral stroma, forming an annulus in the limbus that is sheet-like (Kamma-Lorger *et al.* 2010; Lewis *et al.* 2016), with fibres that extend into the peripheral cornea (Lewis *et al.* 2016; Feneck *et al.* 2018). This elastic fibre network is continuous with that in the trabecular meshwork (Feneck *et al.* 2018).

It was reported in 2013 that there is a sixth, previously undefined layer of the cornea, just anterior to Descemet's membrane (Dua *et al.* 2013). "Dua's Layer" was

described as a thin layer of acellular collagen that was sometimes found to remain attached to Descemet's membrane when it was separated from the overlying stroma by the "big bubble" technique during Deep Anterior Lamellar Keratoplasty. However, it was quickly refuted that this is a distinct corneal layer and is suggested to merely be the posterior-most lamellae of the stroma (McKee *et al.* 2014). Further investigations added to this controversy and the prevailing opinion, at present, is that there is no distinct "pre-Descemet's layer" (Jester *et al.* 2013; Schlötzer-Schrehardt *et al.* 2015).

1.1.4 Descemet's membrane

Descemet's membrane is the penultimate layer of the cornea, posterior to the stroma. As the basement membrane of the endothelium, it is the endothelial cells that secrete this layer and it is composed of anterior and posterior sections (DelMonte and Kim 2011). The former is secreted during *in utero* development and the latter after birth. The posterior section, therefore, grows continuously throughout life – increasing from 3-4 µm to 20-30 µm (Kaji 2002). Again, this layer is mostly composed of collagen, predominantly type VIII with some type IV (Kapoor *et al.* 1986; Fitch *et al.* 1990). Descemet's membrane is arranged in a very regular, hexagonal array of non-collagenous nodes and collagenous filaments (Jakus 1956; Kapoor *et al.* 1986).

1.1.5 Endothelium

The endothelium is the internal layer of the cornea, in contact with the aqueous humour (Remington 2012). It is a single layer of polygonal cells, with 70-80% being hexagonal. There are numerous gap junctions and tight junctions between endothelial cells, but it is still considered a "leaky" barrier that allows solutes – and the subsequent osmosis of water – from the aqueous humour into the stroma. This is a necessary movement so that nutrients can be supplied to the cornea. However, surplus water needs to be removed to maintain the correct hydration of the stroma – approximately 78% water content (Geroski *et al.* 1985).

This precise hydration is facilitated by the endothelial pump mechanism (Remington 2012). Ions, such as sodium and potassium, are removed from the stroma via endothelial cell membrane ion channels and pumped into the anterior

chamber. The altered concentration gradient then draws water from the stroma into the aqueous humour. In a healthy cornea, the net movement of water is zero (Bonanno 2012). If the stroma becomes excessively hydrated, oedema and a loss of transparency can occur.

Corneal endothelial cells are non-mitotic and, therefore, the main repair mechanism for endothelial cell loss is the migration and expansion of remaining cells to cover these areas (Remington 2012). Thus, endothelial cell density decreases with age, with an annual rate of loss of between 0.33-0.6% being reported (Bourne *et al.* 1997; Hollingsworth *et al.* 2001). Endothelial cell density has been reported as between 3000-4000 cells/mm^2 for children and 1000-2000 cells/mm^2 at 80 years of age (Remington 2012). However, it has been suggested that for endothelial pump function to be impaired, cell density needs to fall below 1000 cells/mm^2 (Wilson and Roper-Hall 1982).

1.1.6 The limbus

As aforementioned, the transition area between the peripheral cornea and the sclera is termed the limbus. Here, the epithelial cell layer increases in thickness to 10-12 cell layers and 79.6 ± 7.4 µm from 5-7 layers of cells and 54.7 ± 1.9 µm in the central cornea (Feng and Simpson 2008). The limbal epithelium is where the stem cells that replenish the corneal epithelium are believed to reside, which is discussed in more detail in section 1.2.2. The limbal epithelium then transitions into the conjunctival epithelium peripherally and the limbal stroma into the scleral stroma (Van Buskirk 1989; Remington 2012).

The regularly-arranged lamellae of collagen found in the cornea gradually transition into the much less organised structure of the sclera here (Remington 2012) and, as mentioned in section 1.1.3, there are collagen fibrils that run circumferentially – creating an annulus of collagen – and tangentially within the stroma at the limbus (Meek and Boote 2004). In the bovine corneal stroma, collagen fibril diameter was found to be relatively constant from the centre to the corneolimbal transition but then increased significantly peripheral to this (Ho *et al.* 2014). A similar situation was earlier identified in the human cornea (Borcherding *et al.* 1975).

Bowman's layer terminates at the limbus (Remington 2012), demarcating the anterior boundary of the limbus on the external side of the tissue. The internal boundary is defined as the point where Descemet's membrane meets the trabecular meshwork (Van Buskirk 1989). The posterior boundary is more difficult to define due to the gradual transition of the collagen structure, however, pathologists define it as a line that runs from the scleral spur directly outwards to the surface of the eye globe (Figure 1.4) – though there are varying definitions of the extent of the limbus (Van Buskirk 1989).

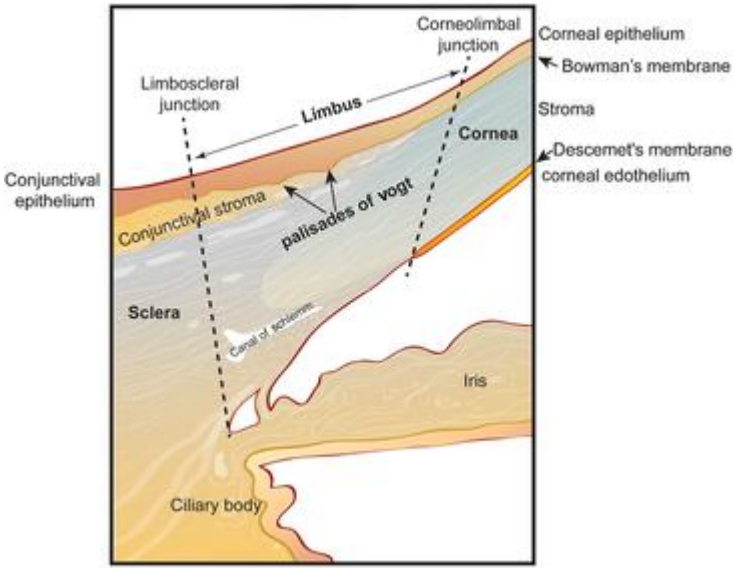

Figure 1.4- Diagram of the anatomy of the limbus.
The definition of the posterior limbal boundary here is just one of several possible demarcations. Adapted from Gonzalez et al. (2018) with permission from the copyright holder.

The limbus is also vascularised, unlike the completely transparent cornea. This vascular network supplies the limbus and the peripheral cornea with nutrients, which is thought to be key to the function of the limbus as the site of the epithelial stem cells (Boulton and Albon 2004; Chen *et al.* 2004).

1.1.7 Porcine corneal anatomy

The porcine eye has often been used as an experimental model for ophthalmological research due to its similarities to the human eye (Ruiz-Ederra *et al.* 2005; Johansson *et al.* 2010; Notara *et al.* 2011; Grieve *et al.* 2015; Lin *et al.* 2018), as has the eye of mini-pigs (Liu *et al.* 2009; Islam *et al.* 2018). However, there are differences that may need to be considered when using a porcine model.

When considering the porcine cornea, it is – first of all – thicker than its human counterpart. The porcine cornea has been measured as 1013 ± 10 µm and 877 ± 14 µm in *ex vivo* experiments (Jay *et al.* 2008; Sanchez *et al.* 2011), suggesting that it is almost twice as thick as the human cornea. Yet, ultrasound pachymetry on live porcine eyes has given an average thickness of 666 µm (range 534-797 µm) (Faber *et al.* 2008), with the difference between *in vivo* and *ex vivo* most likely due to post-mortem corneal swelling. Regal *et al.* (2019) found an even greater corneal thickness for the porcine eye – 1.73 ± 0.47 mm – but the authors acknowledge this is likely due to swelling after storage in saline.

The epithelium of the porcine cornea consists of 8-12 layers of cells (Hayashi *et al.* 2002; Patruno *et al.* 2017), approximately double the amount of the human corneal epithelium, and consists of the same three epithelial cell types in the same positional layout as the human eye (Jay *et al.* 2008; Patruno *et al.* 2017). The thickness of the porcine central corneal epithelium has been measured as 184.4 ± 19.8 µm (Hayashi *et al.* 2002) and 75.77 ± 1.17 µm (Abhari *et al.* 2018) in different studies.

Though some studies have reported Bowman's layer in the porcine cornea (Du *et al.* 2011; Zhang *et al.* 2019), several sources all state that it lacks this structure or that it could not be detected and the porcine cornea consists of just four layers (Merindano *et al.* 2002; Svaldenienė *et al.* 2003; Patruno *et al.* 2017). The porcine corneal stroma comprises most of the thickness of the cornea and is well vascularised at the limbus, and Descemet's membrane and the endothelium are similar to other species (Patruno *et al.* 2017), including humans.

1.2 Limbal epithelial stem cells

A stem cell is a primitive, undifferentiated cell that has unlimited growth potential and the ability to self-renew, whilst also being able to differentiate into specialised cell types (Reya *et al.* 2001). In mammals, stem cells are mostly found in two different forms: embryonic stem cells that are found in the inner cell mass of a blastocyst and are pluripotent (can differentiate into all cell types derived from the

three primary germ layers) (Evans and Kaufman 1981), and adult stem cells that are located within bodily tissues and are multipotent or unipotent (Pauklin *et al.* 2011). It is now also possible to reprogram adult, differentiated cells into a pluripotent state using four factors, creating induced pluripotent stem (iPS) cells (Takahashi and Yamanaka 2006). Adult, or somatic, stem cells are responsible for the repair and maintenance of the tissue in which they are found (Morrison and Spradling 2008) and they can generally only differentiate into cell types that come from the same organ that the stem cell population is located in (Castro-Muñozledo 2013).

Stem cells go through the process of changing from a slow-cycling cell, with unlimited proliferative ability, to a transient amplifying cell (TAC) then to a terminally differentiated cell (Lehrer *et al.* 1998). In general, adult stem cells undergo asymmetric cell division, producing two different daughter cells; one remains as a stem cell whilst the other becomes a TAC, as reviewed by Spradling *et al.* (2001).

In the corneal epithelium, it is these TACs, which cycle quickly, that then migrate centripetally across the corneal surface. As they do this, they undergo several rounds of replication, with peripheral TACs capable of multiple rounds of division and central ones potentially only capable of one more division before becoming fully differentiated (Lehrer *et al.* 1998). During wound healing, the epithelium can employ three different approaches to produce the increased number of terminally differentiated cells required: 1) induce more stem cells to divide and to cycle more rapidly, 2) induce all TACs to utilise their full proliferative potential before terminally differentiating, and 3) reducing the cell cycling time of the TACs.

The limbal epithelial stem cells (LESCs) are often stated to be unipotent, only differentiating to produce corneal epithelial cells. However, it has been suggested that they are multipotent (Ferraris *et al.* 2000) or can be induced to become multipotent (Zhao *et al.* 2002; 2008b). This means that they retain the potential to differentiate into several different, yet very similar, cell types though not as many as totipotent or pluripotent stem cells (Pauklin *et al.* 2011). It appears that LESCs remain unipotent in their physiological *in vivo* environment.

The initial hypothesis regarding replenishment of the corneal epithelium was conjunctival transdifferentiation, in that the conjunctiva was the source of the corneal epithelium due to its epithelial cells crossing the limbus then acquiring a corneal morphology (Shapiro *et al.* 1981). However, despite this prompting the use of conjunctival transplantation for several years to treat corneal epithelial defects, it was found that this was not an appropriate treatment due to conjunctival epithelium being incompatible with the corneal surface (Tsai *et al.* 1990). It has since been refuted by many sources that the conjunctiva replenishes the corneal epithelium (Schermer *et al.* 1986; Kruse *et al.* 1990; Chen *et al.* 1994; Dua 1998).

As aforementioned, it is widely accepted that stem cells for the replenishment of the corneal epithelium are only located at the limbus in humans, but an opposing theory has emerged stating that there are also stem cells throughout the central cornea in other species (Majo *et al.* 2008). Another theory has also argued that there are no stem cells within the corneal or limbal epithelia and that its homeostatic maintenance is entirely via the proliferation of cells from a "germinative basal layer" (Haddad and Faria-e-Sousa 2014). However, a review by West *et al.* (2015) demonstrates the large body of evidence that is incompatible with this theory and, thus, it will not be discussed further.

Majo *et al.* (2008) based their corneal epithelial stem cell hypothesis on mice experiments and stated that during normal homeostasis, the epithelium is solely maintained by central corneal stem cells and LESCs are only activated during wound healing. When limbal epithelium was transplanted, they found that it only migrated onto the host corneal surface if the host corneal epithelium was damaged. They also found that transplanting corneal epithelium could lead to full re-epithelialisation of the corneal surface.

Again, there is a body of evidence that goes against this theory and supports the limbus as the sole location of epithelial stem cells (discussed below). West *et al.* (2015) have suggested that the opposing theories could work together if corneal epithelial stem cells are not slow-cycling or if central basal epithelial cells have a latent proliferative potential that is activated if LESCs are unable to maintain the epithelium. However, these are only speculations. It is also vague as to whether

Majo's theory is believed to apply to all species. It does not match with many of the experimental findings involving human corneas and the LESC hypothesis has prevailed when considering the human corneal epithelium.

A mathematical model designed to assess the centripetal migration of corneal epithelial cells (discussed in section 1.2.3.2) also assessed whether "stem cell leakage" from the limbus could occur and account for Majo and associates' findings (Lobo *et al.* 2016). It was theorised that a small proportion of the time LESCs may undergo symmetric cell division to produce two daughter stem cells, but only one remains within the limbus, whilst the other is pushed into the corneal epithelium. The now corneal epithelial stem cell would still migrate centrally as the other corneal cells do and could accumulate within the central cornea. The model demonstrated that this could be a possibility, but still demonstrates that stem cells would be located mainly within the limbus.

During simple limbal epithelial transplantation (SLET), amniotic membrane is grafted onto the corneal surface and then thin limbal biopsies are grafted on top of this, in the central cornea, away from the visual axis (Sangwan *et al.* 2012). This has been found to lead to potential epithelial stem cells being established in the central cornea, however, this is usually next to retained amniotic membrane (Basu *et al.* 2016). Thus, it is not certain whether the stem cells would persist in the central cornea without this graft that promotes and maintains the LESC phenotype (Tseng *et al.* 1998; Chen *et al.* 2015).

1.2.1 Stem cell niche

The specific site within a tissue in which adult stem cells are located is termed the stem cell niche, as first proposed by Schofield (1978,1983). A stem cell niche can be described as a protective, anatomical, and functional location of the stem cells, consisting of both other tissue cells and ECM components, that sustains them and promotes their proliferation and self-renewal *in vivo* (Spradling *et al.* 2001; Scadden 2006). The asymmetric division of a stem cell results in the daughter stem cell remaining within the niche to maintain its stem phenotype, whilst the daughter TAC loses contact with the stem cell niche and begins the process of differentiation, due

to now being exposed to a different extracellular environment. This then facilitates self-renewal and proliferation respectively.

The limbus represents a good location for the corneal epithelial stem cell niche, as it is a site that can provide protection against ultraviolet light and has a well-developed vascular network for nutrient supply (Davanger and Evensen 1971; Goldberg and Bron 1982). It would be very difficult to maintain a stable stem cell niche within the central cornea, due to the lack of diversity and blood supply in the surrounding environment and the proven centripetal movement of basal cells (West *et al.* 2015), as well as greater exposure to the external environment. This further strengthens the theory of the limbus as the reservoir of the epithelial stem cells.

1.2.2 The limbal stem cell niche

The limbal epithelial stem cell niche in humans is believed to be specifically within structures termed limbal crypts (LCs) or limbal epithelial crypts (LECs), which are projections of epithelial tissue in between fibrovascular ridges in the underlying stroma called Palisades of Vogt – shown in Figure 1.5 (Shortt *et al.* 2007; Grieve *et al.* 2015). There are also focal stromal projections (FSPs), which are spurs of stroma that extend between the crypts. The increased surface area and close contact between the limbal epithelium and stroma are important as it is believed that cells and the ECM of the stroma are key regulators of the LESCs and progenitor cells, as has been suggested by others (Stepp and Zieske 2005; Schlötzer-Schrehardt *et al.* 2007).

Palisades of Vogt are radial, papillae-like protrusions of the limbal stroma, with a distinct vasculature, that project upwards into the epithelium (Davanger and Evensen 1971; Goldberg and Bron 1982). They are approximately 1 mm long and are distributed circumferentially along the superior and inferior limbus; the interpalisade regions contain thickened epithelium that has come to be described as the LCs etc. It was Davanger and Evensen that first proposed the Palisades as the site of the LESC population, citing the pigmentation of the ridges and the spreading of this pigment centrally in response to epithelial injury.

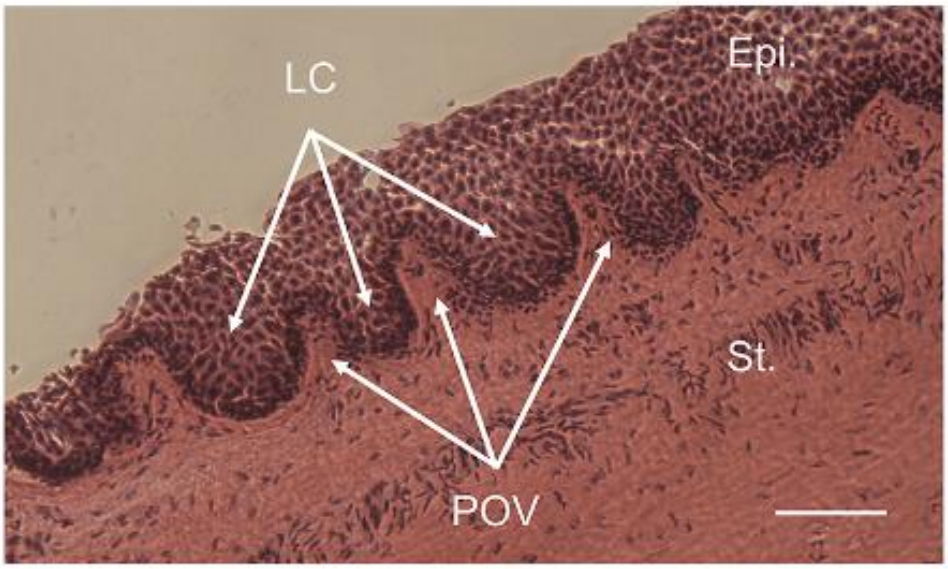

Figure 1.5- Tangential section across the human limbus showing limbal crypts. *Tangential sections of human limbal tissue demonstrate limbal crypts (LC) in between upward spurs of stromal tissue termed Palisades of Vogt (POV). Epi = epithelium, St = stroma, scale bar = 50 µm. Source: Dziasko et al. (2014) with permission under the creative commons user license (https://creativecommons.org/licenses/by/4.0/).*

There are some discrepancies and ambiguity in the literature as to whether the Palisades of Vogt are the areas of thickened epithelium or the fibrovascular stromal papillae. Park *et al.* (2015) refer to the epithelial structures as the Palisades, whilst in *Wolff's Anatomy* (Bron *et al.* 1997), contradictory descriptions of the Palisades are offered in different chapters. The majority consensus appears to be that the Palisades are the fibrovascular stromal structures and the thickened epithelium between the Palisades constitutes the interpalisade tissue (Davanger and Evensen 1971; Goldberg and Bron 1982; Townsend 1991; Shortt *et al.* 2007; Dziasko *et al.* 2014; Grieve *et al.* 2015; Espandar *et al.* 2017) and, thus, this is the nomenclature that will be used for the purpose of this thesis.

Dua *et al.* (2005) were the first to name the epithelial structures, which they termed LECs. These were described as solid cords of epithelial cells that extended either peripherally into the conjunctival stroma or circumferentially into the limbal stroma from the interpalisadal epithelial tissue (Figure 1.6). On average, six of these structures were found per eye, though there is no detail of their positioning around the limbal circumference.

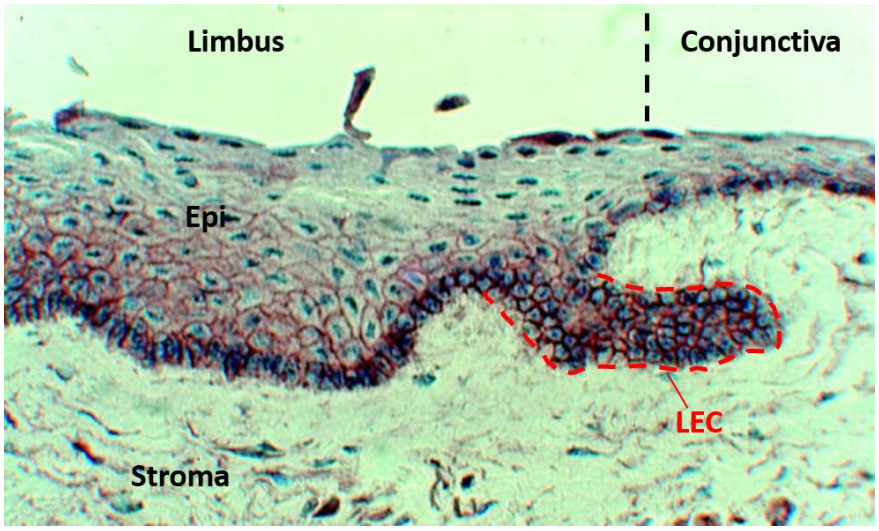

Figure 1.6- Immunohistology image of the human limbus showing a peripherally-oriented limbal epithelial crypt (LEC).
There is stronger staining for a putative stem cell marker within the LEC. Epi = epithelium. Adapted from Dua et al. (2005) with permission from the copyright holder.

Shortt *et al.* (2007) did not find any LEC-like structures in their examination of the human limbal stem cell niche but did define the two structures they believe constitute the niche. LCs were defined as the epithelial invaginations into the underlying limbal stroma, as shown in Figure 1.5, with the Palisades of Vogt forming the lateral walls of the crypts. It was noted that they are similar to the rete pegs of the epidermis. From this point on, LECs and LCs will be referred to together as LCs. FSPs were then found at the corneal end of LCs. These were described as finger-like upward projections of the stroma (Figure 1.7), distinct from the crypts, containing a central blood vessel and densely surrounded by basal cells of a smaller size.

Shortt *et al.* (2007) found several key things upon more detailed examination of the characteristics of the human limbal stem cell niche. The underlying stromal vasculature was in close association with LCs, which presents an excellent source of nutrients and could also provide growth factors essential to the niche's function of maintaining the LESC population. LCs were preferentially located in the superior and inferior quadrants of the limbus, matching the findings of Goldberg and Bron (1982) concerning the Palisades. They also noted that the putative LESCs lined the sides and bases of the crypts and – as mentioned above – surrounded the FSPs, putting the LESCs in close proximity to the underlying stroma. A simplified

illustration of the proposed structure of the limbal stem cell niche can be seen within the inset of Figure 1.1.

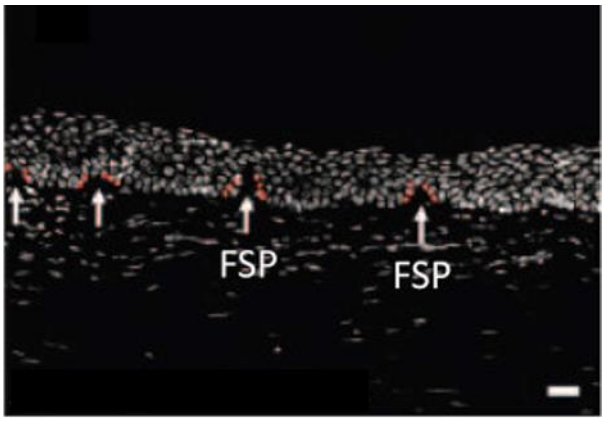

Figure 1.7- Immunofluorescence image of human limbus demonstrating focal stromal projections (FSPs).
FSPs represent small, focal protrusions of the limbal stroma and the cells directly adherent to these structures demonstrate a stem-like morphology. Scale bar = 50 µm. Adapted from Shortt et al. (2007) with permission of the copyright holder.

1.2.2.1 Porcine model of the limbal stem cell niche

The porcine limbus has been investigated previously to see whether it can be used as a model for the human limbus. Notara *et al.* (2011) studied the anatomy of the porcine limbus in detail and Grieve *et al.* (2015) compared the porcine limbus with human and murine tissue. Patruno *et al.* (2017) examined the limbal structures of several different mammalian species, including pigs. All three studies found invaginations of limbal epithelium into the underlying stroma, but not all agreed that these represented "true" LC structures. Grieve and Notara also disagreed on whether the crypt-like structures are found around the entire limbal circumference or are just located superiorly and inferiorly, as in the human eye. What all of these studies did agree upon was that porcine LCs/invaginations of epithelium into underlying stroma contained cells positive for p63α (a putative epithelial stem cell marker), with Notara *et al.* also noting basal expression of β1 integrin – a basal epithelium marker that is associated with a limbal epithelial progenitor cell phenotype.

Colony-forming efficiency – the ability of a single cell to replicate and produce a colony of cells – was also found to be significantly higher for cells taken from

superior/inferior “crypt-rich” limbal biopsies compared to “non-crypt-rich” nasal/temporal areas and the central cornea (Notara *et al.* 2011). This was compared again more recently, and it was again shown that epithelial cells from the limbus have much greater clonal capacity than cells from the central cornea (Seyed-Safi and Daniels 2020). However, Grieve *et al.* still found that colony-forming efficiency was significantly greater in human limbal cells than porcine cells.

Interspecies differences in the locations of potential stem/progenitor cell populations in the corneal epithelium have been observed and it has been indicated that oligopotent stem cells may be found throughout the porcine basal corneal epithelium, as well as the limbus (Majo *et al.* 2008). This study found that colonies could be produced from single cells throughout the corneal epithelium, suggesting stem cells are not exclusive to the limbus in porcine eyes. However, Notara *et al.* (2011) found that central corneal cells had the lowest colony-forming efficiency and this was significantly lower than the result obtained from “crypt-rich” areas of the limbus. It has been pointed out, in response to Majo *et al.*’s work, that any central corneal stem cells cannot be slow-cycling as they are not detected in label retention experiments and that Majo’s other results do not match with existing findings in support of the limbal location of corneal epithelial stem cells (Sun *et al.* 2010). It does not seem to be in doubt that the mammalian corneal surface contains limbal stem cells; however, it may be the case that some species – including the pig – maintain a stem cell population within the corneal epithelium as well.

1.2.3 Evidence for the limbal location of corneal stem cells

1.2.3.1 Cell morphology

Small populations of limbal basal epithelial cells with a high nucleus to cytoplasm ratio and a smaller, rounder morphology have been observed along the sides and bases of LCs, as well as adhered to FSPs (Chen *et al.* 2004; Shortt *et al.* 2007; Dziasko *et al.* 2014). These cells are significantly different, in the attributes mentioned above, to both immediately adjacent suprabasal cells and limbal basal cells from outside the LCs.

The smallest keratinocytes in the epidermis demonstrate the highest clonogenicity and, potentially, represent the stem cell population. Romano *et al.* (2003) have shown that the smallest cells of the corneal epithelium are found in the basal limbal epithelium and believe that this phenotype could represent the LESCs. However, not all basal cells in LCs demonstrate this morphology, with the majority still having a columnar shape (Dziasko *et al.* 2014).

1.2.3.2 Centripetal migration

The known centripetal movement of epithelial cells also supports the limbal localisation of the stem cells. As mentioned above, Davanger and Evensen (1971) noted the movement of pigment from the limbus of a guinea pig eye to an area of epithelium that had been experimentally wounded 24 hours earlier. They then hypothesised that this supports the idea of a migrating cell population, based at the limbus. Kinoshita *et al.* (1981) then demonstrated that host epithelium in rabbit eyes that had undergone lamellar keratoplasty would mix with donor epithelium on the graft over time. However, no mixing occurred in areas peripheral to the graft-host boundary, suggesting it was only host epithelial cells that were migrating and that they were doing so in a centripetal direction.

Buck (1985) went further than this and measured the amount of centripetal movement in mouse corneas. By "tattooing" the epithelium and underlying stroma with India ink, the movement of ink incorporated into the epithelium in relation to the static stromal tattoo could be observed. Centripetal movement was found in most corneas and a mean migration distance of 94 ± 14 µm over seven days was recorded. It was also briefly demonstrated that conjunctival epithelial cells did not migrate over the limbus.

A lineage-tracing experiment by Amitai-Lange *et al.* (2014) demonstrated radial limbal streaks of epithelial cells that grew towards the corneal centre of murine eyes. This was shown to be the case under normal, homeostatic conditions as well as after corneal wounding. They found an average limbal streak development rate of 120 ± 6.2 µm/day after severe wounding, compared to 15.69 ± 4.36 µm/day under normal conditions.

Using the same K14CreERT2-confetti mice as the previous study and mathematical modelling, Lobo *et al.* (2016) have given further impetus to the idea of centripetal migration of corneal epithelial cells. The model demonstrated radial streaks of cells from a common source LESC that looked remarkably similar to the limbal streaks in the confetti mouse (Figure 1.8). This was shown to occur without any external stimuli; the process was driven just by limiting stem cells to a limbal location, TACs having a limited replication capacity, and movement being stimulated by population pressure. This suggests that during homeostasis no extrinsic factors are needed for centripetal migration to occur, though external factors are likely still to be involved during wound healing and inflammation etc.

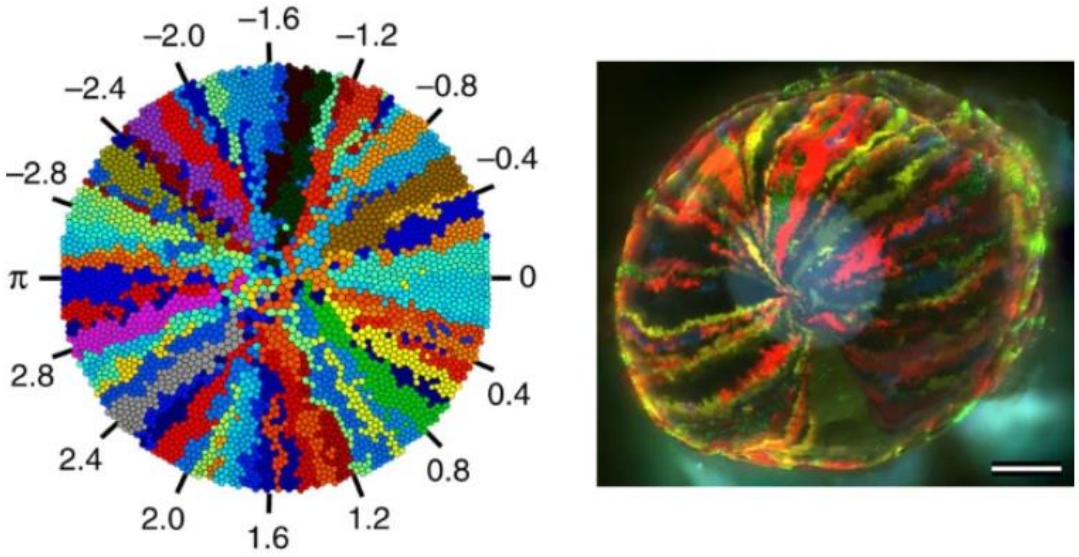

Figure 1.8- A comparison of a mathematical model of the centripetal migration of corneal epithelial cells and the limbal streaks present in the confetti mouse cornea.
Lobo et al.'s mathematical model of limbal epithelial cell migration shows remarkable similarity to the limbal epithelial streaks that appear in the K14CreERT2-confetti mouse, without any external stimuli required. Adapted from Lobo et al. (2016) with permission under the creative commons user license (https://creativecommons.org/licenses/by/4.0/).

1.2.3.3 Wound healing of the epithelium

When investigating wound healing of rabbit corneal epithelium, Huang and Tseng (1991) demonstrated that wound healing in eyes that had the limbal epithelium completely removed was significantly delayed. They also found that conjunctival cells had spread onto the cornea and vascularisation occurred. TACs within the corneal basal epithelium were able to maintain a relatively normal epithelium for at least six months, but impairment of wound healing was believed to demonstrate that the stem cell population had been removed with the limbal epithelium.

Work carried out on rabbits with partial limbal removal showed that consecutive 6 mm epithelial wounds could heal fairly normally, due to the remaining LESC population, and the initial limbal wounds healed rapidly (Chen and Tseng 1990). However, after one large wound, covering most of the remaining central epithelium, healing was significantly delayed – compared to corneas with an intact limbus – from the eighth-day post-wounding and conjunctival epithelial cells started to cover the cornea. It was believed that the large wound almost completely depleted the remaining TAC population and the remaining stem cells could not produce enough TACs to meet the healing demands.

Limbal grafts have been demonstrated to be effective treatments for severe ocular surface disorders, such as chemical or thermal burns, that destroy all of the corneal and limbal epithelium. Grafts of limbal tissue taken from human patients' contralateral, uninjured eyes resulted in very good clinical results in a set of patients that underwent this procedure (Kenyon and Tseng 1989). It was then later shown that limbal epithelial cells could be cultured *in vitro* from small limbal biopsies from patients' uninjured eyes and the resultant epithelial sheets used as successful autologous grafts that form clear and structurally-sound epithelium (Pellegrini *et al.* 1997).

Initial surgical treatment for epithelial damage was through transplantation of grafts of conjunctival tissue on to the corneal surface (Thoft 1977), based on the theory of conjunctival transdifferentiation mentioned above. However, a comparison study of conjunctival and limbal autograft transplantation by Tsai *et al.* (1990) demonstrated the superiority of the latter technique, which produced a new ocular surface epithelium with a corneal phenotype. The former technique was shown to form a conjunctival epithelium over the corneal stroma, with no transdifferentiation observed.

A recent investigation has shown that wound healing of an annular epithelial wound is predominantly due to limbal/peripheral corneal cells and not cells from the central cornea in the mouse (Park *et al.* 2019). This also confirmed that centripetal migration of epithelial cells is much greater than centrifugal during wound healing.

1.2.3.4 Presence of label-retaining cells

As epithelial stem cells are slow-cycling and divide infrequently in their quiescent state, they will retain certain labels for prolonged periods after initial labelling. Cotsarelis *et al.* (1989) verified the existence of label-retaining cells in the basal limbal epithelium of mice by labelling with ^{3}H-thymidine. No corneal epithelial cells were found to retain the label and it was also shown that wounding or applying a tumour promotor to the cornea stimulated the LESCs to proliferate. The results of Zhao *et al.* (2008a) supported the finding of label-retaining cells at the limbus.

Label retention was assessed in the ocular surface of the H2B-GFP/K5tTA transgenic mouse, which expresses green fluorescent protein (GFP) throughout the ocular surface epithelia until chased with doxycycline, which causes the label to dilute by 50% with every cell division (Parfitt *et al.* 2015). At 28 days chase, almost the entire limbal epithelium was still labelled, demonstrating a quiescent cell population here. By 56 days chase, the number of label-retaining cells had greatly reduced at the limbus, with only 3% of limbal epithelial cells still exhibiting label. No label-retaining cells were observed in the corneal epithelium. The authors suggested that this remaining 3% represented the "true" stem cell population. Similar findings were presented by Sartaj *et al.* (2017).

Though it is not possible to carry out label retention experiments *in vivo*, this has been done with organ-cultured pig corneas (Seyed-Safi and Daniels 2020). After four weeks in culture, a larger number of label-retaining cells were found within the porcine limbus than the central cornea: 44.7 ± 6.4 vs 4.7 ± 1.5 respectively. Label retention investigations in organ-cultured human corneas demonstrated label-retaining cells in the limbal epithelium that expressed several putative LESC markers (Figueira *et al.* 2007).

1.2.3.5 In vitro growth characteristics

It was demonstrated in the Eighties that peripheral human corneal epithelial cells grow better in culture than central cells do; then subsequently that limbal epithelial cells grow better than peripheral corneal cells (Ebato *et al.* 1987,1988). Cultured peripheral cells had significantly higher mitotic rates and larger outgrowth sizes than central cells and, also, reached confluence within 14 days whereas the central

cells did not and had begun to die off. Limbal epithelial cells demonstrated a significantly quicker doubling time than peripheral cells and the mitotic rate was also considerably higher. This greater proliferative potential of limbal cells was a meaningful boost to the newly proposed limbal stem cell theory at the time.

Clonal analysis of single cells cultured from limbal and central corneal epithelium further revealed this loss of clonogenic ability towards the centre and suggested that the cornea mostly consists of TACs (Pellegrini *et al.* 1999). Central corneal cells did not form colonies though some peripheral cells did, but these could not be serially cultivated. The cells from limbal colonies were then characterised (based on the characterisation of epidermal progenitor cells) as holoclone, paraclone or meroclone – representing a potential stem cell with high proliferative capacity, a TAC with limited proliferative capacity that produces a terminally differentiated colony, or an intermediary cell respectively (Barrandon and Green 1987). 11 of 58 limbal clones formed were judged to be holoclone, with eight being classed as paraclone and the remainder as meroclone (Pellegrini *et al.* 1999), demonstrating a population of cells with stem characteristics here.

Dziasko *et al.* (2014) took this further by comparing cells specifically from "LC-rich" and "non-crypt rich" limbal areas. They found that a significantly higher proportion of holoclones was produced by cells from the LC-rich limbus – 17.74% compared to 1.61% from the non-crypt rich limbus. The LC-rich limbus also produced a significantly lower proportion of paraclones (38.71% compared to 56.45%), which showed the higher proliferative capacity of cells from these regions. Similar findings were also found when comparing the two reportedly different regions of the porcine limbus, as mentioned above (Notara *et al.* 2011). A more recent study has shown the greater proportion of holoclones produced by cells from the porcine limbus (38.3%) compared to the central cornea (8.3%) (Seyed-Safi and Daniels 2020).

1.2.3.6 Putative stem cell markers

One of the issues when trying to identify the limbal stem cell niche is the lack of a specific stem cell marker for epithelial cells (Chen *et al.* 2004). An issue with many markers is their progressive downregulation in early progenitor cells (Noisa *et al.*

2012), resulting in them being present in both LESCs and early TACs. However, many putative markers have been suggested and several are expressed at the basal limbus.

Pellegrini *et al.* (2001) stated that the transcription factor p63 was expressed specifically by putative LESCs and not the TACs that derive from them. However, Di Iorio *et al.* (2005) found that it was just the isoform ΔNp63α that was expressed in the limbal basal epithelium of undamaged corneas and this is more likely the candidate for a LESC-specific marker. p63 and its isoforms are commonly used when assessing LESCs (Arpitha *et al.* 2008; Levis *et al.* 2013; Grieve *et al.* 2015).

ABCG2, an ATP-binding cassette transporter, is considered a general stem cell marker (Zhou *et al.* 2001) and has been shown to be expressed in limbal basal epithelial cells (Chen *et al.* 2004; Dua *et al.* 2005). However, Watanabe *et al.* (2004) found that ABCG2 is not exclusively expressed by the basal limbal epithelial cells, with some suprabasal staining observed as well. Another member of this family of transporters, ABCB5, has been identified as a regulator of differentiation and can be used as a putative stem cell marker (Frank *et al.* 2003). Ksander *et al.* (2014) demonstrated that ABCB5 maintained LESCs in their quiescent state in mice, and was present in populations of label-retaining cells in mice and in ΔNp63α-positive human basal limbal epithelial cells. More specifically, it marked cells adjacent to the Palisades of Vogt and the proportion of ABCB5-positive cells was much lower in eyes from limbal stem cell-deficient patients. ABCB5 has now become a very promising candidate for a LESC-specific marker, immunofluorescence images for this and p63α can be seen in Figure 1.9.

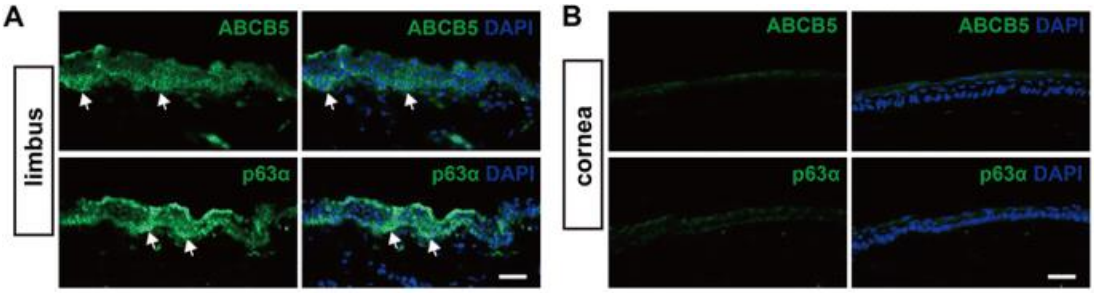

Figure 1.9- Immunofluorescence staining of the rabbit limbus with putative LESC markers. *ABCB5 and p63α both stain more strongly in the limbal epithelium than the corneal, particularly the basal cells. Scale bar = 50 µm. Adapted from Li et al. (2017) with permission under the creative commons user license (https://creativecommons.org/licenses/by/4.0/).*

Vimentin is an intermediate filament and is believed to be a marker of late progenitor cells and mesenchymal cells (Ivaska *et al.* 2007; Schlötzer-Schrehardt *et al.* 2007). Vimentin has been found to label basal epithelial cells that are located at the anterior end of the limbus, where it transitions into the peripheral cornea (Lauweryns *et al.* 1993; Schlötzer-Schrehardt and Kruse 2005; Schlötzer-Schrehardt *et al.* 2007), which is the proposed migration route of the epithelium's TACs. This intermediate filament has also been noted as a marker of epithelial-mesenchymal transition (EMT) (Zeisberg and Neilson 2009).

Another two important markers for assessing the corneal epithelium are the cornea-specific differentiation markers, cytokeratins 3 and 12 (K3/K12). It was Schermer *et al.* (1986) who first specifically suggested that corneal epithelial stem cells are located in the basal limbal epithelium, based on the observation that K3 was found throughout the full thickness of the corneal epithelium and was present in the suprabasal limbal epithelium, but not the basal limbal epithelium. This same staining pattern was also later observed for K12 (Liu *et al.* 1993; Wu *et al.* 1994). This lack of staining at the basal limbus confirms that these epithelial cells are less differentiated than are those throughout the rest of the cornea and limbus. K19 is suggested to be a marker of skin stem cells and has been used to identify these cells in hair follicles (Michel *et al.* 1996). It has also been suggested as a potential marker of the LESCs (Kasper *et al.* 1988) but, again, it is not specific to the stem cell population (Chen *et al.* 2004).

Many other markers have been used when assessing LESCs; just some of those including α-enolase, nestin, connexin 43 and numerous integrins (Matic *et al.* 1997; Chen *et al.* 2004; Schlötzer-Schrehardt *et al.* 2007). However, many of these are not exclusive to the basal limbal epithelium – or even to the cornea. Thus, a distinct LESC marker remains elusive and, usually, several markers are used in unison to attempt to identify LESCs.

1.2.4 Limbal stem cell deficiency

Another key indicator that the limbus – and more specifically the LC – is the site of the limbal stem cell niche is that the crypt structures appear to be absent in human eyes affected by Limbal Stem Cell Deficiency (LSCD). Shortt *et al.* (2007) used *in vivo*

confocal microscopy and neither LCs nor FSPs could be detected in any of the eight patients with the deficiency. Lagali *et al.* (2013) found that progression of stem cell deficiency affected the morphology of the limbus; LCs may be significantly damaged if present or could be lacking entirely.

LSCD often arises due to external influences that destroy the LESCs and the niche. These can include chemical or thermal injury, contact lens wear, medications, and iatrogenic trauma – amongst others (Holland and Schwartz 1997; Schwartz and Holland 1998; Chan and Holland 2013; Bobba *et al.* 2017). The deficiency can also arise from pathologies or congenital conditions such as aniridia (Nishida *et al.* 1995), with a congenital lack of stem cells or an inadequate niche environment for the maintenance of the stem cells being proposed as the aetiology (Ramaesh *et al.* 2005). Autoimmune conditions, such as Stevens-Johnson syndrome and ocular pemphigoid, are difficult-to-treat causes of LSCD that are suggested to cause the deficiency via promotion of LESC apoptosis through inflammatory factors (Hatch and Dana 2009). This list of possible LSCD causes is not exhaustive.

The main symptoms people with LSCD often present with are reduced vision and photophobia (Espana *et al.* 2002; Rama *et al.* 2010; Chan and Holland 2013). Varying degrees of discomfort, from itching/irritation to pain, may also be reported (Pathak *et al.* 2013). Recurrent epithelial erosions, and their associated symptoms, are also reported by LSCD sufferers. Very often conjunctivalisation occurs, conjunctival epithelium growing over the corneal surface (Huang and Tseng 1991), and this then leads to the issues mentioned above (Shortt *et al.* 2007) and loss of transparency of the cornea. This again refutes the idea of conjunctival transdifferentiation.

Limbal transplants can be performed to treat LSCD, using either autografts or allografts (Kenyon and Tseng 1989) and, as aforementioned, grafts cultured from LESCs can also be used successfully (Pellegrini *et al.* 1997). Another development has been the use of amniotic membrane as a transplant material that allows a functional corneal epithelium to grow over the membrane and repopulate the corneal surface (Kim and Tseng 1995). This has then been developed further by either transplanting a limbal allograft along with the amniotic membrane (Tseng *et*

al. 1998) or by culturing autologous epithelial cells on to the membrane and grafting both together (Tsai *et al.* 2000), both demonstrating good clinical results.

More recent developments of surgical treatment of LSCD include trying to revitalise the stem cell niche. Solid platelet-rich plasma has been incorporated into an allogeneic limbal epithelial transplant, as it is a good source of growth factors that aid tissue regeneration, with promising initial results (Alvarado-Villacorta *et al.* 2020). The transplantation of bone marrow-derived mesenchymal stem cells (MSCs) instead of cultured limbal epithelial cells has recently been shown to be as effective as limbal epithelial transplant (Calonge *et al.* 2019). The mechanism of repair after MSC transplant is still not fully understood but could involve MSCs transdifferentiating into corneal epithelial cells (Rohaina *et al.* 2014; Harkin *et al.* 2015; Sánchez-Abarca *et al.* 2015), migrating into the injured tissue and modulating the immune response/inflammation (Omoto *et al.* 2014; Galindo *et al.* 2017), or by stimulating remaining LESCs (Holan *et al.* 2015; Galindo *et al.* 2017).

1.3 Extracellular matrix in stem cell niches

It is now widely believed that the ECM has a highly regulatory role in stem cell niches. As aforementioned, a stem cell niche is not just where the stem cells are located, it is a specific environment of cells and ECM components that maintains the stem cell population. The ECM helps maintain a niche by modulating cell adhesion and through regulation of cell signalling – including via cell-cell interactions and chemical signalling (Ordonez and Di Girolamo 2012). Initial thinking seemed to favour that stem cell niches were maintained just by the interaction of stem cells with surrounding cells, however, new evidence emerged demonstrating the importance of the ECM in niche maintenance, as reviewed by Scadden (2006).

A range of paracrine factors, secreted by niche cells, which affect stem cell behaviour has been identified in *Drosophila* models. Decapentaplegic, a BMP2/4 homologue, maintains germline stem cells and stimulates cell division in the ovaries (Xie and Spradling 1998), Wingless maintains intestinal stem cells in a self-renewal state and Hedgehog then stimulates these cells to differentiate (Takashima *et al.*

2008). Some of these factors have also been identified as regulators of mammalian adult stem cells: Wnt (a Wingless homologue) regulates neurogenesis in the adult hippocampus and stimulates the *de novo* formation of hair follicles after injury in adult mice (Lie *et al.* 2005; Ito *et al.* 2007). Hedgehog is also important in the regulation of neural precursor cells (Palma *et al.* 2004). These are just a small sample of the many paracrine factors that have been implicated in stem cell niches.

Another interesting possibility, when it comes to ECM regulation of stem/progenitor cell populations, is whether the mechanics of the matrix – such as the stiffness of the ECM – modulate cell phenotype in addition to the chemical composition. It has been shown that 3T3 fibroblasts will preferentially migrate from a softer substrate to a stiffer one, in a process termed durotaxis (Lo *et al.* 2000; Lazopoulos and Stamenović 2008). The stiffness of the underlying substrate can also impact other cell behaviours, such as proliferation and differentiation, as shown in an *in vitro* experiment using human epidermal cells (Wang *et al.* 2012). A stiff substrate stimulated migration and proliferation but inhibited differentiation. Contradictory findings were found with 3T3 fibroblasts grown on polyacrylamide substrates, cells migrated more on softer gels, but the effect of stiffness on cell behaviour was still notable (Pelham and Wang 1997).

Stiffness of the underlying substrate, similarly, does affect stem cell behaviour. MSCs, which have multilineage potential, respond to the stiffness of the adjacent matrix in directing cell lineage – as shown in an *in vitro* model (Engler *et al.* 2006). Increasingly stiffer polyacrylamide gels that mimicked brain, muscle and collagenous bone tissue elasticity were found to be neurogenic, myogenic, and osteogenic, respectively. This could be seen in the morphology of the MSCs cultured on each gel, the RNA profiles, and in cytoskeletal markers. In another study, murine muscle stem cells retained stemness; including the ability to self-renew, improved viability and inhibition of differentiation; when cultured on a softer substrate that mimicked the stiffness of muscle tissue (Gilbert *et al.* 2010). In fact, these stem cells could be implanted into damaged muscle and would engraft and even localise themselves to their native *in situ* niche.

Evidence has been gathered suggesting the importance of the ECM in the stem cell niches of a range of tissues. In skeletal muscle, the stem cells are adjacent to the basal lamina of the ECM and numerous components influence them. For example, collagen VI regulates self-renewal and maintains quiescence (Urciuolo *et al.* 2013), whilst laminin and poly-$_D$-lysine may aid differentiation and maturation (Boonen *et al.* 2009). Tenascin-C, by interacting with other signalling pathways, influences the developmental programme of neural stem cells (Garcion *et al.* 2004). Wang *et al.* (2013) found that MSCs taken from trabecular bone differentiated into endothelial cells when cultured in ECM-rich conditions, with laminin being a key driver. This is, again, just a small sample of the vast array of ECM components and proteins that can constitute and regulate a stem cell niche. However, little is still known about the composition of the limbal stem cell niche.

1.3.1 Limbal basement membrane and stromal extracellular matrix

The stiffness of the underlying stromal ECM has been shown to influence epithelial cell fate. Limbal epithelial cells demonstrate increased growth capacity and greater differentiation (as indicated by K3 staining) when cultured on stiffer, compressed collagen gels than on uncompressed (Jones *et al.* 2012). This was demonstrated further both *in vitro* and *ex vivo* by assessing the expression of Yes-associated protein (Yap) in basal epithelial cells (Foster *et al.* 2014). Yap is retained in the cytoplasm when cells are stimulated by a soft substrate (Dupont *et al.* 2011). LESCs expanded on stiffer collagen gels expressed more nuclear Yap, whereas there was more cytoplasmic Yap staining on softer gels (Foster *et al.* 2014). In *ex vivo* bovine corneas, there was significantly more cytoplasmic Yap in limbal basal epithelial cells and more nuclear in corneal basal cells. This indirectly suggests that the limbal ECM is less stiff than the corneal ECM and it was suggested that underlying ECM stiffness might drive epithelial cell differentiation and the centripetal migration of cells.

A novel microscope was developed to assess the biomechanical properties of the cornea using Brillouin scattering (Lepert *et al.* 2016). This technique can assess the relative stiffness of corneal tissue and has shown that there is indeed a difference in stiffness between the human limbal and corneal stroma – with the limbal stroma being softer, as previously hypothesised. The same has been found in the rabbit

cornea, where it has also been shown that the stiffness can be reduced via collagenase treatment and that treatment then resulted in a softer central cornea that supported the growth of epithelial cells that expressed putative stem cell markers (Connon *et al.* 2017).

Further influence of the stroma over the fate of the overlying epithelium has been demonstrated using another rabbit model (Espana *et al.* 2003). Using dispase II to dissociate intact epithelial sheets from rabbit cornea and limbus, the resultant sheets were then recombined with either corneal or limbal stroma. It was seen that corneal epithelium became less differentiated and apoptosis was reduced when it was placed upon limbal stroma, whilst limbal epithelium became more differentiated and apoptosis was increased when it was placed onto corneal stroma. Thus, these results suggested that the stromal composition, and therefore the ECM composition here, was different between the limbus and cornea – with the former creating an environment that favours stemness.

As Espana *et al.*'s technique for isolating epithelial sheets breaks down the basement membrane, they did not believe that the basement membrane had a significant effect on the modulation of the limbal and corneal epithelia. However, in-depth studies have examined the composition of the limbal basement membrane and demonstrated variations that could implicate it in stem cell niche regulation of the LESCs.

Blazejewska *et al.* (2009) have demonstrated that culturing murine hair follicle stem cells in a limbus-specific environment can cause them to transdifferentiate into corneal epithelial cells. It was specifically a microenvironment similar to the limbus, rather than the cornea, that was needed to induce this change. This microenvironment was replicated by obtaining culture media conditioned by limbal and corneal fibroblasts – as well as 3T3 fibroblasts which were used as a control – and by incorporating laminin-5, which is an important component of ocular surface basement membranes (Schlötzer-Schrehardt *et al.* 2007). This again demonstrated the considerable influence the ECM/basement membrane environment of the limbus has over directing cell fate.

It has recently been shown that a decellularised matrix produced by human corneal fibroblasts can be used for ocular surface reconstruction (Mertsch *et al.* 2020). The matrix produced was multi-layered and similar to the corneal stromal ECM. It supported the growth of LESCs and a stem phenotype was maintained. Though it is yet to be tested in humans, it is a good candidate for delivering LESC transplants to the eye as it contains the required cornea-specific matrix and has reduced immunogenicity.

Using an array of different monoclonal antibodies, Schlötzer-Schrehardt *et al.* (2007) assessed the composition of the limbal stromal ECM and epithelial basement membrane. Type IV collagen, an important component of all basement membranes, can be composed of six different α chains (Sado *et al.* 1995) and Schlötzer-Schrehardt *et al.* found that there was more α1 and α2 collagen IV in the limbal basement membrane than in the corneal, a finding agreed upon by others (Ljubimov *et al.* 1995). It was also found that the corneal basement membrane contains more α3 collagen IV in both of these studies. The exact role of collagen IV is not understood, but it is suggested to play a role in adhesion of potential LESCs and promoting differentiation into an epithelial cell line (Li *et al.* 2005; Ahmad *et al.* 2007). The difference in the function of different α chains has not been examined. Type XVI collagen is also one that appears to only be present in the limbal, and not the corneal, epithelial basement membrane (Schlötzer-Schrehardt *et al.* 2007).

Vitronectin is a glycoprotein that is localised either within the limbal epithelial basement membrane or directly subjacent to it but is not found within the central cornea of human eyes (Schlötzer-Schrehardt *et al.* 2007; Echevarria *et al.* 2011). Echevarria *et al.* also found vitronectin within the basement membranes of the epithelia of the hair follicle outer root sheath and the crypts of the small intestine, both epithelia that are host to stem cell populations. The colony-forming efficiency of putative LESCs was demonstrated to be increased with the addition of a vitronectin coating and a higher number of holoclones were formed (Echevarria *et al.* 2011). These results suggest the presence of vitronectin in, or subjacent to, the limbal basement membrane may indeed play a role in stem cell niche maintenance.

It is interesting to note that some basement membrane components, individual to the limbal area, seem to aggregate at the base of LCs and co-localise with putative stem cells based on marker expression (Schlötzer-Schrehardt *et al.* 2007). These include laminin γ3, BM40/SPARC and tenascin-C. In the limbus anterior to LCs, suggested to be the migration route of TACs, other components are found such as chondroitin sulphate, versican, type XVI collagen. Significantly, the ECM/basement membrane components found here are noted to have an effect on cellular changes, including proliferation and migration, via interactions with signalling molecules/cascades.

Gesteira *et al.* (2017) have demonstrated that the ECM of the murine limbal stem cell niche is rich in the glycosaminoglycan hyaluronic acid (HA) (see below). Using HA synthase knockout models, they showed that the loss of these synthases could lead to LSCD and that a change in the distribution of HA led to a change in the distribution of LESCs. They proposed that HA helps maintain the stem cell phenotype in the cornea. This is not the first investigation to examine glycosaminoglycans in relation to stem cell niches; in fact, they have become an area of interest in this field.

1.4 Glycosaminoglycans

1.4.1 Structure

Glycosaminoglycans (GAGs) are extremely diverse molecules comprised of a long sugar chain made of repeating disaccharides, which themselves consist of a hexosamine unit alternating with a uronic acid or galactose (Caterson 2012). The hexosamine unit can be either N-acetyl-glucosamine (GlcNAc) or N-acetyl-galactosamine (GalNAc) and the uronic acid can be either iduronic acid (IdUA) or glucuronic acid (GlcA). There are four different types of GAG: hyaluronic acid (HA), heparin/heparan sulphate (Hep/HS), keratan sulphate (KS) and chondroitin sulphate/dermatan sulphate (CS/DS). When a GAG is attached to a core protein, this is then termed a proteoglycan (PG). One or more GAG chains can covalently

bind to the core protein of a PG and they can be found both intracellularly or extracellularly, as well as on cell membranes (Wight *et al.* 1991).

HA consists of GlcNAc alternating with GlcA and is the only GAG that is never sulphated and does not bind to a protein core (Iozzo 2000). KS is different in that its structure is formed by galactose alternating with GlcNAc and does not involve a uronic acid component. Hep/HS consists of either uronic acid alternating with GlcNAc. The structure of CS/DS is discussed below.

There is a vast number of possible GAG configurations (Cummings 2009). Considering just CS/DS, it is estimated there are as many as 16^{50} theoretical variants of a 50 disaccharide-long chain, based on 16 possible disaccharide variants (Persson *et al.* 2020). One of the reasons for this is that the amount of sulphation of the hydroxyl groups of the disaccharide, and which hydroxyl group the sulphated groups attach to, can vary (Hayes *et al.* 2011). The sulphation, as well as other components of the structures, give GAGs a strong negative charge. This makes the molecules very hydrophilic and gives them the ability to bind to many positively charged molecules within cells and the ECM (Caterson 2012).

1.4.1.1 Chondroitin sulphate and dermatan sulphate

CS consists of GalNAc and GlcA, however, some of the GlcA can be converted into IdUA and when this occurs it is then known as DS (Wight *et al.* 1991). Simplified diagrams of one of many possible structures of CS and DS heptasaccharides are shown in Figure 1.10. The individual monosaccharides can be sulphated in various positions (Caterson 2012). GalNAc can be sulphated at either the 4- or 6-hydroxyl groups, or both in CS chains, and the uronic acids can be sulphated at the 2-hydroxyl group. The glycosidic bonds from the uronic acid are β 1,3 links and those from GalNAc are β 1,4 links (Iozzo 2000).

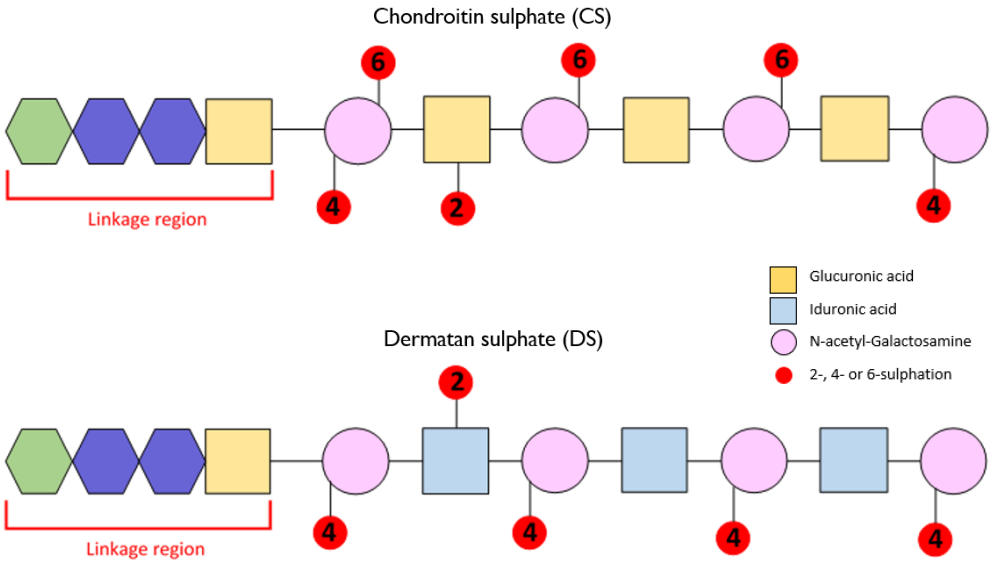

Figure 1.10- Diagram representing the structures of chondroitin sulphate (CS) and dermatan sulphate (DS) polysaccharides.
CS and DS both contain N-acetyl-galactosamine, but different uronic acids. This allows them to form hybrid chains containing both types of glycosaminoglycan. The tetrasaccharide linkage region, consisting of xylose-galactose-galactose-glucuronic acid, binds the glycosaminoglycan to a core protein via a glycosidic bond between the xylose and a serine residue on the protein (Wight et al. 1991).

1.4.1.2 Biosynthesis of CS/DS

The biosynthesis of CS/DS and Hep/HS begins in the same way, with the formation of the tetrasaccharide linkage region. Two different xylosyl-transferases begin this process by transferring a xylose residue from UDP-xylose onto the hydroxyl group of a specific serine residue in the core protein of a PG. Two galactose residues are then added from UDP-galactose and, finally, a GlcA residue added from UDP-GlcA completes the linkage region. These additions are all completed by distinct glycosyl-transferases (Hascall *et al.* 1991; Iozzo 2000; Caterson 2012).

Chain elongation then occurs with the alternate addition of GalNAc and GlcA by further distinct glycosyl-transferases, which is when the biosynthetic pathways for CS/DS and Hep/HS diverge. Further modification occurs when some of the GlcA residues are converted into IdUA by DS epimerases (Table 1.1), thus forming DS disaccharides from CS disaccharides. Sulphate groups are also added to the disaccharides in various positions by numerous sulphotransferases, also shown in Table 1.1. These modifications are believed to occur during or slightly after chain elongation.

Enzyme	Action of enzyme
Chondroitin-4-sulphotransferase-1 (C4ST1)	Adds sulphate residue to 4-hydroxyl group of GalNAc in CS chains
Chondroitin-4-sulphotransferase-2 (C4ST2)	Adds sulphate residue to 4-hydroxyl group of GalNAc in DS chains
Chondroitin-4-sulphotransferase-3 (C4ST3)	Adds sulphate residue to 4-hydroxyl group of GalNAc in CS chains
Dermatan-4-sulphotransferase-1 (D4ST1)	Adds sulphate residue to 4-hydroxyl group of GalNAc in DS chains
Chondroitin-6-sulphotransferase-1 (C6ST1)	Adds sulphate residue to 6-hydroxyl group of GalNAc in CS chains
Chondroitin-6-sulphotransferase-2 (C6ST2)	Adds sulphate residue to 6-hydroxyl group of GalNAc in CS chains
N-acetyl-galactosamine 4-sulphate 6-O-sulphotransferase (GalNAc4-6ST)	Adds sulphate residue to 6-hydroxyl group of an already 4-sulphated GalNAc in CS chains
Uronyl-2-O-sulphotransferase (UST/CS2ST)	Adds sulphate residue to 2-hydroxyl group of either uronic acid in CS/DS chains
DS epimerase-1 (DSepi-1)	Converts GlcA to IdUA before 4-O-sulphation of GalNAc has occurred
DS epimerase-2 (DSepi-2)	Converts GlcA to IdUA before 4-O-sulphation of GalNAc has occurred

Table 1.1- A list of some of the enzymes involved in CS and DS biosynthesis (Caterson 2012). In particular, those involved in sulphation.

The biosynthesis of GAGs occurs intracellularly, mostly within the Golgi/trans Golgi compartments. The core protein is formed in the rough endoplasmic reticulum and is then transferred to the Golgi for the addition of the GAG chains. The completed PGs are then transported to where they are needed: stored in secretory granules for later secretion, embedded in the plasma membrane or secreted into the ECM (Hascall *et al.* 1991; Iozzo 2000).

1.4.2 Functions

Though it is strongly believed that PGs have a role in maintaining the transparency of the corneal stroma, PGs have functions in many different cellular processes and these functions can be enacted by either the protein itself, the GAG side chain or both together (Tiedemann *et al.* 2005). PGs have the ability to bind many different

molecules/entities, including growth factors, morphogens, cytokines, and chemokines (Najjam *et al.* 1997; Kawashima *et al.* 2002; Bao *et al.* 2004; Yan and Lin 2009). Through binding to these different molecules, PGs can then influence biological processes. There are three proposed actions when a PG binds with a growth factor: 1) enhancing/initiating the growth factor's action; 2) prolonged action of the factor due to the PG binding and slowly releasing it; 3) inhibition of the growth factor's action by preventing it from binding to its receptor (Toole 1991). Thus, GAGs and PGs can play both structural and functional roles within a tissue.

Some examples of the influence of PGs include the dependence of vascular endothelial growth factor (VEGF) on heparin to bind to its receptor, in order to initiate angiogenesis and the proliferation of endothelial cells (Gitay-Goren *et al.* 1992). Heparin-binding EGF-like growth factor interacting with HS PGs on the cell surface of smooth muscle cells is also essential for stimulating the migration of these cells (Higashiyama *et al.* 1993). Cell adhesion, both to the ECM and to other cells, is also influenced by PGs/GAGs. Mouse mammary epithelial cells were found to attach to the ECM via cell surface PGs that acted as receptors for ECM components (Saunders and Bernfield 1988), and macrophages and fibroblasts have been shown to aggregate via HA receptors with HA molecules cross-bridging the receptors on adjacent cells (Green *et al.* 1988). These are specific examples of functions within specific tissues, the influence of GAGs is widespread throughout the body and the effects of this have particular importance in the development and regeneration of tissues.

1.4.3 GAGs/PGs regulating stem cells

PGs, particularly HS PGs, have been shown to be key players in stem cell niche regulation and with embryonic stem cells (Kraushaar *et al.* 2013). A study on haematopoietic stem cells found that HS PGs were important in the maintenance of long-term culture-initiating cells (Gupta *et al.* 1998). In particular, it was thought that larger, more highly sulphated HS PGs were responsible for this. Another study, on mouse bone marrow-derived MSCs, also demonstrated the impact HS PGs have on stem cell self-renewal and proliferation (Cheng *et al.* 2014).

The HS PGs syndecan-3 and syndecan-4 have been shown to be expressed exclusively by quiescent satellite cells (the stem cells of skeletal muscle) in adult muscle tissue and these PGs have important roles in the maintenance, activation and proliferation of these cells (Cornelison *et al.* 2001). The *in vitro* proliferation and differentiation of bovine muscle cells was also found to be considerably higher when a mixture of GAGs was added to an enactin-laminin-collagen culture substrate (Rønning *et al.* 2013). However, it cannot be determined from this which GAGs were having the most influence on cell behaviour.

CS/DS has also become the subject of much interest concerning its role in stem cell niches and the functioning of stem cells. Embryonic stem cells in mice are dependent on CS to develop and function properly (Izumikawa *et al.* 2014). This investigation found that pluripotency could not be maintained without CS and that CS was needed to initiate differentiation.

When investigating sections of telencephalon tissue of embryonic mouse brains, and neural cells in culture, Ida *et al.* (2006) found a significant presence of CS around these cells. Fibroblast growth factor (FGF-2)-mediated cell proliferation of the stem cells was stimulated by different types of commercially produced CS and telencephalon-derived CS also produced this effect. Furthermore, e*x vivo* and *in vitro* investigations of neural precursor cells by Sirko *et al.* (2007) corroborated the regulatory role of CS. The reduction of CS by chondroitinase digestion led to a decline in both cell proliferation and differentiation in cultured murine neural cells as well as sections of forebrain.

Karus *et al.* (2012) took this further and found that the sulphation of CS is an important regulator of spinal cord neural precursor cells. Progression of the cell cycle, proliferation and maturation were all affected in mouse neural cells that were treated with sodium chlorate *in vitro*, which reduced the sulphation of CS GAGs.

When examining the *in vitro* differentiation of MSCs into cartilage cells in 3D hydrogel scaffolds designed to mimic the native cartilage environment, the addition of CS enhanced chondrogenesis (Varghese *et al.* 2008). This was believed to be due

to creating a microenvironment that was more similar to the native niche. The cells in the CS hydrogel also exhibited lower rates of proliferation and started producing cartilage ECM components, unlike MSCs cultured without CS.

1.4.4 GAGs in the cornea

GAGs have been studied extensively in the central cornea, but not as comprehensively at the limbus. However, Borcherding *et al.* (1975) examined GAG distribution across the full width of the human cornea and made several interesting observations. KS was found to be the main GAG in the central cornea, but its concentration dropped sharply when transitioning from central to peripheral cornea and from corneolimbus to sclerolimbus. CS and DS were then found to be more prominent in the peripheral cornea and limbus. Ho *et al.* (2014) also examined PG distribution in bovine corneas. The distribution of KS and DS PGs was uniform across both the depth and width of the cornea and CS was only detected in the peripheral cornea and at the limbus, like in the human eye.

Despite Ho *et al*. finding no change in PG distribution with increasing stromal depth, there is an "oxygen-lack" theory that suggests KS is preferentially produced in low oxygen conditions. Therefore, more KS is expected in the less oxygen-rich posterior cornea (Scott and Haigh 1988b), due to the majority of corneal oxygenation coming from the atmosphere via the anterior surface. This effect is only thought to be prevalent in thicker corneas of larger species, where it has been noted in cows, rats and rabbits (Bettelheim and Goetz 1976; Scott and Haigh 1988b). Murine corneas, which are sufficiently thin and do not demonstrate such variation in oxygen conditions, have KS only in very low levels and the KS present is all low sulphated (Scott and Haigh 1988b; Young *et al.* 2005).

Though Borcherding *et al.* reported that it is KS and chondroitin that are dominant in the central cornea, it is usually stated that KS and DS are the most prominent GAGs here (Scott and Haigh 1988a; Iozzo 1998; Lewis *et al.* 2010). In particular, these two GAG chains are bound to PGs in a family known as small leucine-rich proteoglycans (SLRPs) (Iozzo 1998). Some of the most abundant SLRPs in the cornea include decorin, lumican, keratocan, biglycan and mimecan. One role of these PGs is the hydration of the corneal stroma, with the negative charge of GAGs due to

their sulphation being stated as the main driver of the cornea's swelling pressure (Hedbys 1961). This function, along with maintaining collagen fibril spacing, is thought to play a key role in maintaining corneal transparency.

From the numerous studies of PGs in the central cornea, it is well known that they are closely associated to the collagen fibrils of the stroma. Sawaguchi *et al.* (1991) compared the PG distribution in normal and keratoconic human central corneal stromas using cuprolinic blue staining and found that PG filaments ran transversely to the collagen fibrils – a finding agreed upon by Meek *et al.* (1989). Studies creating 3D reconstructions of bovine and mouse corneas using electron tomography demonstrated that the collagen fibrils of the corneal stroma were in a regular "pseudo-hexagonal" arrangement and that CS/DS PGs would contact two or more fibrils, whilst KS PGs occupied the interfibril space (Lewis *et al.* 2010; Parfitt *et al.* 2010). Some CS PG filaments would also run parallel to the fibrils, as well as at angles to them that approached orthogonal. Despite the irregularity of the PGs, it is still thought that they maintain the regular spacing of collagen fibrils that is essential to the transparency of the tissue (Maurice 1962; Benedek 1971). Lewis and Parfitt both propose that two opposing, yet balanced, forces are created by the corneal PGs. The attractive force, induced by the thermal motion of the PGs, causes a retraction of the molecule and brings the core proteins attached to different fibrils closer together. The repulsive force is due to the anionic nature of GAGs attracting positively charged ions and water molecules to the interfibril space, inducing a swelling pressure between fibrils. Parfitt *et al.* also suggested that it is specifically undersulphated KS that is responsible for the attractive force and large CS/DS PGs for the repulsive in mouse corneas.

Corneal PGs also have an effect on the formation of collagen fibrils. An *in vitro* investigation demonstrated that collagen fibrils formed in the presence of lumican (a KS PG) were significantly thinner than those formed without lumican (Rada *et al.* 1993). Decorin (a DS PG) also resulted in thinner fibrils and the investigators found that the effects on fibrillogenesis resided in the core proteins, not the GAG chains. However, a knockout mouse model demonstrated normal corneal collagen packing and fibril sizes in decorin-null mice (Danielson *et al.* 1997), whilst lumican-null mice

presented abnormally shaped, sized and organised fibrils and corneal clouding (Chakravarti *et al.* 1998; Quantock *et al.* 2001). This suggests lumican plays a larger role in corneal collagen fibrillogenesis than decorin does. Additionally, mice lacking keratocan, another KS PG, demonstrate much larger collagen fibril diameters that are arranged further apart and less regularly than in wild type corneas (Liu *et al.* 2003; Meek *et al.* 2003). In a dual decorin/biglycan knockout model, Zhang *et al.* (2009) showed that knocking out each PG individually did not change stromal collagen fibril structure. Decorin was found to be more important for fibrillogenesis than biglycan, as decorin-null mice demonstrated a compensatory increase in biglycan, whilst the decorin-null/biglycan-null mice showed significantly disrupted collagen fibril formation.

The distribution of HA in the murine cornea has also been investigated and has been found to be almost exclusively within the limbus and not the peripheral or central cornea (Gesteira *et al.* 2017). This is true even after epithelial injury; however, HA can be found in the central cornea of HA synthase knockout mice after injury.

1.5 Cell-cell interactions

The other aspect of a stem cell niche is the influence of other cell types on regulating the stem cell population. It has been proposed in a review of the literature that LESCs can potentially receive signals from six different cell types: the corneal and conjunctival epithelia, corneal stromal cells, conjunctival stromal cells, and the endothelial and smooth muscle cells of the episcleral vasculature (Stepp and Zieske 2005). Though the LESCs are not in direct contact with all of these cell lines, there are still numerous sources of potential cell-cell contact.

1.5.1 Corneal stromal cells

As mentioned in section 1.1.3, the corneal stroma contains keratocytes – flattened fibroblast-like cells. However, there is also a population of stem cells within the limbal stroma that are proposed to be MSCs. MSCs are multipotent stem cells, derived from the mesoderm, that can be found in skeletal muscle, bone marrow

and adipose tissues (Dennis *et al.* 1999; Williams *et al.* 1999; Zuk *et al.* 2001). In 2005, Dravida *et al.* identified a population of limbal stromal cells that possessed transdifferentiation potential for several different cell lines. Polisetty *et al.* (2008) then compared human limbal stromal cells to human bone marrow MSCs and found that they were extremely similar in morphology, proliferative capacity, surface marker expression and multilineage differentiation potential – suggesting that these cells are indeed MSCs. They also hypothesised that these cells form a component of the LESC niche.

Chen *et al.* (2011) isolated human LESCs by using collagenase, which kept the basement membrane intact. This resulted in niche cells from the stroma also being harvested via this technique. Through this, and subsequent studies (Xie *et al.* 2012), this group found that the putative LESCs were closely associated to these underlying cells from the stroma, which expressed a range of stem cell markers, and demonstrated that they support and enhance the *in vitro* growth of LESCs. They then showed that these stromal cells expressed MSC markers and suggested that they were MSCs that form part of the limbal stem cell niche (Li *et al.* 2012). Further studies have also shown that limbal MSCs can be used to efficiently support the culturing of LESCs *in vitro* (Branch *et al.* 2012; Nakatsu *et al.* 2014; Kureshi *et al.* 2015). All of this collectively demonstrates the highly regulatory role that MSCs play in maintaining the limbal stem cell niche.

It has been shown that the putative LESCs and stromal cells are in very close proximity to each other – partly due to Bowman's layer terminating at the corneolimbal transition. However, it has been shown that there is an even closer association than this. Chen *et al.* (2004) noted invaginations into the limbal basement membrane from the basal epithelial cells, which they commented made for an excellent route for obtaining nutrients, by bringing the putative LESCs closer to the ECM of the stroma. However, Dziasko *et al.* (2014) have shown that there are actual breaks in the basement membrane of the human limbal stem cell niche, allowing direct cell-cell interactions between the limbal epithelium and stroma.

Using serial block-face scanning electron microscopy (SBFSEM), 3D reconstructions of the LC were created and direct contact between a putative LESC and a stromal

cell was demonstrated (Dziasko *et al.* 2014). Stromal cells were elongated and extended processes towards the basement membrane and a focal, direct contact was observed between a large stromal cell and a basal epithelial cell. This connection was only observed within the LCs. Significant staining for MSC markers was observed in a subpopulation of limbal stromal cells subjacent to the LCs. However, the investigators did suggest that these CD90- and CD105-positive cells may be situated deeper in the stroma than the stromal cells that are interacting with the basal epithelial cells.

These stromal cell-epithelial cell interactions have also been observed in the rabbit limbus (Yamada *et al.* 2015) (Figure 1.11). Mesenchymal cells in the stroma extended long processes that went through discontinuations in the basement membrane to contact basal epithelial cells, with some even extending some distance in between adjacent epithelial cells. With no positive staining for putative MSC markers, it cannot be assumed that these stromal cells are MSCs. 3D reconstructions confirmed these direct interactions between the two cells types, showing that two mammalian species both possess this phenomenon in their putative limbal stem cell niches.

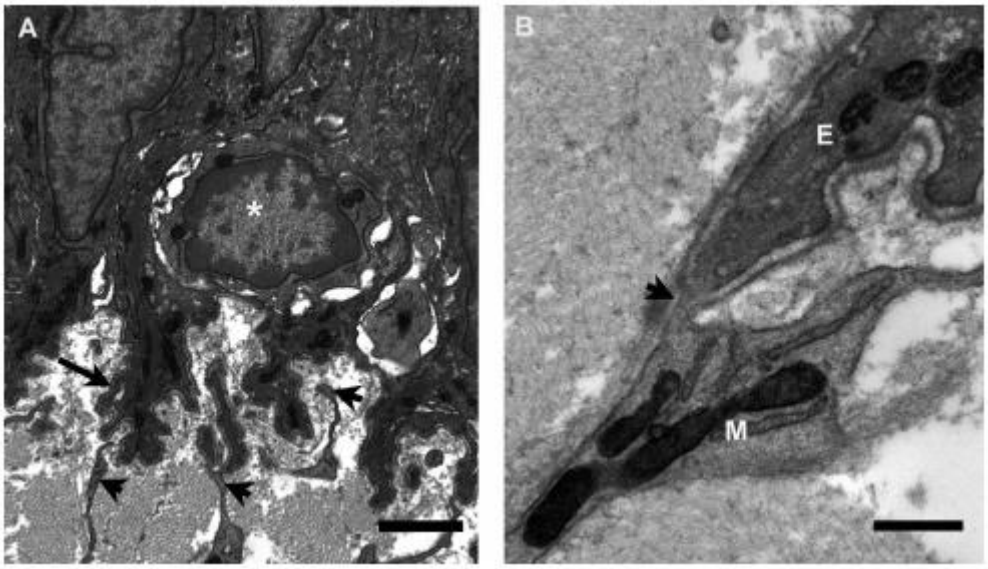

Figure 1.11- Direct contact between an epithelial cell and a stromal cell in the rabbit limbus.
Multiple process from stromal cells (A, arrowheads) extend towards lobed protrusions of basal epithelial cells (A, arrow). A discontinuity in the basement membrane allows the stromal and epithelial cells to come into direct contact (B, arrowhead) in the limbus. E = epithelial cell, M = mesenchymal stromal cell. Scale bars (A) = 2 µm, (B) = 0.5 µm. Source: Yamada et al. (2015) with permission under the creative commons user license (https://creativecommons.org/licenses/by-nc-nd/3.0/).

1.5.2 Limbal melanocytes

As mentioned above, the Palisades of Vogt contain melanin pigment and Higa *et al.* (2005) characterised the limbal melanocytes that are responsible for this. Limbal melanocytes are found within the basal layer of the limbal epithelium, with the pigment preferentially situated apically within the cell, closer to the ocular surface. It is only the melanocytes that produce melanin at the limbus, as in the skin, and Higa *et al.* (2005) suggested a melanocyte to K19-positive epithelial cell ratio of approximately 1:10. The melanocytes exhibit a dendritic morphology, extending to multiple epithelial cells to which they appear to be closely associated. Dziasko *et al.* (2014) observed direct cell-cell interactions at basal epithelial cells' apical surfaces with limbal melanocytes. These limbal melanocytes support the growth of LESCs *in vitro* and maintain the stem cell phenotype (Dziasko *et al.* 2015).

Earlier work by Hayashi *et al.* (2007), demonstrated that subsets of both putative LESCs and limbal melanocytes express N-cadherin in the human limbal stem cell niche. The authors hypothesised that LESCs and N-cadherin-positive melanocytes interact with each other via N-cadherin and that this subset of limbal melanocytes

acts as niche cells in the limbus. A more recent study of cell adhesion molecules within the limbal stem cell niche contradicts Hayashi *et al.*'s findings, suggesting that N- and P-cadherins mediate putative LESC-LESC interactions and that E- and P-cadherins mediate LESC-melanocyte interactions (Polisetti *et al.* 2016). Hayashi *et al.* did not observe any P-cadherin in the limbal or corneal epithelium and E-cadherin was observed throughout the corneal epithelium, but only in the suprabasal limbal epithelial layers. Higa *et al.* (2013) did not observe N-cadherin-positive epithelial cells in association with melanocytes either, also contradicting Hayashi *et al.* However, all the studies do agree that limbal melanocytes certainly seem to be important niche cells within the corneal limbal stem cell niche.

1.5.3 Epithelial-mesenchymal transition

Epithelial-mesenchymal transition (EMT) can be described as the process of an epithelial cell undergoing biochemical and phenotypical changes to become a mesenchymal cell (Kalluri and Weinberg 2009). The changes observed include changing from an apical-basally polarised cell to an elongated, front-to-back leading-edge polarised cell; lack of intercellular adhesions; increased ECM production; increased individual motility and irregularity in shape and composition (Lee *et al.* 2006; Kalluri and Weinberg 2009). The reverse process can also occur, known as mesenchymal-epithelial transition.

The need for EMT has been discussed in a series of review articles (Acloque *et al.* 2009; Kalluri 2009; Zeisberg and Neilson 2009). EMT is essential during embryogenesis, in particular for producing the primary mesenchyme. EMT is also required for producing the mesenchymal cells and fibroblasts that are needed during tissue repair, wound healing and fibrosis. However, metastasis of epithelial cancers is also reliant on EMT, producing invasive, migratory cells that can then establish a secondary tumour elsewhere in the body. Thus, EMT is indispensable for the correct development and maintenance of an organism but is also involved in the most serious of pathologies.

There are various markers that can be used to determine whether EMT has taken place. E-cadherin levels decrease during EMT and in the resultant mesenchymal cells. It is thought that the reduction of E-cadherin and the adherence complexes

they form may stimulate EMT (Behrens *et al.* 1989; Vleminckx *et al.* 1991; Kato *et al.* 1995). β-catenin is a protein that links cadherins to the cytoskeleton and is normally found attached to the cell membrane of epithelial cells and non-migratory tumour cells (Brabletz *et al.* 1998). However, during EMT, the β-catenin dissociates from cadherins and is then localised within the cytoplasm or nucleus of the newly formed mesenchymal cells. β-catenin also acts as a transcription factor by forming complexes with Lymphoid Enhancer Factor-1 (LEF-1) that then activate genes necessary for initiating EMT (Medici *et al.* 2006), thus also explaining the nuclear location of this protein in transitioned cells.

Cytoskeletal markers of EMT include Fibroblast-specific protein-1 (FSP-1) and vimentin – which has been mentioned above. FSP-1 has been shown to promote the early stages of EMT in fibroblast formation (Okada *et al.* 1997) and, also, metastatic development of carcinomas in a murine model (Xue *et al.* 2003). Vimentin is a more uncertain marker of EMT, as it is not found solely in mesenchymal cells (Dellagi *et al.* 1983; Commo *et al.* 2004; Schlötzer-Schrehardt and Kruse 2005). It appears that vimentin is a suitable marker for EMT during metastasis and gastrulation (Burdsal *et al.* 1993; Fléchon *et al.* 2004; Yang *et al.* 2004; Sarrió *et al.* 2008), but cannot be reliably used as a marker for EMT during fibrosis (Witzgall *et al.* 1994; Zeisberg and Neilson 2009).

EMT can be stimulated in the limbal epithelium by air exposure in an *in vitro* model (Kawakita *et al.* 2005). “Air lifting” of rabbit limbal explants caused intrastromal invasion by limbal basal epithelial cells and changes associated with EMT (such as a reduction in E-cadherin and nuclear relocation of β-catenin) were observed in some basal epithelial cells situated at the invading tip. Some p63-positive cells were found subjacent to the invading tips, within the limbal stroma, suggesting that some limbal epithelial progenitor cells had undergone EMT. The authors suggested EMT could play a role in corneal wound healing and the choice of whether regeneration or fibrosis is triggered in LESCs.

A follow-up study to this suggested that EMT is involved in the pathogenesis of human pterygium, in particular, due to the activation of the β-catenin pathway (Kato *et al.* 2007). Several changes associated with EMT were observed in epithelial

cells at the leading edge of pterygia and, again, invasion of basal epithelial cells into the stroma was observed. EMT is also believed to be involved in subepithelial fibrosis that occurs due to LSCD, with similar observations to Kato *et al.*'s investigation found (Kawashima *et al.* 2010).

When examining the putative limbal stem cell populations in the murine ocular surface, Parfitt *et al.* (2015) were surprised to find a very small number of label-retaining cells within the limbal stroma that had potentially migrated from the epithelium, based on keratin 5 staining. The authors believe this supports the notion of EMT at the limbus and, suggests it may be occurring *in vivo*. These findings also appear to support Kawakita *et al.*'s theory (2005) that limbal epithelial stem/progenitor cells undergo EMT.

More recently, using a transgenic mouse model, it has been shown that Krüppel-like factor 4 (KLF4) is a strong mediator of corneal epithelial homeostasis and a suppressor of EMT (Tiwari *et al.* 2017). Ablation of KLF4 resulted in altered gene expression that favoured EMT in corneal epithelial cells. This also affected wound healing, with experimentally induced wounds closing more quickly in the KLF4-deficient mice but failing to re-epithelialise correctly after seven days. Thus, EMT does appear to be a process that occurs in the corneal epithelium *in vivo*, though it may be mostly associated with pathology and not corneal homeostasis.

1.6 X-ray micro-computed tomography

X-ray computed tomography is a technique widely used clinically, but it lacks the resolution to observe finer structures and to examine smaller animals (Holdsworth and Thornton 2002; Ivanishko *et al.* 2017). However, X-ray micro-computed tomography (microCT) was developed to remedy this gap in utility. This technique can be used on much smaller samples – from hundreds of microns to several centimetres – to get micron-level resolution (Leszczyński *et al.* 2018).

In this technique, just as with the clinical application, X-rays are passed through the specimen being examined to gather 3D information about it. An electronic detector placed directly opposite the X-ray source measures the attenuation values of the X-

ray beam as it passes through a cross-section of the specimen (Seeram 2016). The X-ray source is then rotated around the specimen and the attenuation values are processed by a computer to generate 2D image slices that can be used to form 3D volumes. MicroCT works along the same principles as clinical CT but has greatly increased resolution for use on much smaller specimens. In microCT, the sample is rotated by a fraction of a degree through 180˚ or 360˚ after taking each cross-section whilst the X-ray source and detector remain stationary, in contrast to clinical CT which involves a ring-shaped gantry rotating around the patient to collect the images (Seeram 2016).

The advantages of this technique include it being non-destructive and able to be used on unstained/unprocessed samples (Leszczyński *et al.* 2018; Mittone *et al.* 2018). However, as soft tissues do not attenuate X-rays as much as harder or mineralised tissues, staining procedures can be applied to soft tissue samples to improve the image contrast. In addition, as mentioned above, this technique collects 3D information, meaning that cross-sections and surface images can be acquired. Measurements can then be carried out on the resultant data sets.

X-ray microCT will be used in this thesis to create 3D reconstructions of the porcine limbus in an attempt to determine its structure. Analyses can then be applied to determine some characteristics of this area, including of the LCs.

1.7 Electron microscopy

As the name states, electron microscopy utilises electrons instead of light in order to image the structures under investigation. The advantage of this is it allows for much higher resolution than light microscopy. Image resolution is dependent on the wavelength of the light or electron beam used. As the wavelength range of visible light is approximately 400-700 nm, the resolution of light microscopy cannot go below this range. Electrons have a much shorter wavelength than visible light, which results in better resolution and the ability to image much smaller structures.

Low contrast was initially an issue with electron microscopy. This can be countered with the use of staining with heavy metals (Hall *et al.* 1945; Watson 1958), such as

uranium or tungsten, amongst others. These make the sample more electron-dense, increasing the interaction of the structures with the electron beam and producing greater contrast.

There are two main types of electron microscopy: transmission electron microscopy (TEM) and scanning electron microscopy (SEM). During TEM, an electron beam is passed through a thin section (approximately 100 nm) of the specimen to be examined; electromagnets act as condensing lenses to focus the beam. It is then the electrons that have been transmitted through the sample that are collected to form the image.

SEM was developed after TEM and involves raster scanning the electron beam across the surface of a specimen and then collecting the backscattered and secondary electrons from the surface to form the image. Classically, the magnifying power of SEM was not as high as TEM, but it does allow the formation of "three-dimensional" surface images, where depth and contouring can be observed. A modification of SEM called serial block-face SEM (SBFSEM) has been developed that allows the creation of 3D reconstructions of samples at high magnification (Denk and Horstmann 2004). The electron beam is raster-scanned across the surface of a specimen *en bloc*; then an in-chamber, automated ultramicrotome removes a section from the top of the block and the newly-created block-face is raster-scanned (Figure 1.12). This is done repeatedly, gathering a large dataset of many images a set distance apart (usually 50-100 nm) that can then be combined to create a 3D reconstruction. All of the electron microscopy techniques discussed here will be used in this thesis.

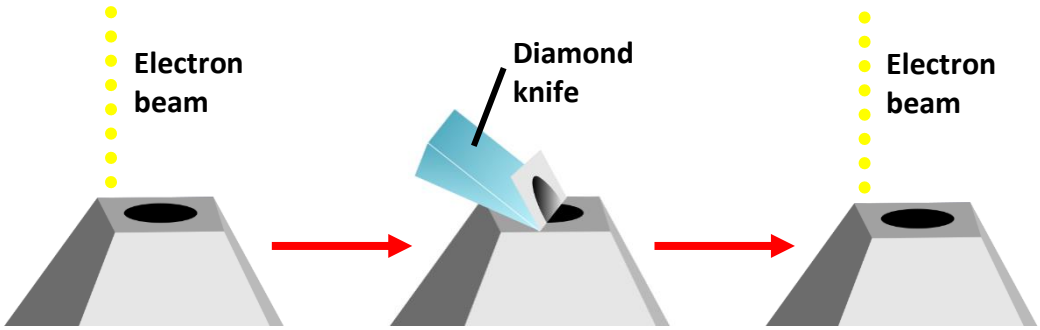

Figure 1.12- A representation of the mechanism of serial block-face scanning electron microscopy. *The electron beam is raster-scanned across the block-face of an* en bloc *sample and the back-scattered electrons are collected to form an image. The diamond knife of the in-chamber ultramicrotome then removes a section of set thickness and the newly exposed block-face is then raster-scanned by the electron beam to create another image. This is done repeatedly to gather a dataset of potentially hundreds of images to then create a three-dimensional reconstruction of the sample.*

1.8 Aims and hypotheses

It is well known that GAGs are abundant within the cornea and their distributions vary with eccentricity, and there is ample support that GAGs exhibit modulatory effects on stem cell populations. Due to the limited knowledge of the ECM composition of the limbal stem cell niche, these factors have motivated the research that will be conducted in this thesis.

The aims of the experimentation described in this thesis are:

1. To further assess the anatomy of the porcine limbus and determine where LCs/LC-like structures are located and how suitable a model porcine tissue is for the human cornea.
2. To determine what the distribution of CS is in the porcine limbal stem cell niche and to assess whether there are differences between the superior/inferior and the nasal/temporal quadrants of the limbus.
3. To examine the ultrastructure of the porcine limbal stem cell niche and determine whether cell-cell interactions are present, looking for regional variations around the limbal circumference.

The hypotheses of this thesis are:

1. 3D tissue reconstructions can be used to determine the distribution of LCs/LC-like structures around the porcine limbus and give further support to one of the opposing theories about LC location in porcine tissue.
2. CS will be present in association with the putative stem cell niche and the distribution of different sulphation motifs will vary between the superior/inferior and nasal/temporal quadrants of the porcine limbus (if a regional variation in the location of LCs is found), as well as varying along the width of the limbal area in a sclerolimbus to corneolimbus direction.
3. Cell-cell interactions between basal limbal epithelial cells and surrounding niche cells will be present in supposed stem cell-rich areas of the porcine limbus, with stromal MSCs potentially involved.

To address these aims and hypotheses, assessment of the ultrastructure of the porcine limbal stem cell niche will be carried out at both high and low resolution, assessing the localisation of CS and CS PGs and forming 3D reconstructions of the tissue to investigate cell-cell interactions and crypt distribution.

2 General Methods

2.1 Orienting porcine corneas

All porcine eyes used for experimentation in this thesis came from the same abattoir (W.T. Maddock, Kembery Meats, Maesteg, UK). The eyes were enucleated within a few hours after death; they were then stored and transported on ice. The pigs were not scalded after death; a procedure often included to facilitate removal of hair before the carcass is butchered, but which may interfere with planned immunolocalisation studies by destroying sensitive epitopes. Upon receipt of the eyes, they were all oriented using the same procedure.

It is known that the horizontal diameter of the porcine cornea is larger than the vertical diameter (Sanchez *et al.* 2011; Abhari *et al.* 2018) (Figure 2.1). This difference is approximately 2 mm and is noticeable to the naked eye (Figure 2.2). This is how each eye was initially oriented, then each diameter was measured with a ruler to confirm which diameter was longer and this was then taken to be the horizontal meridian. For most of the investigations in this thesis, the opposite sides of the same meridian were grouped together – nasal/temporal (N/T) for the horizontal meridian and superior/inferior (S/I) for the vertical meridian – and then the two meridians were compared to each other.

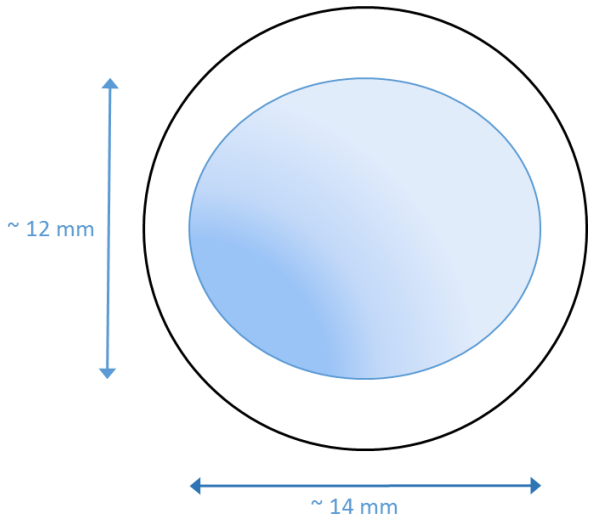

Figure 2.1- Diagram representing the dimensions of the porcine cornea.
All corneas observed during the investigations in this thesis had a noticeable difference in the horizontal and vertical diameters of the cornea. (Not to scale).

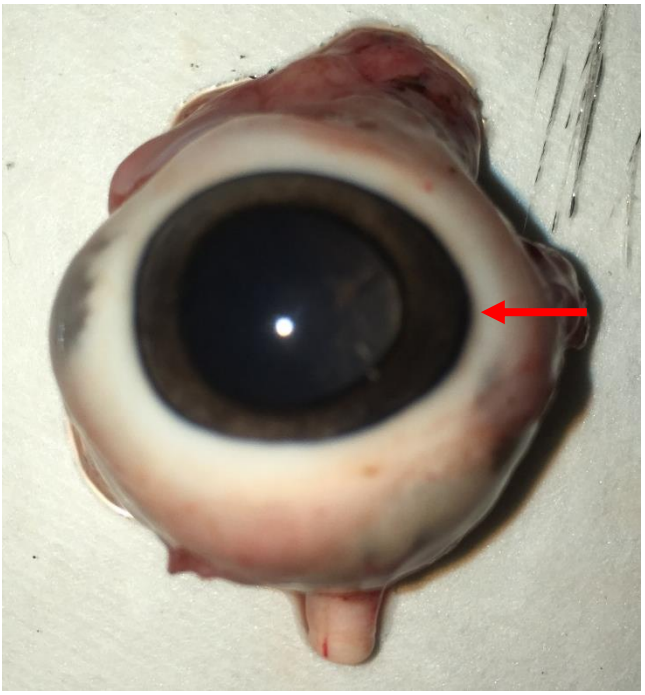

Figure 2.2- An enucleated porcine eye.
The cornea is not round, as in humans, but noticeably oval with a longer horizontal diameter than vertical. The red arrow indicates a side of the limbus (either nasal or temporal) that has much steeper curvature.

2.2 Electron microscopy

2.2.1 Resin embedding

The process for embedding samples in resin was the same for TEM and SBFSEM. After the initial processing for the respective techniques, the tissue segments were dehydrated by immersing in ethanol; first 70% then 90% (both 1 x 15 mins), followed by 100% (2 x 15 mins). After this, the tissue segments were transferred to propylene oxide (Agar Scientific Ltd, Stansted, UK) (2 x 15 mins).

The tissue was then placed into a 1:1 mixture of Araldite resin, without benzyl dimethylamine (BDMA) accelerator (Appendix 2.6), and propylene oxide for at least one hour. After this, the tissue was placed in six changes of Araldite resin without BDMA accelerator, for several hours at a time in each change of resin. The tissue samples were then placed in six changes of Araldite resin with the BDMA accelerator, again for several hours at a time. The segments were then placed into embedding moulds with new Araldite resin and were put into an oven at 60˚C for at least 24 hours to polymerise.

2.3 Immunohistochemistry

Porcine eyes were sourced and orientated in the manner mentioned in section 2.1. Corneoscleral discs were removed from whole eye globes and these discs then had four segments dissected: two S/I segments and two N/T segments (Figure 2.3).

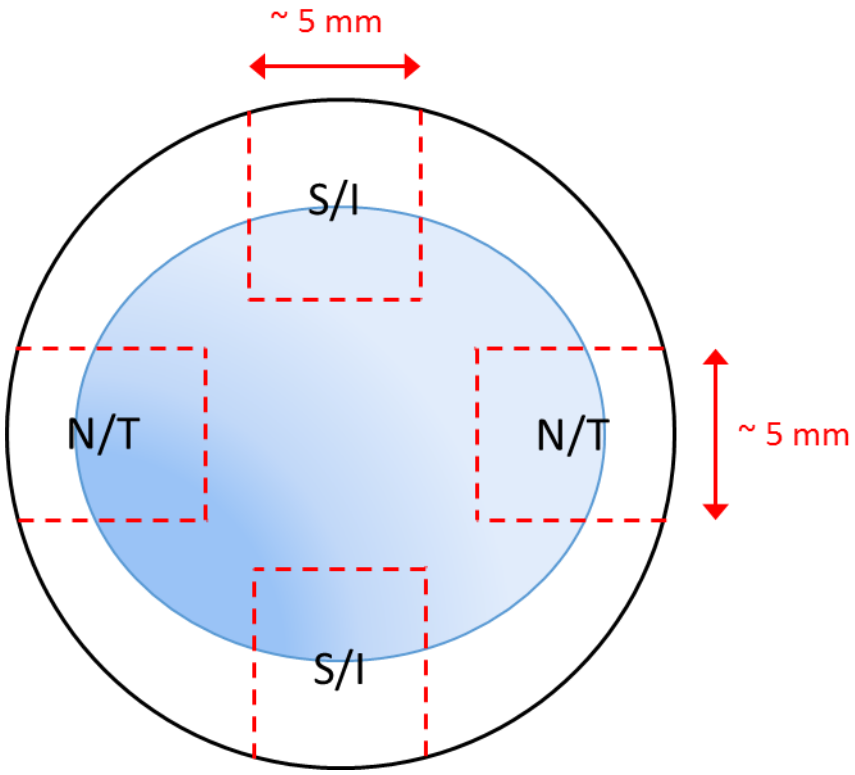

Figure 2.3- Illustration demonstrating how tissue was dissected for immunohistochemistry. *Full-thickness sections were taken and some corneal/scleral tissue was removed to leave approximately 3-4 mm of tissue either side of the limbus. Blue area = cornea, white area = sclera. (Not to scale).*

The limbal segments were washed in phosphate buffered saline (PBS) (Appendix 3.1) for 1 hour and then cryoprotected by immersing in 30% sucrose solution for approximately 15 mins. The tissue was then frozen in optimal cutting temperature (OCT) embedding compound (Fisher Scientific UK Ltd, Loughborough, UK). Frozen tissue blocks were stored at -80°C until used for immunolocalisation.The frozen blocks were mounted on cryostat chucks with OCT compound and further frozen. Sections of 15-20 µm were cut using a cryostat at -21°C, creating radial sections showing scleral, limbal and corneal tissue that were then collected on Superfrost Plus microscope slides (Fisher Scientific UK Ltd, Loughborough, UK). The sections were then rehydrated in PBS with 0.1% Tween 20 for 10 mins and non-specific staining was blocked with PBS with 0.1% Tween 20 and 1% bovine serum albumin

(BSA) for 2 hours (Appendix 3.2). The sections were incubated at 4°C overnight with primary antibodies diluted in PBS/Tween. Primary antibody details can be found in the relevant experimental chapters.

Control sections for the primary antibodies were incubated with the relevant mouse or rabbit immunoglobulins (1:1000), sourced from Vector Laboratories (Peterborough, UK) and Fisher Scientific UK Ltd (Loughborough, UK), instead of primary antibody. Negative controls for the secondary antibodies were incubated with PBS/Tween without any primary antibody.

The sections were washed with PBS/Tween again (3 x 5 mins) and then sections were incubated with the relevant secondary antibodies (details in the relevant experimental chapters) for 1 hour at room temperature. The slides were washed in PBS/Tween (3 x 5 mins) again and, finally, the sections were mounted under glass cover slips using Fluoroshield with 4',6-diamidino-2-phenylindole (DAPI) (Sigma-Aldrich Company Ltd, Gillingham, UK) for cell nucleus staining. Images were obtained using epifluorescence microscopy with an Olympus BX61 microscope and cellSens Dimension imaging software (Olympus UK & Ireland, Southend-on-Sea, UK).

3 Localising the Palisades of Vogt and limbal crypts in porcine limbal tissue using X-ray micro-computed tomography

3.1 Introduction

As mentioned in the introduction, the LESCs are believed to reside in LCs or LECs in human eyes (Dua *et al.* 2005; Shortt *et al.* 2007). These crypt structures are preferentially located in the superior and inferior quadrants of the limbus and are notably absent/damaged in people suffering from LSCD (Shortt *et al.* 2007; Lagali *et al.* 2013). However, there is disagreement as to whether the porcine limbus has these structures and, if they are present, where they are located around the limbal circumference.

Patruno *et al.* (2017) examined the dorso-temporal quadrant of the porcine limbus and stated that though there is certainly an invagination of the limbal epithelium into the underlying stroma, which contained p63α-positive cells, that this was not a "true LC". No specific reason appears to be given for this conclusion. However, this assertion that the epithelial invaginations do not represent true LCs is at odds with Notara *et al.* (2011) and Grieve *et al.* (2015), whose detailed examinations of the porcine limbal stem cell niche led them to believe that these were analogous to human LCs and supported this by demonstrating putative stem cell markers present within these areas.

These two studies did not agree on where these LCs were located around the limbal circumference, however. Notara *et al.* (2011) found that Palisade of Vogt- and LC-like structures were located in the superior and inferior sections of the porcine limbus, with non-crypt areas at the nasal and temporal sides, much like in human tissue. In contrast, Grieve *et al.* (2015) found that the crypts were distributed more evenly around the entire circumference of the porcine limbus. These are the two most in-depth assessments of the porcine limbal crypt location; thus, it is interesting that they produced contradictory findings.

In this investigation, X-ray microCT will be used to image the entire porcine corneoscleral disc, creating a 3D reconstruction of the tissue, which will then allow assessment of the distribution of LCs/Palisades of Vogt. The use of either osmium or phosphotungstic acid contrasting, which are expected to increase the X-ray attenuation of the corneal epithelium and stroma respectively, will be compared to uncontrasted tissue to determine the optimal tissue preparation method for visualising the epithelium.

Due to the contradictory data already available, it is difficult to form a hypothesis about where LCs will be located around the porcine limbus. However, the aim is to provide more supporting data for one of the opposing theories, with the hypothesis for this investigation being that 3D reconstructions can be used to determine the location and characteristics of the LCs.

3.2 Materials and Methods

3.2.1 Sample preparation

Eight porcine eyes were sourced from a local abattoir, transported on ice, and then refrigerated immediately prior to dissection. Corneoscleral discs were manually dissected, after being oriented as in section 2.2, with a notch being cut into the sclera to mark the vertical meridian, and were fixed in 4% PFA in 0.01 M PBS (Appendix 1.1) for 24 hours at 4°C. As part of the method refinement for this experiment, two corneas each were prepared in three different ways, described below. These were then examined to see which provided the best contrast for the X-ray microCT imaging. The remaining two corneoscleral rims were then prepared in the method that provided optimum contrast for use in the full scans.

3.2.1.1 Unstained corneas

After initial fixation, two corneas were stored in 0.5% PFA in 0.01 M PBS (Appendix 1.2) at 4˚C for five days. The corneoscleral rims were then dehydrated in ethanol: 2 hours in 30% ethanol, followed by 2 hours in 50% ethanol and then 2 hours in 70% ethanol. Next, the rims were transferred to 100% ethanol and stored in this at 4˚C until used for imaging.

3.2.1.2 Phosphotungstic acid-stained corneas

After initial fixation, two corneas were dehydrated in ethanol: 2 hours in 30% ethanol, followed by 2 hours in 50% ethanol and then overnight in 70% ethanol at 4˚C. The corneoscleral rims were then transferred to 0.6% phosphotungstic acid (PTA) in 70% ethanol (Appendix 1.3) for four days at room temperature on a rotator. The tissue was then washed in 70% ethanol (1 x 1 hour) and then stored in 100% ethanol at 4˚C until used for imaging.

3.2.1.3 Osmium tetroxide-stained corneas

After initial fixation, two corneas were transferred to 0.5% PFA in 0.01 M PBS and stored at 4˚C for one day. The tissue was then washed in 0.01 M PBS for 15 mins and then transferred to 1% osmium tetroxide in PBS (Appendix 1.4) for four days on a rotator in a fume hood. The corneoscleral rims were washed in PBS again for 15 mins and were then dehydrated in ethanol: 2 hours in 30% ethanol, followed by 2 hours in 50% ethanol and then 2 hours in 70% ethanol. Finally, the rims were transferred to 100% ethanol and stored in this at 4˚C until used for imaging.

3.2.2 X-ray micro-computed tomography

3.2.2.1 Pilot scans

For these scans, 5-6 mm long strips of full-thickness superior/inferior limbal tissue were dissected from one of the prepared corneas for each staining method (Figure 3.1). These limbal segments were then inserted into 1 ml pipette tips filled with 100% ethanol and sealed at both ends using Blu Tack® (Bostik Ltd, Stafford, UK) (Figure 3.2). The tissue segments were gently pushed down into the pipette tip to ensure they were securely in place and would not move as the samples were rotated.

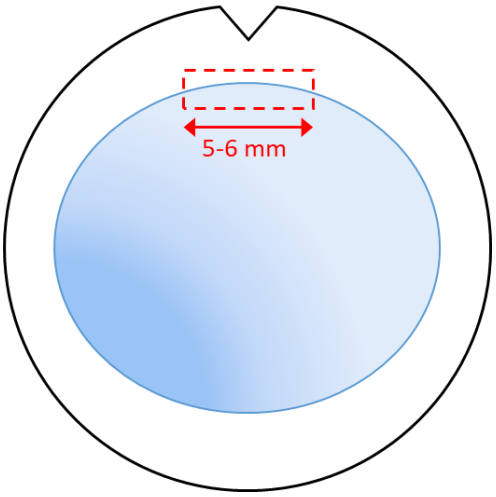

Figure 3.1- Diagram demonstrating where limbal samples were taken for pilot scans.
A notch was cut into the sclera to mark the vertical meridian and the limbal segments were therefore dissected from either the superior or inferior limbus. Not to scale.

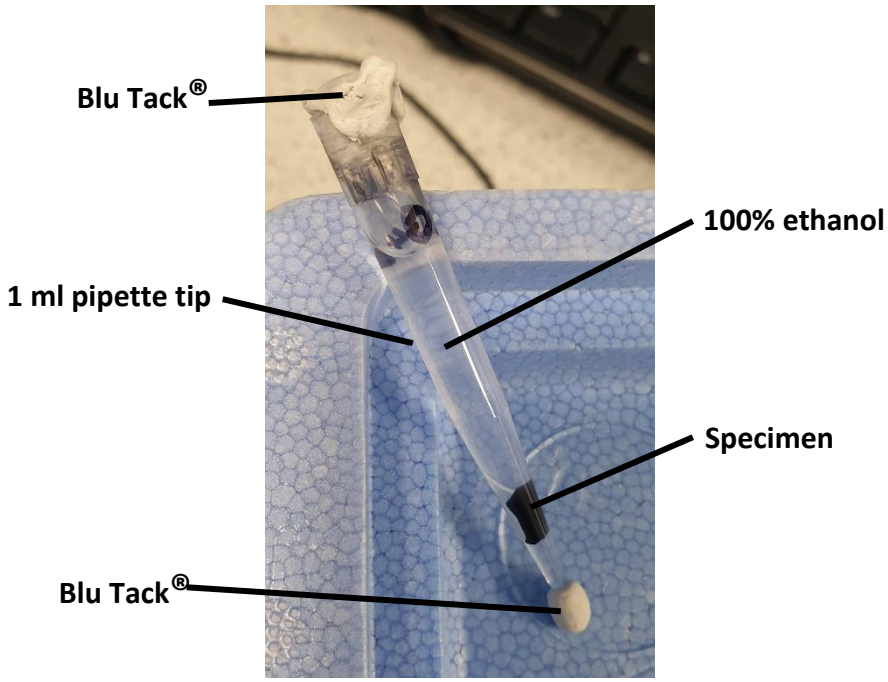

Figure 3.2- Mounting system for a segment of porcine limbus for microCT.
A plastic pipette tip was chosen as it is virtually X-ray transparent.

The pipette tip was then placed into a polystyrene tube of the appropriate diameter so that the pipette tip was held securely in a vertical position (Figure 3.3). The polystyrene tube was then mounted into a brass holder and the holder was secured into the microCT imaging chamber.

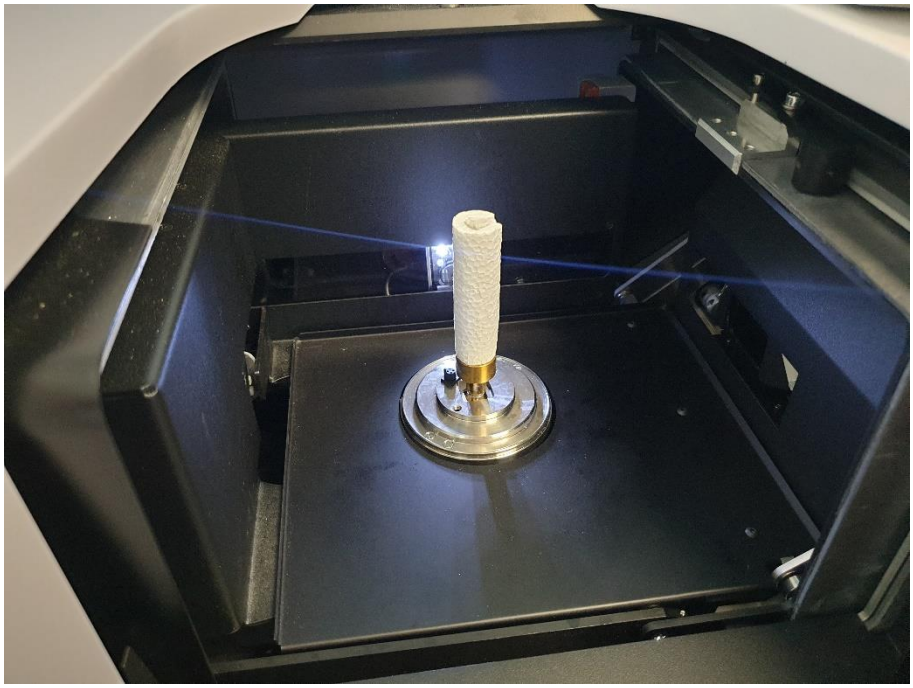

Figure 3.3- Scanning set up for a porcine limbal segment within the imaging chamber of the Bruker microCT.
The pipette tip is in the centre of the polystyrene tube, which is also virtually X-ray transparent, and allows the sample to be mounted in the brass holder whilst keeping the sample upright.

Imaging of each sample was carried out using a Bruker-SkyScan 1272 microCT scanner (Bruker microCT, Kontich, Belgium) under the following settings: source voltage 80 kV, source current 125 µA, 1 mm thick aluminium filter applied, image pixel size 19 µm, two frames averaging, samples rotated through 180° in 0.5° steps. Each scan took approximately 15 minutes. A second scan of the unstained sample was performed at the following settings, as the previous settings were not optimised for an unstained, soft tissue: source voltage 50 kV, source current 200 µA, no aluminium filter applied, image pixel size 19 µm, two frames averaging, samples rotated through 180° in 0.5° steps. Finally, a high-resolution scan of the osmium tetroxide-stained sample was performed, after it was deemed to provide the best contrast, under the following settings: source voltage 80 kV, source current 125 µA, 1 mm thick aluminium filter applied, image pixel size 11 µm, three frames averaging, samples rotated through 180° in 0.2° steps. All microCT scans were carried out by Dr David Williams at Cardiff University's School of Engineering.

The X-ray images collected for each sample were then transferred to NRecon software (Bruker microCT, Kontich, Belgium) to create a 3D reconstruction of the

sample. The 3D reconstructions were then opened in the programme CTVox (Bruker microCT, Kontich, Belgium) to assess the samples and to carry out transformations to best visualise the epithelium and the LCs.

3.2.2.2 Full corneoscleral disc scans

Visual inspection of the pilot scans revealed that osmium tetroxide provided the best contrast and, thus, the two remaining corneoscleral rims were stained as discussed in section 3.2.1.3. This resulted in three corneoscleral discs for full imaging.

The corneoscleral rims were placed into 20 ml syringes (Terumo UK Ltd., Bagshot, UK), epithelial side upwards, that were sealed with Blu Tack® at the tip and cling film at the top and were filled with 100% ethanol (Figure 3.4A). The gradations on the syringes were removed with acetone (Fisher Scientific UK Ltd, Loughborough, UK). They were again placed so that they were secure and would not move as the samples were rotated. The syringes were then placed into a brass holder that was filled with more Blu Tack® (Figure 3.4B) to hold the syringe securely in place and ensure the syringe tip was sealed and would not leak.

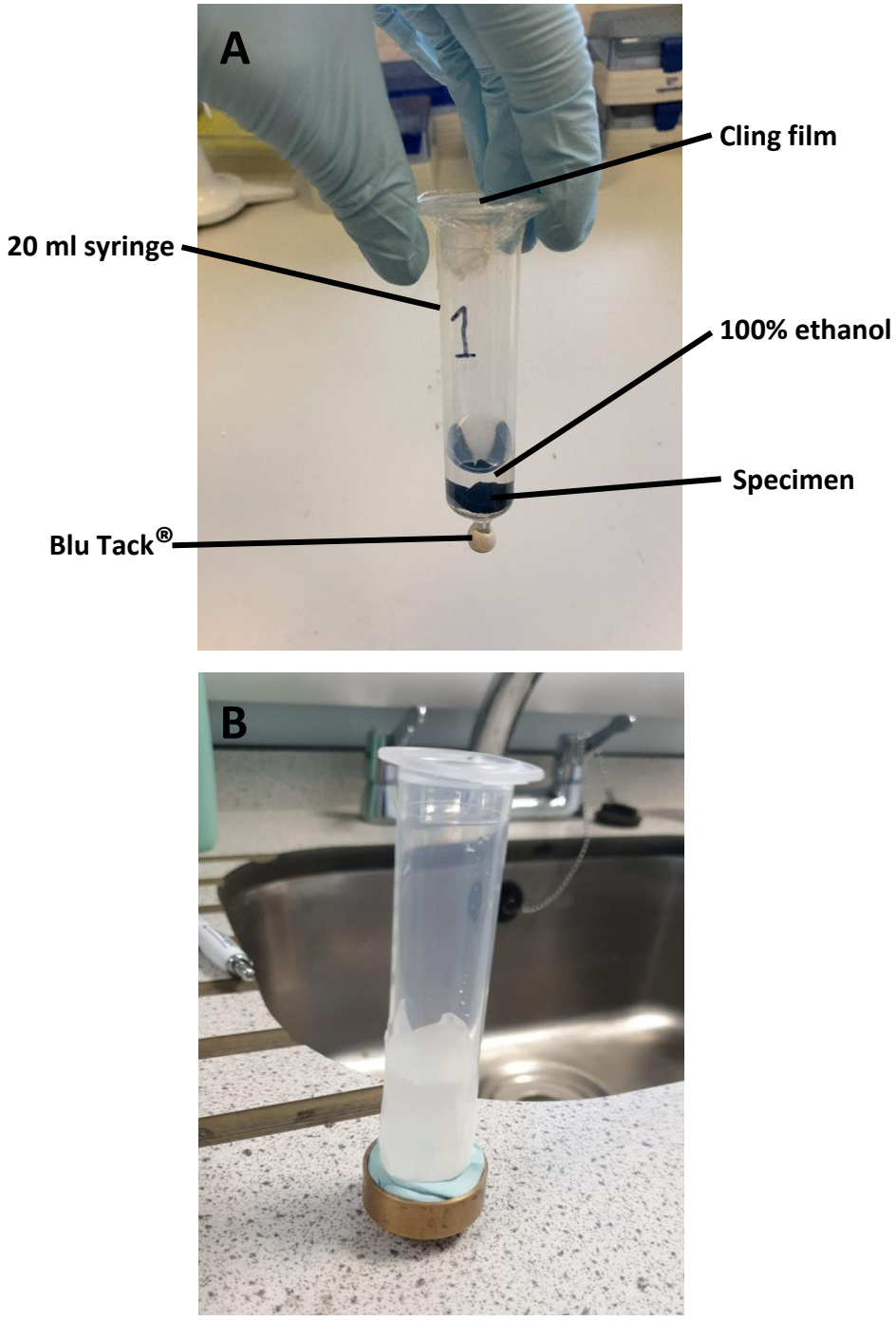

Figure 3.4- Mounting system for a porcine corneoscleral disc for microCT.
The corneoscleral disc was placed, epithelial side up, in a 20 ml syringe which was the right diameter to hold the disc firmly in place (A). To ensure the syringe could be mounted within the microCT upright, watertight, and capable of being manoeuvred fully, it was secured with more Blu Tack® within the brass holder (B).

The scans were then carried out at the following settings: source voltage 80 kV, source current 125 µA, 1 mm thick aluminium filter applied, image pixel size 9 µm, three frames averaging, samples rotated through 180° in 0.2° steps. Each scan took approximately 1.5 hours. These scans, again, were carried out by Dr David Williams. As with the pilot scans, the X-ray images were then transferred to NRecon software to create a 3D reconstruction of each cornea. CTVox was then used to assess the samples and to carry out transformations that had been determined the best to view the tissue when assessing the pilot scan data.

3.3 Results

3.3.1 Osmium tetroxide vs. PTA vs. no staining

The pilot scans revealed that osmium tetroxide staining provided the best contrast of the corneal/limbal epithelium, including being able to see a protrusion of epithelium where LCs would be expected (Figure 3.5A, B). PTA staining also contrasted the epithelium well, but this blended with contrasting of the stroma which led to the limbal epithelium being indistinguishable from the stroma (Figure 3.5C). The pilot scan of the unstained cornea, performed at the same settings as the stained samples, resulted in the limbal sample being virtually indistinguishable from the surrounding media (Figure 3.6A) and, thus, no 3D reconstruction was made for this image set. The scan of the unstained cornea under more optimised settings did result in better distinction of the sample from its surrounding media, but none of the features of the sample could be distinguished and the surrounding media were also highly visible (Figure 3.5D).

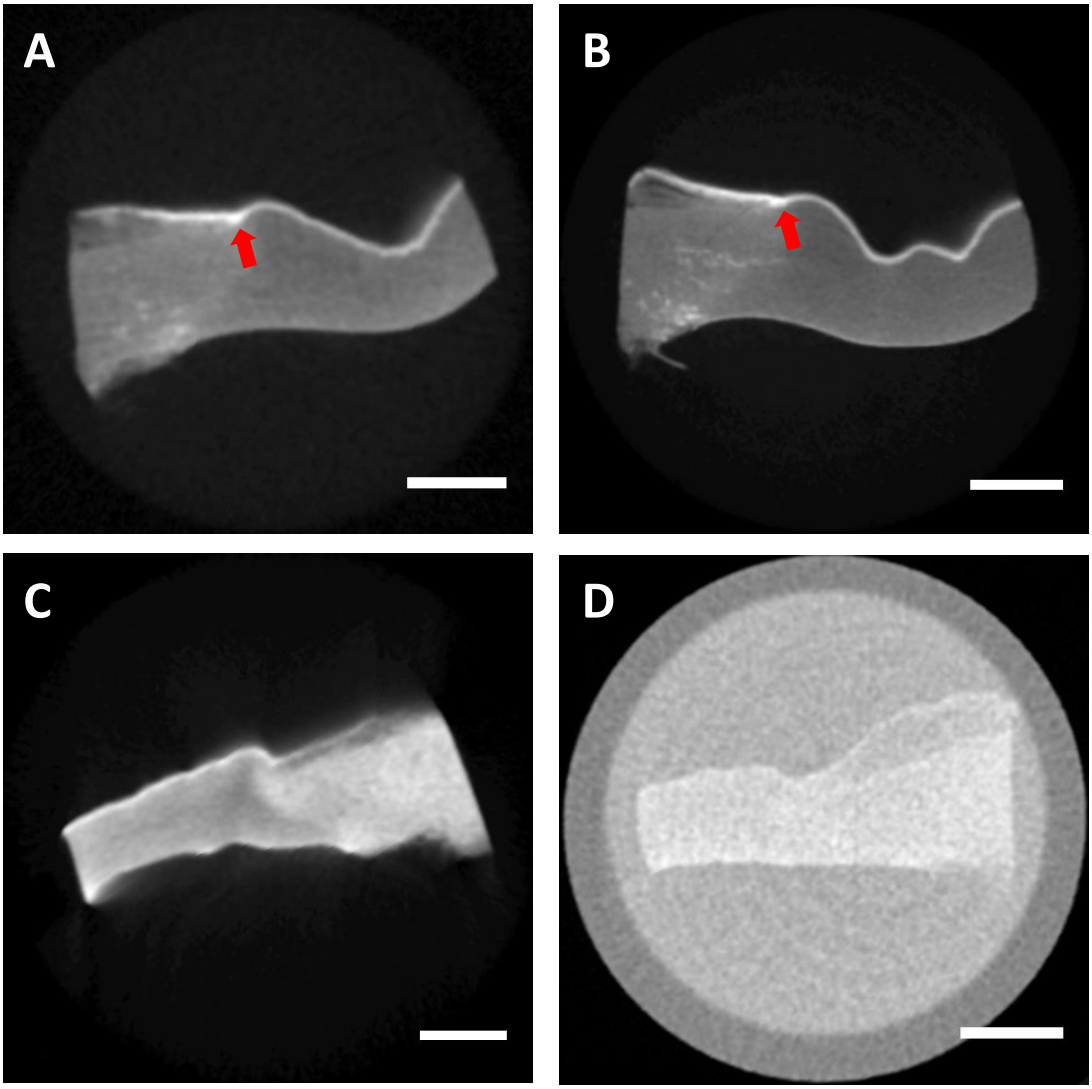

Figure 3.5- Cross-sections of limbal segments obtained via microCT under different staining conditions.

A and B are from a sample stained with osmium tetroxide, with B obtained at higher resolution. The epithelium appears as a bright, white strip and a limbal protrusion of epithelium into the underlying stroma is visible (red arrows). C shows the sample stained with phosphotungstic acid; the epithelium is also a bright, white strip but blends into the limbal and scleral stromas. The unstained cornea is barely distinguishable from the surrounding media, even under more optimised scanning conditions (D). Scale bar = 500 µm.

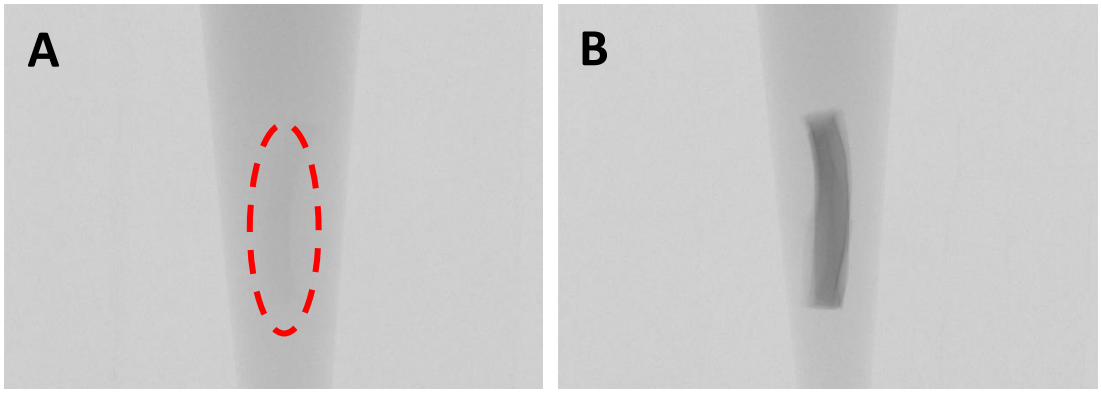

Figure 3.6- X-ray images of limbal segments with and without additional staining.
Without any staining (A), the limbal segment (within red, dashed oval) is virtually indistinguishable from the surrounding ethanol. Whereas with osmium tetroxide staining, the limbal segment can be easily seen (B).

The high-resolution scan of the osmium tetroxide-stained sample, which provided the best differentiation of the epithelium, was selected for further examination of the 3D reconstruction. Transformation functions were applied to the reconstructions, which are settings that can be customised to assign colours/levels of opacity to different greyscale values in order to enhance the features of the specimen being assessed. A pre-made transformation function designed to enhance the visualisation of soft tissues was used first and led to the epithelium being enhanced as a dark blue volume (Figure 3.7). Again, a limbal epithelium protrusion is clearly visible (Figure 3.7, red arrow). Interestingly, what can be seen in the cross-section throughout the tissue (supplementary video 1) is that this protrusion of epithelium seemed to be one continuous structure. Figure 3.8 shows a diagram to demonstrate the orientation of the tissue in supplementary video 1, in which a radial section of the limbus is shown. Though it did undulate slightly, there did not appear to be any stromal tissue, reminiscent of the Palisades of Vogt, which separated out smaller, distinct limbal crypts. The limbal epithelial protrusion did seem to disappear and merge into the rest of the limbal epithelium as the end of the tissue block is reached.

Supplementary video 1: MicroCT 3D reconstruction of a section of pig limbus stained with osmium tetroxide to demonstrate a continuous limbal crypt-like structure (dark blue) that is present along most of the limbal circumference. The view presented here is a radial cross-section, with sclera to the left and cornea to the right. As the cross-section moves through the tissue, it is doing so along the limbal circumference. https://figshare.com/s/0eddcc5935d2b78ae43a

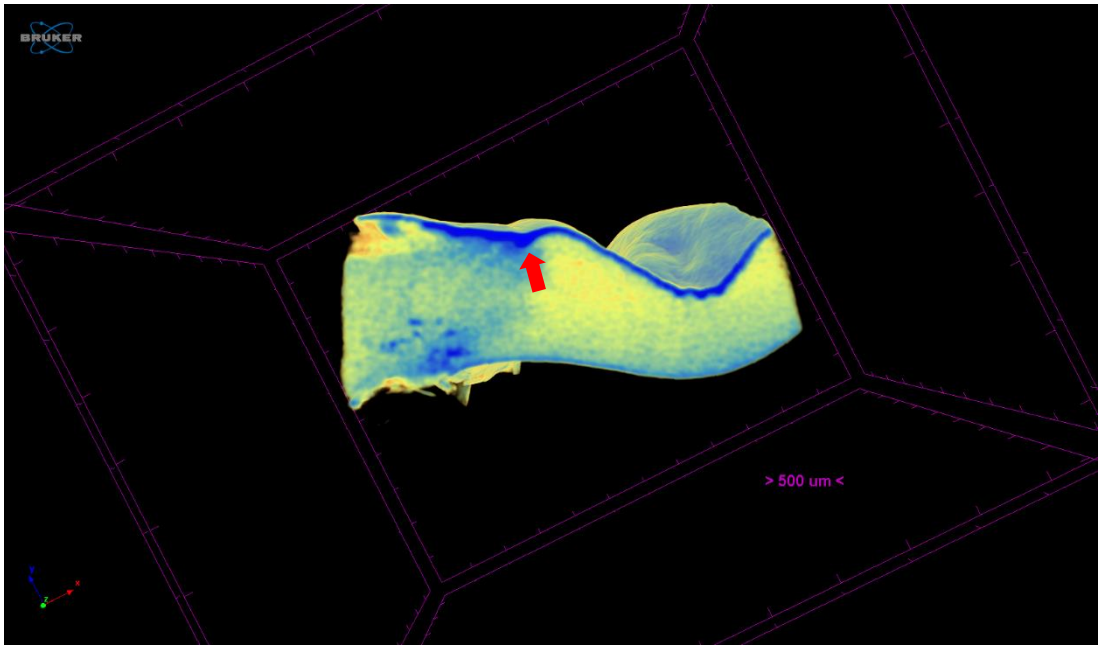

Figure 3.7- 3D reconstruction of a porcine limbal sample obtained via microCT.
A transformation function designed to enhance the visualisation of soft tissues leads to the limbal epithelium appearing as a dark blue volume, whilst the stroma appears as a lighter blue and yellow. An area of thickened limbal epithelium can be seen as an area of the dark blue volume protruding into the underlying stromal volume (red arrow).

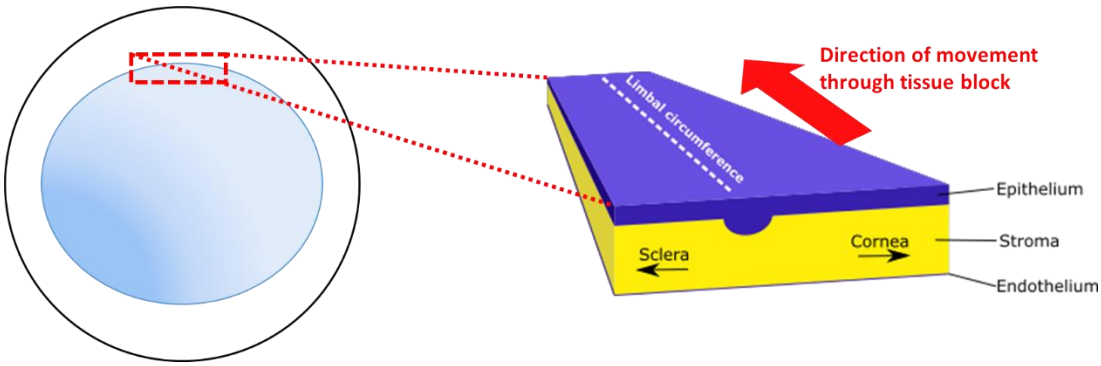

Figure 3.8- A diagram demonstrating the orientation of the tissue presented in supplementary video 1.
The video presents a cross-section of the limbus, centred on the projection of limbal epithelium. This is a radial cross-section, with the sclerolimbus to the left and the corneolimbus to the right. The movement through the tissue is along the limbal circumference.

The soft tissue transformation function was altered so that all but the deepest blue volumes appeared transparent. This produced a transformation function that isolated the epithelium (Figure 3.9A). When the tissue reconstruction was flipped upside-down, so that the basal epithelial surface was facing upwards, a continuous ridge of epithelium that correlates to the limbal protrusion seen in cross-section could clearly be seen (Figure 3.9B, between the red lines). This can also be seen in supplementary video 2. Again, there are no indentations in this crypt-like structure that would suggest the presence of Palisades of Vogt and multiple, distinct limbal crypts.

Supplementary video 2: MicroCT 3D reconstruction of the basal surface of the limbal epithelium of an osmium tetroxide-stained segment of porcine limbus, demonstrating a continuous ridge of thickened limbal epithelium that is present along most of the limbal circumference.
https://figshare.com/s/1d315d7b2ed26e1fc810

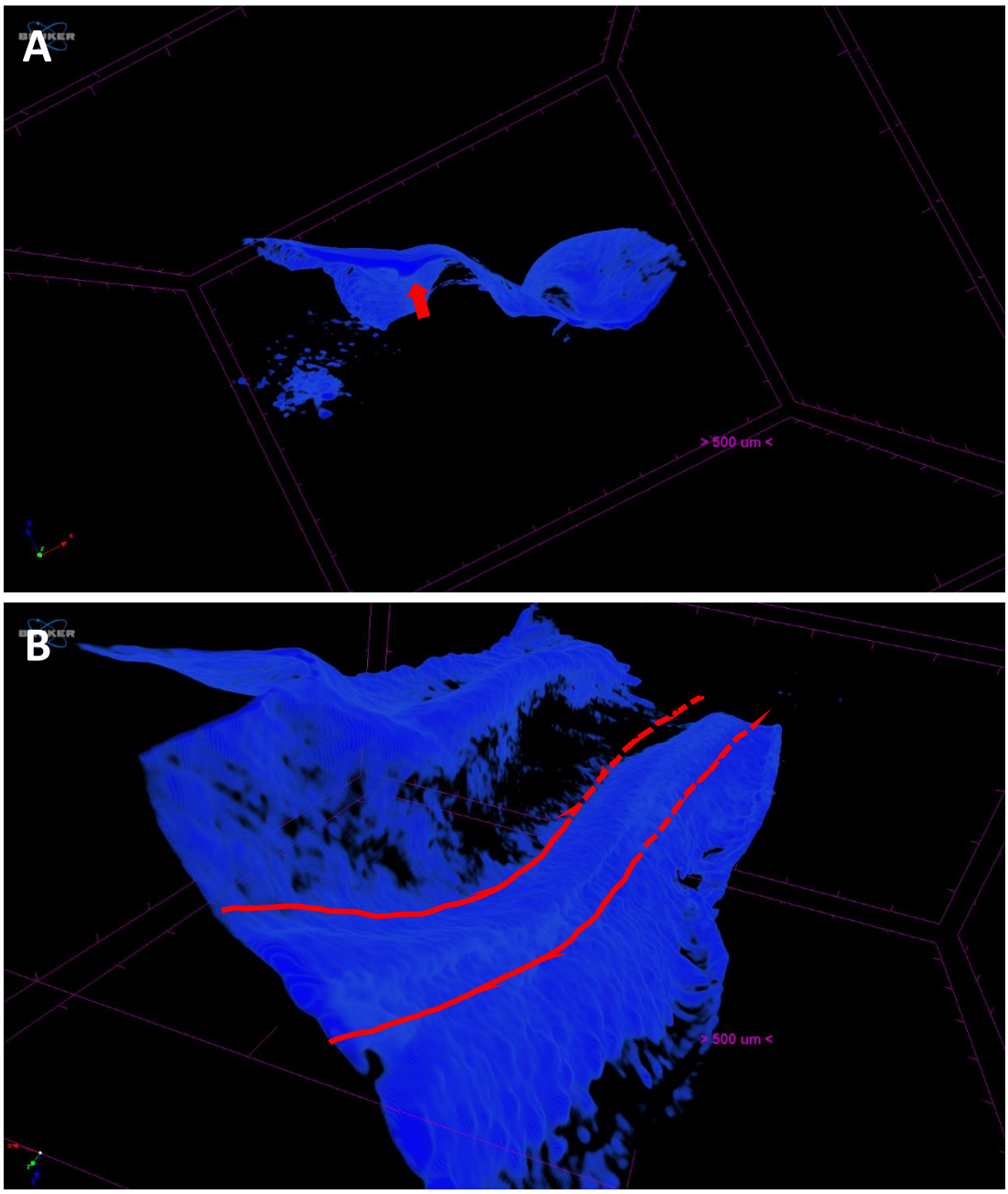

Figure 3.9- A view of the isolated epithelium of a porcine limbal 3D reconstruction obtained via microCT.

The soft tissue transformation function was adjusted to isolate the epithelium and, once again, a limbal epithelial protrusion can be seen (A, red arrow). When the reconstruction is turned upside down, it can be seen that this protrusion is one continuous structure (B, between red lines). Though there are undulations in this structure, there are no gaps within it that would suggest Palisade of Vogt-like structures. Dashed red lines indicate where the protrusion appears to diminish.

3.3.2 Limbal epithelial architecture

Reconstructions from a full corneoscleral disc stained with osmium tetroxide are presented below. It can be seen that the epithelium was contrasted very well and a structure similar to a LC could easily be distinguished in greyscale and with transformations (Figure 3.10). With the soft tissue transformation function applied, the epithelium appears as a dark blue volume again (Figure 3.10B) and a downward protrusion of the epithelium, reminiscent of a LC, could be seen in almost all areas of the limbus when viewed in cross-section (supplementary video 3). This was a continuous structure, with no Palisades of Vogt or ridges of stromal tissue visible, but with some slight variations in the prominence of the crypt. There were some areas where the invagination seemed to recede, such as at 22-27 seconds in supplementary video 3. This corresponds to the N/T area of the limbus shown in Figure 3.13B. Additionally, there were sometimes one or more smaller crypt-like structures posterior to the main, continuous crypt that would emerge (Figure 3.11, supplementary video 3). These appeared to be focal projections of epithelium and not continuous structures around the full limbal circumference.

The isolated epithelium transformation function (Figure 3.10C) allowed for visualisation of the full limbal circumference to determine the location of the protrusion of epithelial tissue. Once the tissue reconstruction was flipped upside down, with the basal epithelial surface facing upwards once more, a continuous ridge of limbal epithelial tissue could be seen around the full circumference (Figures 3.12 and 3.13). This ridge was present in both of the S/I quadrants and the N/T quadrants, with no breaks in the epithelial ridge that would suggest Palisades of Vogt seen anywhere. However, as mentioned above, the ridge did recede along a considerable length of one of the N/T quadrants (Figure 3.13B, between yellow arrows). There is also a large break in the continuous ridge in one of the S/I quadrants (Figure 3.12B), where much of the surrounding epithelium also appears to be missing. There are undulations in the profile of the ridge, as was seen in the pilot scan. It should be noted that the regular, parallel lines across the reconstructions in Figures 3.12 and 3.13 are artefacts of the reconstruction process and are not features of the tissue. Supplementary video 4 presents a flyover of the

limbal epithelium, demonstrating the singular, continuous nature of this epithelial protrusion.

Supplementary video 3: MicroCT 3D reconstruction of an osmium tetroxide-stained porcine corneoscleral disc demonstrating a radial cross-section showing a continuous limbal-crypt like structure found around almost the entire circumference of the limbus. There are also smaller, secondary crypts that emerge posterior to the main, annular crypt.
https://figshare.com/s/77047f0a9f525a6ad592

Supplementary video 4: MicroCT 3D reconstruction of an osmium tetroxide-stained porcine corneoscleral disc demonstrating the basal surface of the limbal epithelium. Here, a continuous limbal-crypt like structure can be found around almost the entire circumference of the limbus.
https://figshare.com/s/586a295227a141e49cb9

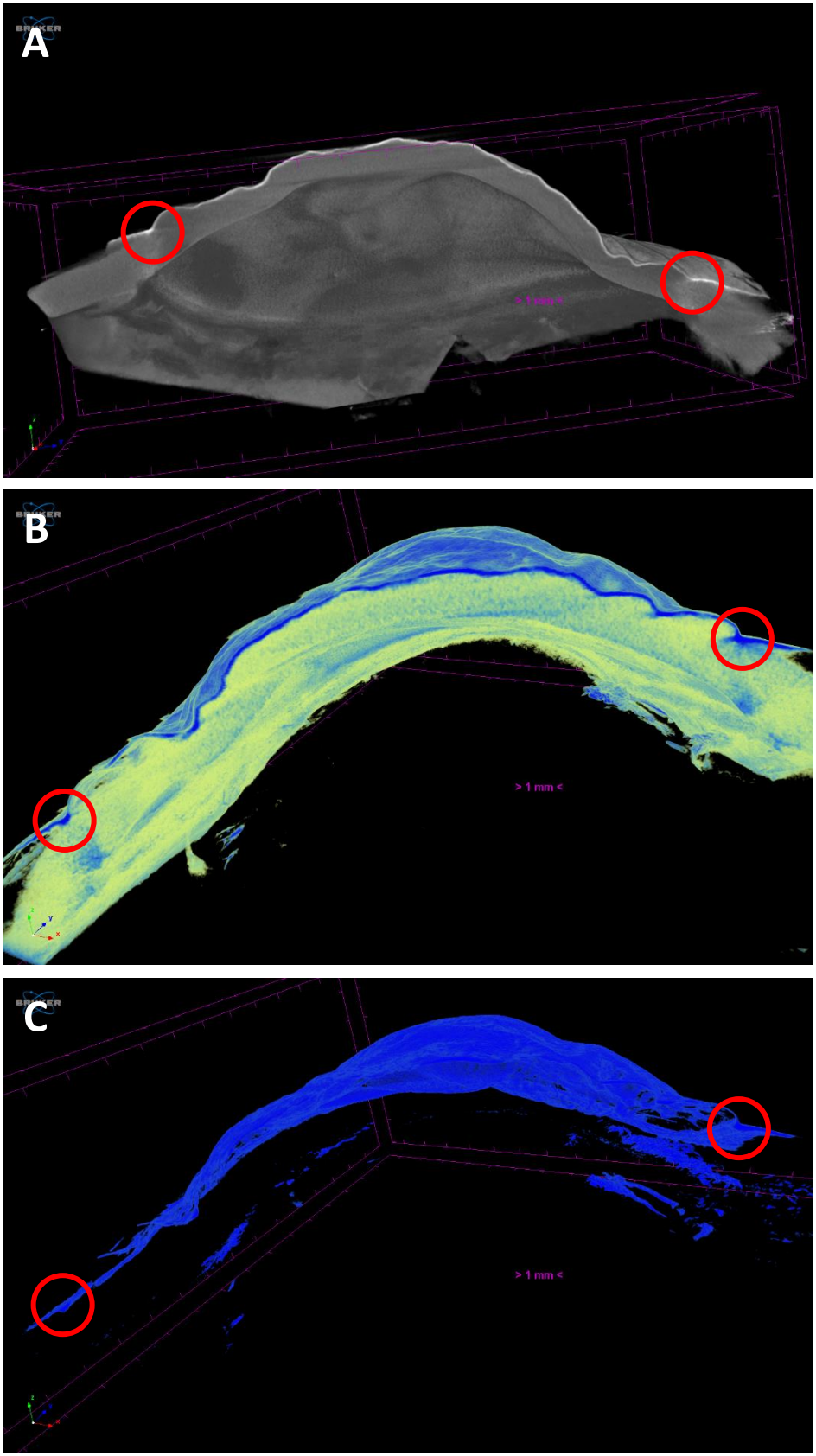

Figure 3.10- 3D reconstruction of a porcine corneoscleral disc obtained via microCT under different transformation functions.
Under greyscale conditions (A), the corneal and limbal epithelia appear as a bright, white strip again. With the soft tissue transformation (B), the epithelium can be seen with much greater contrast and it was also possible to isolate the epithelium again (C). Red circles indicate the structure reminiscent of a limbal crypt in opposite quadrants.

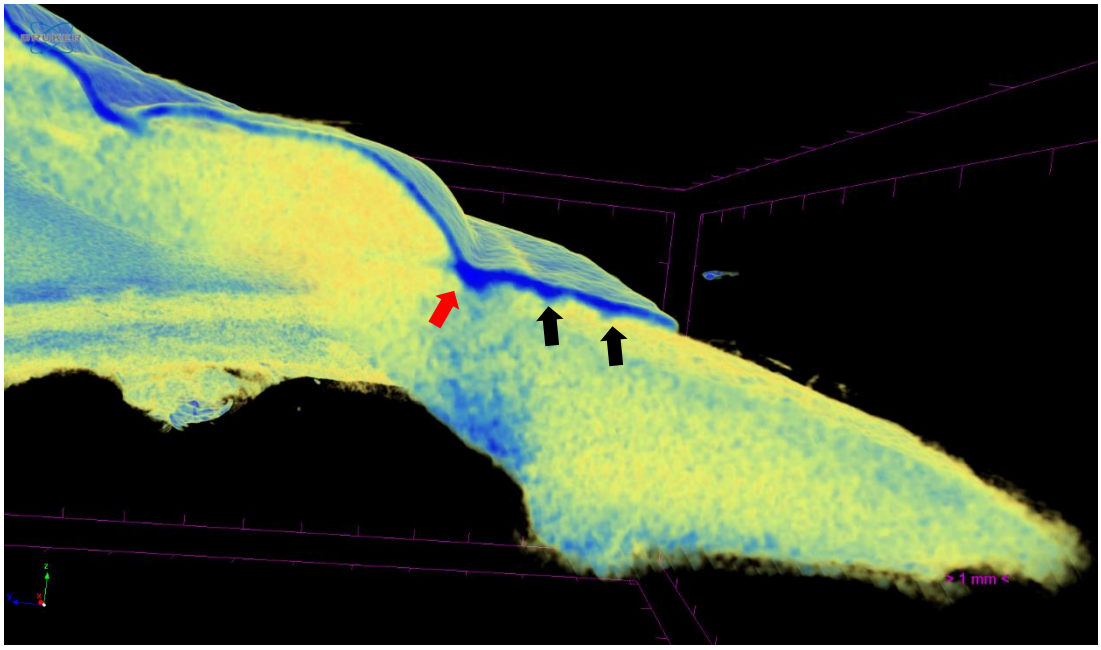

Figure 3.11-The presence of smaller, secondary crypts within the limbal epithelium posterior to the main, larger crypt.

Posterior to the main, continuous crypt (red arrow) smaller crypts would sometimes emerge (black arrows). These secondary crypts were not continuous and would quickly recede, being only a few microns in width.

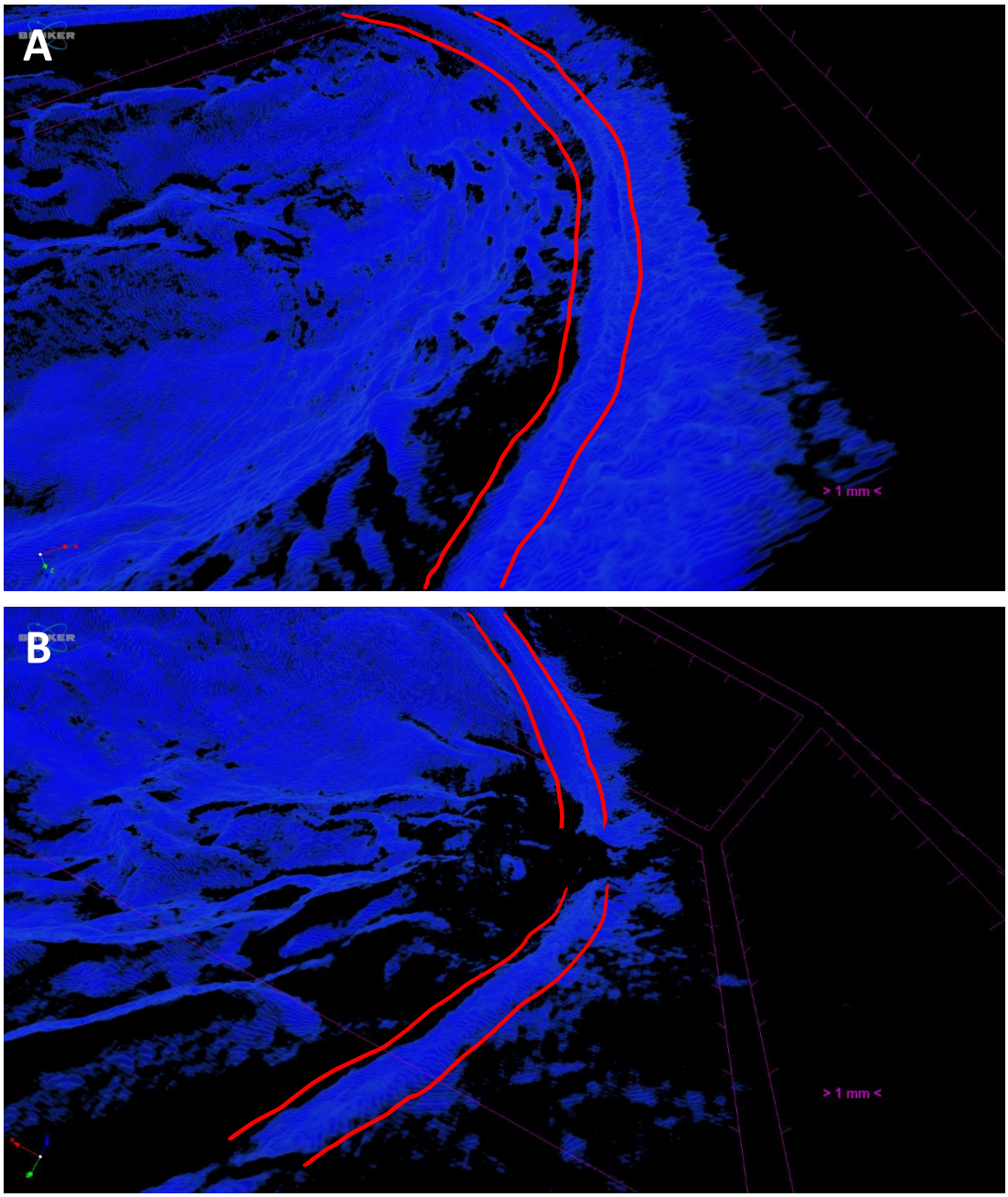

Figure 3.12- Views of the basal surface of the isolated epithelium of superior and inferior quadrants.

A continuous ridge of epithelium can be seen in both the superior and inferior limbus (between red lines). There are no distinct breaks in the ridges that would suggest the presence of Palisades of Vogt. The large gap in the epithelium in B is potentially due to damage during processing. As mentioned in section 2.2, a distinction cannot be made as to which quadrant is the superior or inferior.

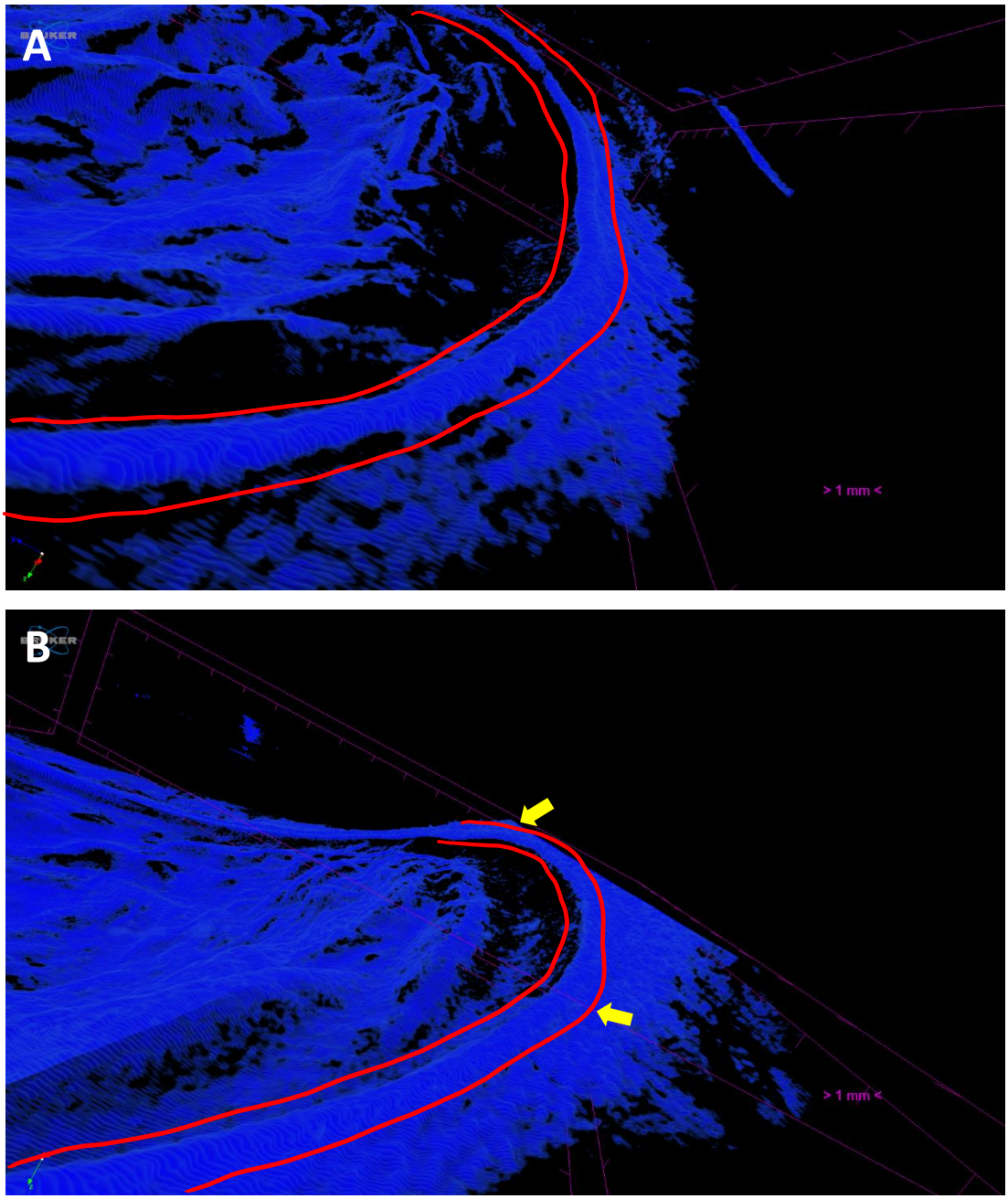

Figure 3.13- Views of the basal surface of the isolated epithelium of nasal and temporal quadrants. *A continuous ridge of epithelium can also be seen in both the nasal and temporal limbus (between red lines). The appearance is similar to the superior and inferior limbus, with no suggestion of Palisades of Vogt. However, in the horizontal quadrant shown in B, the crypt structure is less prominent and potentially has completely regressed between the yellow arrows. As mentioned in section 2.2, a distinction cannot be made as to which quadrant is the nasal or temporal.*

After pilot scans revealed the superiority of osmium tetroxide staining for visualising the epithelium, two more corneas were stained to examine alongside the previously stained cornea discussed above. However, these samples proved to be suboptimal. The differences between the three corneoscleral discs can be seen in Figure 3.14.

The second cornea (Figure 3.14B, E) appeared to have lost much of its epithelium, as identified by the absence of blue across the corneal surface when compared to the first and third corneas (Figure 3.14A, D and C, F respectively). The third cornea also demonstrates a partial loss of epithelium. Both the second (Figure 3.14E) and third corneas (Figure 3.14F) had much stronger attenuation of the X-rays within the sclera, as indicated by the dark blue appearance of the sclera. These circumstances led to it being much more difficult to visualise the basal surface of the epithelium with the isolated epithelium transformation function (Figures 3.15 and 3.16), due to a lack of visible epithelium or being unable to separate the scleral volume from the epithelium. However, it did appear that a limbal crypt-like structure could be discerned around various quadrants of the limbus in these two samples (supplementary videos 5 and 6). When this structure could be seen, it once again appeared to be a continuous structure, without interspersed Palisades.

Much of the limbal epithelium posterior to the LC-like structure has been lost in these two samples. However, at certain points in supplementary videos 5 and 6, smaller focal crypts can be seen posterior to the main continuous crypt, as was seen in the first sample. Again, these do not appear to be particularly large and are not continuous around the full limbal circumference.

Supplementary video 5: MicroCT 3D reconstruction of an osmium tetroxide-stained porcine corneoscleral disc demonstrating a radial section showing a potential continuous limbal-crypt like structure. This is much less prominent than in supplementary video 3 due to a partial loss of epithelial tissue and the much stronger attenuation of X-rays seen in the subjacent stroma, as demonstrated by the darker shade of blue here. https://figshare.com/s/0171f33846898aa2f409

Supplementary video 6: MicroCT 3D reconstruction of an osmium tetroxide-stained porcine corneoscleral disc demonstrating a radial section showing a potential continuous limbal-crypt like structure. As with the cornea shown in supplementary video 5, this is much less prominent due to the same reasons discussed above. https://figshare.com/s/67de498fbef059472330

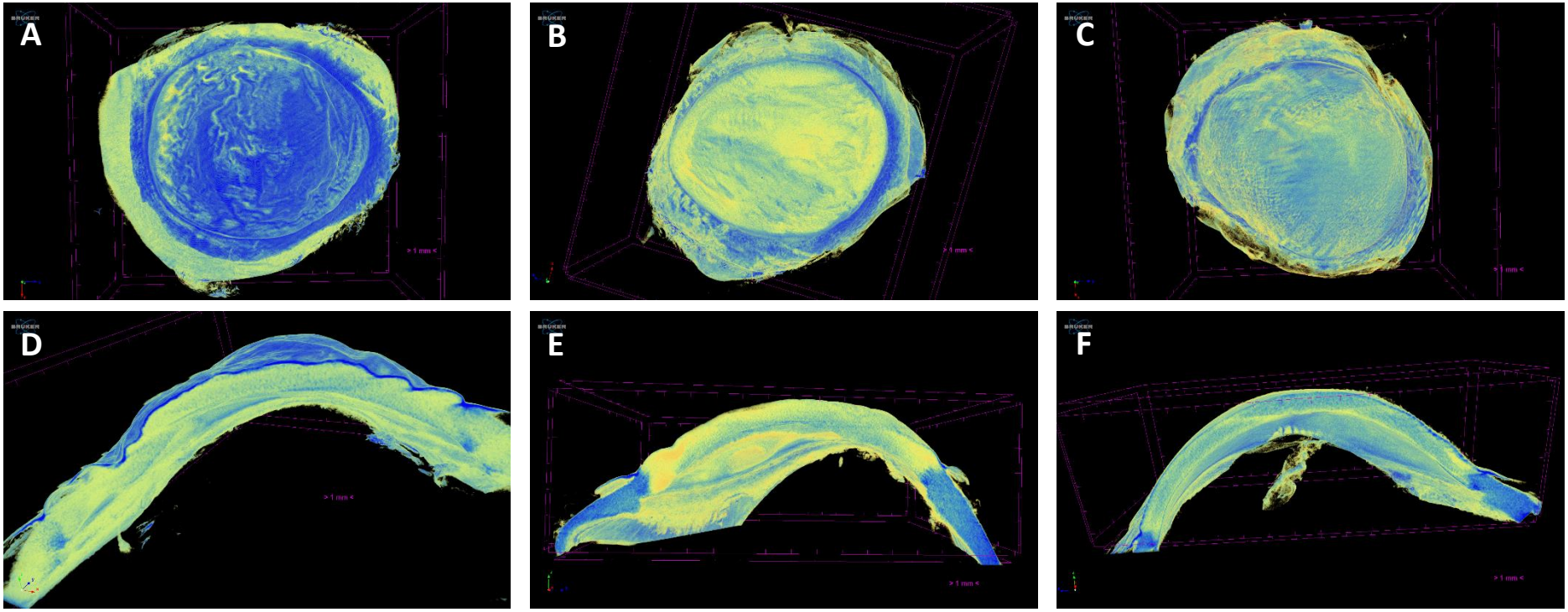

Figure 3.14- A comparative view of three porcine corneoscleral discs imaged via microCT.
En face views of the three utilised corneas (A, B, C) show the lack of epithelium in the second cornea (B) and a moderate amount of loss in the third cornea (C), as demonstrated by a lack of dark blue coloration. This lack of epithelium can also be seen in a cross-section of the second cornea (E). Cross-sections also reveal the much stronger X-ray attenuation generated in the scleras of the second (E) and third (F) specimens, when compared to the first (D).

The continuous limbal epithelial protrusion can also be seen to some extent in Figures 3.15 and 3.16. For the second cornea, this continuous protrusion of epithelium can be distinguished most successfully in one of the N/T quadrants (Figure 3.15C). There is a thin strip of limbal epithelium visible around almost the entire limbal circumference, but this does not necessarily mean this all correlates to a continuous limbal crypt. Similarly, for the third cornea, a continuous strip of limbal epithelium can be seen around the full circumference (Figure 3.16). There was some residual scleral volume in most quadrants. However, there did seem to be a continuous epithelial protrusion in all quadrants, except for one S/I quadrant where most of the epithelium had been lost (Figure 3.16D), once as much of the scleral volume as possible was removed. Supplementary videos 7 and 8 present flyovers of the basal epithelial surface for the second and third corneas respectively.

Supplementary video 7: MicroCT 3D reconstruction of the basal epithelial surface of an osmium tetroxide-stained porcine corneoscleral disc. The presence of a continuous limbal-crypt like structure is much more difficult to discern here than in supplementary video 4 due to loss of much of the limbal epithelial tissue. However, a ridge of thickened epithelium along the limbal circumference can be seen in multiple areas. *https://figshare.com/s/c63c4de55f73a0f86516*

Supplementary video 8: MicroCT 3D reconstruction of the basal epithelial surface of an osmium tetroxide-stained porcine corneoscleral disc. As in supplementary video 7, a continuous limbal-crypt like structure is present in multiple areas, but is often difficult to discern. This is again due to loss of much of the limbal epithelial tissue and also due to remaining scleral volume that sometimes obscures the view of the limbal epithelium. *https://figshare.com/s/e18e3d9194084c18d681*

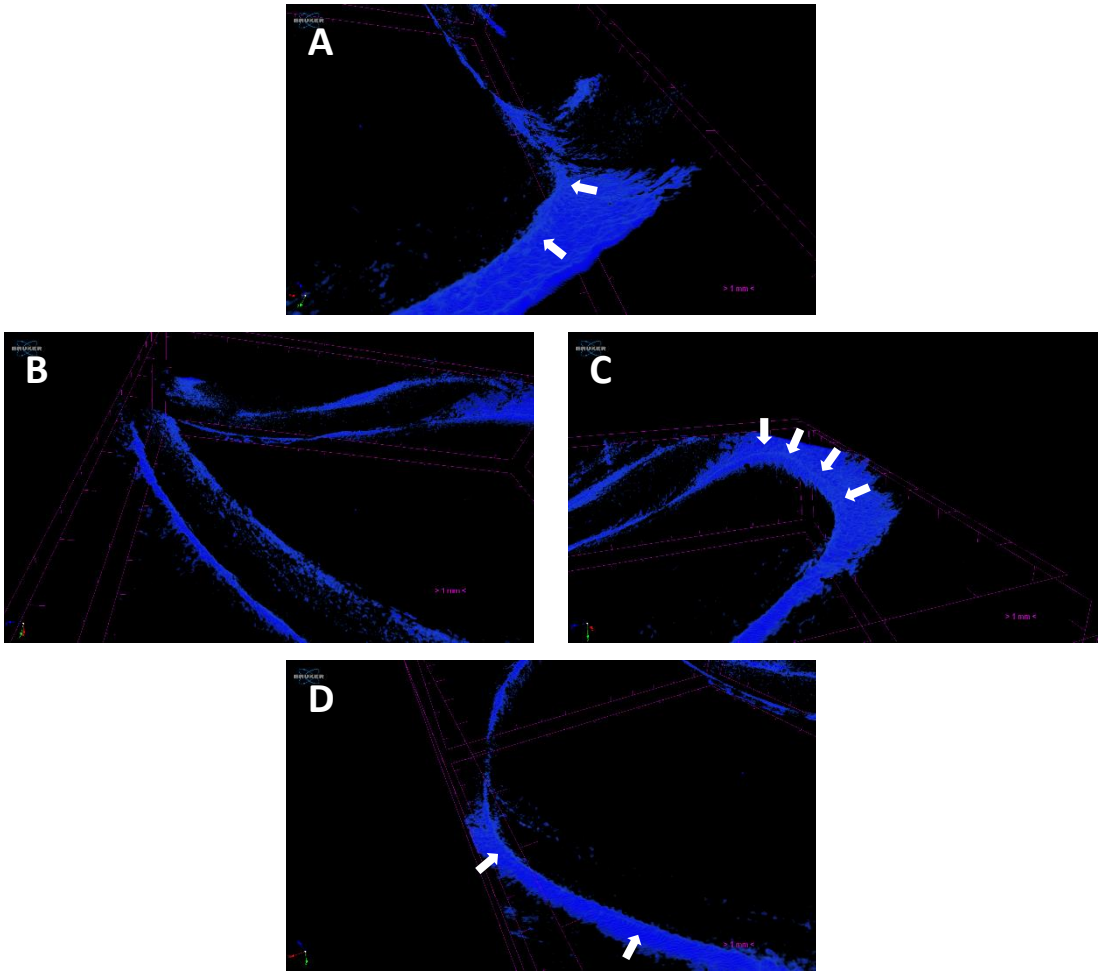

Figure 3.15- The isolated limbal epithelium of the second examined cornea.
A continuous limbal epithelial protrusion (white arrows) can potentially be seen in the superior/inferior quadrants (A and D) and also in one of the nasal/temporal quadrants (B). The protrusion can be seen most clearly in the nasal/temporal quadrant shown in C.

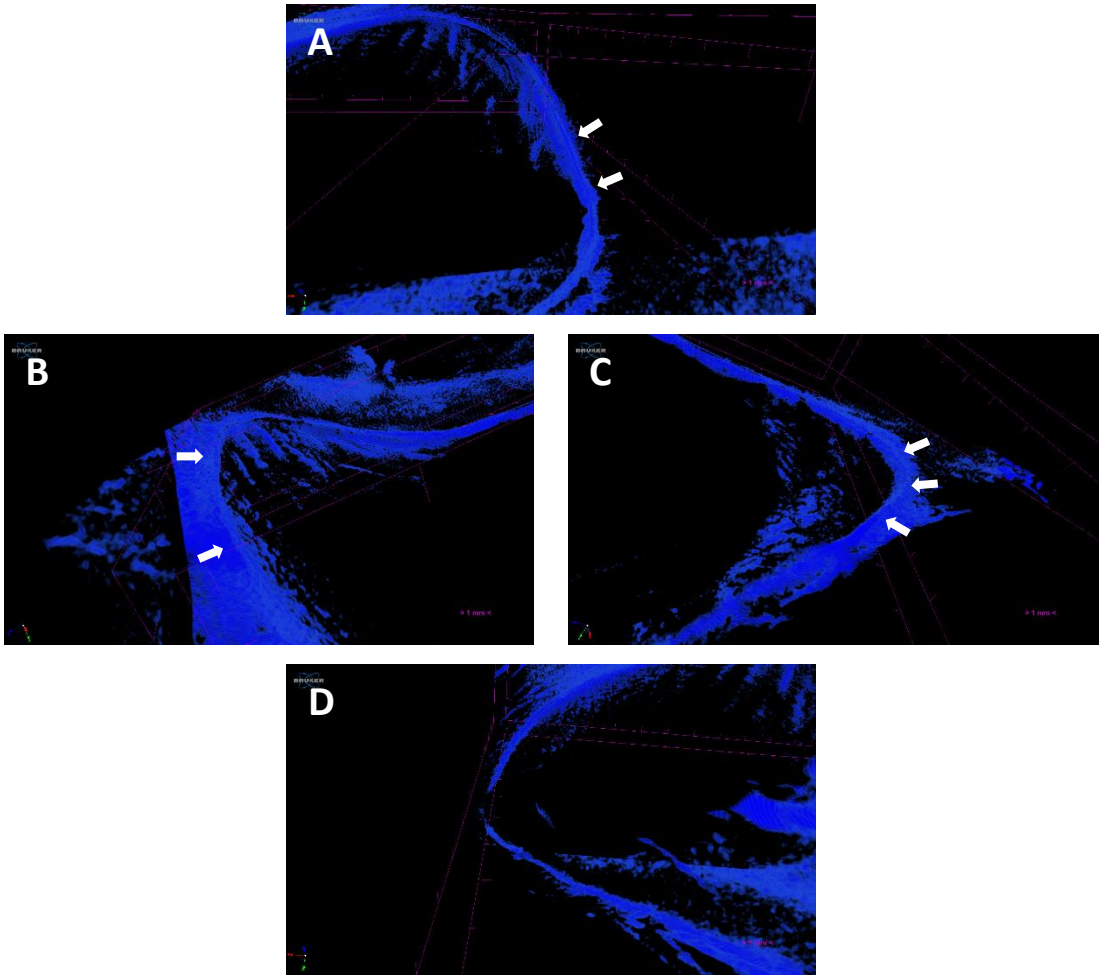

Figure 3.16- The isolated limbal epithelium of the third examined cornea.
A section of a continuous limbal epithelial protrusion (white arrows) can be seen best in most quadrants (A, B, C), though some residual sclera volume sometimes obscures the view of this. Much of the epithelium is lost in one superior/inferior quadrant (D).

3.4 Discussion

3.4.1 MicroCT of ocular tissues

This investigation has revealed that microCT can be used on ocular tissue to visualise the corneal epithelium and to assess the limbal architecture. The method refinement and pilot scans in this investigation revealed that osmium tetroxide contrasting is by far the best method of preparation to allow visualisation of the corneal epithelium. This result was expected based on previous findings by Leszczyński *et al.* (2018) when investigating microCT imaging of whole porcine eye globes. They found that contrasting with 1% osmium tetroxide or 100% Lugol's solution was the best for contrasting ocular tissues with osmium tetroxide, in particular, contrasting the epithelium most effectively.

The reason that osmium tetroxide provides the best contrast of the epithelium is most likely due to its characteristic of binding to lipids and staining cell membranes (Seligman *et al.* 1966; Riemersma 1968). As the epithelium is an entirely cellular stratum, it would have bound large amounts of the reagent and, therefore, generated the greatest attenuation of the X-rays. Though the stroma does also have a cellular component, keratocytes are widespread throughout this layer and do not comprise the bulk of its composition. This then generates a large contrast differential between these two corneal layers. In contrast, PTA acts as a positive stain of proteins (Silverman and Glick 1969), in particular of collagen (Watson 1958). The hypothesis was that this would lead to high X-ray attenuation within the corneal stroma during the current investigation, creating a high contrast with the lesser-stained epithelium. However, this was not the outcome as the epithelium also took up much of the PTA staining.

Osmium tetroxide contrasting has also been used to improve the contrast of human ocular tissue during microCT investigation (Hann *et al.* 2011). Leszczyński *et al.* (2018) also used PTA and iodine as contrasting agents and note that all contrasting methods improved the visibility of ocular tissues above unstained tissue. Another microCT investigation on porcine tissue demonstrated how iodine staining can improve contrast (Enders *et al.* 2017); however, they did not examine the cornea.

The current investigation has clearly demonstrated that unstained corneas cannot be used to examine the epithelium via microCT.

High-resolution examinations of ocular tissue have also been done via microCT without staining in combination with phase contrast imaging (Coudrillier *et al.* 2016; Ivanishko *et al.* 2017; Liu *et al.* 2018; Mittone *et al.* 2018). Fine details of ocular structures were revealed – including the lamina cribrosa, retina, and ciliary body – despite the lack of staining. The species examined included rats, rabbits, pigs and monkeys, and it has been suggested that this technique could potentially be used for *in vivo* experiments in future (Ivanishko *et al.* 2017). However, the scans did involve thousands of images at very high resolution, took up to several hours and required synchrotron facilities to achieve the necessary X-ray beam coherency. Thus, it appears that contrasting agents are still necessary for detailed visualisation of soft tissues with more widely available microCT equipment.

3.4.2 Limbal epithelial architecture

As aforementioned, two comprehensive studies produced contradictory findings about the location of LCs in the porcine cornea and the current investigation has revealed greatly differing results to both of these studies. The findings presented here revealed that a LC-like structure can be found in all quadrants of the porcine limbus, similar to the assertion by Grieve *et al.* (2015), rather than preferentially in the superior and inferior quadrants as stated by Notara *et al.* (2011). However, the current investigation's results certainly are not in agreement with Grieve and associates, as the reported morphology of these limbal epithelial structures differs considerably.

Both Grieve and Notara state that the porcine limbus includes multiple, distinct LCs separated by stromal processes similar to Palisades of Vogt, as seen in human tissue. No similar features were found during microCT investigation. A protrusion of epithelium similar to a LC was seen in almost all areas of the porcine limbus, which was continuous, and no breaks were seen in this that would suggest the presence of Palisades. Sometimes the LC would regress, with the epithelium becoming the same thickness at the limbus as in the peripheral cornea, but these areas without an apparent LC were too large to be analogous to Palisades of Vogt. The previous

investigations both used high-resolution microscopy techniques that led to the investigators stating they had observed Palisades of Vogt. The possibility must be considered that the resolution used in the current investigation was too low to discern these stromal ridges. However, if pigs have a similar average palisade width as humans of approximately 40 µm (Goldberg and Bron 1982; Townsend 1991), the resolution should have been sufficient to detect these structures if present. Neither of the studies on porcine tissue provided measurements of the dimensions of the stromal palisades.

Another possible reason why previous investigators have identified what they believe are LCs/Palisades of Vogt could be due to the plane of imaging. As mentioned in the results, there are slight undulations in the profile of the base of the limbal trough. If the imaging plane used in previous investigations was at the level of the base of the trough, then this could give rise to the appearance of repeated ridges of stromal tissue that separate protrusions of limbal epithelium. Without volume imaging or additional imaging at more superficial planes, these small undulations could easily be mistaken for Palisades of Vogt.

As shown here, there are smaller protrusions of limbal epithelium posterior to the main, large, continuous crypt. These are present in both meridians, concurring with an investigation by Seyed-Safi and Daniels (2020), where these ancillary crypts were clearly demonstrated in all four limbal quadrants. Additional posterior crypts may be more similar to LCs observed in the human eye. They do not appear to be continuous structures, rather they are distinct invaginations of limbal epithelium that are several microns wide. However, they do not appear as regularly as human LCs, with large gaps between these secondary crypts in the porcine limbus that, again, are not analogous to the Palisades of Vogt.

Interestingly, whilst Grieve and associates stated both humans and pigs possess LCs, they also found that mice have a continual depression of the limbal epithelium similar to that observed in the porcine cornea with microCT. They referred to this type of structure as a “limbal trough”. Thus, the results of the current investigation lead to the proposal that the porcine limbus also possesses a limbal trough. The porcine limbus does not have Palisades of Vogt or a series of regularly repeating,

narrow protrusions of epithelium into the underlying stroma, but a continuous protrusion that spans almost the entire limbal circumference similar to the limbal trough described in the mouse cornea. The data presented here have shown that this limbal trough does regress at points, thus it cannot be said that the trough is a full ring. It may also be possible that the trough regresses in more than one area and, therefore, that a porcine eye may contain more than one limbal trough.

Further investigations in this thesis will examine whether the porcine limbal trough functions in a similar way to the human LCs, in that it is the site of LESCs. The fact that there are not smaller, protective structures like LCs does not preclude the limbal trough from hosting a population of putative LESCs. Grieve *et al.* (2015) demonstrated the presence of p63α-positive cells within the limbal trough of the mouse, and rabbit eyes do not have LCs (Gipson 1989) but the limbal epithelium is still believed to play host to a LESC population (Kinoshita *et al.* 1981; Huang and Tseng 1991; Li *et al.* 2017).

3.4.3 Limitations

The major limitation of this investigation is the quality of the scans from the second and third corneas. Though the presence of a limbal trough-like structure can potentially be discerned in these scans, it is certainly not as distinct as in the first scan. Thus, the full nature of the porcine limbal trough cannot be accurately determined and how the trough may vary between individuals is also not known.

The reason these scans were not of as good quality as the first scan is believed to be due to the amount of time these samples were in storage before being stained with osmium and imaged. Due to restrictions imposed during the Covid-19 pandemic, these corneas were stored in 0.5% PFA for several months before they were stained. The first cornea was immersed in 0.5% PFA for only one day before being stained. This may have led to more degradation of the epithelium under conditions of long-term storage in dilute monoaldehyde fixative; however, the reasons for greater uptake of osmium by the sclera in these specimens is not known.

Two human corneas, sourced from NHS Blood and Transplant Eye Banks, were also processed for microCT imaging. These specimens were contrasted with osmium tetroxide using the same method as the porcine eyes. They were transplant-expired eyes, meaning they had been stored in organ culture medium for more than 28 days. Once scanned, it was found that the epithelium was almost completely absent for both specimens and no LCs could then be discerned. This loss of epithelium was expected due to the length of time in storage, but also demonstrated the difficulty in preserving the corneal epithelium and how it is necessary for viewing the limbal epithelial architecture with microCT after osmium contrasting.

The disadvantage of using already enucleated porcine eyes, with no extraocular muscles attached, is that a distinction cannot be made between superior and inferior or between nasal and temporal. Anecdotal advice from members of the research group suggested that the nasal and temporal sides of the porcine cornea could be distinguished based on the shape of the cornea. The porcine cornea is not a symmetrical ellipse, but rather oval or "egg-shaped" (as shown in Figure 2.2). The advice from research group members was that the more steeply curved end (Figure 2.2, red arrow) was the temporal side of the cornea. However, an investigation by Faber *et al.* (2008) on live pigs' eyes includes a diagram of the porcine cornea that suggests this steeply curved end is the nasal side. Due to this contradiction, it was decided not to distinguish between the opposite sides of each meridian and to group the two sides together as superior/inferior (S/I) and nasal/temporal (N/T) and to look for differences between the two meridians, as mentioned in section 2.1, in all of the investigations in this thesis due to the known differences in the human cornea (Goldberg and Bron 1982; Shortt *et al.* 2007).

This experiment was also subject to time constraints. More detailed, high-resolution scans are possible with microCT; however, these increase the length of time taken to complete the scans. The scan times were optimised in this investigation to provide sufficient resolution, whilst also taking an appropriate length of time. Even greater resolution can be achieved, but scan times would increase significantly, which was not possible in the current investigation. Increasing the resolution of the scans may reveal whether the porcine limbus does

possess Palisades, which are significantly narrower than the human counterpart, that were not detectable at the current resolution.

3.4.4 Conclusions

This investigation has shown microCT can be used as an effective tool for visualising the corneal epithelium when paired with the staining agent osmium tetroxide. This has allowed for the visualisation of the architecture of the porcine limbal epithelium, revealing that the porcine cornea may not have Palisades of Vogt or LCs, but a continuous limbal trough that is present in all quadrants. Throughout the rest of this thesis, this structure will be referred to as the limbal trough wherever a protrusion of the limbal epithelium is seen in the porcine cornea. Other studies have revealed labelling of putative stem cell markers within this protrusion of epithelium, suggesting it may still be the site of the porcine LESCs. This will be examined further during this thesis.

Future work that could come from this investigation include higher resolution scans of the porcine cornea and to assess the limbal architecture of the human cornea. It will be interesting to see how the LCs appear in a tissue where they are known to be present and compare this to the porcine results.

4 Visualising proteoglycans in the porcine corneal limbus using cupromeronic blue staining

4.1 Introduction

The distribution and role of PGs in the central cornea have been investigated extensively (Scott and Haigh 1988a; Sawaguchi *et al.* 1991; Müller *et al.* 2004; Parfitt *et al.* 2010). It is widely agreed that within the central cornea, PGs are associated with the collagen fibrils of the stroma and maintain the regular arrangement of the fibrils that facilitates the transparency of the tissue.

The distribution of PGs at the corneal limbus has not been examined in detail at high resolution. Borcherding *et al.* (1975) examined which GAGs are present with increasing eccentricity from the central cornea using electrophoresis and Ho *et al.* (2014) have also investigated the distribution of KS and CS throughout the bovine cornea. However, neither of these examined the microstructure of the limbus, though they showed the presence of CS and DS here. As aforementioned, CS/DS has been implicated in stem cell niches, including the limbal stem cell niche (Ashworth *et al.* 2021), as has heparan sulphate (Gupta *et al.* 1998; Hayes *et al.* 2008). Thus, potentially, this change in the PG/GAG profile may fulfil a role in providing a matrix composition that favours maintenance of the stem cell phenotype.

Many of the investigations into the central corneal PGs have used cuprolinic or cupromeronic blue dye to visualise the PGs during transmission electron microscopy. However, it does not appear that this has ever been done specifically at the limbus. Cuprolinic/cupromeronic blue dyes are copper-based phthalocyanin-like dyes that are cationic and, therefore, attracted to the negative charges of sulphated GAG molecules (Scott 1972; Holst and Powley 1995). When used in a "critical electrolyte concentration", these dyes can stain sulphated PGs with higher specificity, staining very little of other polyanions in the tissue (Scott 1985). This is due to cations in the salt solution competing with the dye molecules for binding sites on the polyanion (Figure 4.1). As the concentration of cations in the solution

increases, there is not a gradual change in the balance of stained polyanion vs. unstained polyanion, but rather a sharp, critical cut-off. Above a certain concentration, no dye molecules will bind to the desired polyanion, as all binding sites will be occupied by electrolyte cations instead (Figure 4.1B).

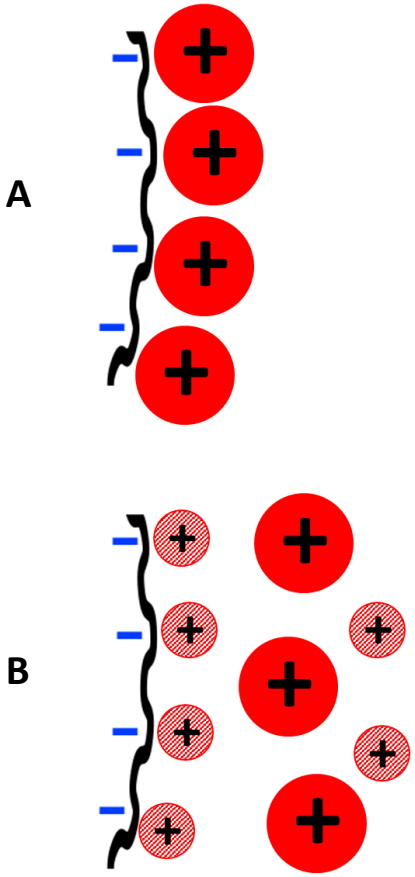

Figure 4.1 - Diagram representing the competition between dye molecules and electrolyte cations that is utilised in a "critical electrolyte concentration".
In (A), four cationic dye molecules (red circles) are bound to four negatively charged binding sites on the polyanion in the absence of any electrolyte cations. In (B), adding cations (dashed red circles) to the solution introduces competition between these and the dye molecules for binding sites on the substrate. Above a certain concentration, only electrolyte cations bind to the polyanion, resulting in no staining of the substrate with the dye. Adapted from Scott (1985).

Depending on how negatively charged the substrate is, the critical electrolyte concentration needed to block any dye binding increases. Therefore, with a certain cation concentration, the binding of dye to any substrates that are less negatively charged than the desired substrate can be blocked (Scott 1985). KS and CS are more negatively charged than HS and HA; thus, with the correct critical electrolyte

concentration, the binding of cuprolinic/cupromeronic blue dyes can be limited to the KS and CS PGs as well as heparin. The addition of anions to the salt solution then allows more dye molecules to bind to the desired substrate by occupying three of the dye's four binding sites (Scott 1980) (Figure 2). These electrolyte anions can then be replaced with heavy metal ions, such as tungsten, to enhance the dye as these are better scatterers of electrons than the dye's copper ion.

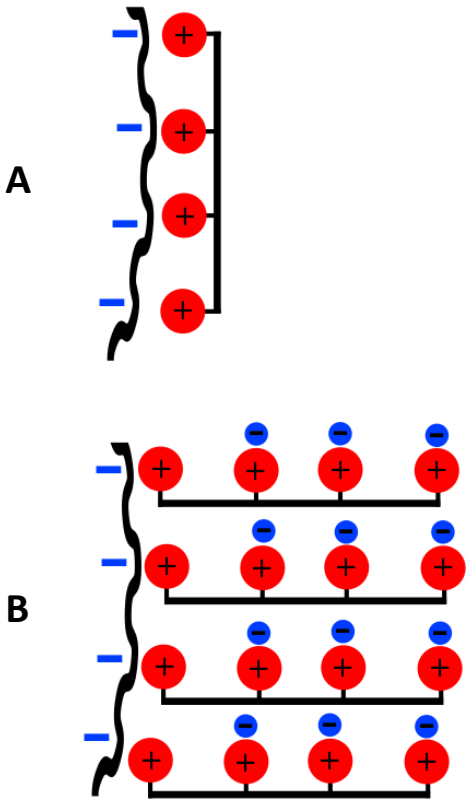

Figure 4.2- Diagram representing how anions in the salt solution can increase the amount of stain bound to the desired polyanion.
In (A), the four positive charges of one molecule of dye bind to four negative charges on the polyanion. However, in (B), adding anions (blue circles) to the salt solution allows these to occupy three of the molecule's positive charges and now four dye molecules can bind to the polyanion. Adapted from Scott (1980).

This study aims to localise the PGs in the porcine corneal limbus, using cupromeronic blue dye, and to examine the limbal ultrastructure to determine if this differs from the central cornea. The hypothesis is that CS/DS PGs will be present at the limbus, in close association to the limbal epithelial basement membrane, with a different distribution than the central cornea due to collagen fibrils being less rigidly organised here and transparency being less important.

Differences are not expected in PG profile between the S/I limbus and the N/T limbus due to the findings of the previous chapter.

Some of the findings in this chapter were published in an article by Hammond *et al.* (2020).

4.2 Materials and Methods

4.2.1 Preparation of tissue samples

Sixteen porcine eyes were sourced from a local abattoir, transported on ice, and refrigerated immediately prior to dissection. Firstly, the eyes were oriented as indicated in section 2.2 and corneoscleral discs were manually dissected from whole eye globes. The endothelium of the 13 corneas used for transmission electron microscopy was removed via mechanical scraping with a scalpel blade in order to facilitate penetration of the cupromeronic blue dye. Limbal tissue segments were then taken from four positions, at the assumed 3, 6, 9 and 12 o'clock positions (Figure 4.3), and also a central corneal section to use as a positive control. Thus, two limbal segments per eye were taken from the S/I quadrants and two from the N/T quadrants.

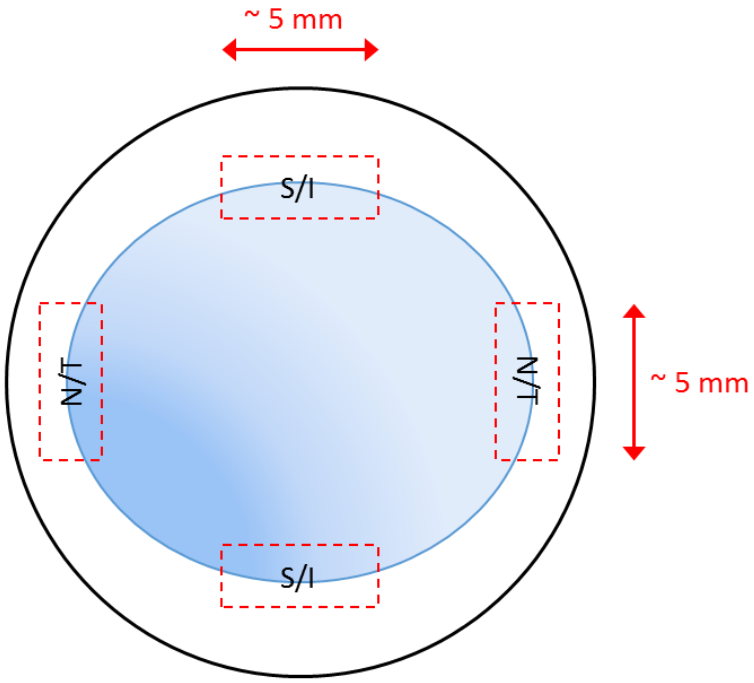

Figure 4.3- Diagram demonstrating limbal tissue dissection.
Limbal segments approximately 5 mm long – with approximately 1 mm of scleral and corneal tissue either side of the limbus – were manually dissected, along with a similarly sized central corneal segment. Blue area = cornea, white area = sclera. (Not to scale).

4.2.2 Chondroitinase ABC digestion

To remove the CS/DS PGs, some corneas were treated with chondroitinase ABC. Another set was incubated with enzyme buffer without chondroitinase ABC as a control and the rest were left untreated so that all PGs were left *in situ*.

Corneal/limbal segments from eight porcine corneas, dissected as above, were fixed in 4% PFA in single strength Tris/sodium acetate buffer (without bovine serum albumin (BSA), pH 7.2) (Appendix 2.1) for 10 mins. They were then rinsed in Tris/sodium acetate buffer for 2 x 5mins. The samples from four eyes were incubated in 2 units/ml chondroitinase ABC (Appendix 2.3) at 37°C for approximately 16 hours. The remaining four eyes were incubated in just Tris/sodium acetate buffer with 0.02% BSA, pH 8 (Appendix 2.2), including 1:100 protease inhibitor cocktail, at 37°C for approximately 16 hours as a control. The tissue segments were then washed in Tris/sodium acetate buffer for 2 x 5 mins, followed by 2 x 5 mins washing in 25 mM sodium acetate buffer (pH 5.7) with 0.1 M $MgCl_2$ (Appendix 2.4).

4.2.3 Transmission Electron Microscopy

The procedure to stain the PGs is based on that described by Scott (1980). The tissue segments were stained with cupromeronic blue dye at a "critical electrolyte concentration". After the tissue was excised/had completed enzyme digestion, it was immediately fixed in a solution of 2.5% glutaraldehyde in 25 mM sodium acetate buffer (pH 5.7) with 0.1 M $MgCl_2$ and 0.05% cupromeronic blue dye (Appendix 2.4), at room temperature on a rotator for approximately 36 hours. Then, segments were washed with single-strength sodium acetate buffer without cupromeronic dye or glutaraldehyde (3 x 5 mins). Next, the segments were washed in aqueous 0.5% sodium tungstate (3 x 5 mins) followed by 0.5% sodium tungstate in 50% ethanol (1 x 15 mins) (Appendix 2.5). The tissue was then dehydrated and embedded in Araldite resin as described in section 2.3.1.

Tissue sections were cut from the polymerised blocks using a Reichert-Jung Ultracut E microtome (Reichert Inc, Depew, USA). The blocks were trimmed using razor blades so that only a small region of interest, usually the area adjacent and subjacent to the limbal trough, was sectioned. Several semi-thin sections of 300 nm

were cut first and stained with toluidine blue. These were then assessed on a light microscope to check the quality of tissue processing and select appropriate regions of interest. Ultrathin sections of 100 nm were then cut and collected on uncoated G300 copper electron microscopy grids (Gilder Grids, Grantham, UK). Finally, the sections were contrasted by staining with saturated aqueous uranyl acetate (UA) for 12 minutes and were then assessed and imaged with a Jeol 1010 transmission electron microscope (Jeol (UK) Ltd, Welwyn Garden City, UK).

4.2.4 Scanning Electron Microscopy

The tissue segments from three corneas, dissected as above and including a central corneal segment, were prepared for imaging with SEM. One end of each limbal segment was cut off, as shown in Figure 4.4, and processed with the main segment. All segments were fixed in 2.5% glutaraldehyde/2% PFA in 0.1 M sodium cacodylate buffer (pH 7.2) (Appendix 2.7) for approximately 16 hours at room temperature. They were then washed in 0.1 M sodium cacodylate buffer (3 x 10 mins).

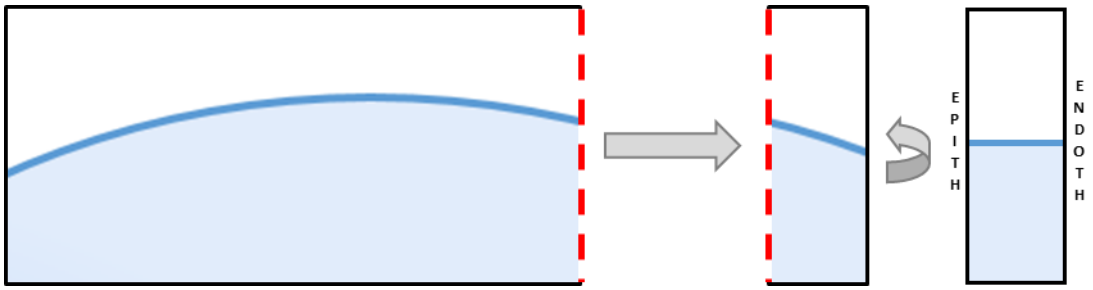

Figure 4.4- A diagram of the limbal segments used for scanning electron microscopy.
One end of each limbal segment was cut from the main segment and then rotated so that one of the side surfaces was facing upwards to then be imaged.

Cell maceration was then carried out by immersing the tissue in 10% aqueous sodium hydroxide over five days, at room temperature, with five changes of solution. Next, they were washed in distilled water over approximately 24 hours at room temperature, with three changes of water in that period, followed by immersing in aqueous 2% tannic acid (Appendix 2.8) for 6 hours. The tissue segments were washed in distilled water again (3 x 30 mins) and then immersed in aqueous 1% osmium tetroxide (Appendix 2.8) for 2 hours.

The tissue was washed in distilled water again (3 x 5 mins), then dehydrated in an ethanol series: starting with 70% then 90% (both 1 x 30 mins), then 100% (2 x 30 mins). The dehydrated tissue was dried using hexamethyl-disilazane (HMDS) (Alfa

Aesar, Heysham, UK). The tissue segments were immersed in a 1:1 solution of 100% ethanol and HMDS for 1 hour, followed by 2 x 1 hour in 100% HMDS. The tissue segments were then left in fresh HMDS in a desiccator in a fume hood until all the liquid had evaporated.

Finally, the dried tissue segments were mounted on 12.5 mm aluminium stubs, with the epithelial side up for the main segments and with the cut-off segments on their sides so that the cross-section was facing upwards (Figure 4.4), using Leit-C carbon cement (Agar Scientific Ltd, Stansted, UK). The samples were then sputter-coated with ~15 nm of gold-palladium using a Bio-rad SC500 sputter coater (Bio-Rad Laboratories Ltd, Watford, UK) with argon as the sputtering gas. The samples were imaged using a Zeiss Sigma HD field emission gun SEM (Carl Zeiss Ltd, Cambridge, UK) with the accelerating voltage set to 5 kV and the aperture size at 30 µm. Images for the first eye were collected by Dr Duncan Muir, and by myself for the second and third eyes.

The orientation of collagen fibrils in the SEM images was assessed using the ImageJ plug-in "FibrilTool" (Boudaoud *et al.* 2014). Three distinct areas in the limbal samples were quantified: peripheral cornea, a transition zone and the limbal annulus of collagen. The images analysed with FibrilTool were acquired at 10,000x magnification. One image was used from each of the three aforementioned areas in all four limbal sites from the three eyes, and four images of different areas from the central cornea of each eye. The same five set regions of interest were analysed in each image, resulting in 60 values generated for each distinct area (central cornea, peripheral cornea, transition zone and limbal annulus). The means were calculated from these values and Student's independent sample t-Test was then performed to compare the averages.

4.3 Results

Light microscopy images demonstrate the areas of tissue that were subsequently sampled for TEM imaging. The limbal trough was observed in all limbal tissue samples (Figure 4.5) – though it varied in appearance, usually being more prominent and defined in S/I segments. As expected, no noticeable protrusions of the epithelium were visible in the central cornea; the epithelium was generally of uniform thickness and number of layers across the width of the section (Figure 4.6).

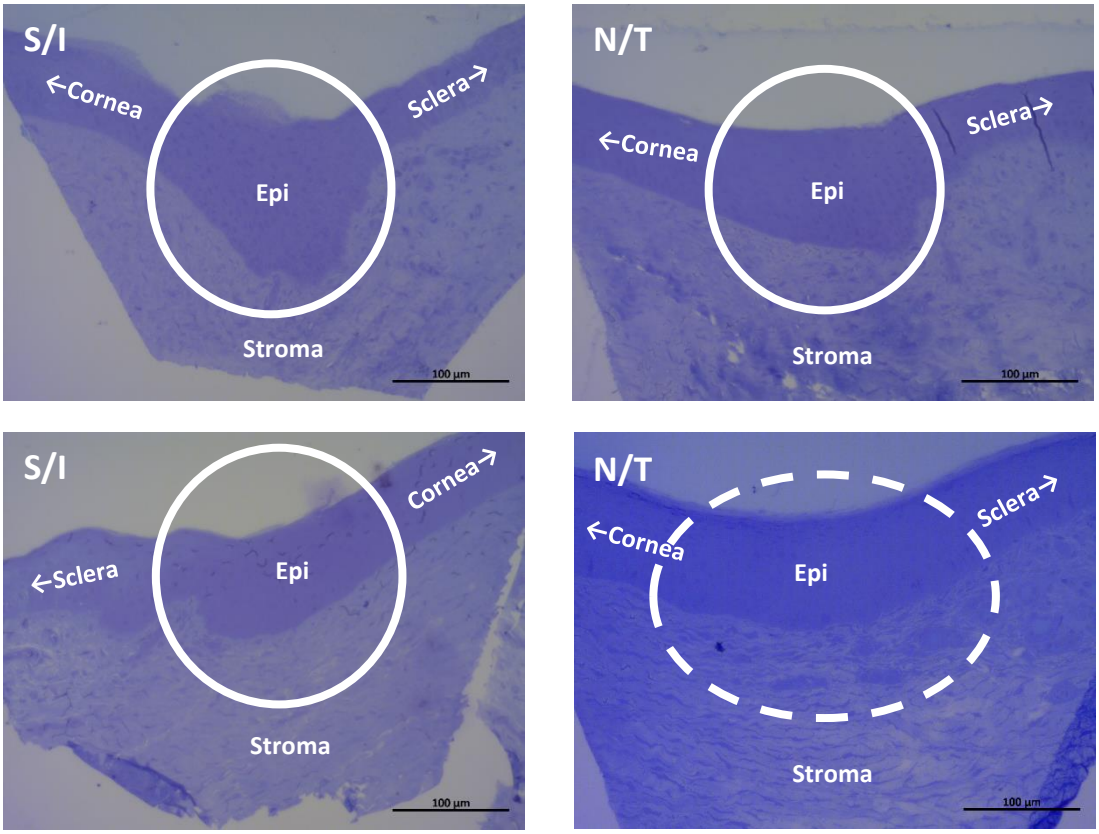

Figure 4.5- The presence of the limbal trough around the porcine limbus.
A section of the limbal trough (circled) is found in all limbal tissue sections, though it varies in its appearance and prominence. Some areas of the nasal/temporal samples, in particular, have a much less pronounced trough (dashed circle). Epi = epithelium.

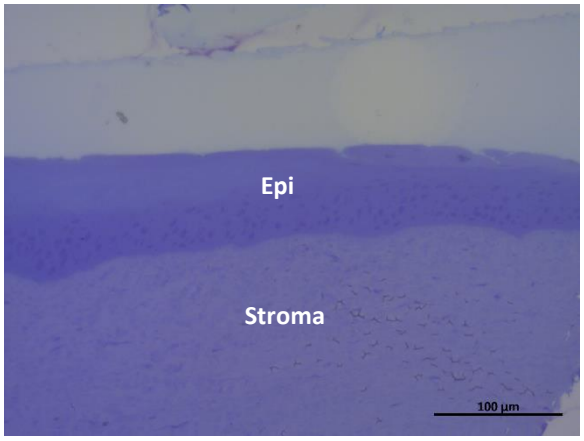

Figure 4.6- The central corneal epithelium lacking a limbal trough.
Though there are some variations in the thickness of the central corneal epithelium, it lacks any prominent protrusions, as would be expected. Epi = epithelium.

The TEM results presented here are from one cornea each for untreated, chondroitinase-digested, and enzyme control conditions, following numerous attempts to optimise the experimental protocol. The first three untreated corneas and the first chondroitinase-digested and enzyme control corneas were stained with a new source of cupromeronic blue dye which was found to be of dubious quality immediately. It did not stain the PGs as expected; all PGs appeared to have collapsed in all samples and no filamentous PGs were visible. The second chondroitinase-digested and enzyme control corneas were not fixed before enzyme incubation, resulting in total degradation of corneal structure and, thus, these samples were also abandoned.

Chondroitinase ABC-treatment appeared to have been ineffective – presumably because of lack of enzyme activity – on the third chondroitinase-digested cornea and so this sample, as well as the accompanying enzyme control and untreated corneas, were again abandoned. Consequently, the enzyme incubation time was increased from four hours to approximately 16 hours and these corneas, in addition to the accompanying untreated cornea, produced the results presented below.

4.3.1 Distribution of CS and KS PGs

4.3.1.1 Anterior stromal collagen lamellae

Electron micrographs taken of the central corneal stroma of the undigested cornea showed that the cupromeronic blue dye had stained CS and KS PGs as expected (Figure 4.7). The periodic banding pattern of the collagen fibrils was not clearly evident in these sections; however, vast amounts of PGs were seen associated with the fibrils in both transverse and longitudinal lamellae (Figure 4.7B, C).

PG filaments were of varying lengths, with some appearing to span the gap between adjacent collagen fibrils and some appearing to bridge more than one fibril. The PGs also displayed varying orientations; both perpendicular and parallel alignments, in relation to collagen fibrils, can be seen as well as oblique orientations.

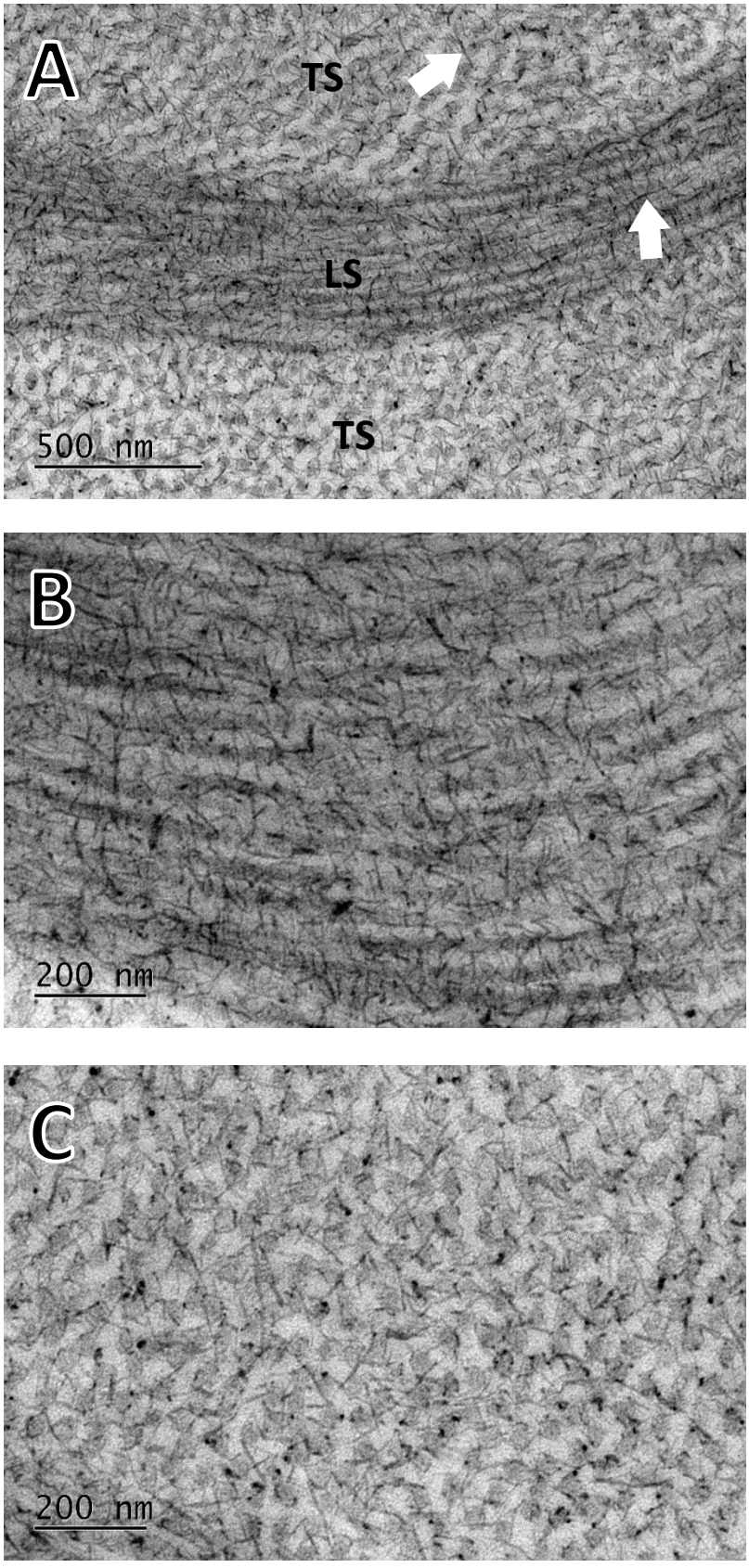

Figure 4.7- Anterior stromal collagen lamellae of the central cornea.
A: Collagen lamellae of the porcine cornea demonstrate a quasi-orthogonal arrangement of adjacent lamellae. Vast amounts of proteoglycans (darker filaments crossing and in between collagen fibrils, white arrows) can be seen in association with the collagen fibrils. B: Longitudinal collagen fibrils demonstrate large amounts of proteoglycans both running alongside and at angles to the fibrils. C: In transverse section, proteoglycans bridge the gaps between collagen fibrils, connecting with two or more fibrils. LS = longitudinal section, TS = transverse section.

Abundant PGs, associated with collagen fibrils within the stroma, were also seen in limbal sections (Figures 4.8 and 4.9). Adjacent lamellae still appeared to have quasi-orthogonal orientations in relation to each other and the positioning of attached PGs to longitudinal collagen fibrils seemed to have a very regular D periodicity in some areas (Figures 4.8A and 4.9A). There did not appear to be any considerable difference in the PG profiles between the S/I limbal areas or the N/T areas. Equally, there were no significant differences between the two S/I areas sampled or the N/T areas respectively.

Figure 4.8- Anterior stromal collagen fibrils of the superior/inferior limbus. →
A lamellar structure, like that of the central cornea, can still be found at the limbus. However, the arrangement of PGs along collagen fibrils seems more regular here – with some areas demonstrating D periodicity (A, white arrows). The appearance that some PGs are within collagen fibrils (B) is most likely an artefact due to potential oblique sectioning of the 100 nm thick sections.

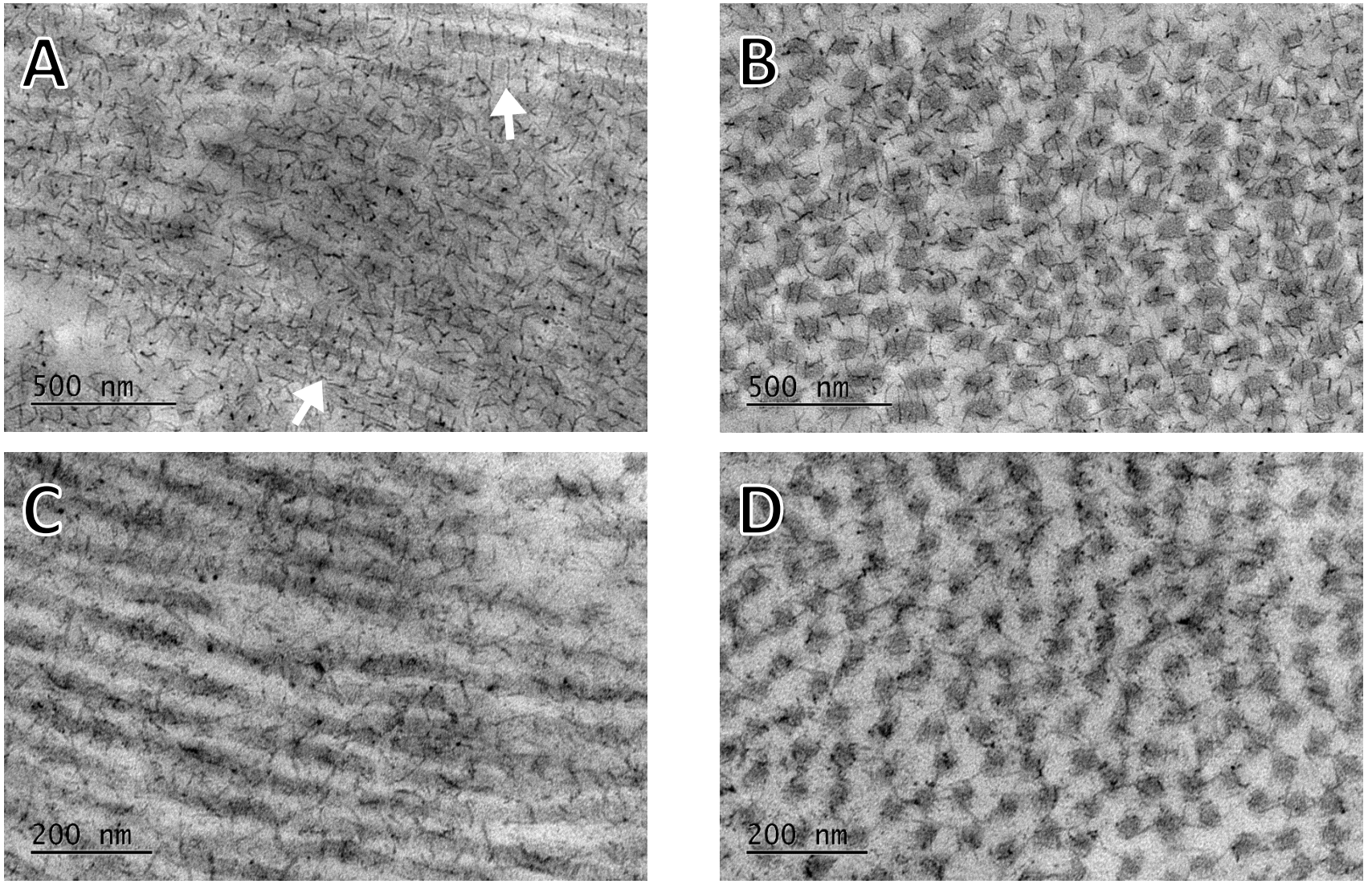
A
500 nm
B
500 nm
C
200 nm
D
200 nm

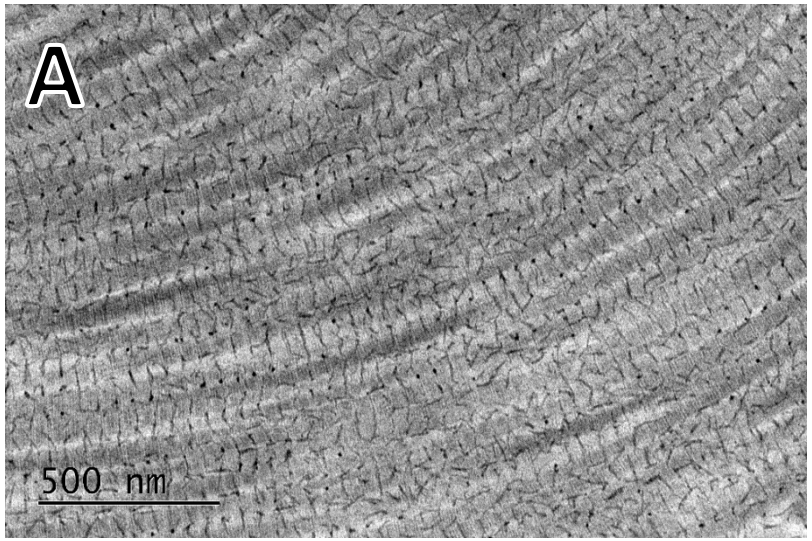
A
500 nm

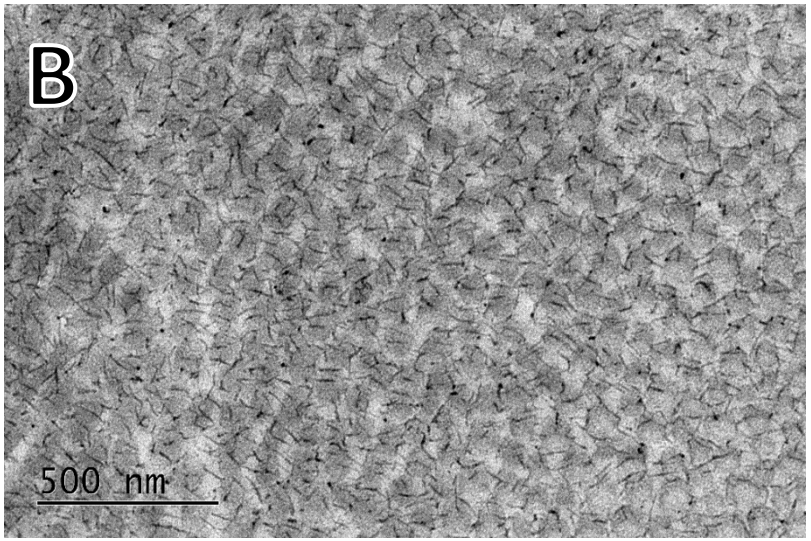
B
500 nm

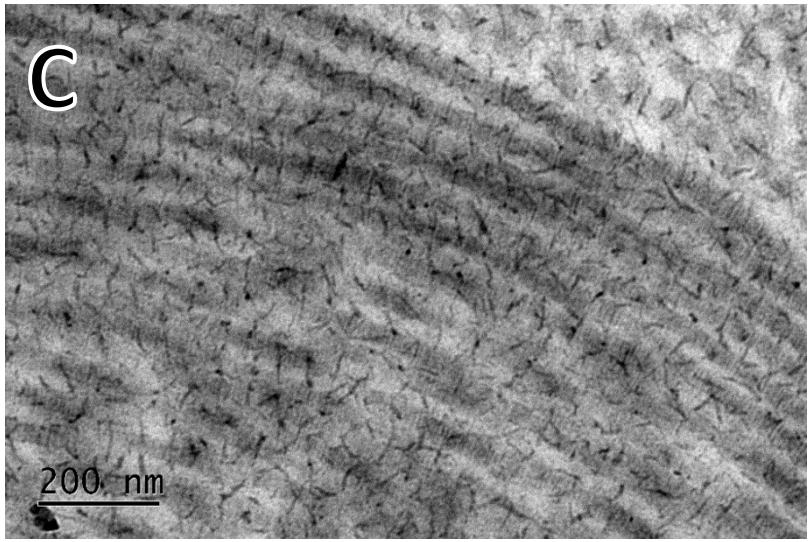
C
200 nm

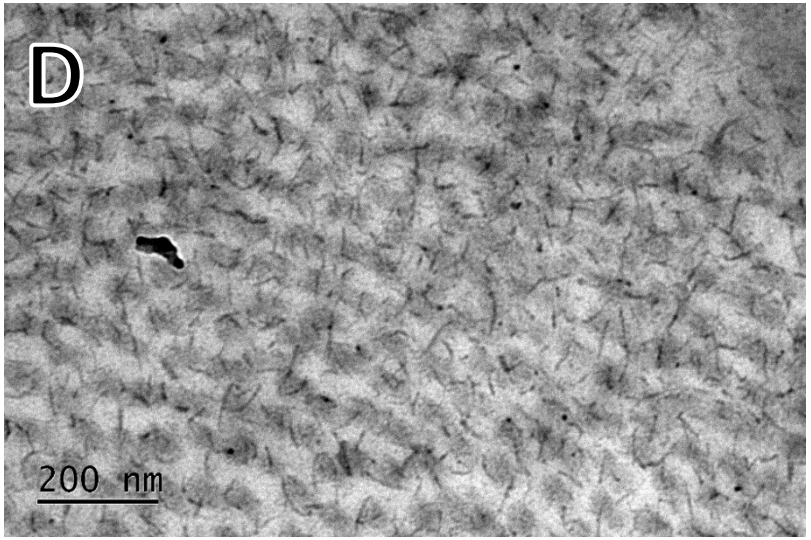
D
200 nm

Figure 4.9- Anterior stromal collagen fibrils of nasal/temporal limbus. ←
The structure appears to be the same in the nasal/temporal areas of the limbus as the superior/inferior. The adjacent collagen lamellae have differing orientations of their fibrils, but proteoglycans are arranged with a regular periodicity along the collagen fibrils (particularly evident in A).

4.3.1.2 Epithelial basement membrane

The epithelial basement membrane was identified in all tissue samples and appeared to consist of three parts, as defined by associated staining with cupromeronic blue: a lining of PGs on the stromal side, a gap which is presumably composed of collagen, and another lining of PGs on the epithelial side (Figures 4.10-4.12). This was true for the central corneal basement membrane (Figure 4.10) and the limbal basement membrane (Figures 4.11 and 4.12). The PGs lining the epithelial side of the basement membrane all appeared to be moderately short with limited variation in length. The central part of the basement membrane, most likely the lamina densa and lamina lucida, was usually completely devoid of PGs. There were some instances where PGs could be seen to be bridging across this gap. The lamina densa appeared as a clear gap as no conventional osmium tetroxide/UA contrasting *en bloc* was used in this method. Also, epithelial cell membranes are indistinct owing to the lack of osmium contrasting the lipid.

The basement membrane of the S/I limbus (Figure 4.11) and the N/T limbus (Figure 4.12) had the same configuration as the central corneal basement membrane. However, there were less PGs along the epithelial side of the basement membrane in the limbal regions than in the central cornea. The basement membrane had an undulating profile in the N/T limbus (Figure 4.13). Some of the stromal processes observed in N/T sections were very elaborate, with a lot of branching, but there were also areas of flatter profile. Though some undulation and processes of stromal tissue extending into the epithelial layer could be seen in S/I sections, these were less numerous, pronounced, and extensive than can be seen in N/T sections.

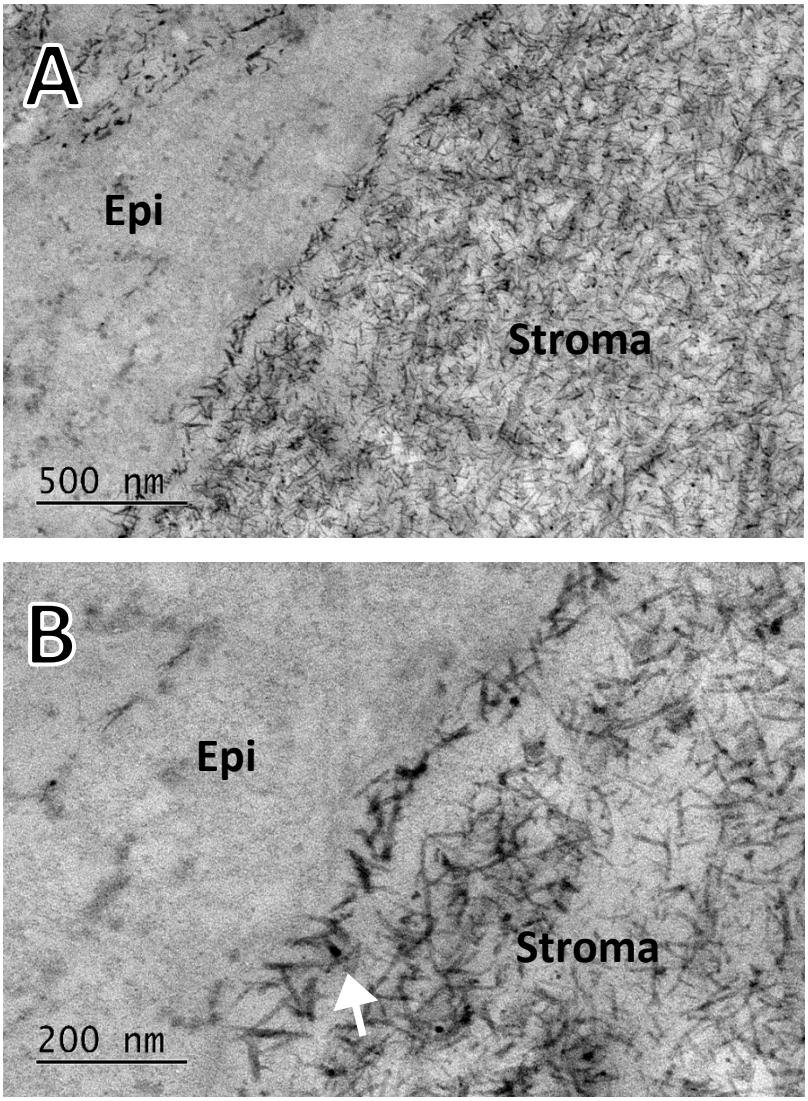

Figure 4.10- Epithelial basement membrane of the central cornea.
The basement membrane demonstrates linings of proteoglycans on both its epithelial-facing and stromal-facing surfaces, with a clear gap between these linings. However, proteoglycans do sometimes cross this gap (B, white arrow). Proteoglycans along the epithelial lining appear to be shorter than those found within the stroma. Epi = epithelium.

Figure 4.11- Epithelial basement membrane of superior/inferior limbus. →
The structure of the basement membrane is the same here as in the central cornea. There are less proteoglycans lining the epithelial surface of the basement membrane than in the central cornea. No notable differences can be seen in the basement membrane composition at the opposite limbal positions of the vertical meridian (A, C and B, D respectively). White arrow indicates areas where proteoglycans cross the lamina densa/lamina lucida. Epi = epithelium.

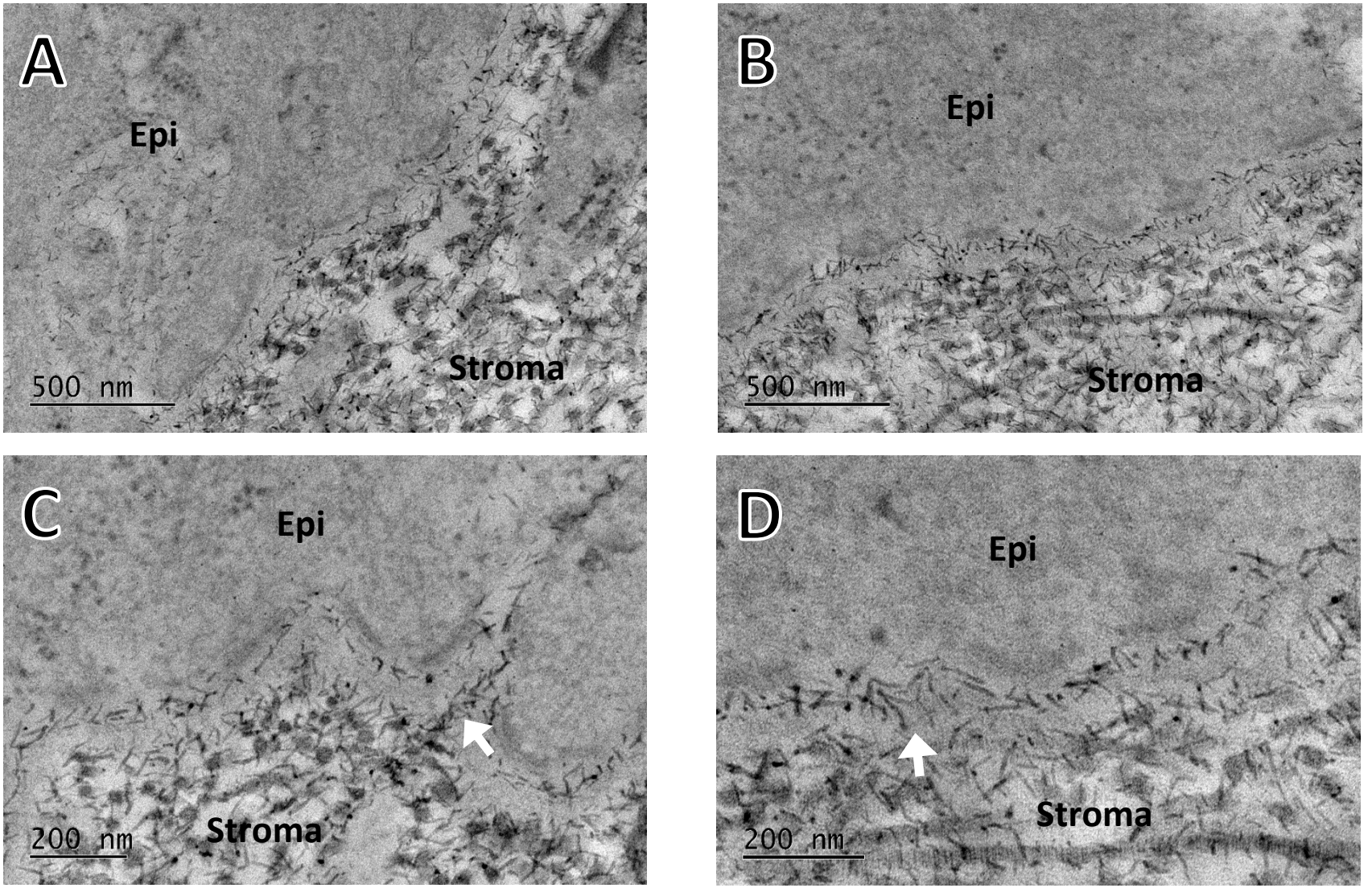
A
Epi
Stroma
500 nm
B
Epi
Stroma
500 nm
C
Epi
Stroma
200 nm
D
Epi
Stroma
200 nm

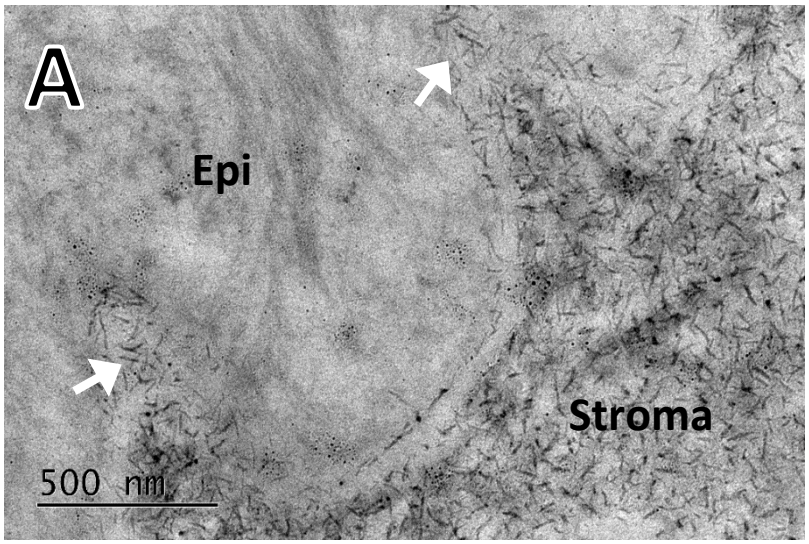
A
Epi
Stroma
500 nm

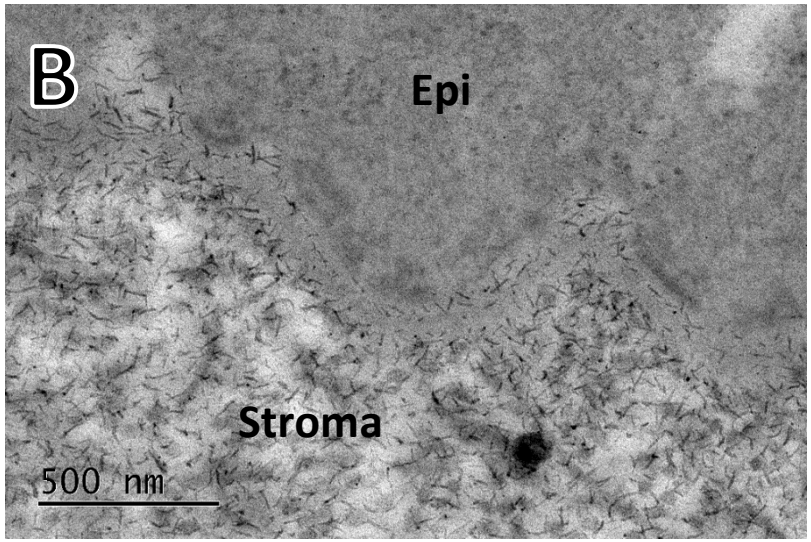
B
Epi
Stroma
500 nm

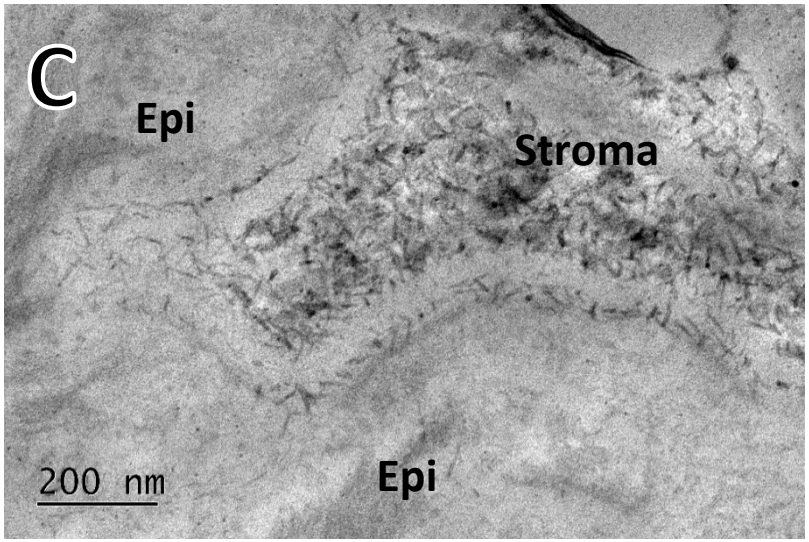
C
Epi
Stroma
Epi
200 nm

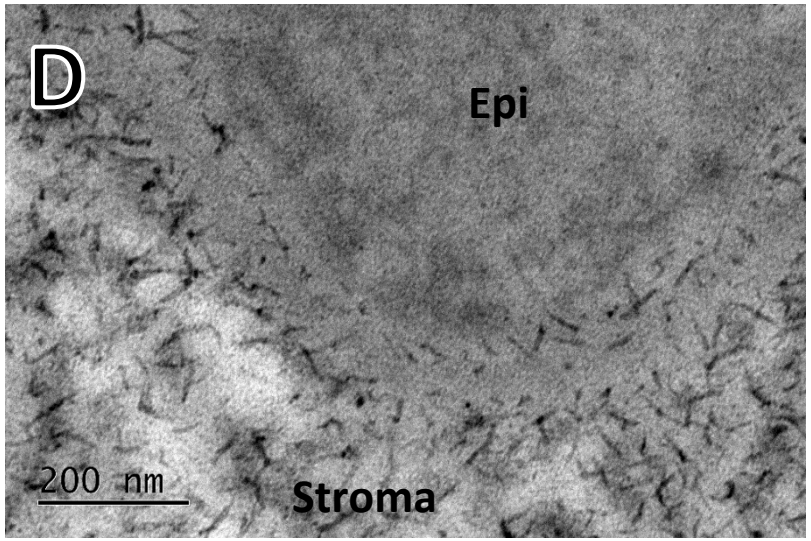
D
Epi
Stroma
200 nm

Figure 4.12- Epithelial basement membrane of nasal/temporal limbus. ←
The structure of the basement membrane is the same as the central cornea and the superior/inferior limbus. There are, again, points where proteoglycans are found within the gap between proteoglycan linings (white arrows). There are no noticeable differences between the two sides of the horizontal meridian (A, C and B, D respectively). Epi = epithelium.

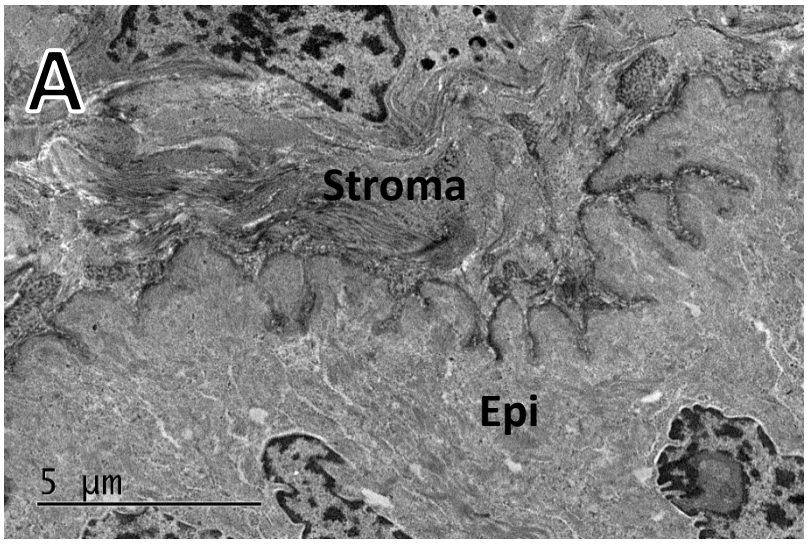

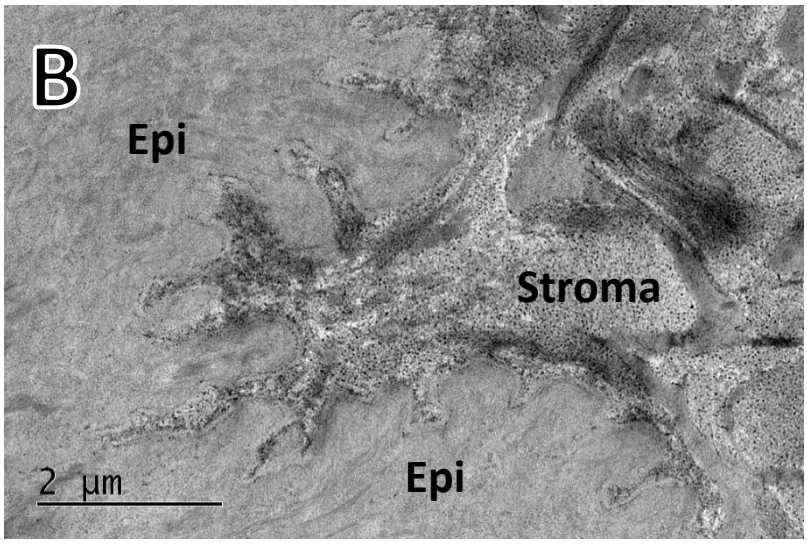

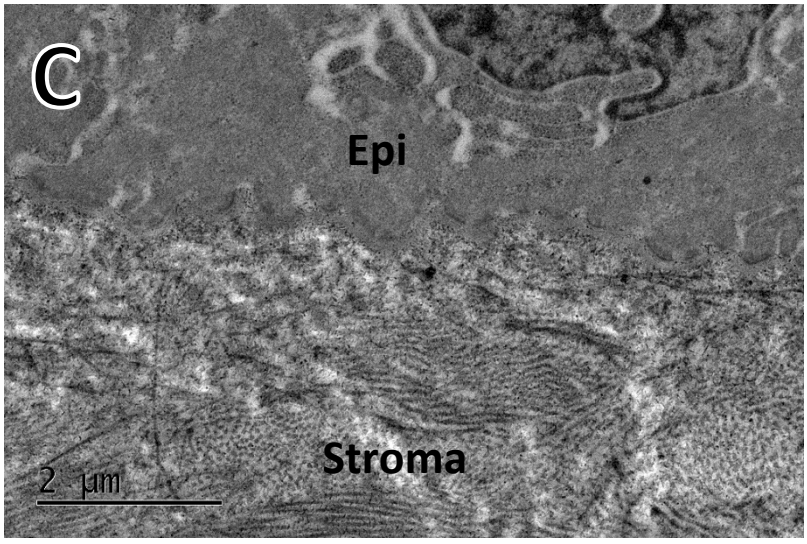

Figure 4.13- Undulating basement membrane of the nasal/temporal limbus.
Lower magnification images clearly demonstrate the irregular profile of the limbal epithelial basement membrane in nasal/temporal areas. Many processes of stromal tissue, with branching elements, into the basal epithelium can be seen. However, there are also some areas of flatter profile (C). Epi = epithelium.

4.3.2 Distribution of PGs after exposure to chondroitinase ABC

Due to cupromeronic blue dye staining both KS and CS/DS PGs, the preceding images do not provide specific information about the distribution of the two types of PGs individually. By digesting all of the CS/DS PGs with chondroitinase ABC, this should leave just the KS PGs *in situ*. By comparing the remaining PGs in the enzyme-exposed tissue to non-exposed, the distribution of CS/DS PGs can be indirectly observed.

4.3.2.1 Anterior stromal collagen lamellae

In the central cornea, exposure to chondroitinase ABC appeared to have reduced the amount of PGs in the stromal collagen lamellae (Figure 4.14). In both transverse and longitudinal lamellae, there was a lack of longer, thinner PG filaments in the chondroitinase-exposed cornea (Figure 4.14B, D) compared to the enzyme control (Figure 4.14A, C).

Figure 4.14- Anterior stromal collagen lamellae of the enzyme control (A, C) and chondroitinase ABC-exposed (B, D) central corneas. →
Lower amounts of proteoglycans can be seen both along and in between the collagen fibrils in the chondroitinase-exposed cornea than in the enzyme control cornea. In particular, the longer, thinner proteoglycan filaments have been removed by enzyme exposure.

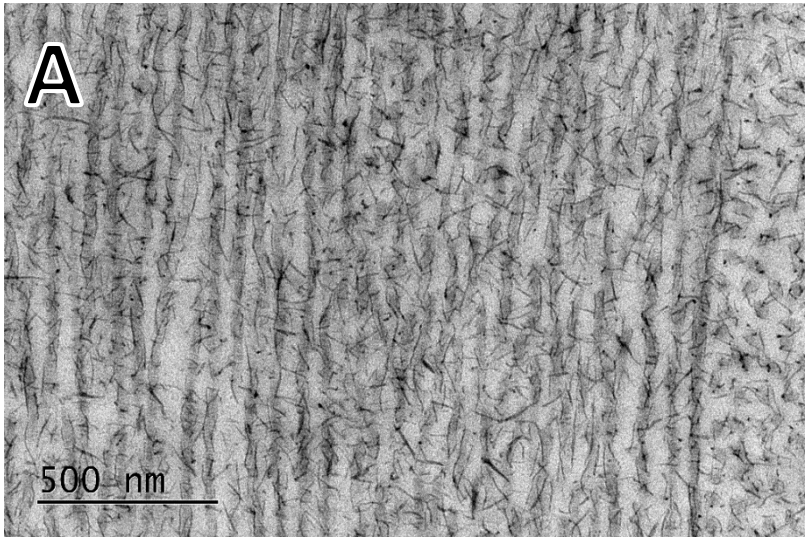
A
500 nm

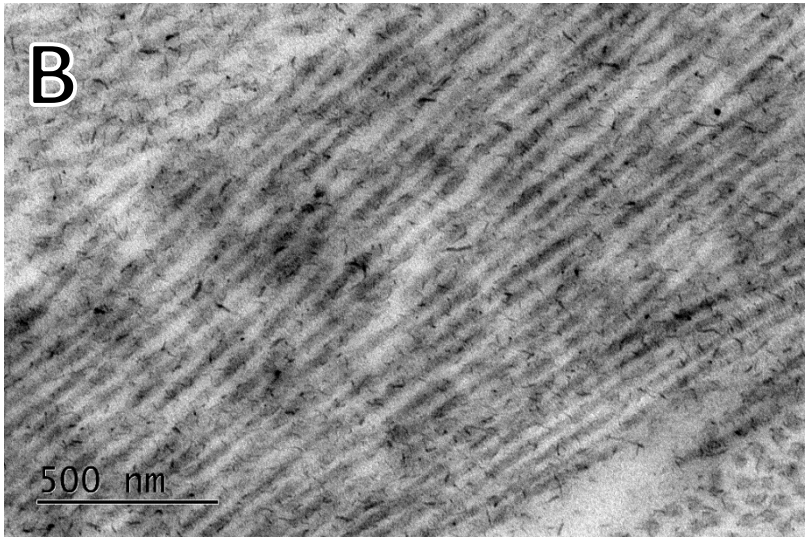
B
500 nm

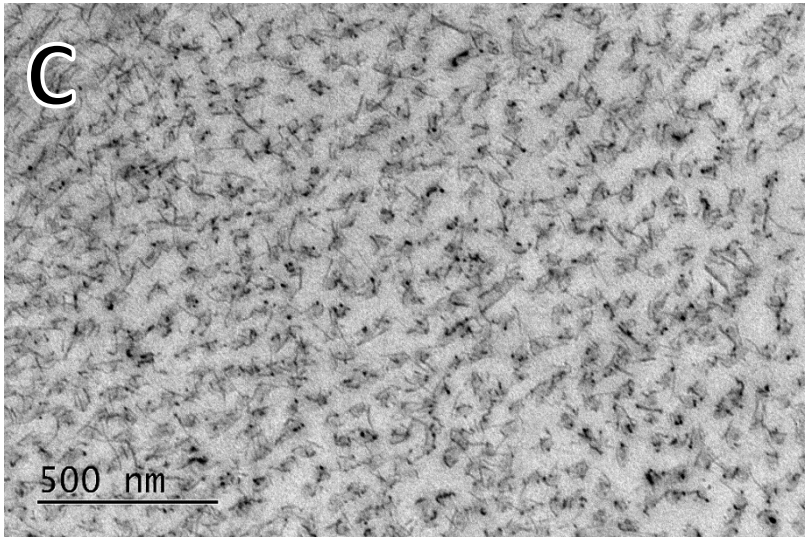
C
500 nm

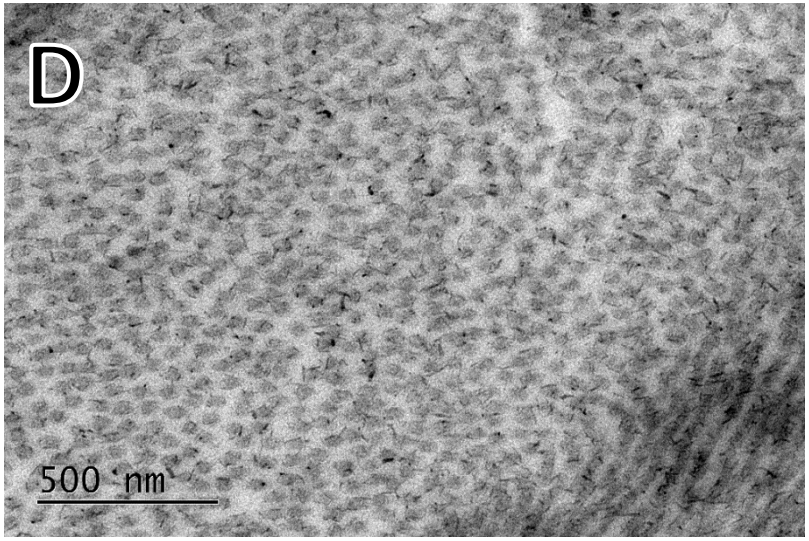
D
500 nm

There was not such a noticeable reduction in the number of PGs in the limbal areas as in the central cornea. The amount of PGs appeared to be the same in the S/I limbal areas of both the chondroitinase-exposed cornea and the control tissue (Figure 4.15). The collagen fibrils were again arranged in quasi-orthogonal lamellae and a regular D periodicity in the attachment of PGs to the collagen fibrils was observed in both limbal sites. There were no substantial differences between the opposite sides of the S/I meridian.

The same organisation was observed for N/T sections in both enzyme-exposed and control tissue (Figure 4.16). However, there appeared to be a reduction in the number of PGs along one side of this meridian in the chondroitinase-exposed tissue, compared to the controls (Figure 4.17). However, many of the PGs here may have collapsed and no longer demonstrated a filamentous configuration. These fibrils may also be deeper within the stroma than demonstrated in other images. The opposing side of this meridian did not seem to have a reduction in PGs and looked similar to the control tissue.

Figure 4.15- Anterior stromal collagen fibrils of the superior/inferior limbus of enzyme control (A, C) and chondroitinase ABC-exposed (B, D) tissue. →
There does not appear to be a notable reduction in the amount of proteoglycans between the two samples and both appear similar to the untreated tissue.

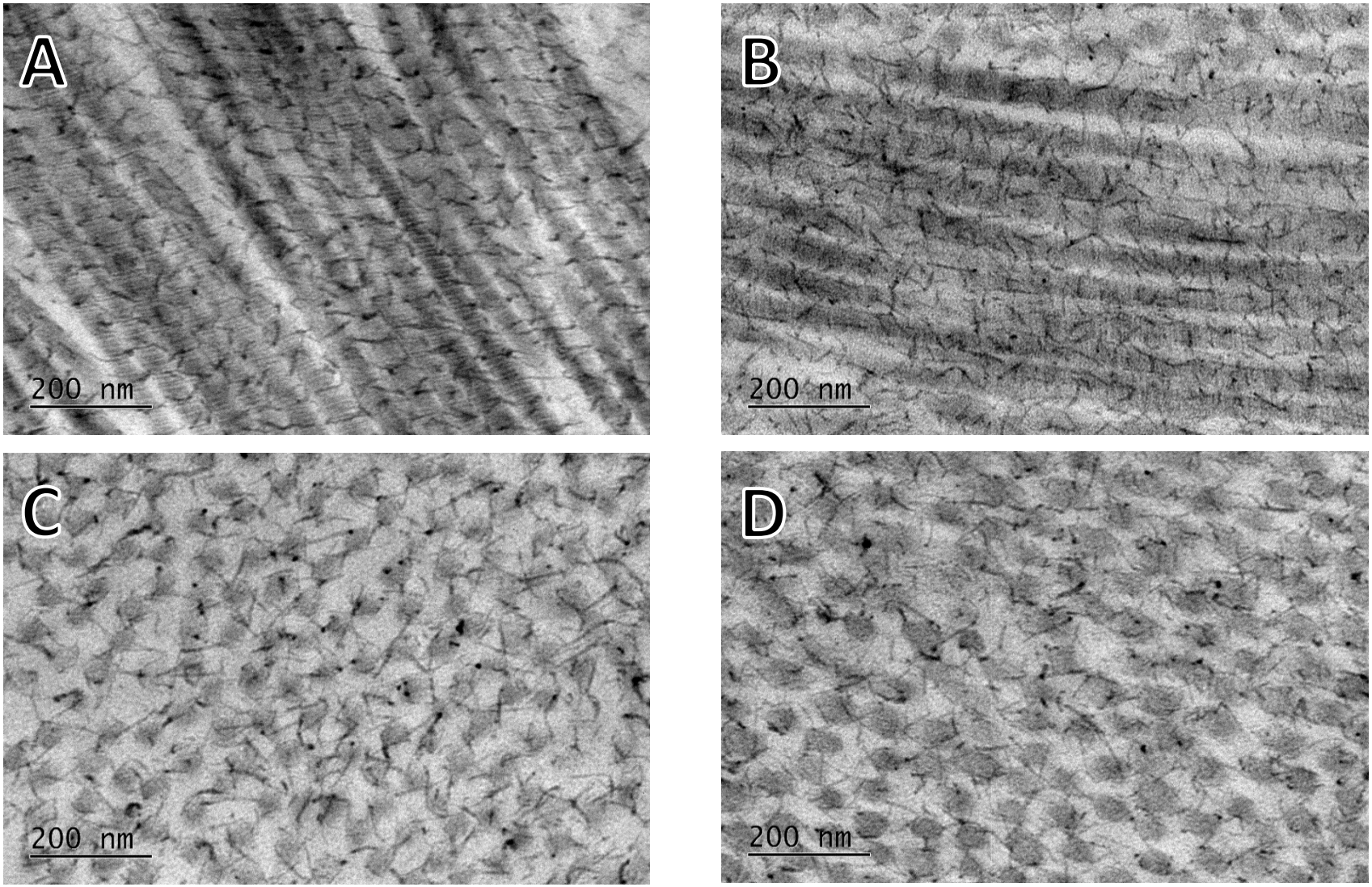
A
200 nm
B
200 nm
C
200 nm
D
200 nm

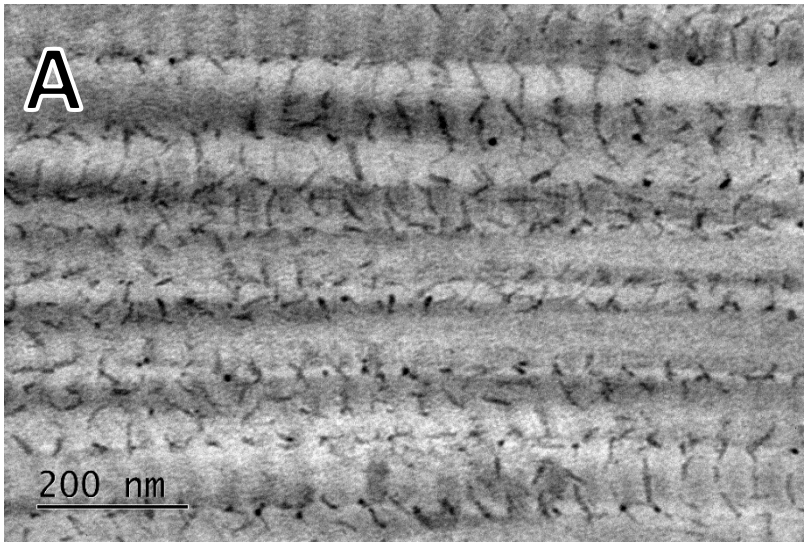
A
200 nm

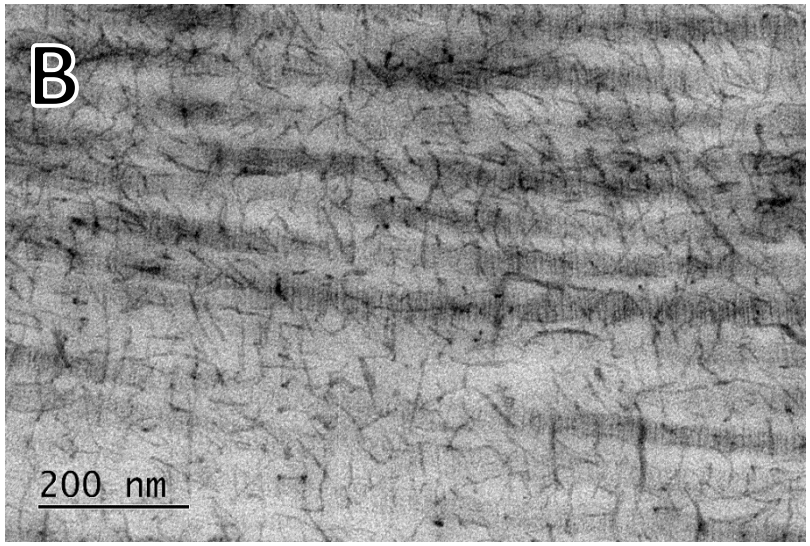
B
200 nm

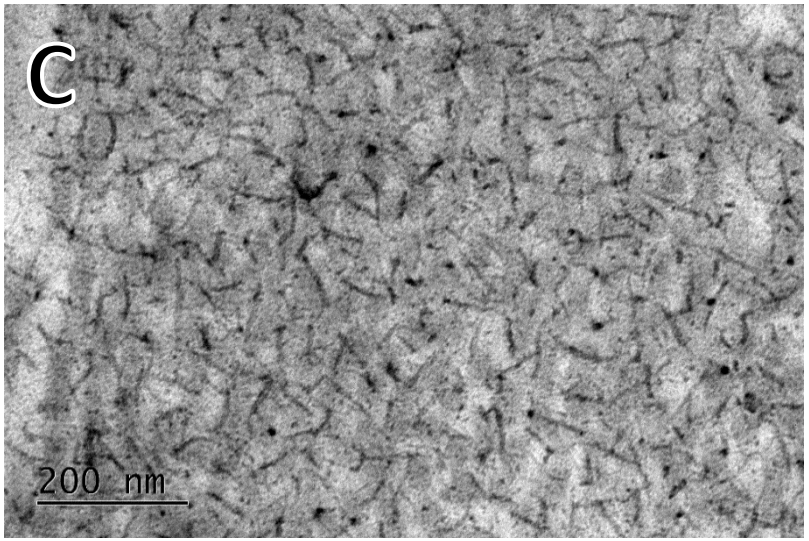
C
200 nm

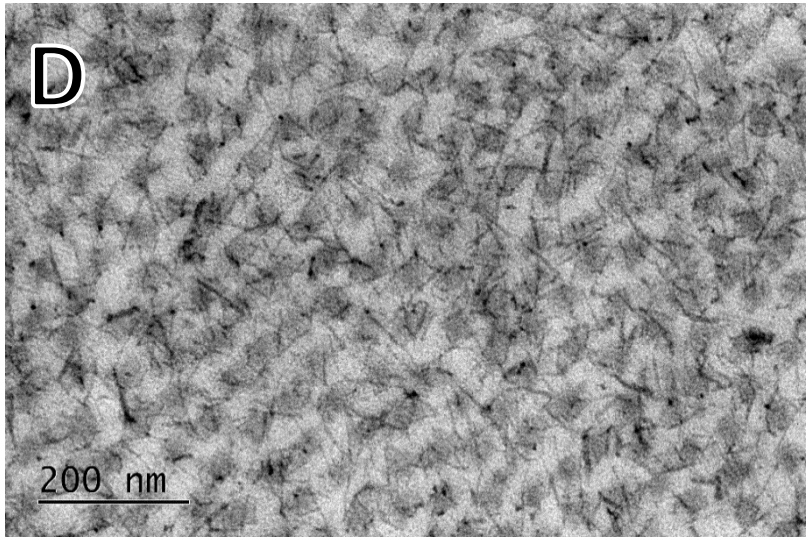
D
200 nm

Figure 4.16- Anterior stromal collagen fibrils of the nasal/temporal limbus of enzyme control (A, C) and chondroitinase ABC-exposed (B, D) tissue. ←
The side of the nasal/temporal limbus in chondroitinase-exposed tissue shown here does not demonstrate a reduction in the amount of proteoglycans compared to both sides of the nasal/temporal limbus of the control cornea.

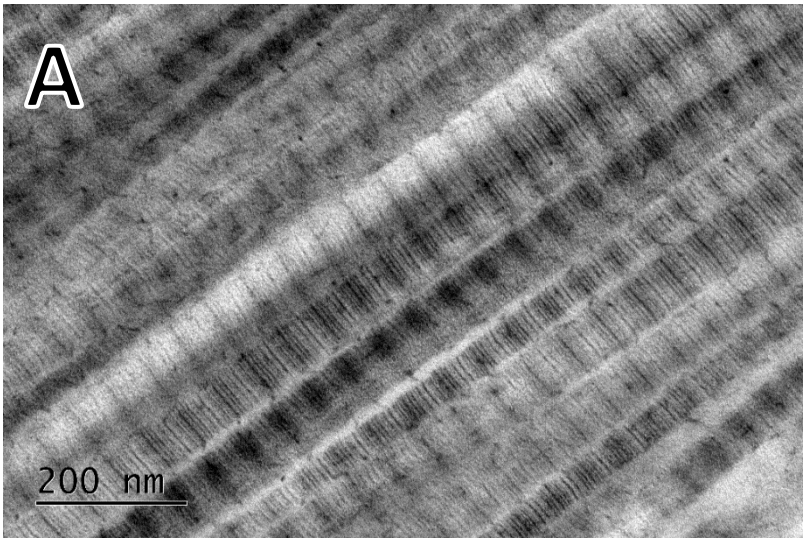

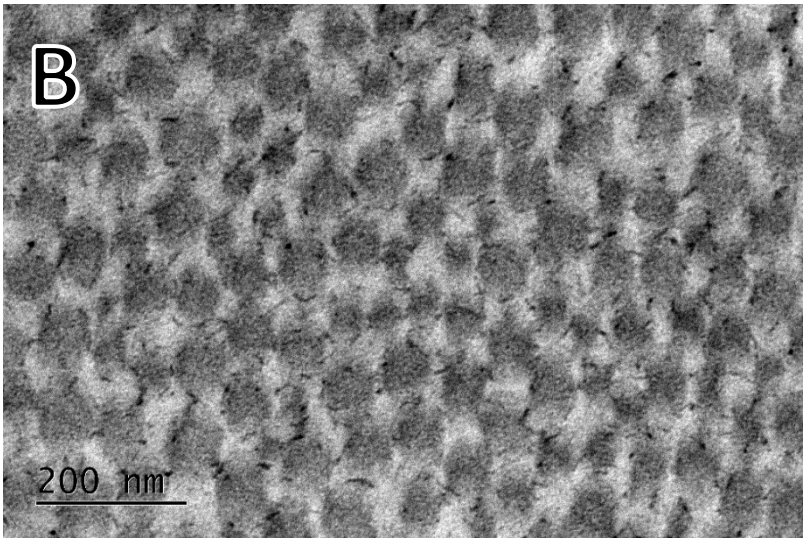

Figure 4.17- Collagen fibrils in the nasal/temporal corneoscleral limbus of chondroitinase ABC-exposed tissue (opposite to that shown in Figure 4.16).
Proteoglycans observed in this nasal/temporal section appear to have collapsed but the number of proteoglycans may also have been reduced by chondroitinase ABC exposure. These fibrils may be deeper in the stroma than shown in previous images, though still within 100-200 µm of the epithelial basement membrane.

4.3.2.2 Epithelial basement membrane

In all chondroitinase ABC-exposed and enzyme control tissue samples, the epithelial basement membrane had the same appearance as in the untreated corneal and limbal tissue, consisting of two linings of PGs separated by a PG-free zone (Figures 4.18-4.20). Again, there were some areas where PGs bridged this gap presumably representing the uncontrasted basal lamina.

As in the anterior stromal collagen lamellae, chondroitinase ABC exposure appeared to have reduced the amount of PGs along the central corneal basement membrane (Figure 4.18). Again, some of the longer, thinner PG filaments were absent in the chondroitinase-exposed tissue when comparing to the controls.

Figure 4.18- Epithelial basement membrane of the central cornea in enzyme control (A, C) and chondroitinase ABC-exposed (B, D) tissue. →
Though not as obvious as in the anterior stromal collagen lamellae, there is also a reduction in the number of proteoglycans along the epithelial basement membrane of the central cornea of chondroitinase-exposed tissue when compared to the enzyme control. White arrows indicate areas where proteoglycans are crossing the presumed collagen component of the basement membrane. Epi = epithelium.

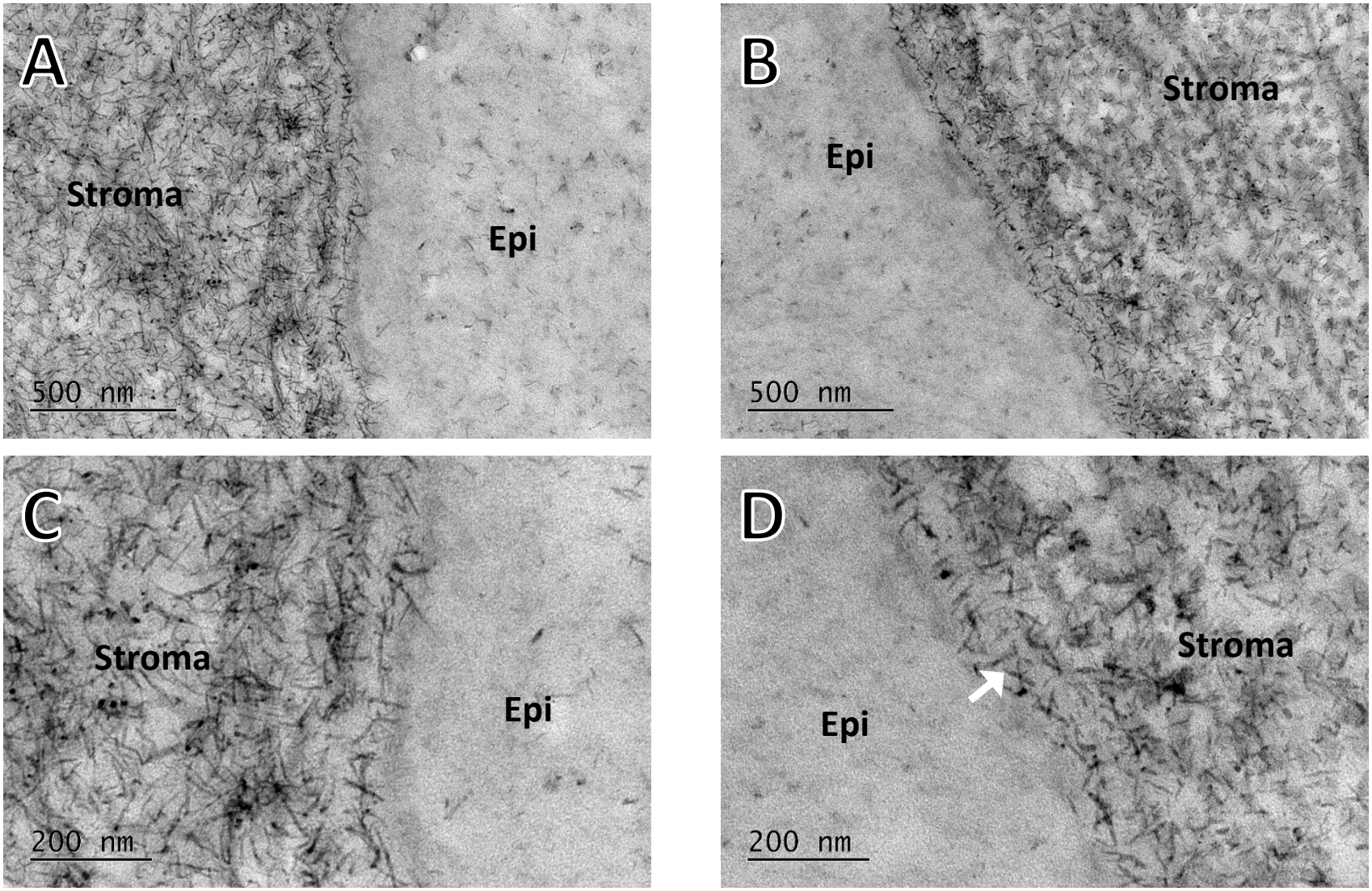
A
Stroma
Epi
500 nm
B
Stroma
Epi
500 nm
C
Stroma
Epi
200 nm
D
Stroma
Epi
200 nm

No similar level of reduction could be seen between the chondroitinase-exposed tissue and the enzymes controls for three of the four limbal areas (Figures 4.19 and 4.20). Both S/I samples did not demonstrate a reduction in PGs; neither did one of the N/T sections. However, the other chondroitinase-exposed N/T section did demonstrate some reduction in PGs (Figure 4.21) when compared to both N/T controls. The PGs that were present had collapsed, with very few filamentous structures visible just as in the stromal collagen lamellae of this sample – shown in Figure 4.17.

Figure 4.19- Epithelial basement membrane of the superior/inferior limbus in enzyme control (A, C) and chondroitinase ABC-exposed (B, D) tissue. →
No significant difference in the proteoglycan profile can be seen between the enzyme-exposed and control tissue here. White arrows again demonstrate areas of basement membrane where proteoglycans are crossing the typically proteoglycan-free gap. Epi = epithelium.

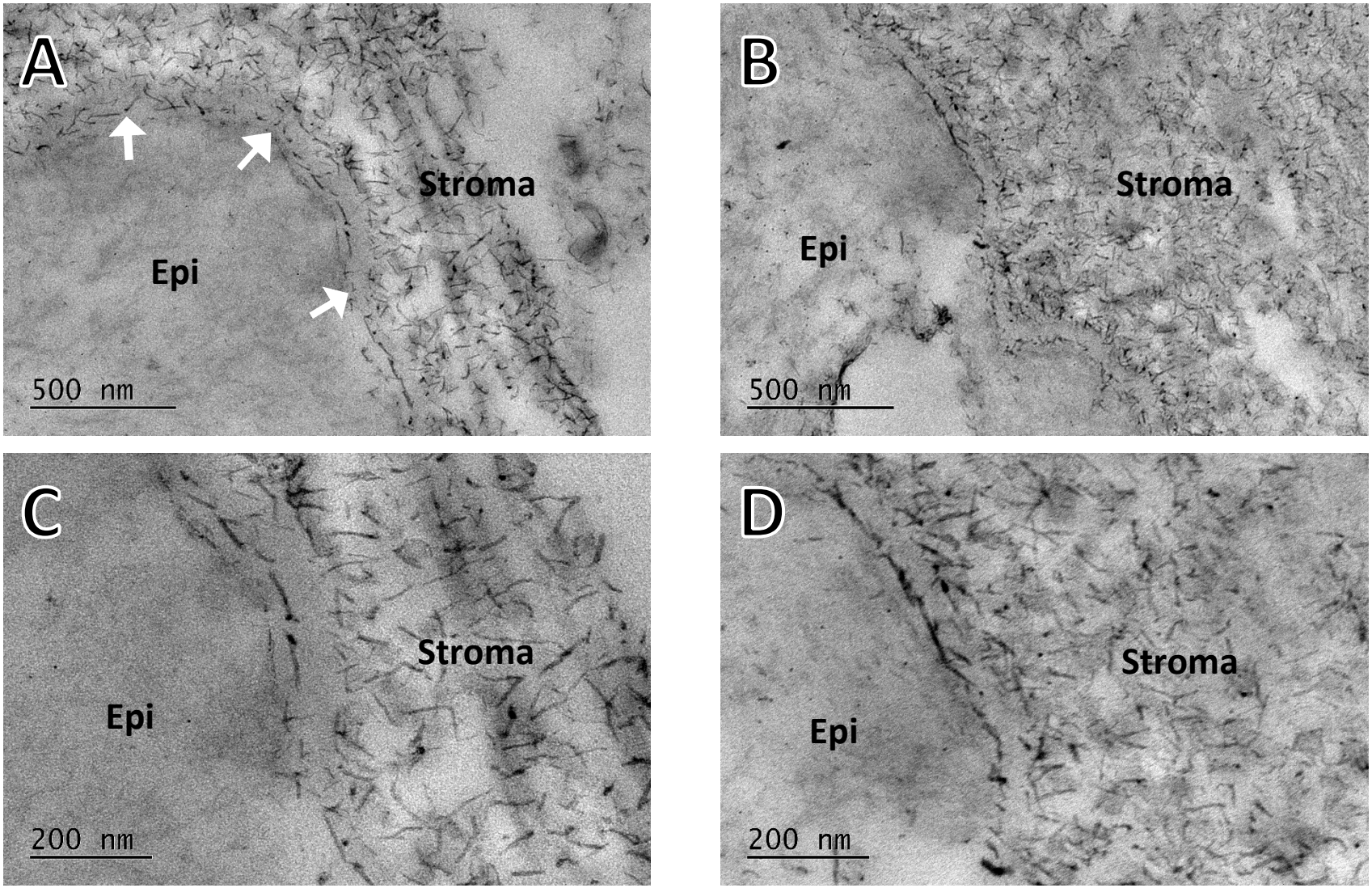
A
Stroma
Epi
500 nm
B
Stroma
Epi
500 nm
C
Stroma
Epi
200 nm
D
Stroma
Epi
200 nm

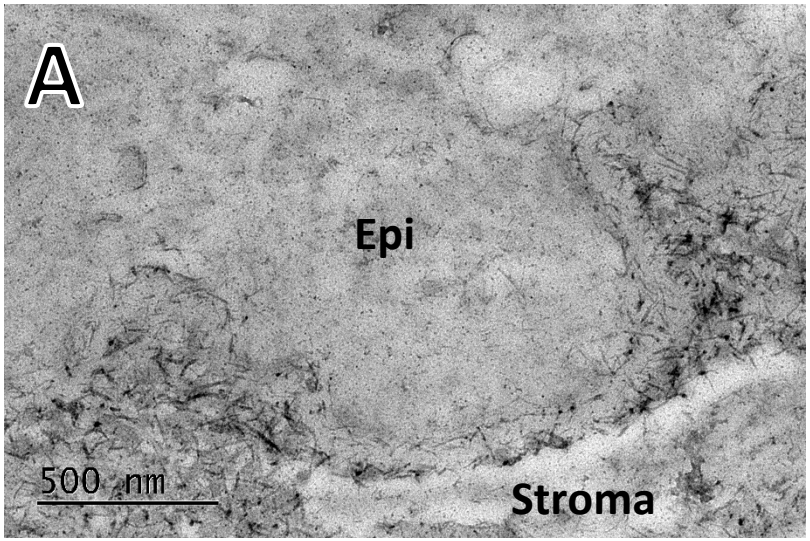
A
Epi
500 nm
Stroma

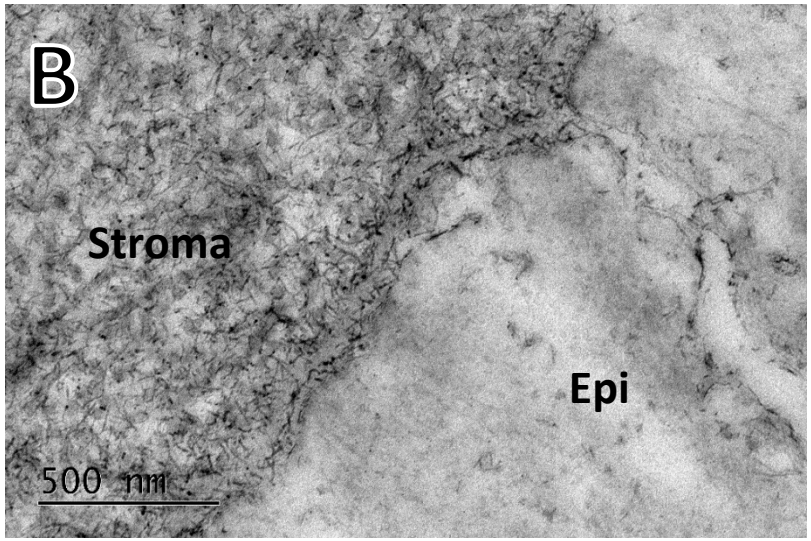
B
Stroma
Epi
500 nm

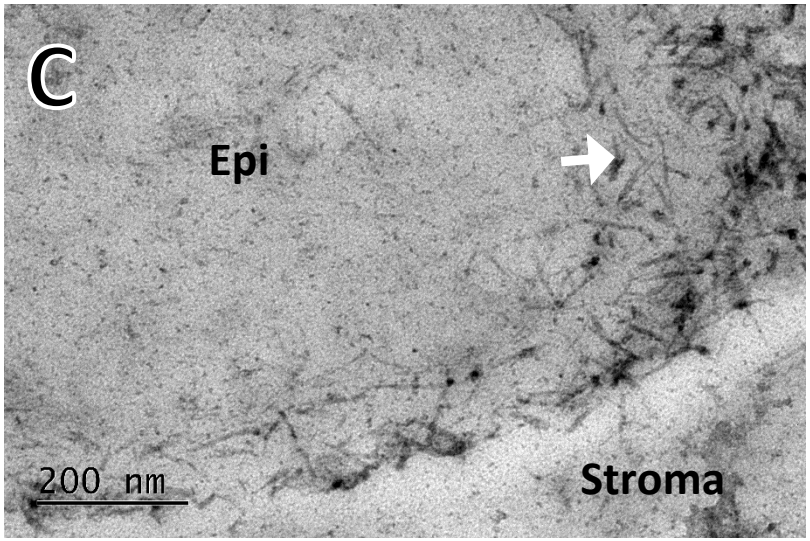
C
Epi
200 nm
Stroma

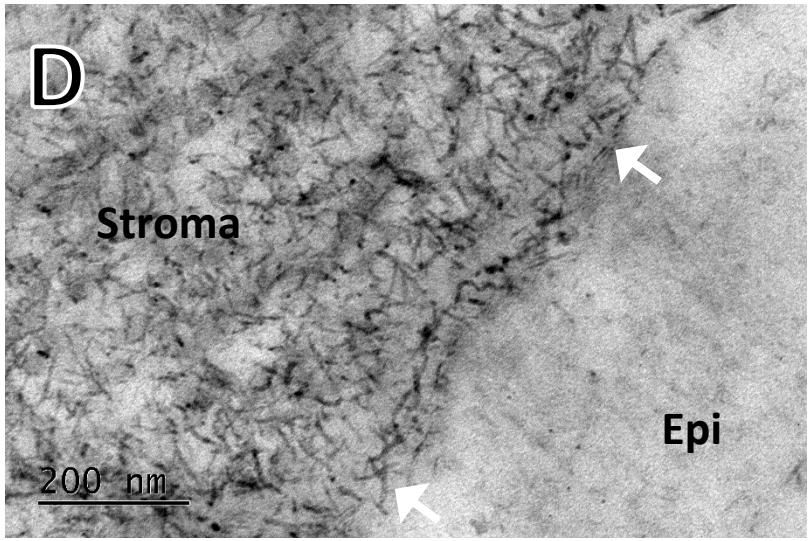
D
Stroma
Epi
200 nm

Figure 4.20- Epithelial basement membrane of the nasal/temporal limbus in enzyme control (A, C) and chondroitinase ABC-exposed (B, D) tissue. ←
Only one side of the nasal/temporal limbus of the chondroitinase-exposed tissue is shown here and no substantial reduction in proteoglycans compared to the control tissue can be seen. White arrows indicate areas of basement membrane where proteoglycans are crossing the gap between proteoglycan linings. Epi = epithelium.

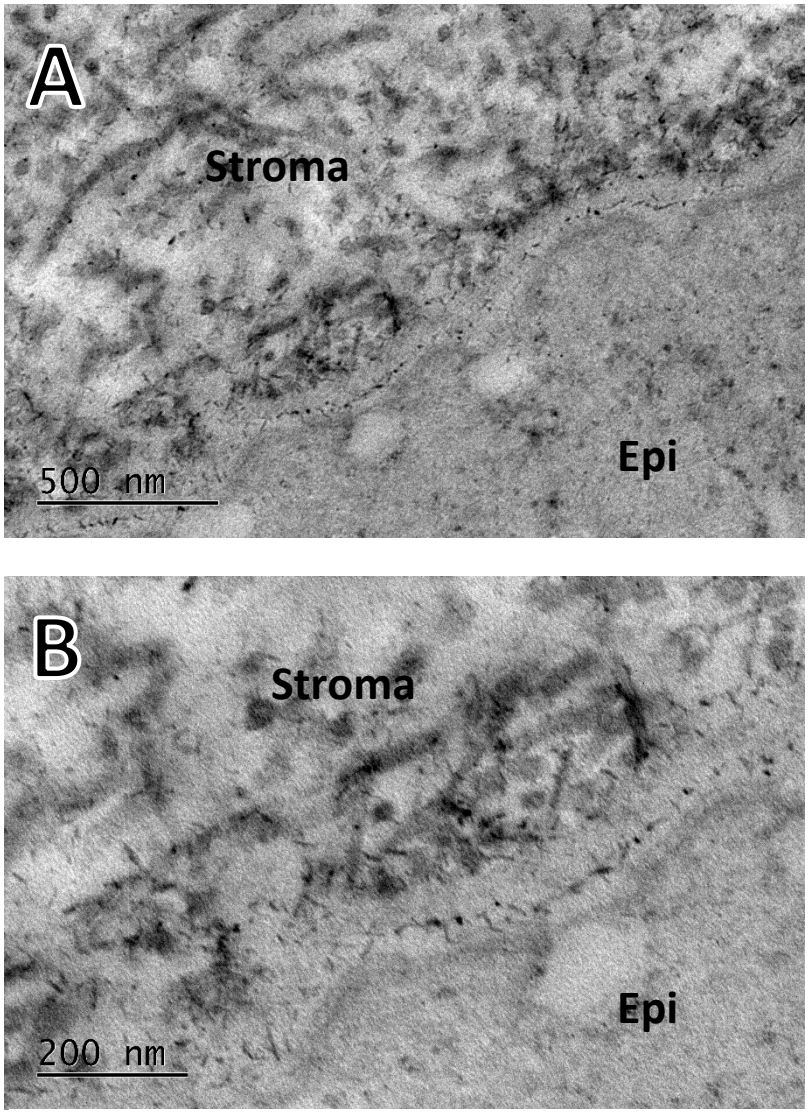

Figure 4.21- Epithelial basement membrane of one side of the nasal/temporal meridian in chondroitinase ABC-exposed tissue (opposite to that shown in Figure 4.20).
Again, the proteoglycans that are present here have collapsed. It also appears that chondroitinase ABC may have reduced the number of proteoglycans. This is the same tissue sample as that shown in Figure 4.17).

As with the untreated eye, an extensively undulating basement membrane was seen in some areas of the limbal samples, in contrast to the central corneal basement membrane where a flat profile was evident. In the chondroitinase ABC-exposed tissue, an irregular basement membrane profile was seen in one of the N/T sections and in one of the S/I sections (Figure 4.22). However, in the enzyme control cornea, both sides of the N/T meridian demonstrated areas of undulating basement membrane (Figure 4.23), as well as one of the S/I sections (Figure 4.24) – though this was to a lesser extent. In all sections, the areas of irregular profile did not constitute the entire length of the limbal basement membrane, with areas of flatter profile also evident.

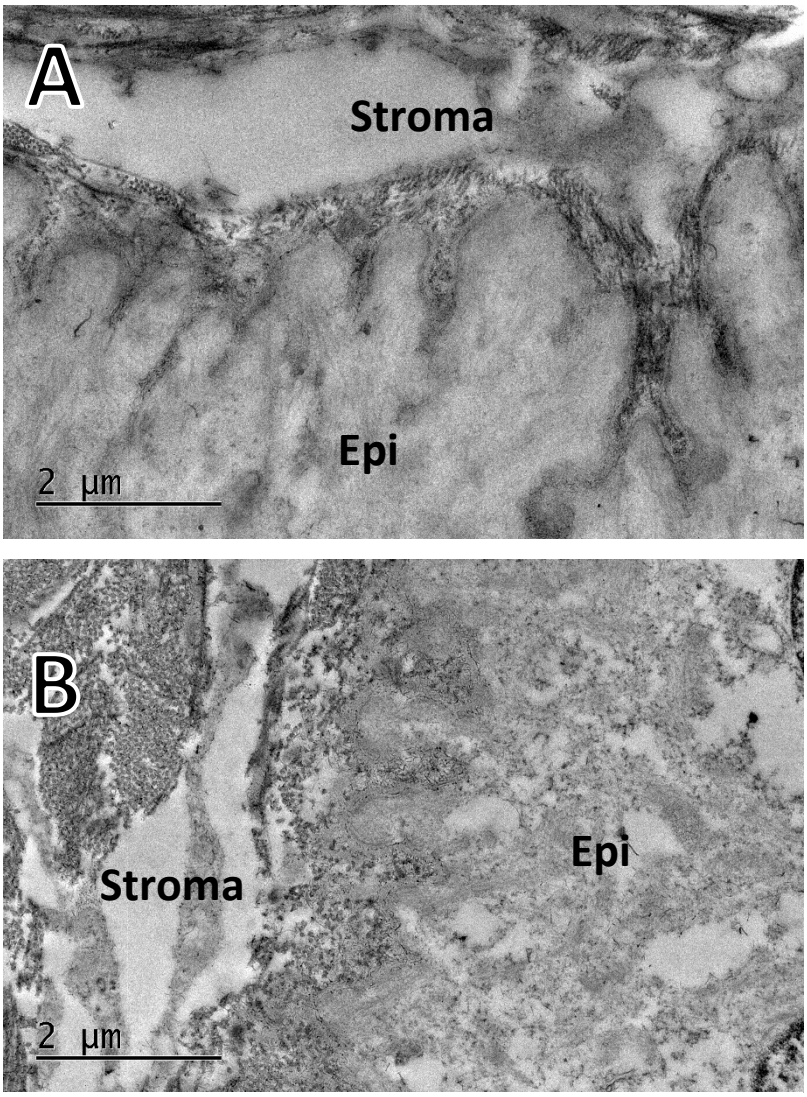

Figure 4.22- The undulating basement membrane of the nasal/temporal (A) and superior/inferior (B) limbal areas of the chondroitinase ABC-exposed cornea.

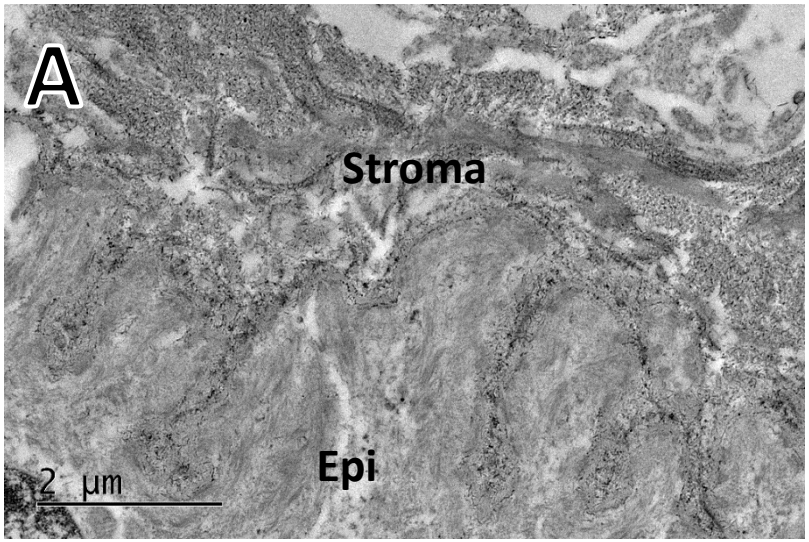
A
Stroma
Epi
2 µm

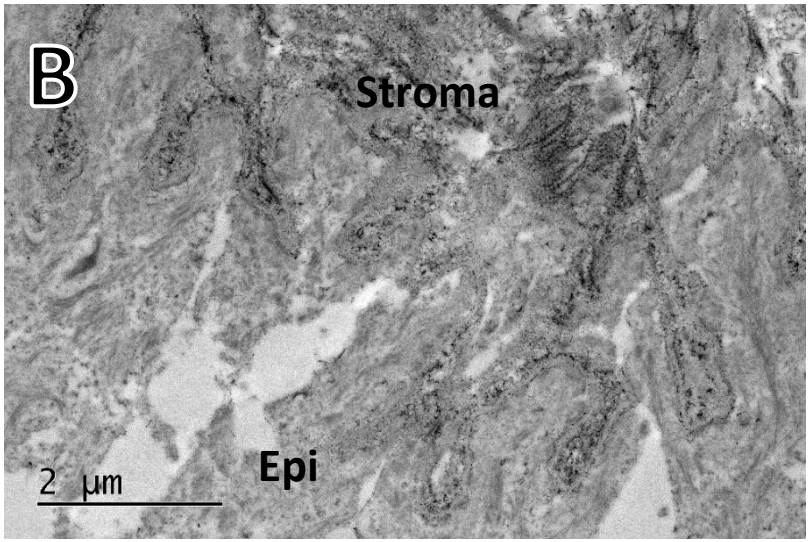
B
Stroma
Epi
2 µm

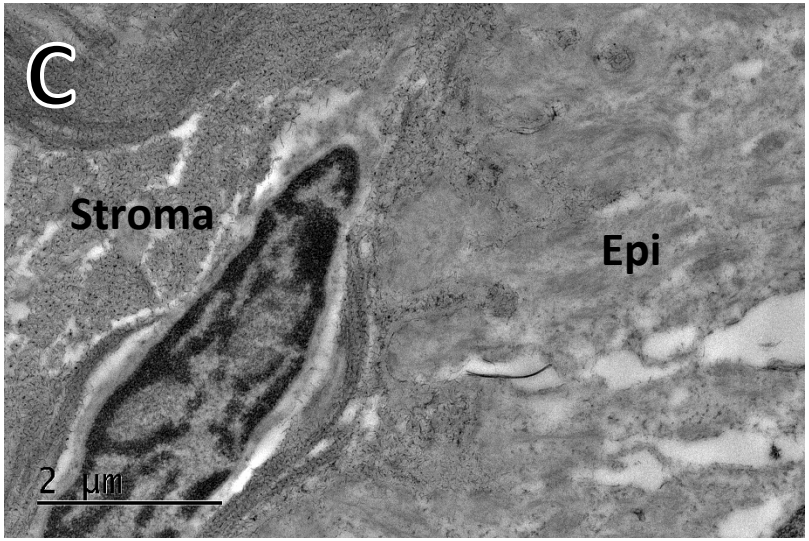
C
Stroma
Epi
2 µm

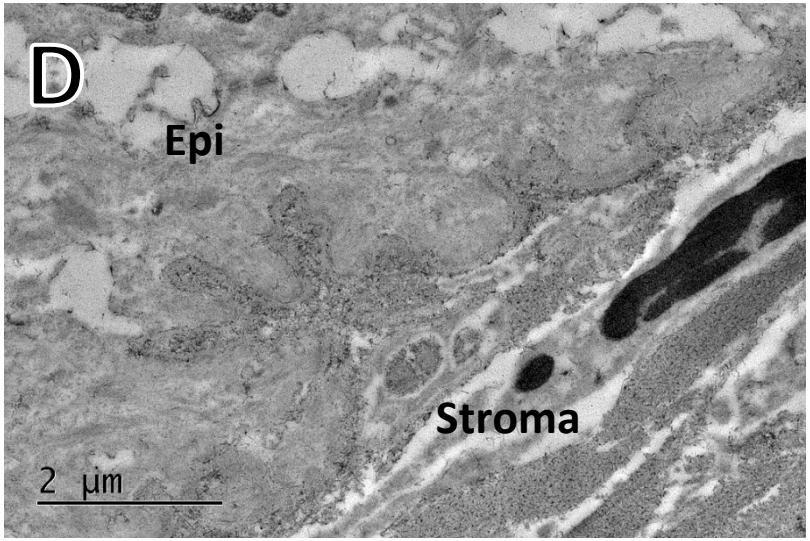
D
Epi
Stroma
2 µm

Figure 4.23- The undulating basement membrane of the nasal/temporal limbus of the enzyme control cornea. ←
A and B demonstrate one side of the nasal/temporal limbus and C and D the other side. One side (A, B) potentially has a more irregular profile than the opposite side. Epi = epithelium.

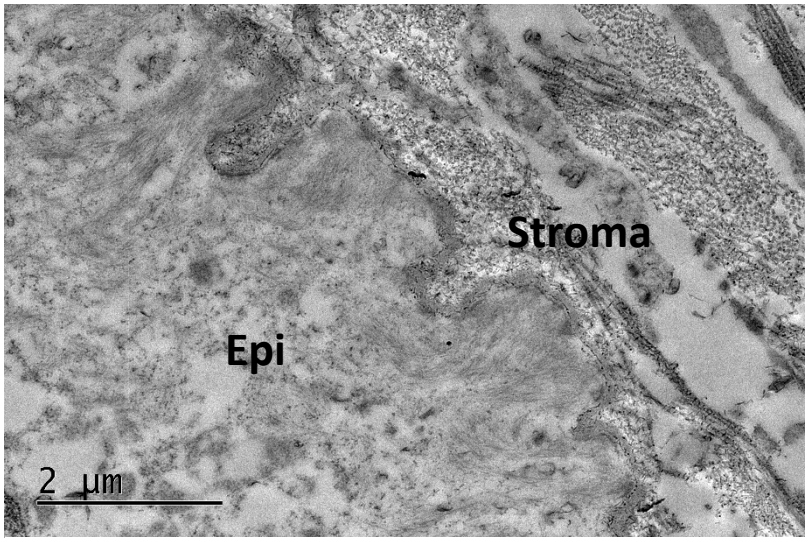

Figure 4.24- The undulating basement membrane of one of the superior/inferior limbal areas of the enzyme control cornea.
Though there are some undulations in the basement membrane, they are less prominent than those seen in the nasal/temporal areas of the same eye (Figure 4.23). Epi = epithelium.

4.3.3 Presence of Bowman's layer

During the TEM investigation, there appeared to be a band of disorganised collagen fibrils subjacent to the basement membrane of the central cornea, distal to stromal lamellae and more organised collagen fibre bundles (Figure 4.25). This was consistently seen in electron micrographs of the central corneal epithelial basement membrane.

This band of disorganised collagen was approximately 1-2 µm wide and was not detected in images taken of the porcine limbus. This was believed to be a potential Bowman's layer within the porcine cornea. There are currently conflicting notions as to whether the porcine cornea does include this layer. This prompted further investigation using SEM to determine if this was Bowman's layer, based on studies by Komai and Ushiki (1991) and Hayashi *et al.* (2002), and to assess whether the limbal trough could also be observed.

Figure 4.25- A transmission electron micrograph of a potential Bowman's layer within the porcine cornea. →
A disorganised band of collagen, with many proteoglycans, can be seen between the epithelial basement membrane (yellow line) and the boundary of the emergence of more organised collagen fibrils (pink line). Epi = epithelium.

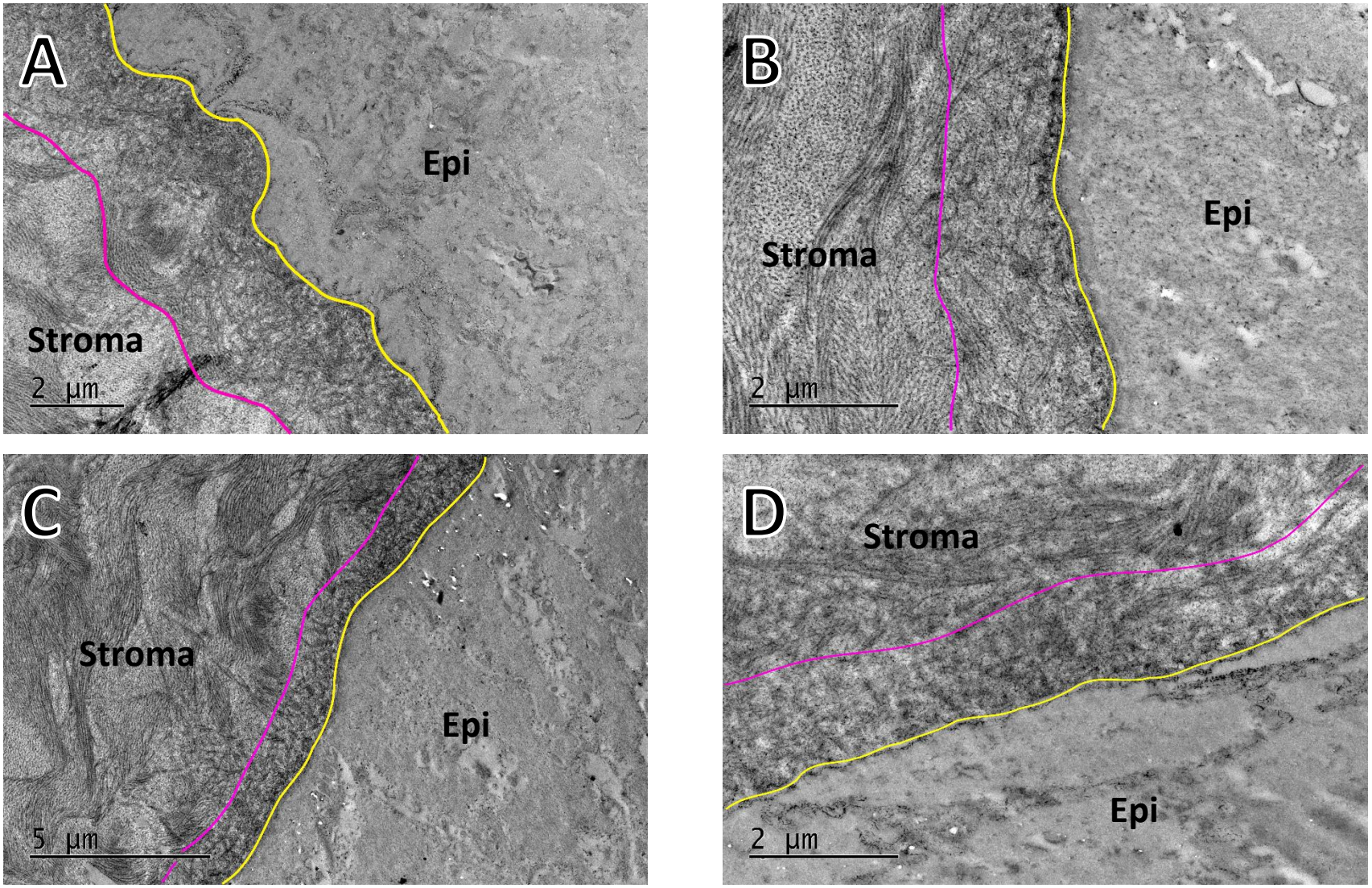
A
Epi
Stroma
2 µm
B
Stroma
Epi
2 µm
C
Stroma
Epi
5 µm
D
Stroma
Epi
2 µm

The decellularised anterior surface of the central cornea was composed of a disorganised meshwork of uniform diameter collagen fibrils (Figure 4.26). This was also true of the peripheral corneal decellularised surface (Figure 4.27). Pores were also seen sporadically across the corneal surface (white arrows).

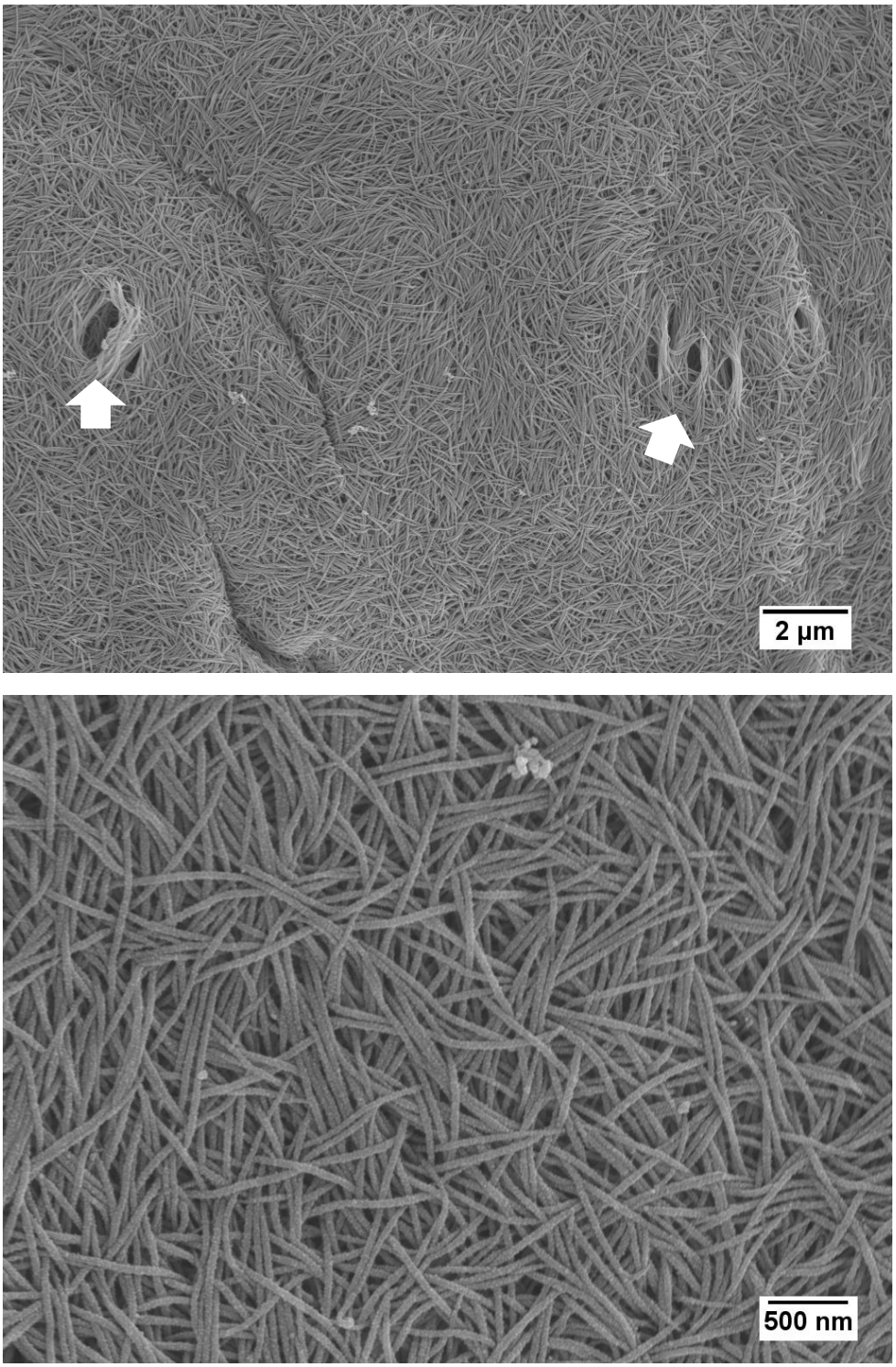

Figure 4.26- Scanning electron micrograph of the central corneal decellularised surface. *The collagen fibrils show no organised alignment in their arrangement. Fibrils run in many different directions and interweave, though all appear to be of the same thickness. White arrows indicate pores in the corneal surface.*

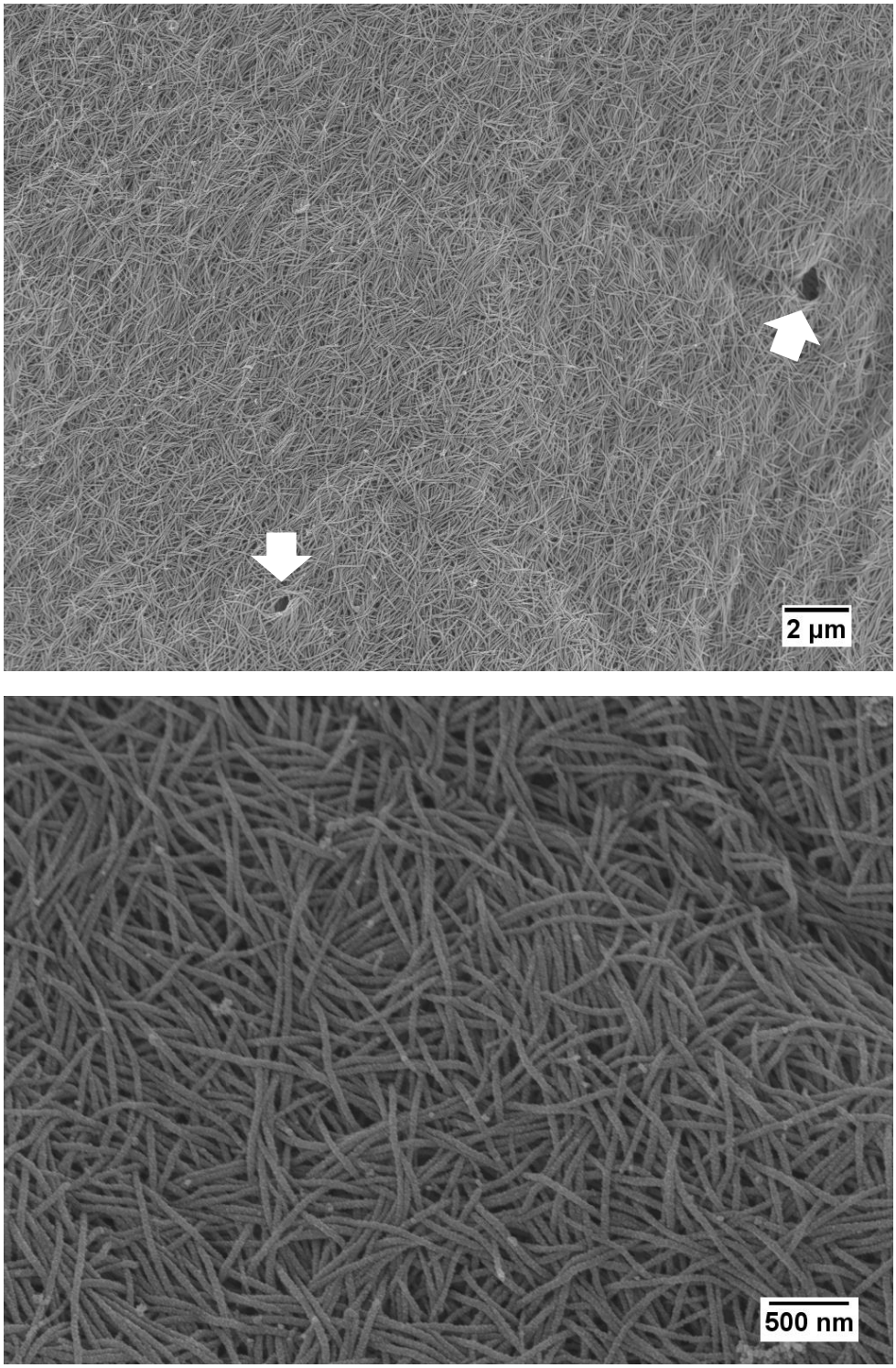

Figure 4.27- Scanning electron micrograph of the decellularised peripheral corneal surface. *Like in the central cornea, the collagen fibrils of the decellularised peripheral corneal surface do not demonstrate any alignment and appear as an interwoven mesh of uniform diameter fibrils. White arrows indicate pores in the corneal surface.*

It was evident in all of the cross-sections of the limbus that the cutting of the tissue had destroyed the structure (Figure 4.28). The collagen lamellae, as well as any other features, could not be distinguished. Thus, these samples were not examined further.

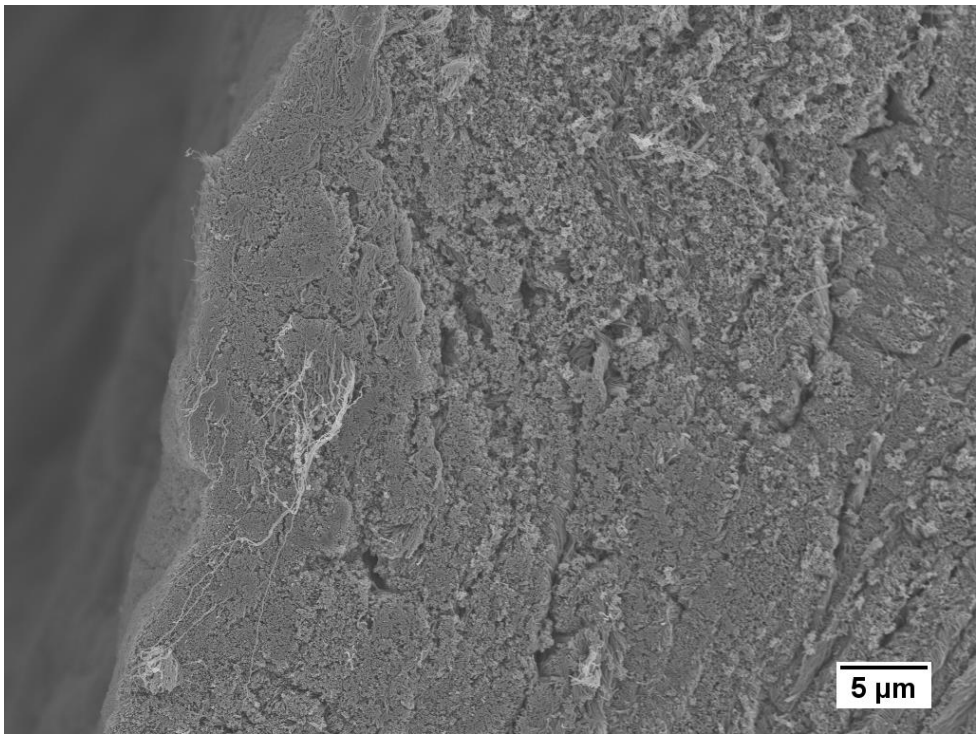

Figure 4.28- Scanning electron micrograph of a cross-section of the limbus.
Cutting through the tissue using a scalpel damaged and distorted the structure and led to all of these sections being unsuitable for examination.

The corneolimbal region had a very different appearance to the central cornea. Distinct zones were identified across the limbal decellularised surface that had differing arrangements of their collagen fibrils (Figure 4.29); this included the peripheral cornea (Figure 4.29, blue arrow) discussed above. Between the peripheral cornea and a relatively highly aligned limbal annulus was a “transition zone” (Figure 4.29, green arrow), which demonstrated the initial stages of alignment of the collagen fibrils. However, interweaving and cross-cutting fibrils were still present (Figure 4.30).

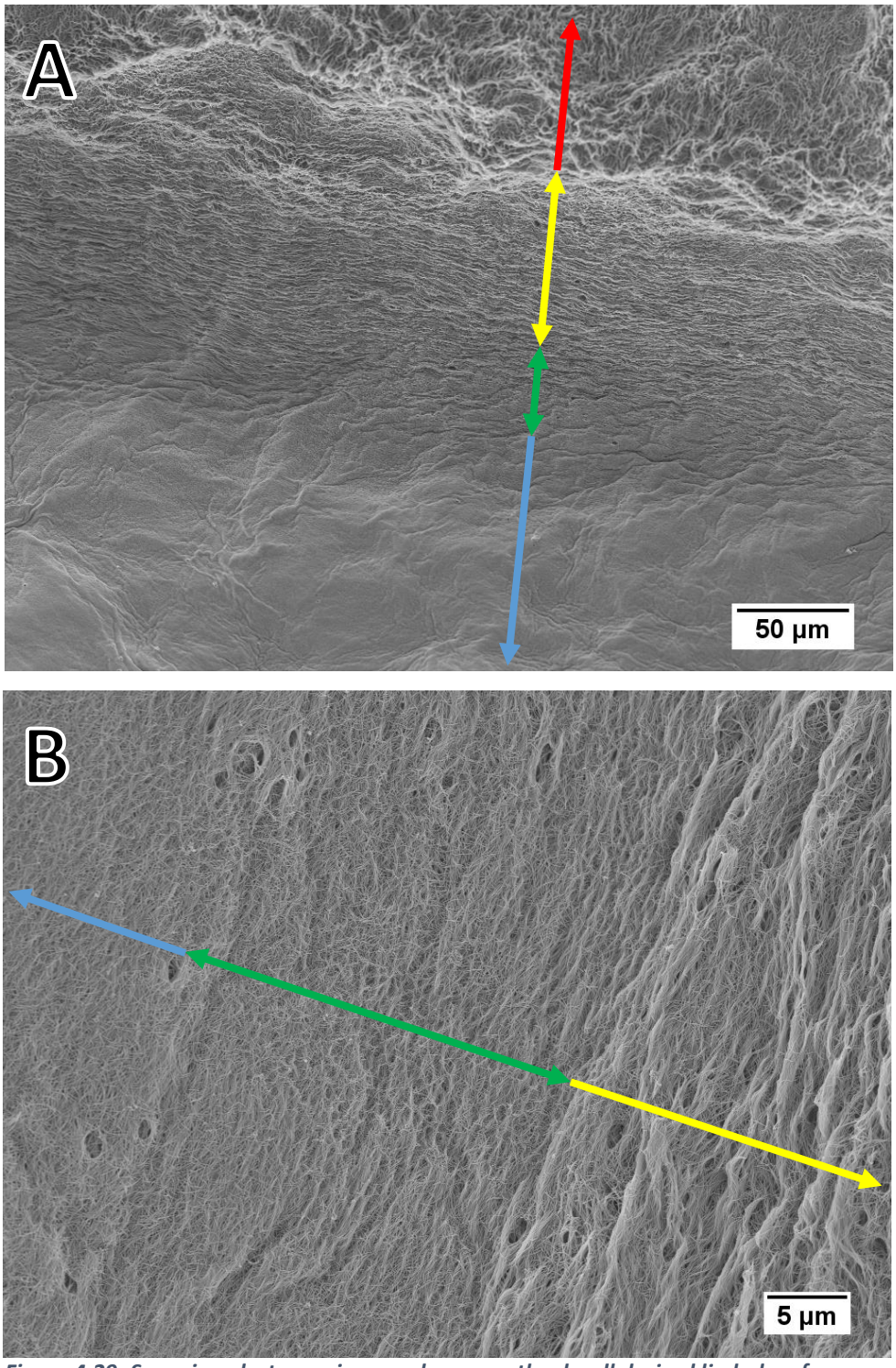

Figure 4.29- Scanning electron micrographs across the decellularised limbal surface. *This region is split into four zones with varying levels of organisation of the collagen fibrils: the peripheral cornea (blue arrow), a transition area (green arrow), an annulus of limbal collagen fibrils (yellow arrow) and the sclera (red arrow) (A). The transition area can be seen at higher magnification in B.*

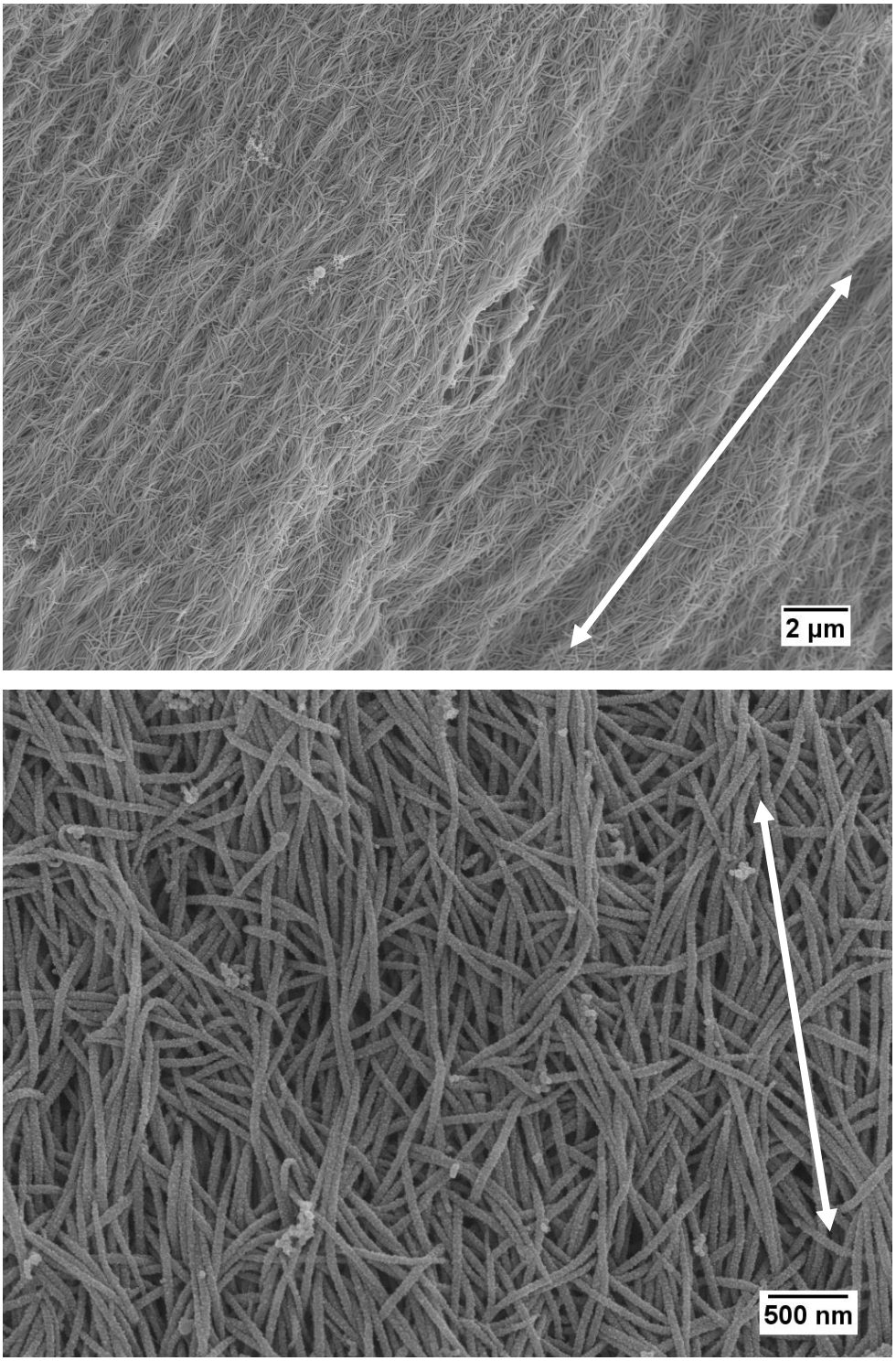

Figure 4.30- Scanning electron micrograph of the "transition zone" between the peripheral cornea and limbus.
In this area, collagen fibrils start to exhibit a more aligned arrangement compared to the central or peripheral cornea. White arrows indicate the direction of this alignment, as calculated by FibrilTool.

A band of highly aligned collagen fibrils, in relation to the rest of the cornea, was seen beyond the transition zone where most of the fibrils were parallel to each other and to the limbal circumference (Figure 4.29, yellow arrow and Figure 4.31). This may be the limbal annulus of collagen, which has been identified in humans and pigs, and consists of aligned fibrils that run circumferentially around the cornea (Newton and Meek 1998; Meek and Boote 2004; Hayes *et al.* 2007).

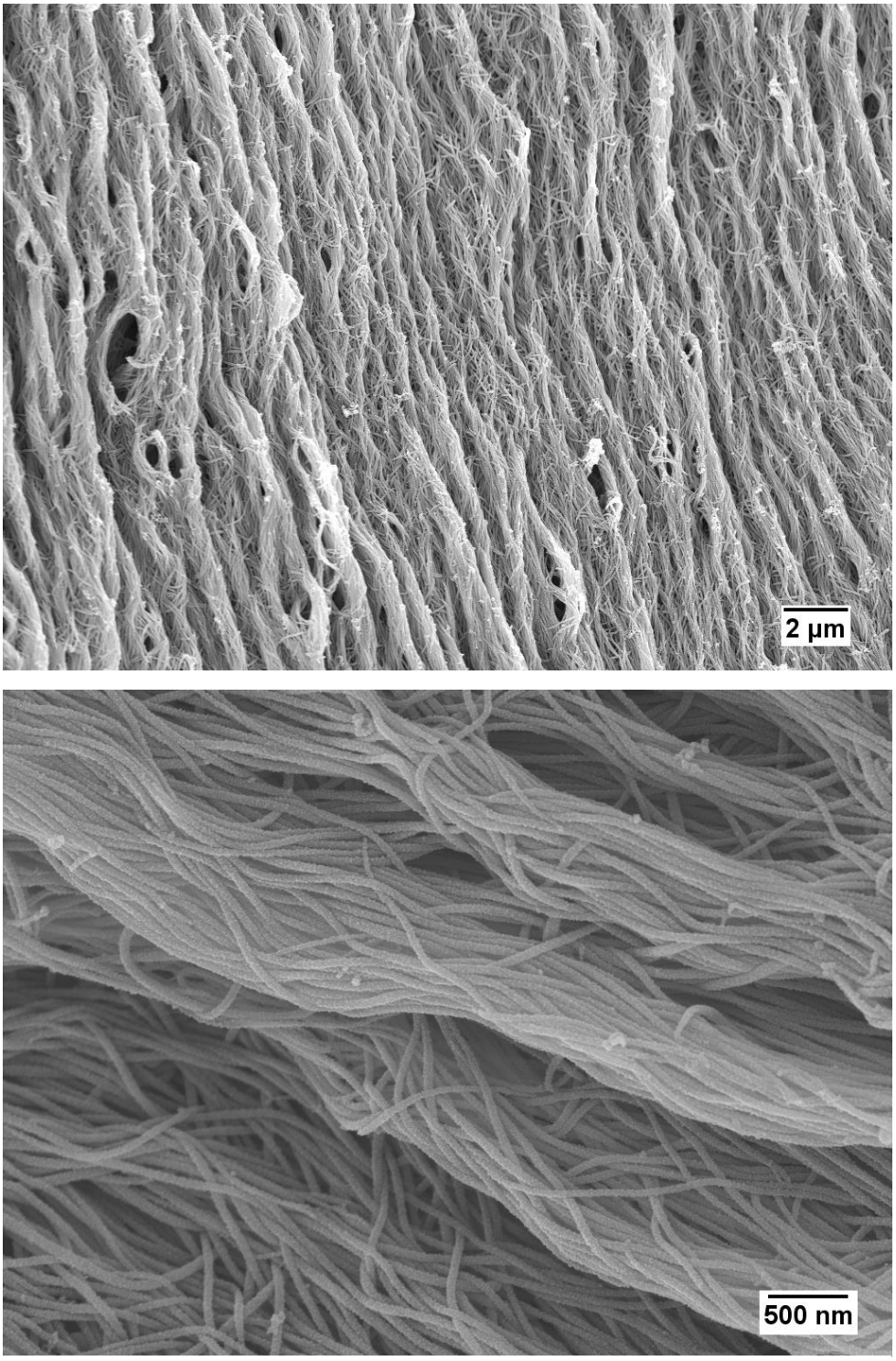

Figure 4.31- Scanning electron micrograph of a limbal annulus of collagen.
Collagen fibrils here are much more aligned than elsewhere and run parallel to the limbal circumference. The different orientations of the fibrils above are due to being from different limbal sites.

Beyond the limbus was the sclera (Figure 4.29, red arrow), which also consisted of disorganised collagen fibrils, though these were very different in appearance to the central corneal surface (Figure 4.32). The collagen fibrils were arranged in bundles and created a very irregular, porous surface. There was no difference in the appearance of the decellularised limbal surface between the different quadrants. No structures resembling the limbal trough were identified.

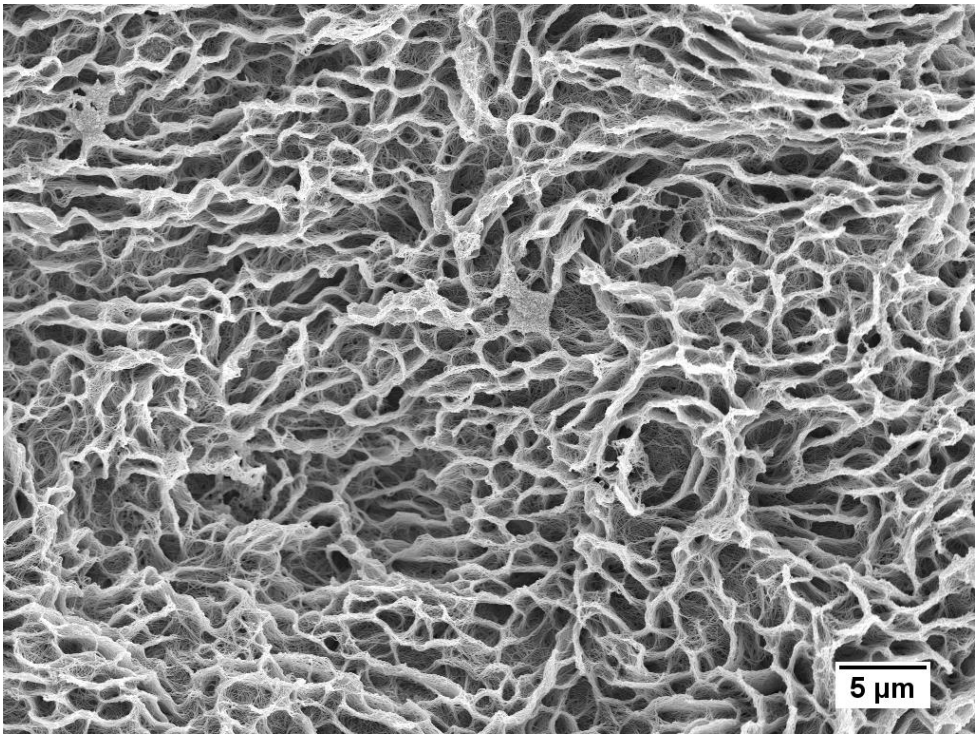

Figure 4.32- Scanning electron micrograph of the decellularised scleral surface.
The collagen organisation of the sclera is noticeably different to that in the cornea and limbus. Though fibrils bundle together, the sclera has a much more irregular surface profile than the limbus or cornea.

The alignment of the collagen fibrils was quantified using the FibrilTool plug-in for ImageJ, which measures the anisotropy of fibrillar arrays within an image and produces a value between 0 (no alignment) and 1 (perfectly aligned) (Boudaoud *et al.* 2014). The data for each of the four regions were normally distributed (Table 4.1). The mean fibril alignment was low for both the central and peripheral cornea at 0.08 ± 0.04 and 0.11 ± 0.05 respectively. These values were found to be significantly different ($p < 0.01$). The transition zone generated a much higher value at 0.23 ± 0.06, which was statistically significantly different to both corneal areas ($p < 0.001$). The limbal annulus produced the highest alignment value of 0.33 ± 0.07, which was significantly different from all other regions ($p < 0.001$). These data are summarised in Figure 4.33.

Location	Test statistic	df	p value
Central cornea	0.111	60	0.063
Peripheral cornea	0.053	60	0.200
Transition zone	0.085	60	0.200
Limbal annulus	0.074	60	0.200

Table 4.1- Kolmogorov-Smirnov test for normality results for the pooled data.
A p value < 0.05 indicates data are not normally distributed.

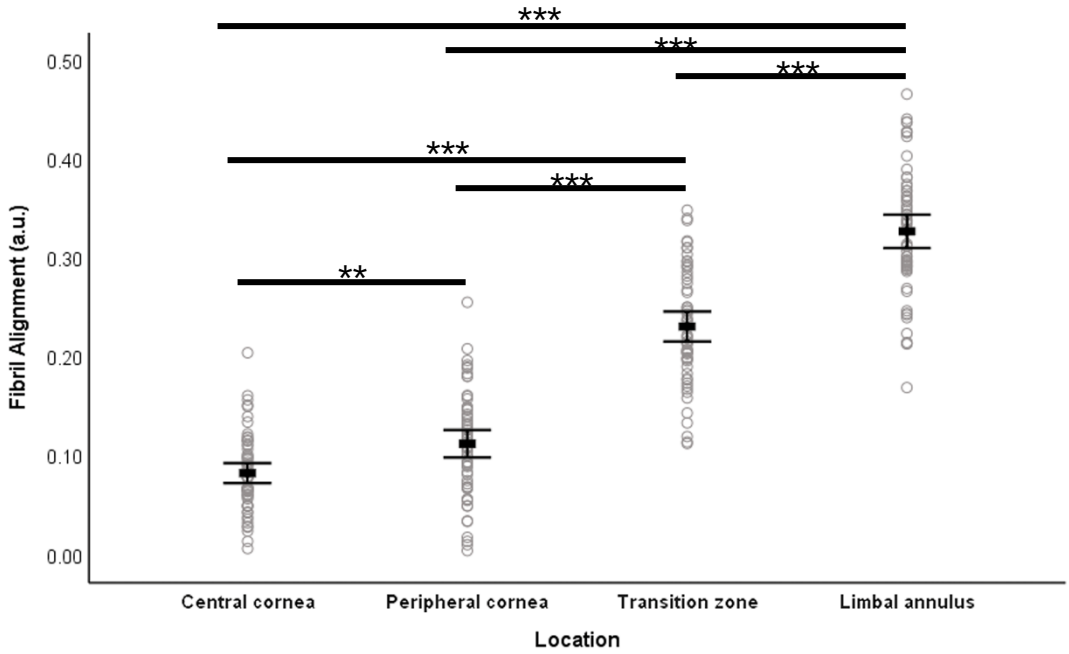

Figure 4.33- Collagen fibril alignment data for four different areas of the corneal and limbal decellularised surface.

*All of the areas have significantly different levels of collagen fibril alignment. Minimal fibril alignment in the distal stroma of both central and peripheral regions of the porcine cornea appears to represent a genuine Bowman's layer, which transforms across the transition zone, via a noticeable change in the isotropic nature of the fibrils, into the significantly more aligned limbal annulus of collagen. ** p < 0.01, *** p < 0.001. Black bars represent means with 95% confidence intervals.*

The data presented above were pooled from all three eyes that were investigated; differences within and between the three eyes were also examined (Figure 4.34). All of the data were normally distributed, except for the central cornea of the first eye (Table 4.2). However, this dataset does include two outliers and when 80% Winsorisation is applied then the distribution becomes normal. Thus, when comparing the different regions of the first eye, and when comparing the central corneas of all three eyes, both the original mean and the 80% Winsorised mean will be included. The mean fibril alignment of the central cornea of the first eye was 0.07 ± 0.03 and this became 0.06 ± 0.02 after 80% Winsorisation.

Eye	Location	Test statistic	df	p value
1	Central cornea	0.209	20	0.022
	Central cornea (80% Winsorised)	0.141	20	0.200
	Peripheral cornea	0.144	20	0.200
	Transition zone	0.128	20	0.200
	Limbal annulus	0.121	20	0.200
2	Central cornea	0.136	20	0.200
	Peripheral cornea	0.111	20	0.200
	Transition zone	0.152	20	0.200
	Limbal annulus	0.138	20	0.200
3	Central cornea	0.143	20	0.200
	Peripheral cornea	0.082	20	0.200
	Transition zone	0.164	20	0.164
	Limbal annulus	0.111	20	0.200

Table 4.2- Kolmogorov-Smirnov test for normality results for separate eyes.
A p value < 0.05 indicates data are not normally distributed.

For all eyes, significant differences were found between the mean fibril alignment of all the different areas of the corneal/limbal surface (Figure 4.34) except for between the central and peripheral cornea of the second eye (0.11 ± 0.04 and 0.12 ± 0.05 respectively, $p > 0.05$) (Figure 4.34B). The Winsorised mean of the central cornea of the first eye and the original mean resulted in the same levels of statistically significant differences when compared to the other regions of that eye.

Between the three eyes, there was no significant difference between the mean alignments of the peripheral cornea or the transition zone. However, fibril alignment of the central cornea of the second eye was significantly higher than the first and third eyes; 0.11 ± 0.04 compared to 0.07 ± 0.03 [original mean] ($p < 0.001$)/0.06 ± 0.02 [80% Winsorised mean] ($p < 0.001$) and 0.07 ± 0.03 ($p < 0.001$) respectively. The limbal annulus was also found to be significantly less aligned in this eye than the other two (0.28 ± 0.05 compared to 0.35 ± 0.05 ($p < 0.001$) and 0.36 ± 0.06 ($p < 0.001$)). Yet, the same general pattern could be seen in each eye, in that fibril alignment increased with increased eccentricity.

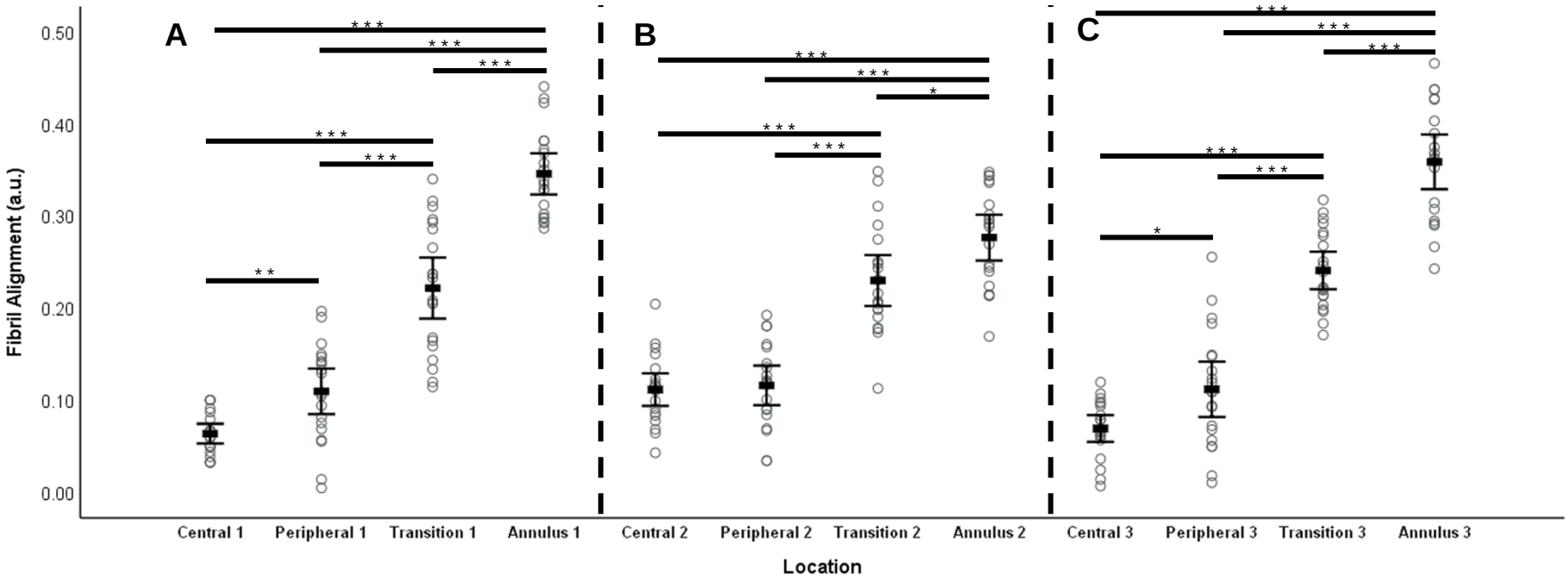

Figure 4.34- Collagen fibril alignment data for different areas of the ocular surface for each individual eye examined.
*Each eye demonstrates greater alignment of the collagen fibrils with increased corneal eccentricity. There are significant differences between all areas in each eye, except between the central and peripheral cornea of the second eye (B). The data shown here for the central cornea of the first eye (A) have undergone 80% Winsorisation. * $p < 0.05$, ** $p < 0.01$, *** $p < 0.001$. Black bars represent means with 95% confidence intervals.*

4.4 Discussion

4.4.1 Anterior stromal collagen lamellae

In the current study, PGs were observed along the length of central corneal collagen fibrils and in between them in a seemingly disorganised arrangement. Bovine corneas were examined using cupromeronic blue staining by Scott and Haigh (1988a) and keratanase/chondroitinase ABC treatment revealed apparently specific axial associations of PGs with collagen fibrils. Collagen fibrils consist of repeating sections, termed a D period, comprised of twelve bands: a_1, a_2, a_3, a_4, b_1, b_2, c_1, c_2, c_3, d, e_1 and e_2 (Chapman 1974; Chapman *et al.* 1990). Scott and Haigh found that KS is associated with the a and c bands of fibrils, whilst CS/DS is associated with the d and e bands. An earlier study on rabbit corneas matches these findings (Scott and Haigh 1985). In the current investigation, the banding of collagen could not be easily seen in the untreated tissue samples, thus it is not possible to say where the PGs are binding. This was also found to be true for much of the enzyme-digested and enzyme control tissues. Cellular features are also not well contrasted in cupromeronic blue-stained specimens due to the lack of osmium staining.

Vast amounts of PGs are found within the corneal limbus, which is comparable to the central cornea (Scott and Haigh 1985; Meek *et al.* 1989; Lewis *et al.* 2010). The collagen arrangement here is still in a lamellar format, as in the central cornea, however, the PG arrangement along the fibrils is more similar to that of the sclera. The PGs are very regularly spaced along longitudinal collagen fibrils, seemingly appearing once within a D period. PGs have been found to associate with the d band of scleral collagen fibrils in both humans and rabbits (Young 1985; Quantock and Meek 1988), thus demonstrating this very regular periodicity. As the limbus is the transition zone between the cornea and sclera, it seems logical that the collagen/PG arrangement here would have characteristics of both tissue types. As the banding pattern could not be resolved clearly in the current study, it is not possible to say whether the limbal PGs also associate to the d band in the porcine cornea.

The PG distribution in normal and keratoconic human central corneal stromas has been compared by Sawaguchi *et al.* (1991) using cuprolinic blue staining. Both "thin" and "medium" types of cuprolinic blue-positive filaments are present in the cornea. These were found to run transversely to longitudinal collagen fibrils, which matches the current investigation's findings, though some PGs will also run parallel to the fibrils. By using the enzyme treatments chondroitinase ABC and keratanase, Sawaguchi and associates found that the medium and thin filaments are DS and KS PGs respectively. From images taken of the porcine central stromal collagen lamellae, where chondroitinase ABC appeared to have removed certain PGs, the thin and long PG filaments were removed. This suggests that these were the CS/DS PGs and the remaining shorter and thicker PGs were KS in the porcine cornea.

Ho *et al.* (2014) expanded on Borcherding *et al.'s* study (1975) into corneal PG distribution when investigating bovine corneas. They showed that the distribution of KS and DS PGs is uniform across both the depth and width of the cornea. However, CS is only detected towards the outer periphery of the tissue/at the limbus. The total amount of sulphation of GAGs does not change with corneal eccentricity suggesting that, despite a change in the proportion of GAG molecules, the amount of sulphation of all the GAGs combined does not change. Interestingly, it was found that the amount of low-sulphated KS increases significantly in the outer periphery/limbus, whilst high-sulphated KS maintains a uniform distribution. Ho's study examined PG distribution in relation to collagen organisation and they found that the increase in low-sulphated KS does not correspond to any changes in collagen diameter or spacing. Potentially, the results of Ho *et al.* could relate to Hayes *et al.*'s theory (2008) based on the distribution of CS/DS in the cartilage stem cell niche: that higher-sulphated CS epitopes may be responsible for inducing differentiation, whilst non- or minimally 4-sulphated CS PGs block binding of growth factors by acting as a physical barrier to this and maintain stemness. Particularly as no change in collagen organisation was found to correlate with the changes in GAG distribution in the bovine cornea, potentially this could relate to other functions, such as directing cell fate. However, the effect of KS in stem cell niches has not been examined in detail before.

4.4.2 Epithelial basement membrane

PGs are a prominent feature of the epithelial basement membrane in both the central cornea and at the limbus. There do not appear to be any significant differences between the central corneal basement membrane and the limbal basement membrane, though there are potentially less PGs lining the epithelial side of the limbal basement membrane compared to the central in all the tissue samples examined. It is not possible to say whether this is due to an equal reduction in both KS and CS/DS PGs in the limbal basement membrane, or whether one of these GAG types is less numerous here, due to the amount of PGs being similar between the chondroitinase-exposed tissue and the control tissue. However, there does seem to be a reduction in basement membrane PGs in the central cornea after exposure to chondroitinase ABC. Again, it appears to be the longer, thinner PGs that have been removed. The PGs present along the corneal basement membrane after chondroitinase exposure do not look the same as those along the limbal basement membrane, so it can be tentatively assumed that the lesser number of PGs along the limbal basement membrane is not due to a lack of CS PGs here.

There also appeared to be a reduction in the number of PGs after chondroitinase ABC exposure in one quadrant of the N/T meridian. However, many of the PGs had collapsed; thus, the number of PGs may not have actually reduced, with it only appearing so as the PGs are much smaller in this form. This brings into doubt whether there was any genuine chondroitinase ABC activity in this tissue segment.

No differences could be seen between the basement membrane of the S/I limbus and the N/T; however, the basement membrane seemed to have a much more undulating profile in some areas. This is reminiscent of Yamada *et al.*'s work on the rabbit limbus (2015). Though no LC- or Palisade of Vogt-like structures were observed in any quadrant of the rabbit limbus, the limbal basement membrane was found to be very irregular in all areas and was believed to represent a "miniaturised" version of the Palisade structures. This is interesting, as no LCs were found in the porcine limbus in the previous chapter – instead the limbal trough was identified – and there is potentially another stem cell niche-associated feature in the porcine limbus. This undulating basement membrane was also seen in both the

S/I and N/T limbus, though the most irregular profile was usually found in the N/T quadrants.

When comparing the opposite sides of the same meridian, i.e. comparing the superior limbus to the inferior and the nasal to the temporal, no major differences could be seen. The only possible variation was that either the nasal or temporal limbus had a more undulating basement membrane profile than the opposite side in two of the eyes examined, but this was not the case in the third. However, as previously stated, it is not possible to differentiate superior from inferior or nasal from temporal in this experiment. This is something that requires further attention.

4.4.3 Bowman's layer

The presence of Bowman's layer in the porcine cornea has been debated for several years. Du *et al.* (2011) and Zhang *et al.* (2019) report finding Bowman's layer in decellularised porcine corneas and Bueno *et al.* (2011) mention detecting Bowman's layer in the porcine cornea using second harmonic generation microscopy, stating that it was 15-20 µm thick. Lange *et al.* (1989) also report a porcine Bowman's layer of 10 µm thick, but do not present any images or data to support this. Multiple sources state that there is no Bowman's layer within porcine tissue (Merindano *et al.* 2002; Svaldenienė *et al.* 2003; Nautscher *et al.* 2016; Patruno *et al.* 2017). In the current investigation, a layer of disorganised collagen fibrils directly subjacent to the porcine central corneal epithelium was observed, reminiscent of the human Bowman's layer presented by Komai and Ushiki (1991) and Birk (2001).

Using the measured thicknesses of Bowman's layer and of the substantia propria (stroma + Bowman's layer) from electron microscopy images analysed by Hayashi *et al.* (2002), the relative percentage contribution of Bowman's layer to corneal thickness for several mammalian species can be calculated (Table 4.3). Species classically considered as lacking Bowman's layer often yield a very low percentage, considerably below the 2.9% recorded for the human cornea. From measurements taken from 3 points across 10 images of Bowman's layer in the current investigation, an average thickness of 0.94 ± 0.15 µm was calculated for a potential porcine Bowman's layer. This equates to the porcine Bowman's layer comprising

approximately 0.2% of corneal thickness, based on an approximate stromal thickness between 465 and 573 µm (from measurements collated by Akhbanbetova et al. (2017), Nautscher et al. (2016) and Abhari et al. (2018)). As the representative proportion of total corneal thickness is so low in the porcine cornea, a lack of imaging resolution may have prevented identification of Bowman's layer in previous investigations.

Species	Thickness of Bowman's layer (µm)	Thickness of stroma + Bowman's layer (µm)	% of substantia propria thickness comprised of Bowman's layer
Rabbit	3	250	1.2
Guinea pig	1	270	0.4
Rat	1	88	1.1
Pig	0.94	~465-573	0.2
Cow	5	800	0.6
Human	10	340	2.9

Table 4.3- The proportions of the substantia propria thickness, comprising stroma and Bowman's layer, that is contributed by Bowman's layer.
Measurements for all species, except the pig, are from Hayashi et al. (2002). The human stromal thickness measured here is considerably less than the physiological thickness, presumably due to the shrinkage of collagen fibril diameter and spacing that is caused by processing for electron microscopy (Fullwood and Meek 1993).

In all species examined by Hayashi *et al.* (2002), the epithelial surface of Bowman's layer is composed of randomly-arranged collagen fibrils, in contrast to the well-organised structure of the corneal stroma. The same is also true for human tissue, as demonstrated by Komai and Ushiki (1991). The porcine cornea was not included in Hayashi *et al.*'s work and has hitherto been omitted from other investigations of this unique stromal layer. The decellularised epithelial surface of the central porcine cornea also demonstrates the disorganised collagen fibril arrangement as found in other species. It is particularly similar to rat and rabbit corneas presented in Hayashi *et al*.'s investigation and to the appearance of the human Bowman's layer in Komai and Ushiki's investigation.

The collagen arrangement of the peripheral cornea of the porcine eye demonstrates the same organisation as the central cornea. This leads to the conclusion that there is a structure representative of Bowman's layer in the porcine

cornea. The similarity between the central and peripheral cornea also includes the presence of pores, which have been proposed as the channels for corneal nerves (Komai and Ushiki 1991). However, in the periphery, these pores may also represent a conduit for the passage of processes from stromal cells that have been identified, and their direct interaction with epithelial cells confirmed, in the peripheral cornea/limbal region of rabbits and humans (Dziasko *et al.* 2014; Yamada *et al.* 2015). These keratocyte processes are believed to be a component of the limbal stem cell niche. Whether these processes are also present in porcine tissue will be investigated later in this thesis.

The collagen arrangement in the porcine limbus is significantly different to the central and peripheral cornea. As Bowman's layer terminates at the limbus (Remington 2012), this change is to be expected and a transition zone between the peripheral cornea and a significantly more organised limbal annulus of collagen has been identified in this investigation. Here, collagen fibrils demonstrate a significant degree of isotropy, but the initial stages of alignment are evident. The limbal annulus of collagen observed here may not be the same annulus that was proposed by Newton and Meek (1998) and Hayes *et al.* (2007), as later investigations found that this was situated in the posterior stroma of human corneas (Kamma-Lorger *et al.* 2010). However, the depth of this annulus in the porcine cornea has not been determined; thus, the limbal annulus presented in this investigation could be part of an annulus that spans much of the thickness of the cornea or could represent a separate, superficial limbal annulus. The statistically significant differences in fibril alignments between the transition zone and the peripheral Bowman's layer, and between the transition zone and the limbal annulus, further demonstrate the distinct nature of this zone. However, though the limbal annulus is highly aligned relative to the rest of the corneal/limbal surface, it still demonstrates a sizeable degree of isotropy. A value of 1 using FibrilTool represents perfect alignment (Boudaoud *et al.* 2014) and the annulus generated mean values of approximately 0.3.

It is surprising that the collagen fibrils of the porcine Bowman's layer become significantly more aligned between the central and peripheral cornea. Visually,

these two areas look identical and it was unexpected that collagen fibril alignment would be significantly different between them. Potentially, this means there is a very gradual increase in fibril alignment across the corneal surface with greater distance from the centre, until a sudden increase in alignment at the transition zone and another significant increase in alignment within the limbal collagen annulus. However, these highly significant increases in alignment demonstrate the notable change in collagen organisation and give further support to the presence of a Bowman's layer in the porcine eye.

The three eyes used to assess collagen fibril alignment mostly provided similar results. The first and third eyes showed no significant difference to each other in their anisotropy values for any of the four regions. The peripheral cornea and transition zone of the second eye were also not statistically different to the other two eyes. However, the central Bowman's layer was significantly more aligned in this eye and the limbal annulus significantly less aligned than the other two eyes. One possibility for the difference in the limbal annulus could be the presence of a greater number of pores here in this eye. Collagen fibrils run circumferentially around the pore openings, leading to the fibrils being less aligned to the general direction of alignment of the rest of the collagen in the annulus. The opposite occurs around pores in the putative Bowman's layer – fibrils become more aligned around these pores than the surrounding fibrils.

4.4.4 Limitations

There were numerous obstacles in this investigation. Chief amongst these was the uncertain activity of the chondroitinase ABC enzyme. As aforementioned, the enzyme appears to have been effective on the central corneal tissue segment, with a very clear reduction of PGs visible. Furthermore, it is a clear subtype of cupromeronic blue dye-stained PGs that have been removed in this segment – the longer, thinner PG filaments. However, there does not appear to be any removal of PGs in three of the four limbal segments. The limbal segment that does potentially show some removal of PGs is ambiguous, as the PGs that are present appear to have collapsed. Thus, potentially there has been no reduction in the amount of PGs and it only appears so as the collapsed PGs are so much smaller.

There are three possibilities concerning this lack of chondroitinase ABC activity at the limbus:

- The limbus contains a much larger population of KS PGs than CS/DS PGs and therefore a negligible reduction in PGs will be visible
- The CS/DS PGs found at the limbus are chondroitinase ABC-resistant
- The chondroitinase ABC did not fully penetrate into the limbal tissue.

The first two options seem unlikely, with the third being the most probable. The tissue segments needed to be fairly large due to limitations in dissecting the tissue and ensuring they could be handled easily. The tissue segments also had to be kept rectangular in shape to allow correct orientation after staining with cupromeronic blue dye, as the tissue became uniformly dark blue throughout after this. This large size could have limited the penetration of the enzyme into the limbal tissue, particularly as it includes tougher, denser scleral tissue. In addition, central corneal tissue is more prone to swelling than peripheral or limbal tissue; this may have facilitated greater penetration of the enzyme into the central tissue and account for the degradative activity seen here but not in limbal tissue.

This theory is brought into question if the chondroitinase ABC was effective on one of the four limbal segments. However, as the same batch of enzyme was used for all limbal segments and the central cornea, and all segments were of similar size, it seems unlikely that it would have different activity in just one of the limbal samples. It is more likely that all PGs are present in the one N/T sample and have all collapsed, though the reason for this collapse is also difficult to determine.

One possible remedy to this issue would be to use keratanase or endo-β-galactosidase to remove the KS PGs. Using this alongside the chondroitinase ABC could help support or reject the first and third possibilities mentioned above. If the first theory is correct, then a near total removal of PGs would be observed in keratanase- or endo-β-galactosidase-digested tissue and if the third is correct, then no enzyme activity would be observed. Ultimately, the inclusion of KS degradation was decided against due to the greater difficulty in accessing the appropriate enzymes, the already considerable number of failed experiment attempts, and time

constraints. However, utilising both KS and CS/DS PG digestion would be the best route to explore in future investigations.

Another issue is the inability to distinguish between superior and inferior limbus, and between nasal and temporal. Differences between two sides of the same meridian were not expected in this investigation and, so, this inability was not considered to be of too much concern. Yet, there were some differences – such as the undulations of the limbal basement membrane. If these differences were found to be consistent across all the eyes examined, then further effort would have been made to ensure the full orientation of the eyes. As these differences varied between specimens, it was decided not to endeavour to orient the eyes fully due to the considerable extra effort this would require.

4.4.5 Conclusions

An unexpected conclusion of this investigation is that the porcine cornea does include Bowman's layer, despite previous reports to the contrary. However, it is very thin and constitutes a small percentage of the corneal thickness, particularly when compared to the human cornea. Yet, this does mean that the porcine cornea is more similar to its human counterpart than currently believed, making it an even more suitable model for the human cornea.

PGs are clearly an important part of corneal and limbal structure, with vast amounts seen in both areas. The finding of limbal stromal collagen lamellae that start to demonstrate a PG distribution more similar to the sclera is coherent, as this is the transition area between the cornea and sclera. Thus, there is a difference in PG arrangement between the central cornea and the limbus, and this includes the epithelial basement membrane. This could potentially contribute to the difference in the extracellular environment that drives different cell fate decisions.

It appears that the PG profile around the limbus may be similar for all quadrants. At present, it appears that the porcine limbus is fairly homogenous around its entire circumference, a finding in agreement with the previous chapter. However, it is still not certain whether the porcine LESCs actually reside within the limbal trough that has been identified and this needs clarification. Yet, so far, it appears that the

general PG distribution does not differ and LESCs may potentially be found around the entire limbal circumference.

5 Immunolocalisation of chondroitin sulphate sulphation motifs and putative stem cell markers in the porcine limbus

5.1 Introduction

Stem cells, from both developing and more mature joint tissue, and their interactions with CS in the ECM have been investigated previously (Hayes *et al.* 2008; Hayes *et al.* 2011; Melrose *et al.* 2012; Hayes *et al.* 2016). Much of this work has been carried out with the use of monoclonal antibodies. Hayes *et al.* (2008) used antibodies to different CS/DS epitopes and found that these could potentially be used to sort stem/progenitor cells in cartilage. The results led the authors to hypothesise that different forms of CS may regulate stem cells in different ways – with higher sulphated CS chains responsible for inducing differentiation of stem cells, whilst non- or minimally 4-sulphated CS chains and HA maintain the stem phenotype by acting as a physical barrier that prevents the binding of growth factors that would stimulate differentiation.

The monoclonal antibodies used in the aforementioned study recognise distinct sulphation motifs that comprise part of the GAG chains. Sulphation motifs are specific sequences within a GAG chain comprising of oligosaccharides and the distinct locations of the sulphated groups attached to the monosaccharide units. These sulphation motifs can be located at different points along a GAG chain, as demonstrated in Figure 5.1, and some need to be exposed by pre-digestion with an enzyme such as chondroitinase ABC. Anti-CS antibodies have been successfully used on a range of species – including humans, rats, sheep and cows (Hayes *et al.* 2008; Hayes *et al.* 2011; Shu *et al.* 2013) – but have thus far not been used on porcine tissue.

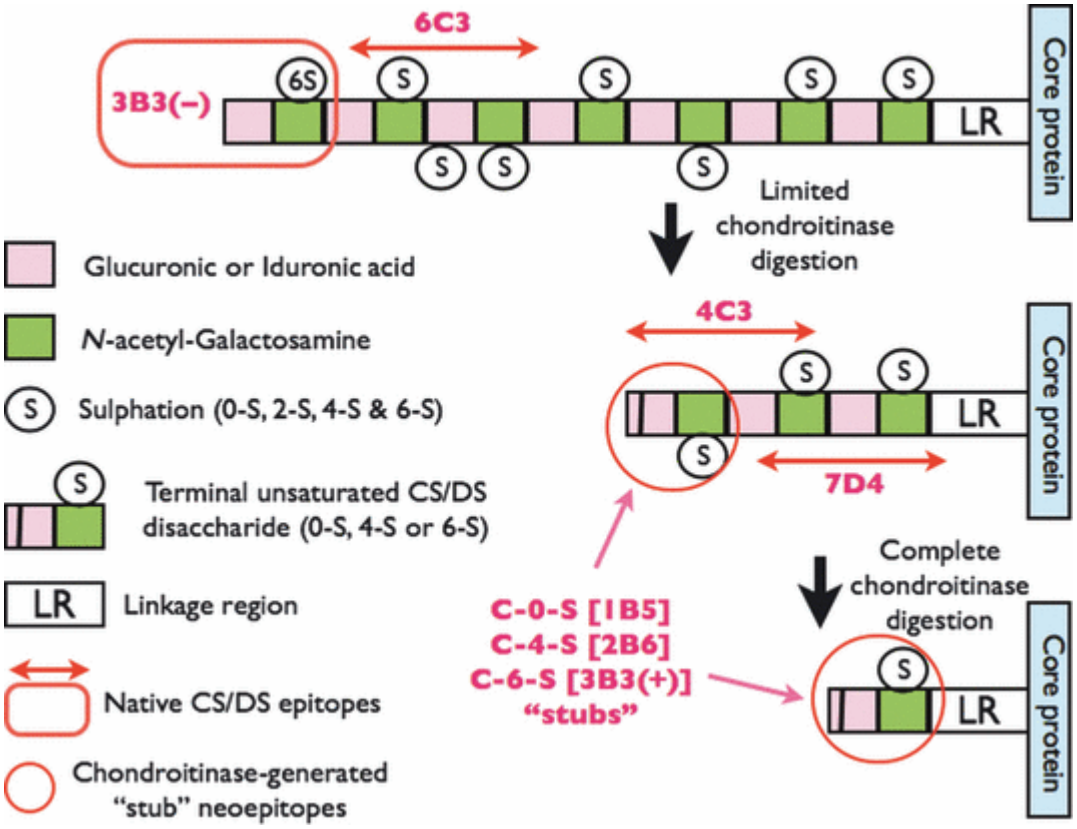

Figure 5.1- Diagram demonstrating the location of the epitopes recognised by certain anti-CS/DS monoclonal antibodies.
Source: Caterson (2012) with permission from the copyright holder.

In Schlötzer-Schrehardt *et al.*'s extensive investigation into the composition of the human corneal, limbal, and conjunctival ECMs and basement membranes (2007), they found that the components varied between the "anterior" (adjacent to the cornea) and "posterior" (adjacent to the sclera) portions of the limbus. This led the investigators to propose that the limbus is split into two compartments: a "posterior compartment" in the region of LCs that maintains the stem cell phenotype and an "anterior compartment" at the corneolimbal transition that promotes the proliferation and differentiation of late progenitor cells or TACs. If this is true, then it may be that there is a difference in CS sulphation motif distributions across the limbal area, based on the aforementioned theories proposed by Hayes *et al.* (2008) and Schlötzer-Schrehardt *et al.* (2007).

In this investigation, a range of monoclonal antibodies that label distinct sulphation motifs was used to assess the distribution of CS in the porcine limbus. The S/I limbus was compared with the N/T limbus to determine whether the distribution of CS differs between the two areas. The hypothesis is that different CS epitope

distributions will be observed at the corneal and scleral sides of the limbus, based on the theories mentioned above, and that epitope distribution may vary between the S/I limbus and the N/T if the LESCs are preferentially located in the S/I limbus as in the human cornea. However, this is not expected based on the findings of a continuous limbal trough, the proposed porcine equivalent of human LCs that hosts the stem cell population, in all quadrants of the limbus demonstrated in chapter 3.

5.2 Materials and Methods

5.2.1 Immunohistochemistry

Immunohistochemistry was carried out on three porcine eyes as detailed in section 2.4. The primary antibodies utilised are shown in Table 5.1. For HA staining, sections were incubated with biotinylated HA binding protein (Sigma-Aldrich Company Ltd, Gillingham, UK) diluted to 5 µg/ml, instead of primary antibody, overnight at 4°C.

Antibody (dilution)	Clonality/Isotype	Specificity	Source/Reference
3B3 (1:1000)	Mouse monoclonal, IgM	A CS sulphation motif recognising a non-reducing terminal end disaccharide consisting of glucuronic acid next to a 6-sulphated N-acetyl-galactosamine	Gifted by Prof. Clare Hughes (Sorrell *et al.* 1988; Caterson *et al.* 1990; Sorrell *et al.* 1990; Caterson 2012)
4C3 (1:100)	Mouse monoclonal, IgM	A "native" CS sulphation motif close to the linkage region	
6C3 (1:20)	Mouse monoclonal, IgM	A "native" CS sulphation motif in peripheral areas of the GAG chain	
7D4 (1:100)	Mouse monoclonal, IgM	A "native" CS sulphation motif close to the linkage region	
p63-α Antibody #4892 (1:100)	Rabbit polyclonal, IgG	p63α protein, including full-length TAp63α and truncated ΔNp63α	Cell Signaling Technology, Leiden, The Netherlands (Notara *et al.* 2011)
EPR21122 (1:100)	Rabbit monoclonal, IgG	ABCG2/BCRP	Abcam, Cambridge, UK (Lee *et al.* 2020)
NBP1-77687 (1:100)	Rabbit polyclonal, IgG	ABCB5	Bio-Techne Ltd, Abingdon, UK (Ksander *et al.* 2014)
AE5 (1:100)	Mouse monoclonal, IgG1	Cytokeratin 3/cytokeratin 12	Abcam, Cambridge, UK (Schermer *et al.* 1986)
EP1580Y (1:100)	Rabbit monoclonal, IgG	Cytokeratin 19	Abcam, Cambridge, UK (Tateishi *et al.* 2008)

Table 5.1- Details of the primary antibodies used in this experiment, including the dilutions used.

The secondary antibodies used were as follows: sections labelled with anti-CS monoclonal antibodies were incubated with a 1:1000 dilution of Alexa Fluor® 488-conjugated goat anti-mouse IgG/IgA/IgM secondary antibody (Invitrogen, Loughborough, UK). Sections labelled with AE5 were incubated with a 1:1000 dilution of Alexa Fluor® 594-conjugated goat anti-mouse IgG secondary antibody (Abcam, Cambridge, UK) and sections labelled with p63-α antibody #4892, EPR21122, NBP1-77687 and EP1580Y were incubated with a 1:1000 dilution of Alexa Fluor® 594-conjugated goat anti-rabbit IgG secondary antibody (Abcam, Cambridge, UK), all for 1 hour at room temperature. Sections labelled with HA binding protein were incubated with a 1:500 dilution of NeutrAvidin protein conjugated with DyLight 488 (Invitrogen, Loughborough, UK) for 1 hour at room temperature.

5.2.2 Chondroitinase ABC digestion

Some sections were subjected to enzyme digestion with chondroitinase ABC prior to immunohistochemistry. After the initial rehydration by washing in PBS with 0.1% Tween 20 for 10 mins, the sections were then incubated in 0.1 units/ml chondroitinase ABC (Appendix 3.3) at 37°C for 2 hours. Following this, the sections were washed in PBS/Tween (2 x 5 mins) and the procedure for immunohistochemistry was followed as in section 2.4 from the point of blocking with 1% BSA onwards.

5.3 Results

From the first eye, all four quadrants were examined. No differences in either CS or stem cell marker staining were found between the opposite sides of the same meridians, thus, only one section from each meridian was examined in the second and third eyes. Representative images are presented below as similar staining patterns were observed in all three eyes.

5.3.1 Chondroitin sulphate sulphation motifs

5.3.1.1 3B3(-)

There was no significant staining with 3B3(-) (Figure 5.2): the (-) denotes that pre-digestion with chondroitinase ABC has not been performed. There was some weak staining throughout the epithelium; however, this was also observed in the IgM controls but not the negative controls, and thus was non-specific binding of this antibody. There was no difference between the N/T limbus and the S/I limbus.

5.3.1.2 3B3(+)

After treating tissue sections with chondroitinase ABC, the neoepitope recognised by 3B3 was revealed. 3B3(+) staining was found beneath the limbal trough in both the S/I and N/T limbus (Figure 5.3); in particular, it was skewed towards the scleral side of the limbal trough. This staining seemed to be mostly concentrated around stromal cells, close to the epithelial basement membrane.

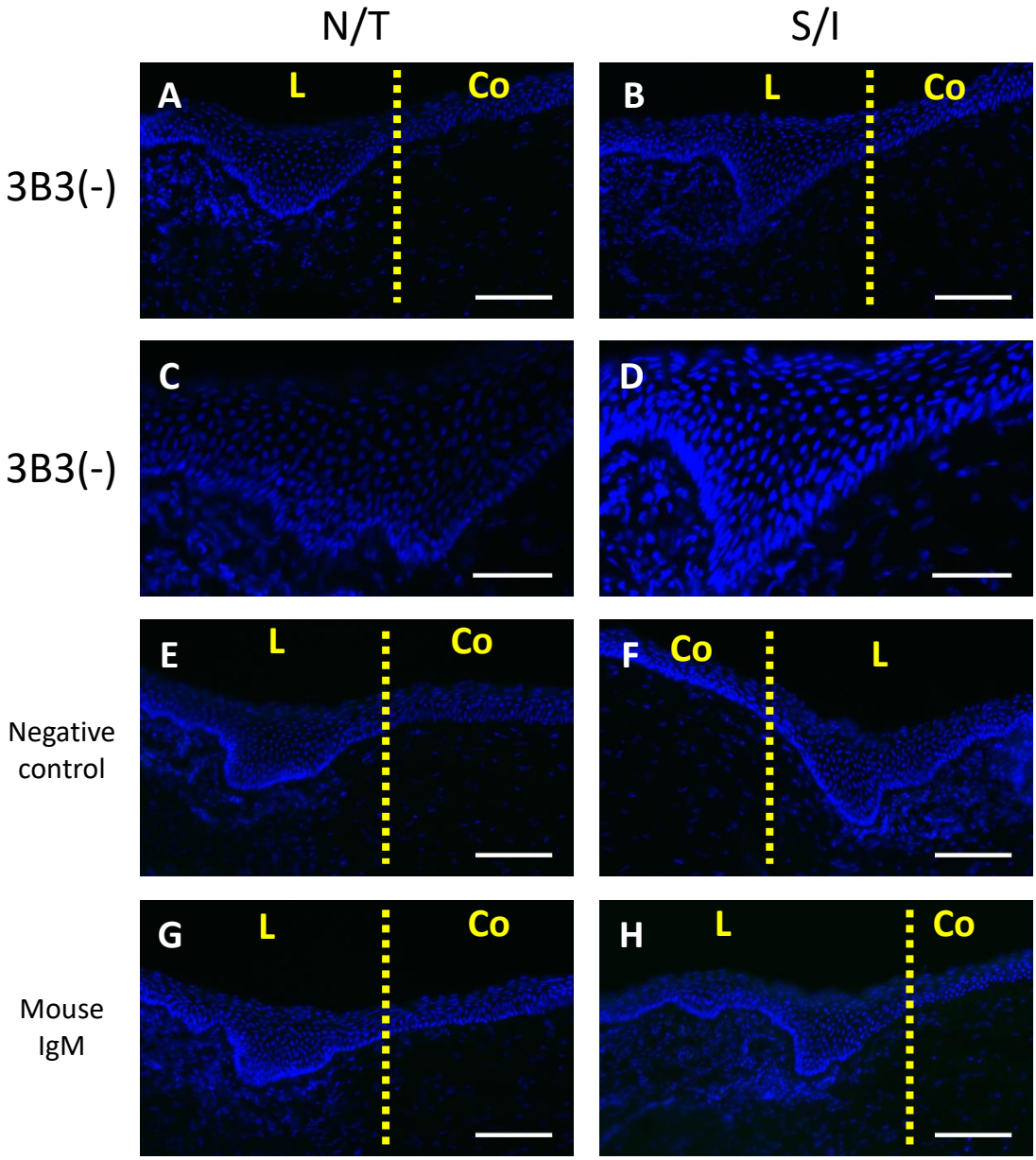

Figure 5.2- Staining of the porcine limbus with anti-chondroitin sulphate antibody 3B3 without enzyme pre-digestion.

No significant staining can be observed with this antibody, without chondroitinase ABC pre-digestion (A-D), compared to negative controls (E, F). There is some weak epithelial staining, but this is also observed in the mouse IgM controls (G, H) and was judged to be non-specific staining. No difference is seen between the nasal/temporal or superior/inferior limbus. Scale bars (A, B, E, F, G, H) = 100 µm, scale bars (C, D) = 50 µm. DAPI- blue, 3B3- green. L = limbus, Co = cornea.

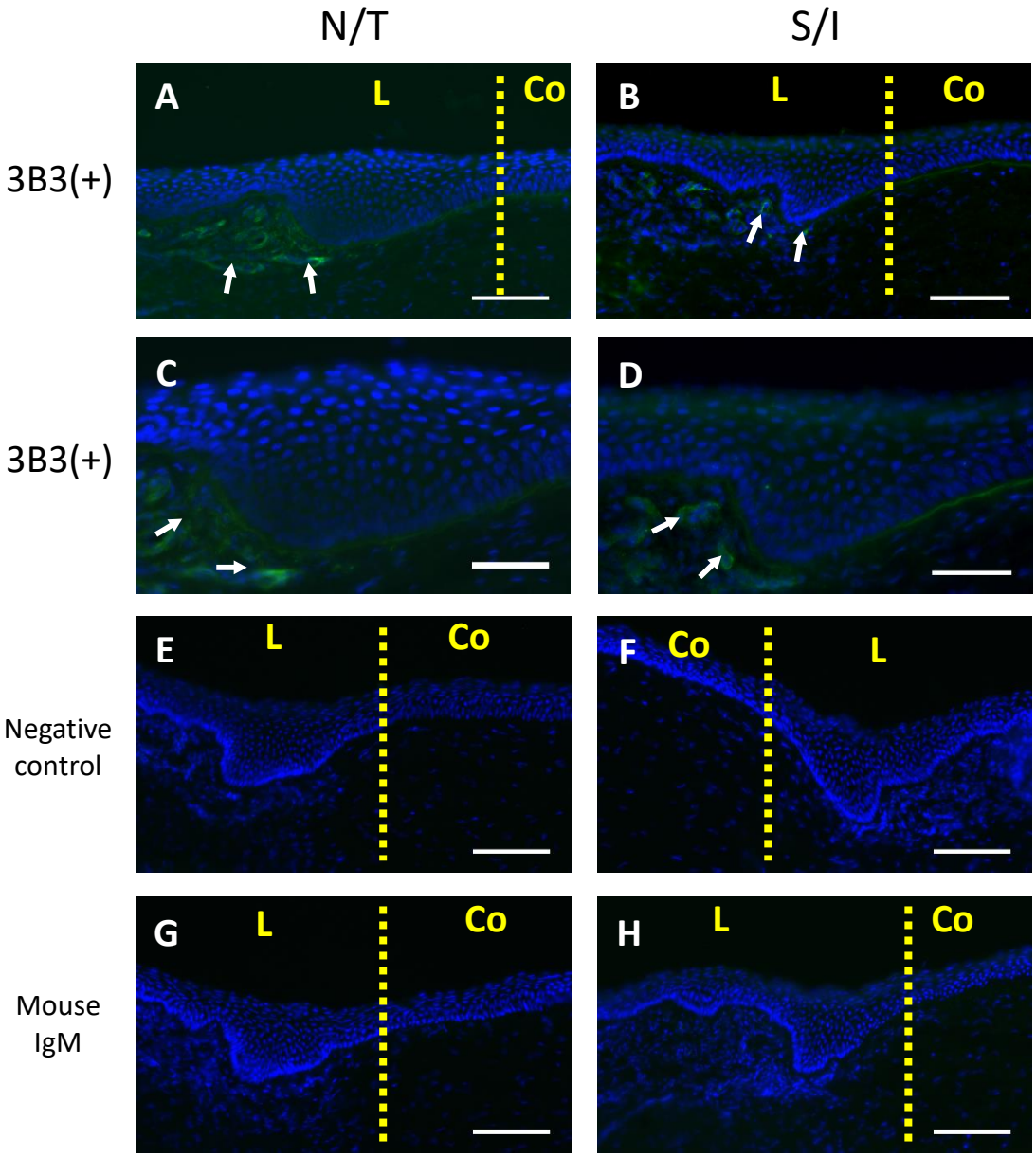

Figure 5.3- Staining of the porcine limbus with anti-chondroitin sulphate antibody 3B3 after exposure to chondroitinase ABC.
Exposure to chondroitinase ABC reveals an epitope recognised by 3B3 that is present subjacent to the limbal trough (arrows). This staining is found in both the nasal/temporal and superior/inferior limbus. Scale bars (A, B, E, F, G, H) = 100 µm, scale bars (C, D) = 50 µm. DAPI- blue, 3B3- green. L = limbus, Co = cornea.

5.3.1.3 4C3

There was generalised staining throughout the full thickness of the stroma with antibody 4C3 (Figure 5.4). There was no specific localisation of the staining and there was no difference between the N/T and S/I limbus.

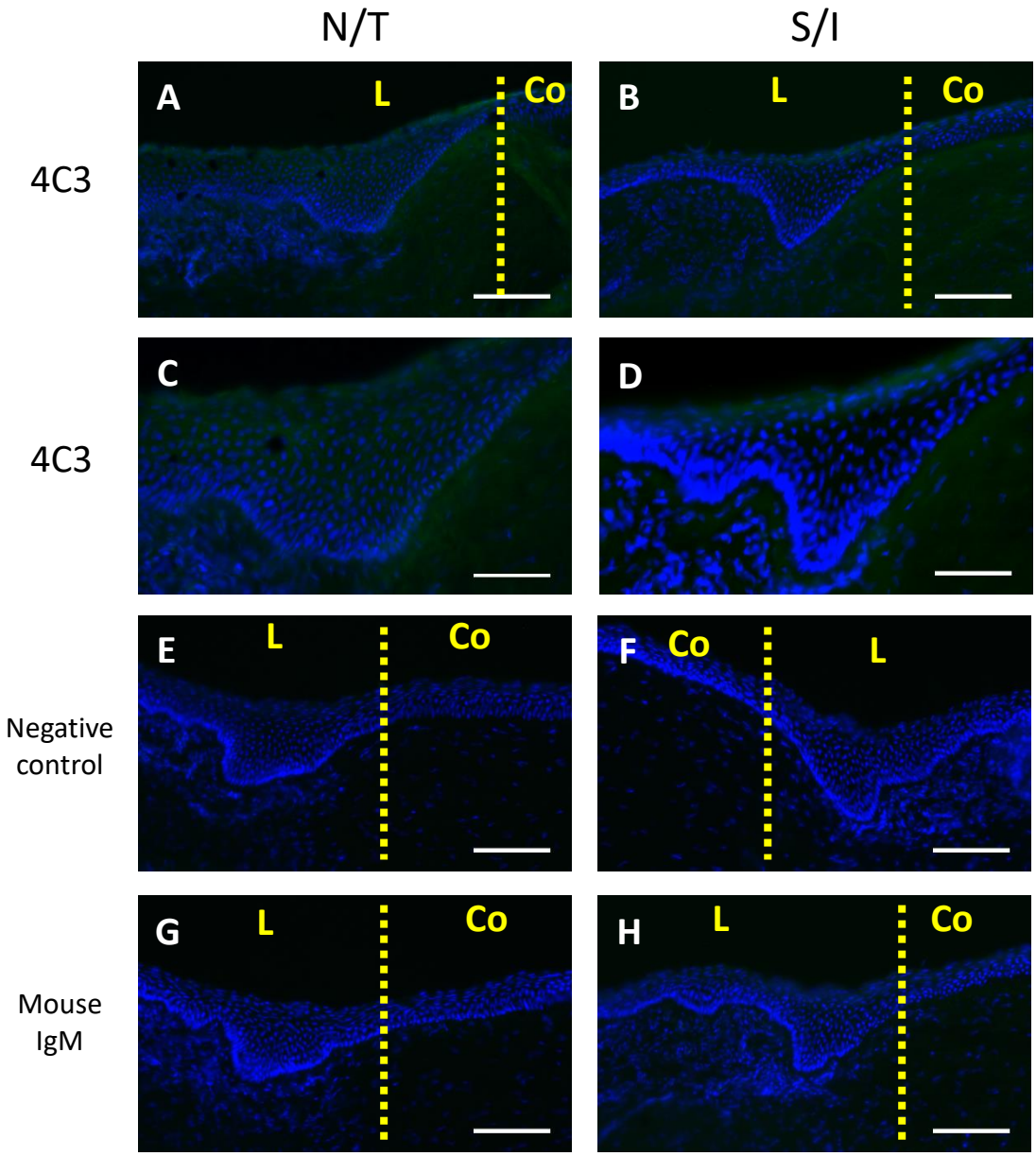

Figure 5.4- Staining of the porcine limbus with anti-chondroitin sulphate antibody 4C3.

There is generalised, weak staining with 4C3 throughout the limbal and corneal stroma (A-D) that is not seen in control sections (E-H). Scale bars (A, B, E, F, G, H) = 100 µm, scale bars (C, D) = 50 µm. DAPI- blue, 4C3- green. L = limbus, Co = cornea.

5.3.1.4 6C3

Significant 6C3 labelling was observed in all sections that were assessed. The staining was focussed around the limbal trough, the porcine equivalent of human LCs (Figure 5.5).

A thin band of subepithelial stroma, directly beneath the trough was strongly labelled with the 6C3 antibody in both N/T and S/I areas. The band often appeared to be skewed towards the scleral side of the trough. 6C3 staining was also observed in the scleral mid-stroma (Figure 5.5A, B) and this area of positive staining would sometimes connect with the subepithelial band beneath the limbal trough. However, subepithelial labelling was found exclusively beneath the trough. Treatment with chondroitinase ABC completely removed 6C3 and any associated staining in both S/I and N/T sections (Figure 5.6).

It was also found that on the rare occasion that the limbal trough was not observed in a tissue section, 6C3 staining was still present beneath the limbal epithelium (Figure 5.18). A lack of a prominent trough was only ever found in N/T sections, S/I sections always demonstrated the limbal trough.

Figure 5.5- Staining of the porcine limbus with anti-chondroitin sulphate antibody 6C3. *→ Positivity for 6C3 is observed in the superficial stroma beneath the limbal trough (*) in all sections, both nasal/temporal and superior/inferior. This staining does not extend to the subepithelial stroma beneath the peripheral corneal epithelium or very far along the limbal epithelium posterior to the trough. Often the staining band was skewed to the scleral side of the limbal trough. Scale bars (A, B) = 100 µm, scale bars (C, D) = 50 µm. DAPI- blue, 6C3- green. L = limbus, Co = cornea.*

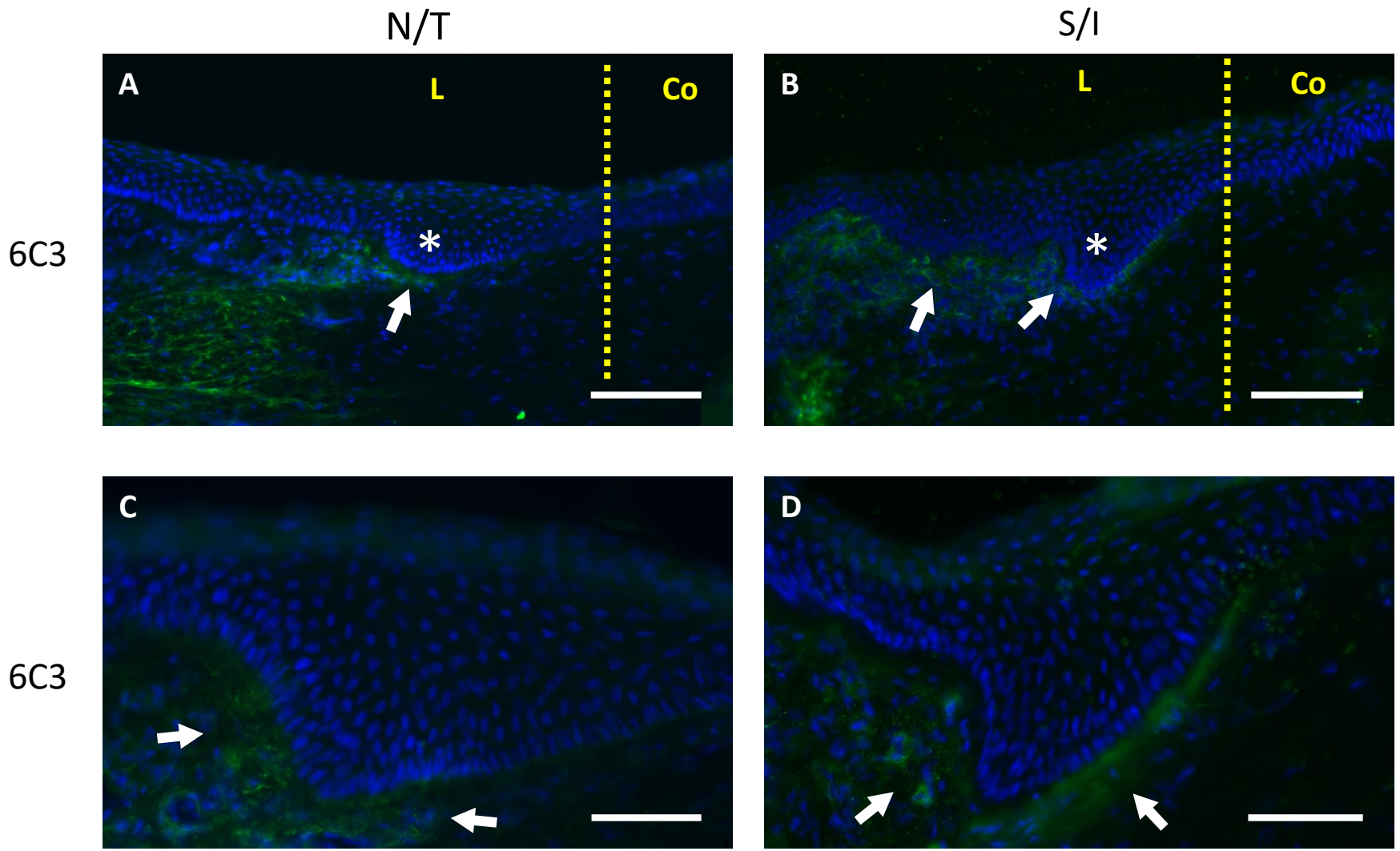
N/T
S/I
6C3
6C3
A
L
Co
B
L
Co
C
D

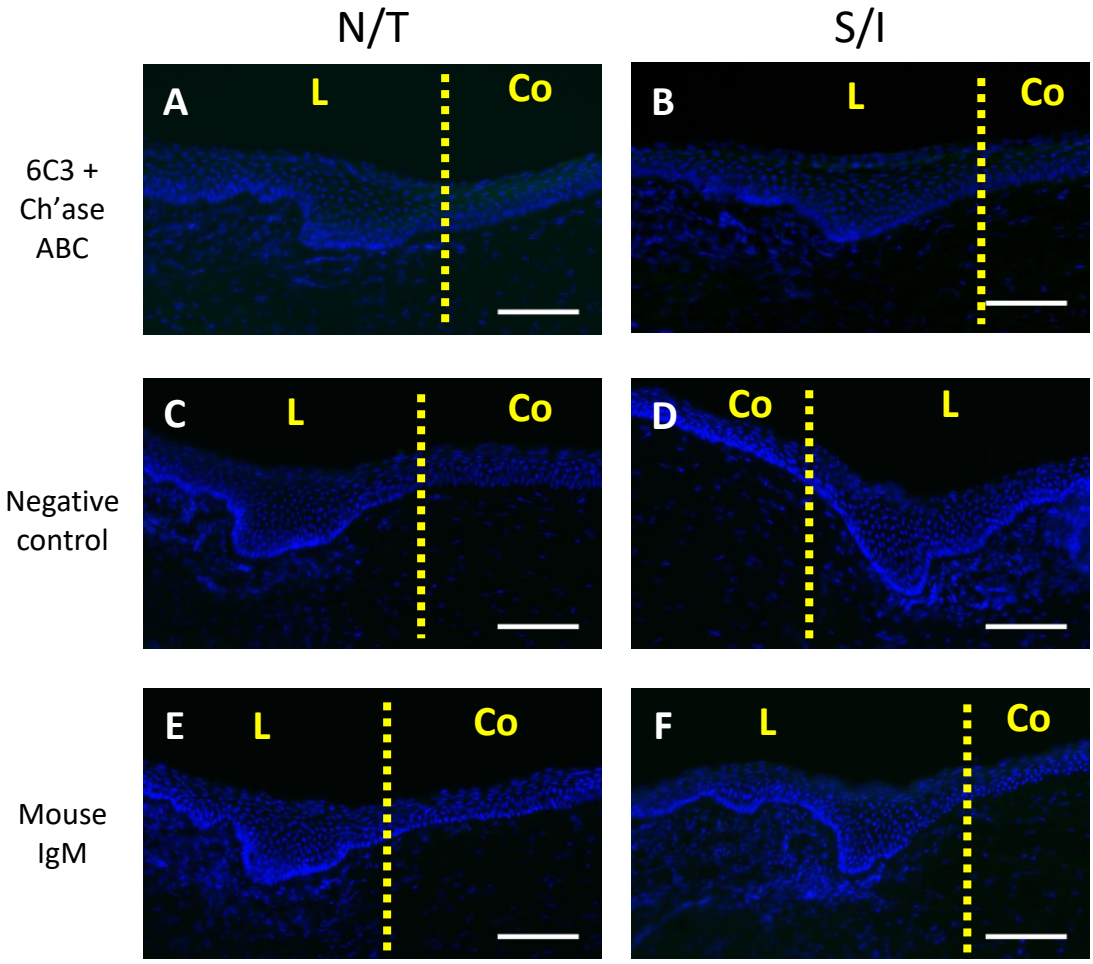

Figure 5.6- Control sections for 6C3 staining of the porcine limbus.
Treatment with chondroitinase ABC completely removes all of the subepithelial 6C3 staining (A, B) observed in Figure 5.5. There is no significant staining in negative control or isotype control sections (C, D and E, F respectively). Scale bars = 100 µm. DAPI- blue, 6C3- green. L = limbus, Co = cornea.

5.3.1.5 7D4

Staining with 7D4 was variable (Figure 5.7). Most often, it appeared to be ubiquitous throughout the corneal and limbal stroma. Yet, in some instances, there was a more intense band of subepithelial staining in the corneolimbal transition area (Figure 5.7A, arrow). However, this was not consistent and in the majority of sections this band was not observed. There was, again, no difference between the N/T or S/I limbus.

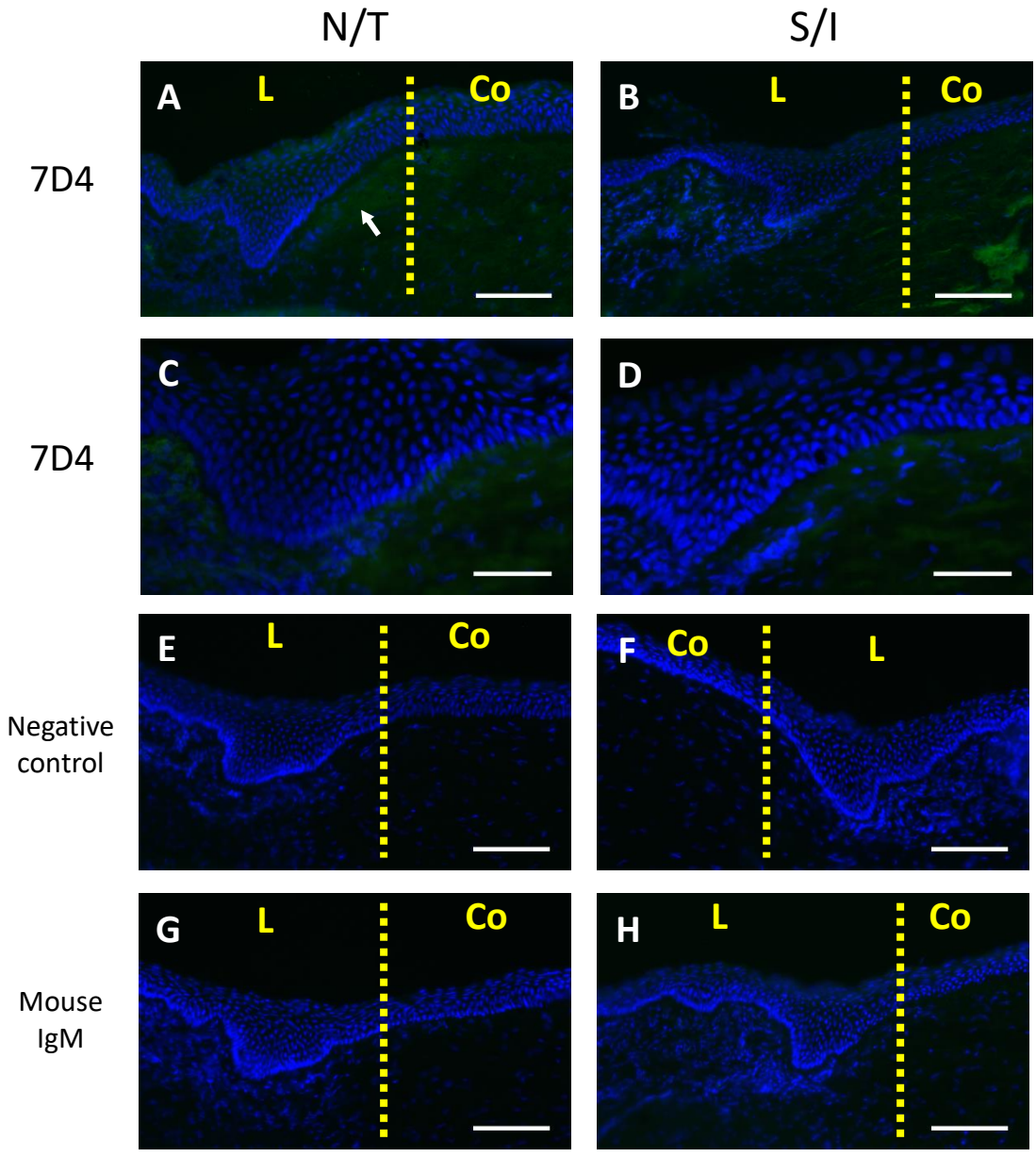

Figure 5.7- Staining of the porcine limbus with anti-chondroitin sulphate antibody 7D4. *7D4 staining is present throughout the full depth of the corneal and limbal stroma. Infrequently, a more intense band of staining is found beneath the corneolimbal transition area (arrow), but this is not consistent. Scale bars (A, B, E, F, G, H) = 100 µm, scale bars (C, D) = 50 µm. DAPI- blue, 7D4- green. L = limbus, Co = cornea.*

5.3.2 Hyaluronic acid

HA staining was observed only in the limbal area of porcine tissue (Figures 5.8 and 5.9). The staining was strongest directly subjacent to the epithelium, in particular beneath the limbal trough and limbal epithelium posterior to the trough, though it also extended deeper into the limbal stroma. There was a sharp cut-off between stromal staining in the limbus and the lack of staining in the peripheral cornea (Figure 5.9A, B). There was no staining in the peripheral cornea and no differences between the S/I and N/T limbus.

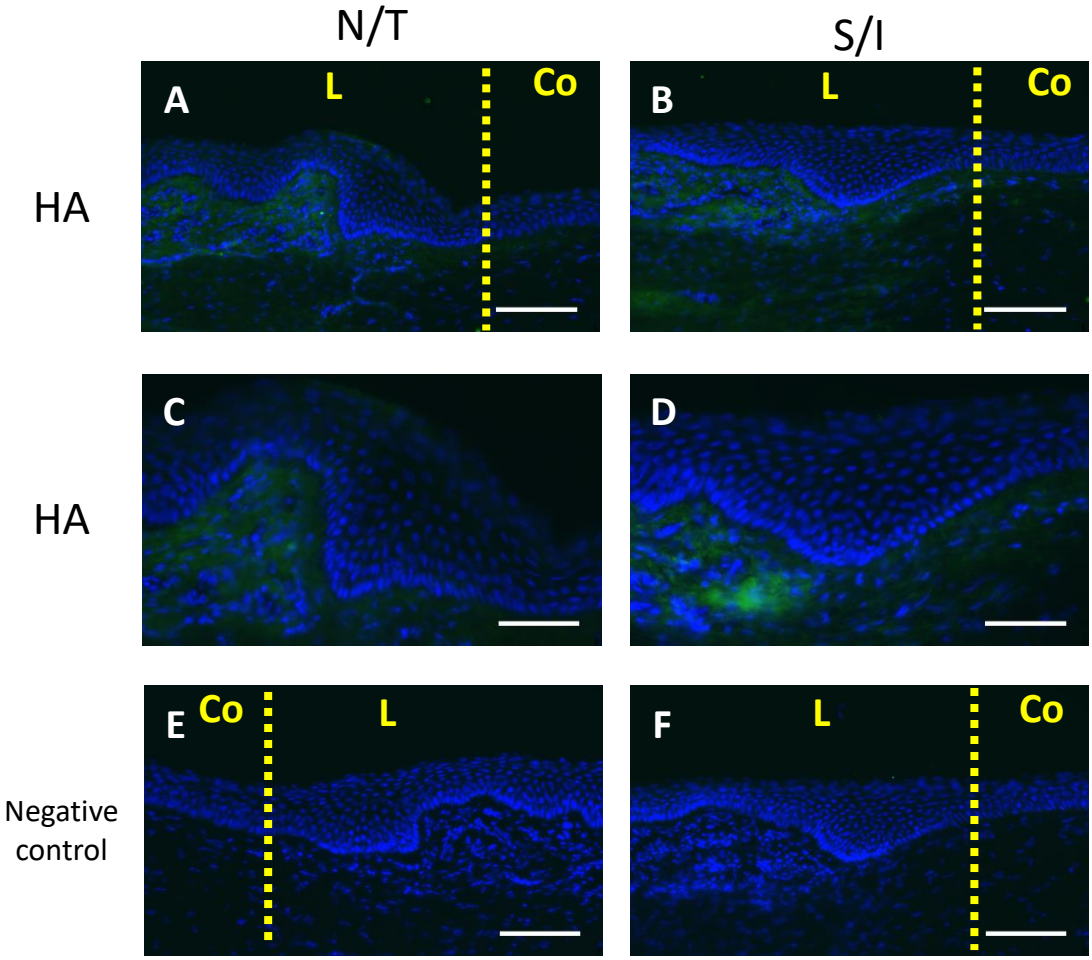

Figure 5.8- Staining of hyaluronic acid in the porcine limbus.
Staining for hyaluronic acid is present subjacent to the limbal trough in the superior/inferior and nasal/temporal limbus. Scale bars (A, B, E, F) = 100 µm, scale bars (C, D) = 50 µm. DAPI- blue, hyaluronic acid- green. L = limbus, Co = cornea.

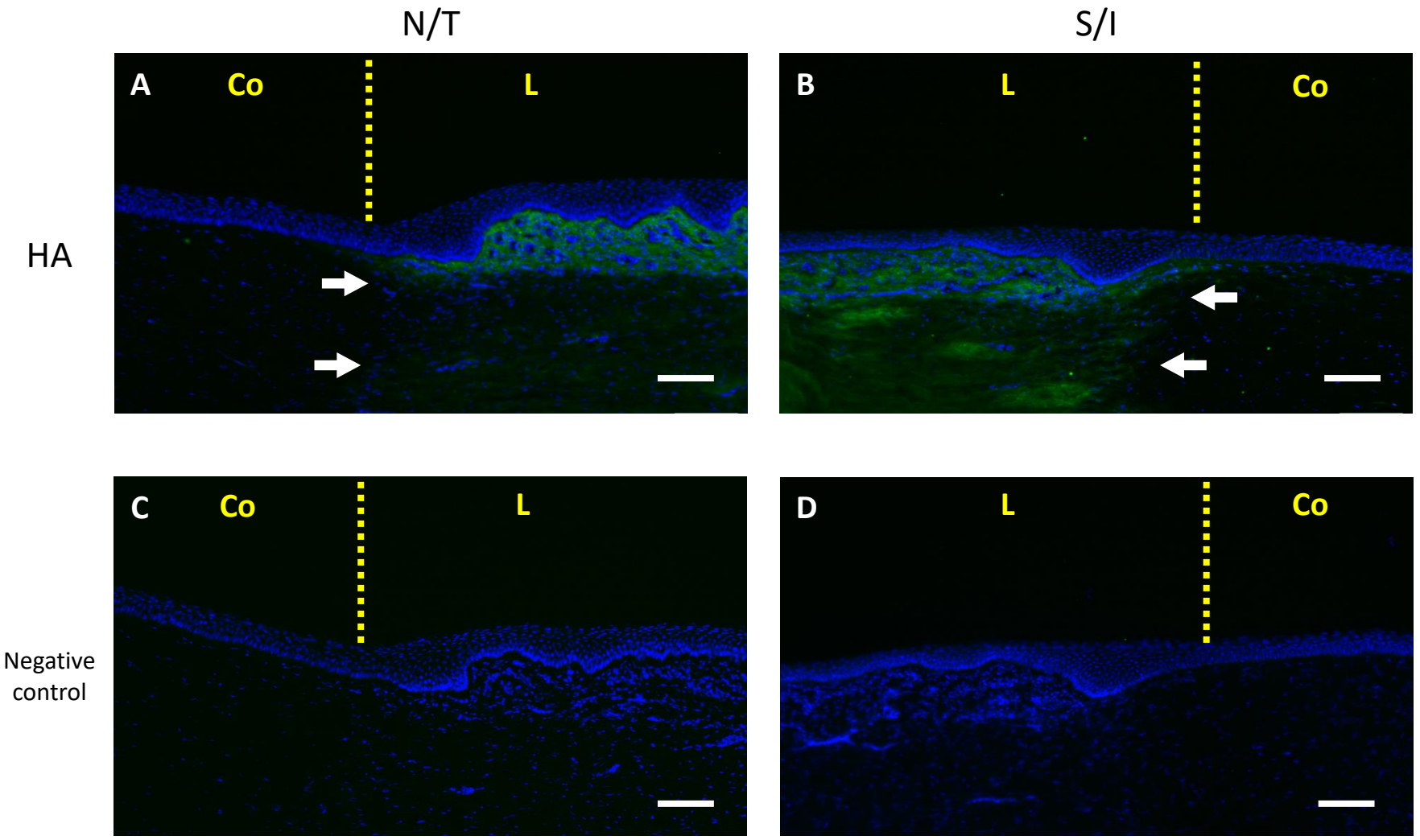
N/T
S/I
HA
Negative control
A
Co
L
B
L
Co
C
Co
L
D
L
Co

Figure 5.9- Staining of hyaluronic acid across the porcine peripheral cornea and limbus. ←
There is no hyaluronic acid staining in the peripheral cornea, but substantial staining subjacent to the limbal epithelium. There is also some hyaluronic acid staining deeper within the limbal stroma and a distinct cut-off to this staining in the peripheral corneal stroma can be seen (A, B white arrows). Scale bars = 100 µm. DAPI- blue, hyaluronic acid- green. L = limbus, Co = cornea.

5.3.3 Stem cell markers

5.3.3.1 p63α

Staining with this putative epithelial stem cell marker was non-specific. Cell nuclei throughout the full thickness of the limbal epithelium appeared to be very weakly labelled (Figure 5.10), not just basal cells. Labelling also extended into the peripheral corneal epithelium. There was also significant, non-specific staining with naïve rabbit IgG in the superficial epithelium (Figure 5.10G, H also seen in Figures 5.11, 5.12 and 5.15). There were no meridional differences.

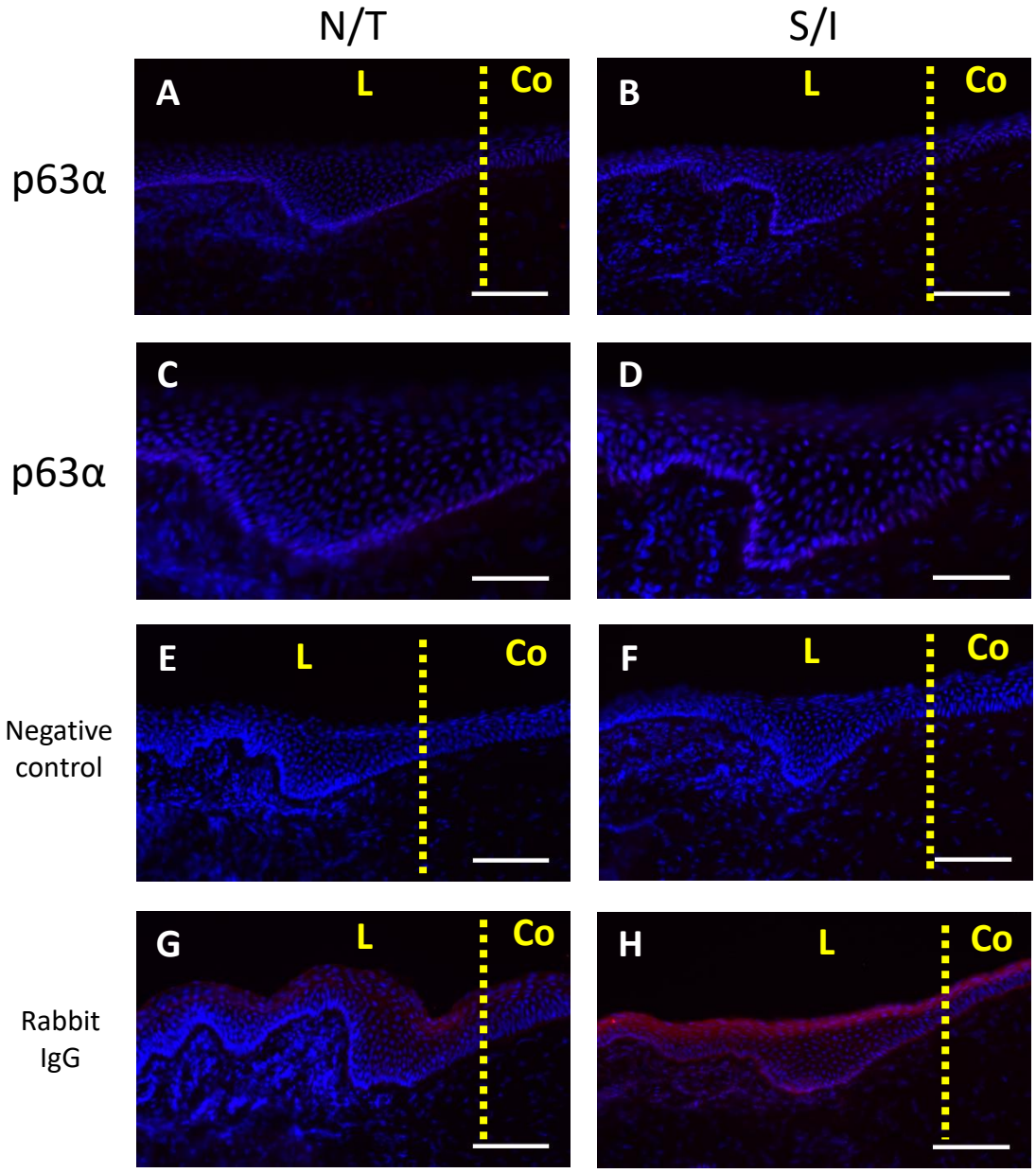

Figure 5.10- Staining of p63α within the porcine limbal epithelium.
Cell nuclei throughout the limbal epithelium label positively for p63α, though this is very weak. This also extends into the peripheral corneal epithelium (not shown). Scale bars (A, B, E, F, G, H) = 100 µm, scale bars (C, D) = 50 µm. DAPI- blue, p63α- red. L = limbus, Co = cornea.

5.3.3.2 ABCG2 and ABCB5

ABCG2 also labelled the limbal epithelium non-specifically in both the N/T and S/I limbus (Figure 5.11). Though there is focal labelling of epithelial cell nuclei, there was no specific localisation of this staining and ABCG2-positive cells can be seen throughout the epithelium.

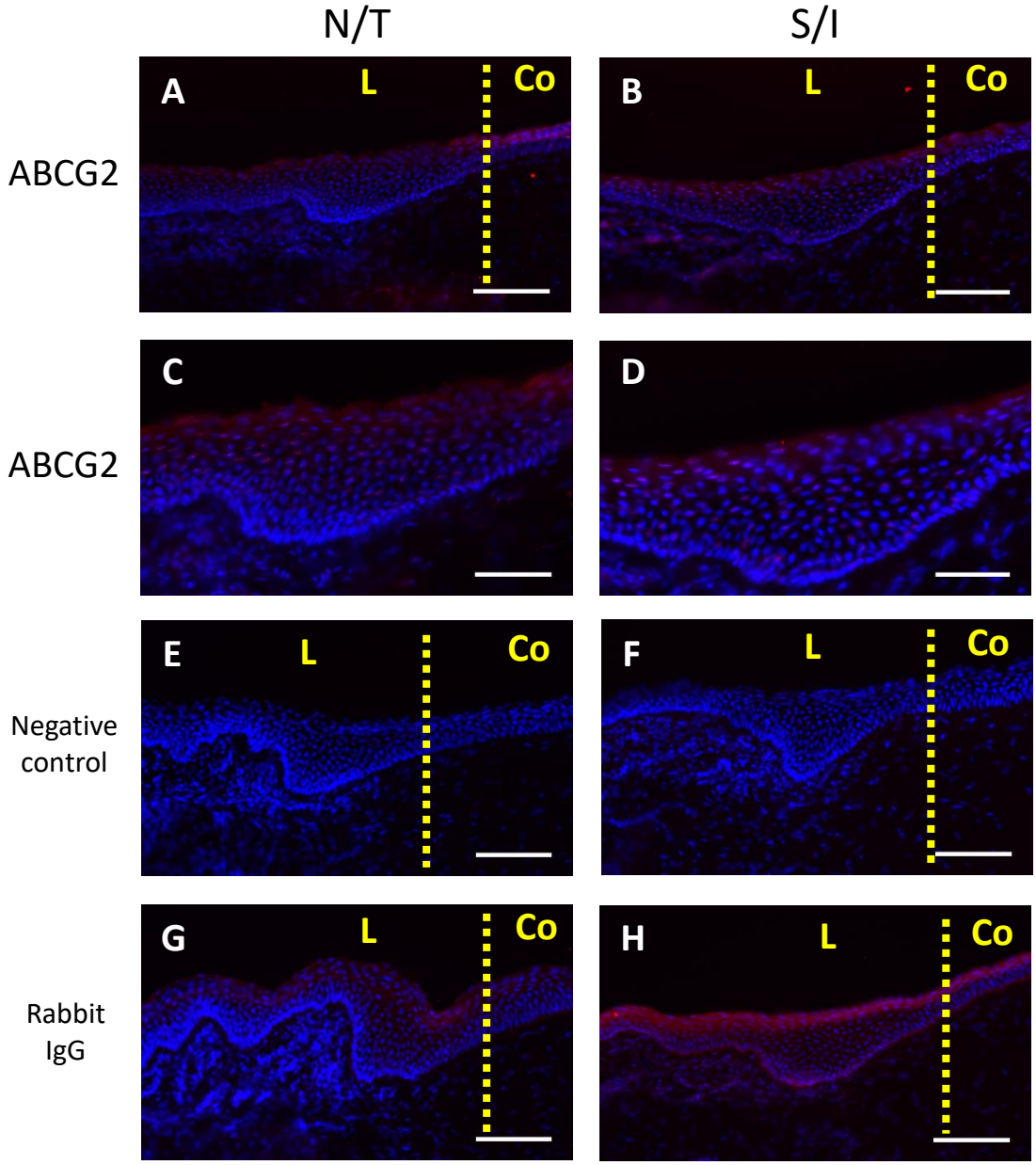

Figure 5.11- Staining of ABCG2 within the porcine limbal epithelium.
The labelling of ABCG2 is non-specific. It is found throughout the limbal epithelium, with focal labelling of cell nuclei in all layers. Scale bars (A, B, E, F, G, H) = 100 µm, scale bars (C, D) = 50 µm. DAPI- blue, ABCG2- red. L = limbus, Co = cornea.

In contrast, the anti-ABCB5 antibody specifically stained basal limbal epithelial cells and those within the limbal trough most intensely (Figure 5.12). The labelling seemed to be strongest at the base of the trough, before continuing along the scleral side of the trough to join with the rest of the basal limbal staining. ABCB5-positive cells were also found to coincide with subepithelial 6C3 staining (Figure 5.17). There was a considerable amount of background staining throughout the superficial epithelium with this antibody, which matches with the non-specific staining found with rabbit IgG. No meridional differences were observed.

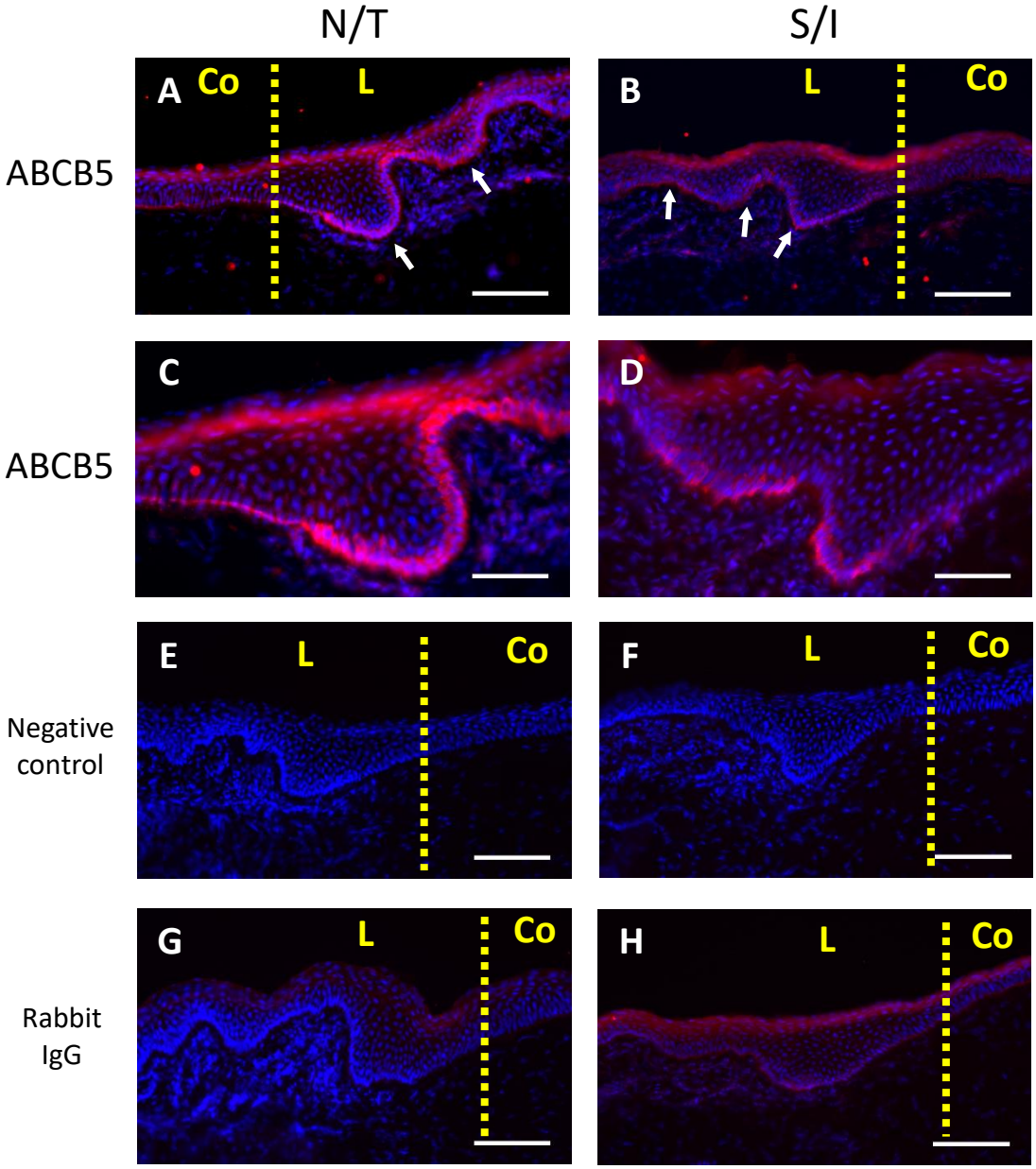

Figure 5.12- Staining of ABCB5 within the porcine limbal epithelium.
Cells demonstrate ABCB5-positivity most intensely within the basal epithelium of the limbus. In particular, cells at the base of the limbal trough and scleral wall of the trough demonstrate the strongest signal. Scale bars (A, B, E, F, G, H) = 100 µm, scale bars (C, D) = 50 µm. DAPI- blue, ABCB5- red. L = limbus, Co = cornea.

5.3.3.3 Cytokeratins K3/K12 and K19

Staining for cytoskeletal components K3/K12 was observed throughout the entire thickness of the corneal and limbal epithelia, including all cellular layers within the limbal trough (Figures 5.13 and 5.14). There were no meridional differences in the labelling of K3/K12.

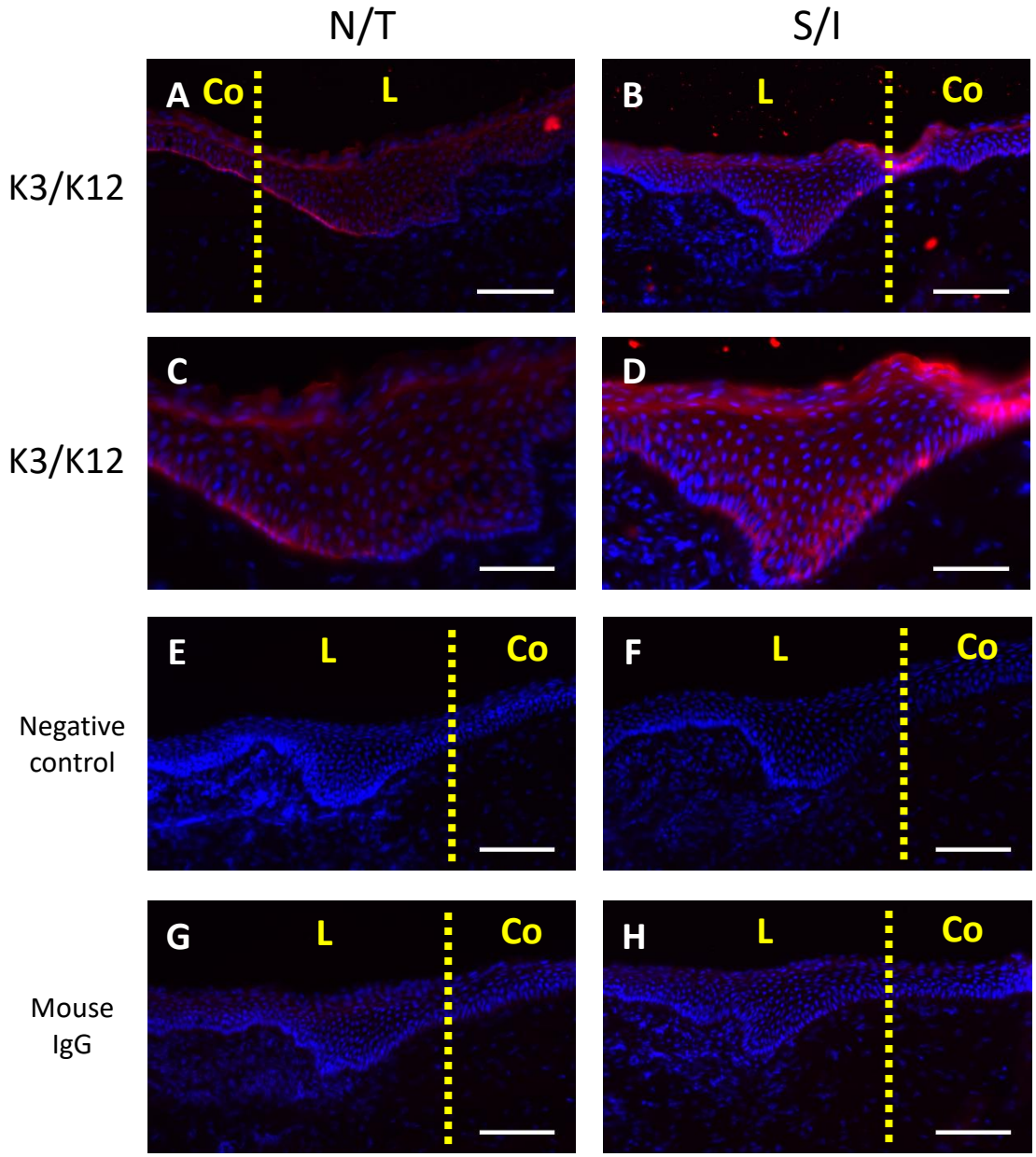

Figure 5.13- Staining of cytokeratins 3 and 12 within the porcine limbal epithelium. *Cytokeratins 3 and 12 are found throughout the full thickness of the limbal epithelium, including the basal cell layer. Scale bars (A, B, E, F, G, H) = 100 µm, scale bars (C, D) = 50 µm. DAPI- blue, cytokeratins 3/12- red. L = limbus, Co = cornea.*

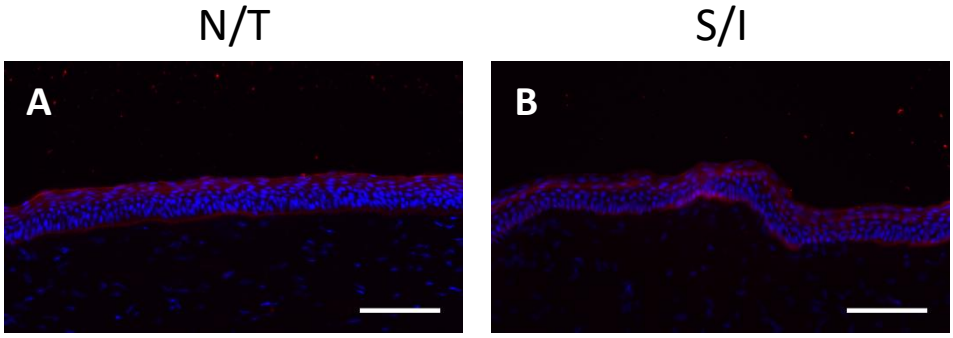

Figure 5.14- Staining of cytokeratins 3 and 12 within the porcine corneal epithelium. *As expected, cytokeratins 3 and 12 are expressed throughout the full thickness of the corneal epithelium. Scale bars = 100 µm. DAPI- blue, cytokeratins 3/12- red.*

On the other hand, within the limbal area, K19 seemed to be specific to limbal epithelial cells at the very base of the limbal trough (Figure 5.15) and to the basal limbal epithelium posterior to the trough (Figure 5.16A, B); which includes secondary, smaller crypt-like structures as identified with microCT in chapter 3. Additionally, K19-positive limbal epithelial cells coincided with areas of subepithelial 6C3 staining (Figure 5.17) and there was some overlap with ABCB5 distribution.

There was also some weaker K19 staining in the basal corneal epithelium (Figure 5.16C, D). This does appear to be true staining, separate from the background, non-specific staining that is observed with rabbit IgG controls. There did not appear to be any differences in K19 staining in the limbus or cornea between the N/T or S/I areas. In fact, K19-positive basal limbal epithelial cells could still be observed in the N/T limbus even when there was no obvious limbal trough apparent (Figure 5.18B).

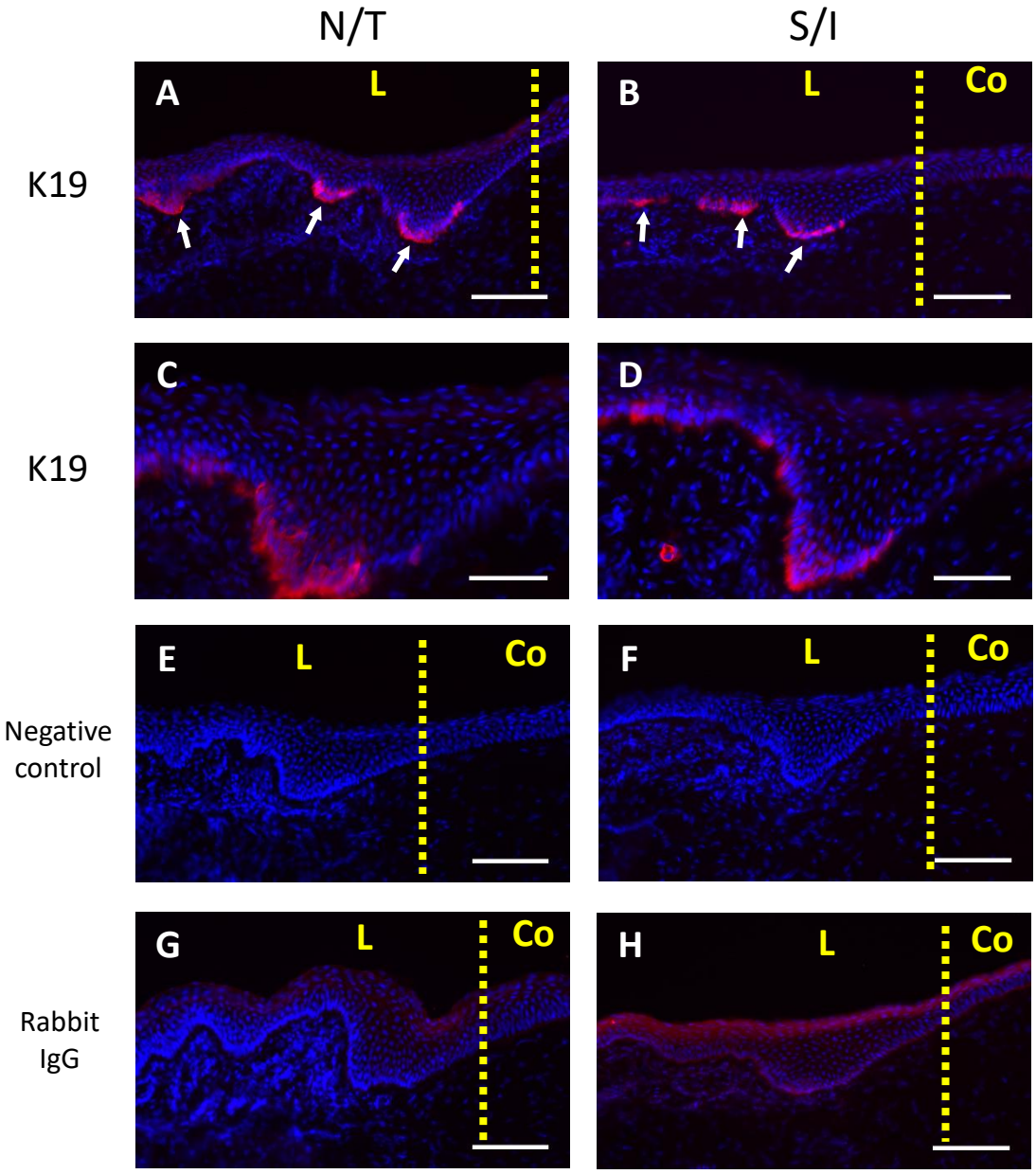

Figure 5.15- Staining of cytokeratin 19 within the porcine limbal epithelium.
Cytokeratin 19 very strongly labels basal epithelial cells at the base of the limbal trough in both the nasal/temporal and superior/inferior limbus and also at the base of smaller protrusions posterior to the main trough. Scale bars (A, B, E, F, G, H) = 100 µm, scale bars (C, D) = 50 µm. DAPI- blue, cytokeratin 19- red. L = limbus, Co = cornea.

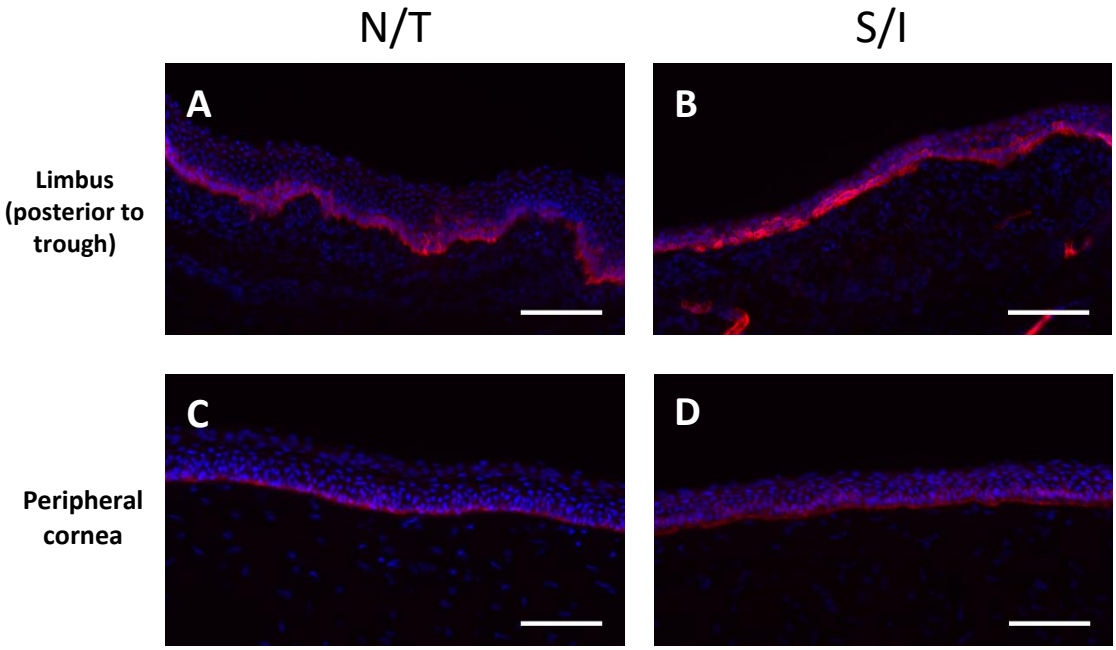

Figure 5.16- Staining of cytokeratin 19 within the porcine posterior limbal and peripheral corneal epithelia.
Cytokeratin 19 strongly labels basal cells of the limbal epithelium (A, B), as well as some weaker labelling of the basal epithelium of the peripheral cornea (C, D). Scale bars = 100 µm. DAPI- blue, cytokeratin 19- red.

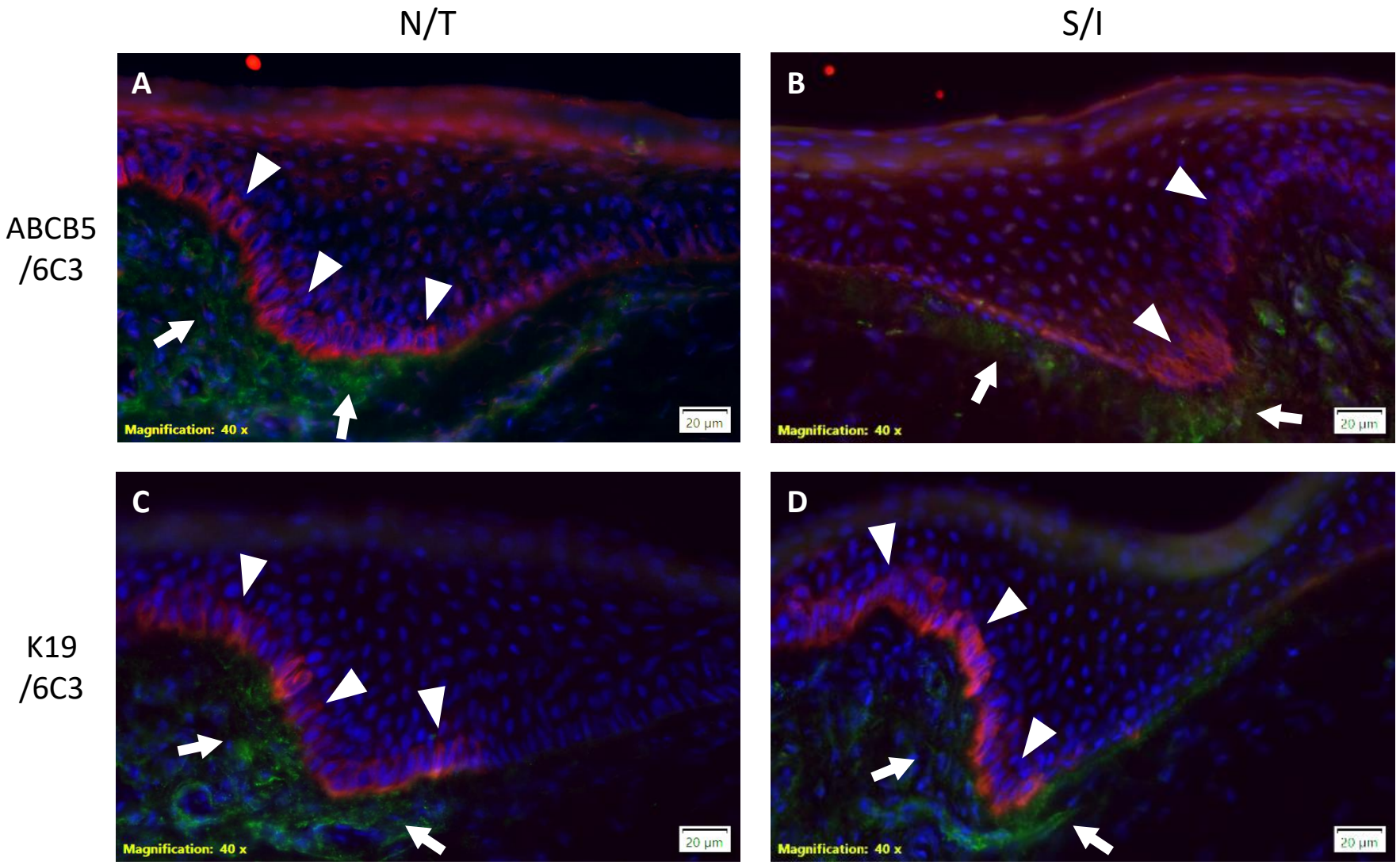
N/T
S/I
ABCB5
/6C3
K19
/6C3
A
B
C
D
Magnification: 40 x
20 µm

Figure 5.17- Dual-labelling of the porcine limbus with anti-chondroitin sulphate antibody 6C3 and stem cell markers ABCB5 or cytokeratin 19. ←
Basal limbal epithelial cells positive for ABCB5 (A, B) and K19 (C, D) (red, arrowheads) are found in the limbal trough directly adjacent to areas of subepithelial 6C3 staining (green, arrows). There is also overlap in the areas of the limbal trough that are positive for these two putative stem cell markers. Scale bars = 20 µm. DAPI- blue.

ABCB5 /6C3

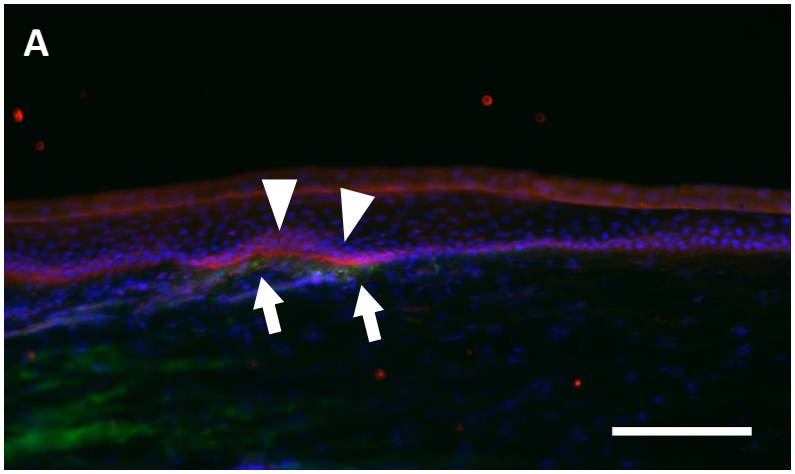

K19 /6C3

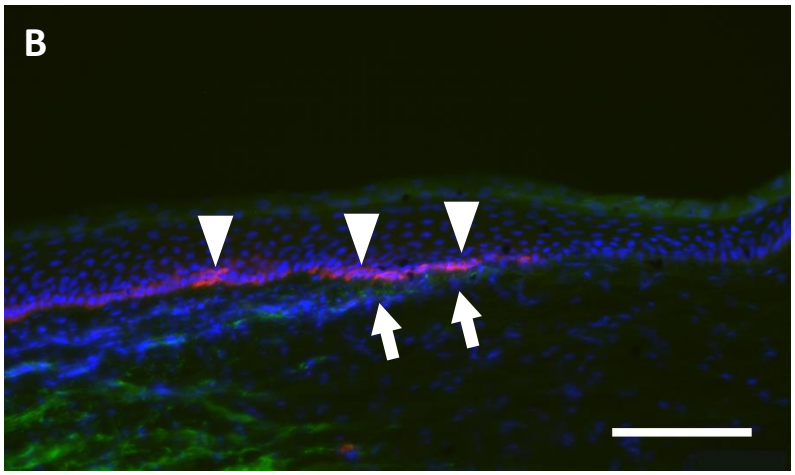

Figure 5.18- Dual-labelling of the nasal/temporal porcine limbus with anti-chondroitin sulphate antibody 6C3 and stem cell markers ABCB5 or cytokeratin 19 where there is no apparent limbal trough.
In some sections – taken from the nasal/temporal limbus – no discernible limbal trough structure is present. This was only observed in the nasal/temporal limbus; superior/inferior sections always demonstrated the limbal trough. Even when the trough is not apparent, subepithelial 6C3 staining (green, arrows) and basal epithelial ABCB5 (A) or K19 (B) staining (red, arrowheads) can still be found. Scale bars = 100 µm. DAPI- blue.

5.4 Discussion

5.4.1 Chondroitin sulphate sulphation motifs

3B3 is an anti-CS antibody that was originally raised against epitopes exposed by chondroitinase ABC digestion (Sorrell *et al.* 1988) and was then later found to recognise native epitopes as well (Sorrell *et al.* 1990), with the 3B3(-) notation being used when enzyme digestion has not been carried out. Investigations on CS sulphation motifs in the rabbit limbus by Yamada *et al.* (2015) demonstrated an absence of 3B3(-) staining in the subepithelial limbal matrix and the epithelium. In contrast, 3B3(+) staining (after chondroitinase ABC digestion) was observed throughout the subepithelial and mid-stromal ECM. In the current investigation, 3B3(-) was not present in the stem cell niche area of the porcine limbus and 3B3(+) had a similar distribution to that observed in the rabbit cornea. The porcine limbus has more defined stem cell niche structures than the rabbit eye and 3B3(+) certainly seems to be associated with these in the porcine eye. In both rabbits (Yamada *et al.* 2015) and pigs, no specific staining of the limbal stem cell niche area was observed with antibody 4C3.

7D4 potentially showed some positive signal in the current investigation and sometimes appeared more noticeably in a subepithelial band just anterior to the limbal trough. However, this was not consistent and more often 7D4 staining appeared to be widespread throughout the limbal and corneal stroma. Mid-stromal 7D4 staining was observed in the peripheral rabbit cornea by Yamada *et al.* (2015), but none was observed subepithelially in the cornea or limbus.

The most interesting results of the current study came from the 6C3 monoclonal antibody. There was a strong signal clearly visible immediately subjacent to the limbal trough in both N/T and S/I sections. This antibody also provided a strong signal in a subepithelial band in the limbus of rabbit eyes in Yamada *et al.*'s work. Importantly, this signal was eliminated with the use of chondroitinase ABC in both Yamada's investigation and the current one, validating the staining observed here. Preliminary work on the human limbus in Yamada's study also found 6C3 staining of the subepithelial ECM in the putative stem cell niche area. 3B3 and 4C3 were also applied, but 6C3 was the only anti-CS antibody that provided a positive result in

human tissue. Thus, the current results now demonstrate that the native CS epitope recognised by 6C3 is associated with the putative limbal stem cell niche of three different mammalian species. From observing the images in Yamada *et al.*'s study, which is the only other work to date that has investigated CS sulphation motifs at the limbus, it would appear there might be a similar mid-stromal patch of 6C3 staining as was found in the current investigation. Yet this is unlikely to have implications on the epithelial stem cell population.

The stem cell niche of the corneal epithelium is often compared to that of the epidermis. As mentioned above, the LCs have been noted to be similar to the rete ridges of the epidermis (Shortt *et al.* 2007) and the stem cells for the human epidermis are believed to reside in the basal layer of the epithelium (as reviewed by Fuchs and Raghavan (2002)). The distribution of CS sulphation motifs, using the same monoclonal antibodies utilised in this investigation, has also been described in skin. Interestingly, 3B3(+) was found directly subjacent to the epidermis and 4C3 was identified within all layers of human skin (Sorrell *et al.* 1990; Willen *et al.* 1991), which is comparable to the staining of the limbus. 6C3 has been identified in the papillary dermis, directly subjacent to the epidermis (Sorrell *et al.* 1990). However, in a more elderly individual, 6C3 was observed throughout the epidermis, as well as in the underlying papillary dermis (Willen *et al.* 1991). There was also weak expression of 7D4 throughout all layers of the skin (Sorrell *et al.* 1990). The distribution of CS sulphation motifs is remarkably similar between the putative stem cell niches of human skin and the porcine limbus.

5.4.2 Hyaluronic acid

HA has been suggested to be important in maintaining the LESC phenotype, based on Gesteira *et al.*'s work (2017). HA was found to be almost exclusively within the limbus and not the peripheral or central cornea of the murine eye. However, there are cable-like extensions of HA from the limbal network that extend into the peripheral cornea. In the porcine eye, HA is not found within the peripheral cornea; it is distributed throughout the limbal stroma with particularly strong staining in the subepithelial stroma. However, Gesteira *et al*. found that HA was located

throughout the limbal epithelium, whereas it was only stromal in location in the porcine eye.

This distribution changed after experimentally induced alkali wounds in HA synthase knockout mice; HA expression was greatly increased and was even present in the central cornea. However, HA was still only present at the limbus of wild-type mice, even after alkali injury. This spread of HA to the central cornea also coincided with the appearance of K15-positive epithelial cells here, suggesting cells had taken on a putative stem cell phenotype. Thus, the distribution of HA in the porcine limbus could suggest it contributes to an environment that sustains the LESC population.

5.4.3 Stem cell markers

The staining patterns of p63α, ABCG2 and K3/K12 observed here were not typical of those reported in the limbus in previous studies. p63α has been stated as a very promising stem cell marker in the limbal stem cell niche, only marking basal limbal epithelial cells that are likely candidates to be LESCs (Di Iorio *et al.* 2005; Sartaj *et al.* 2017). However, the anti-p63α antibody was found to label practically all epithelial cells – both limbal and corneal – in the current investigation. The antibody used was also utilised by Notara *et al.* (2011) in porcine tissue, with different results. They found that basal epithelial cells in both crypt-rich and non-crypt-rich areas most strongly expressed p63α – there was no such basal specificity in the current investigation. It is difficult to determine a reason for this difference, but it could potentially be due to age of the animals that tissue was acquired from. Older specimens may have a reduced number of LESCs and, therefore, lesser staining of p63. However, the age of the pigs used in this investigation are not known. Another possibility is inter-batch variability of the antibody, with a suboptimal batch having been acquired for the current investigation.

ABCG2, as aforementioned, is often still used as a putative LESC marker in studies (Kethiri *et al.* 2017; Latta *et al.* 2018; Gouveia *et al.* 2019) and is regarded as a general stem cell marker (Zhou *et al.* 2001). Chen *et al.* (2004) and Budak *et al.* (2005) agree that ABCG2-positive cells are mostly found within the basal limbal epithelium, often in clusters. However, Watanabe *et al.* (2004) also showed notable

staining of suprabasal limbal epithelial cells with an anti-ABCG2 antibody. In the porcine limbus, it was found that the majority of limbal epithelial cells were positive for ABCG2 and, in fact, the lowest level of staining was observed in the basal epithelium. However, this result is inconsistent with the data mentioned above concerning human tissue. This may be due to the chosen antibody not being appropriate for use with porcine tissue, discussed in section 5.4.6.

K3 and K12 are known to be markers of corneal epithelial cell differentiation (Kasper *et al.* 1988; Schlötzer-Schrehardt and Kruse 2005), and it follows that putative LESCs should be negative for this marker. The basal limbal epithelium has been found to be negative for these two cytokeratins (Schermer *et al.* 1986; Liu *et al.* 1993; Wu *et al.* 1994; Chen *et al.* 2004), implying a less differentiated phenotype here. However, K3/K12 were found throughout all layers of the porcine corneal and limbal epithelium in this investigation, suggesting that the basal limbal cells had taken on a corneal epithelial morphology. A recent study has shown the lack of K3 staining within the basal limbal epithelium of the pig using a different antibody (Seyed-Safi and Daniels 2020). Potentially, as mentioned with ABCG2, the reason for the difference in staining patterns is that the antibody used in the current investigation did not have the appropriate reactivity for use in porcine tissue (discussed in section 5.4.6).

Conversely, two other putative LESC markers demonstrated much more specific localisation within the basal limbal epithelium. ABCB5 was expressed specifically by basal limbal epithelial cells in porcine tissue. Ksander *et al.* (2014) found that ABCB5-positive cells were located in the basal limbal epithelium of both mouse and human corneas. Label-retaining cells in the mouse cornea were found to be positive for ABCB5 and knockout mouse models demonstrated that ABCB5 is required for corneal development and wound healing, and to properly regulate apoptosis. Human ABCB5-positive basal limbal cells were found to be associated with the Palisades of Vogt and co-expressed ΔNp63α. These results demonstrated the strong support for ABCB5 being a LESC marker. Li *et al.* (2017) also showed the co-localisation of ABCB5 and p63α in the rabbit limbus. In rabbit tissue too, ABCB5 was

exclusively expressed by the basal limbal epithelium. Thus, the porcine staining pattern matches that of the other three previously examined species.

K19 is more uncertain as a LESC marker. Though it has often been used and mentioned as a putative LESC marker (Kasper *et al.* 1988; Schlötzer-Schrehardt and Kruse 2005; Shanmuganathan *et al.* 2007; Parfitt *et al.* 2015), it is also a marker of conjunctival epithelial cells (Ramirez-Miranda *et al.* 2011; Poli *et al.* 2015). K19 staining has been found uniformly throughout the conjunctival epithelium and has been observed in the suprabasal cells of the limbal epithelium and particularly in the basal limbal cells (Kasper *et al.* 1988; Lindberg *et al.* 1993; Poli *et al.* 2015). This makes it difficult to consider it as a definitive LESC marker due to its lack of specificity to the basal limbal epithelium. Chen *et al.* (2004) also found K19-positivity throughout the human central corneal epithelium, however, this is contradictory to findings from Ramirez-Miranda *et al.* (2011) and Poli *et al.* (2015). Parfitt *et al.* (2015) also did not observe limbal basal specificity of K19 in mouse tissue; all epithelial cells demonstrated positivity, including label-retaining cells. However, the current investigation has shown a specific localisation of K19-positive cells in porcine tissue. They were found to be specifically within the basal limbal epithelium, with a specific localisation to the base of the limbal trough. This staining pattern is remarkably similar to that observed by Ramirez-Miranda *et al.* (2011) in the human limbus. The K19 staining also overlaps with ABCB5, so potentially cells positive for both of these markers represent a more likely LESC candidate than the markers individually.

5.4.4 Proximity of CS sulphation motifs and stem cell markers

As mentioned above, the staining for putative LESC markers ABCB5 and K19 overlapped. However, these markers also coincided with CS sulphation motifs recognised by antibodies 6C3 and 3B3(+), and also with HA. In particular, the two CS sulphation motifs were observed directly subjacent to the limbal trough and often skewed towards the scleral side of the trough. This matches the distribution of K19- and ABCB5-positive basal limbal epithelial cells within the trough. HA staining was found to extend more peripherally than just the limbal trough, yet this still co-localises with the distribution of the two potential LESC markers.

As HA and the sulphation motif epitopes recognised by 6C3 and 3B3 are all certainly present in the putative limbal stem cell niche area, this does raise the possibility that these GAGs play a role in regulating the LESCs. This could include maintaining the stem cell phenotype as suggested by Gesteira *et al.* (2017) for HA.

6C3 staining is located directly beneath the limbal trough but does not appear in subepithelial limbal stroma anterior or posterior to the trough. Based on the theories of Hayes *et al.* (2008) and of Schlötzer-Schrehardt *et al.* (2007), it may be expected that 6C3 would recognise a non- or low-sulphated CS epitope so that it can help maintain the stem cell phenotype at the trough. Unfortunately, the exact structure of the 6C3 epitope is yet to be determined but it has been shown to contain both 4-sulphated and 6-sulphated CS (Sorrell *et al.* 1993); however, the overall level of sulphation is uncertain.

The 7D4 epitope has been shown to involve low-sulphated CS (Hayes *et al.* 2008), yet its distribution at the porcine limbus does not fit in with the aforementioned hypotheses. A stronger 7D4 signal was occasionally seen subepithelially along the transition zone between the anterior limbus and peripheral cornea, which is the migration route of TACs, and it would therefore be expected that higher amounts of sulphation would be observed here in order to stimulate differentiation.

Schlötzer-Schrehardt *et al.* (2007) considered CS generally to be part of the anterior compartment of the limbal stem cell niche, responsible for inducing differentiation. This was based on the use of the CS-56 antibody to 4- and 6-sulphated CS. However, Hayes *et al.*'s theory is based on the structure of the cartilage stem cell niche, with 3B3(-), 7D4 and 4C3 labelling the superficial zone which is believed to constitute an area accommodating stem/progenitors cells, and is not directly comparable to the limbus. It is also important to note that the limbal stem cell niche of the porcine eye has not been examined in as much detail as the human. Therefore, it is not known for certain how far the stem cell compartment extends into the peripheral cornea and whether this could be different to humans. According to Majo *et al.* (2008), stem cells could be found throughout the porcine corneal epithelium and this could impact upon where one would expect to find CS within the tissue.

The epitopes of the CS antibodies used in this investigation have been implicated as developmental markers in foetal joint tissues, associating with the proposed stem/progenitor cells in these forming tissues. Studies on human foetal elbow tissue found that CS epitopes were expressed in developing cartilage and hair bulbs, in areas well established to host stem cell populations (Hayes *et al.* 2016). This was also found to be true in developing articular cartilage of human foetal knee joints, where CS (alongside HS PGs) was proposed to regulate cell behaviour, including proliferation and differentiation (Melrose *et al.* 2012). Further investigations using these monoclonal antibodies have shown that CS sulphation motif expression changes in a spatiotemporal manner in developing rat intervertebral disc and that the distributions of epitopes 3B3(-), 4C3 and 7D4 at embryonic day 19 may indicate a population of CS that regulates differentiation (Hayes *et al.* 2011). However, the studies mentioned above have not compared the sulphation motif distributions with those of putative stem cell markers.

5.4.5 Meridional differences

There do not appear to be any differences in the CS sulphation motif distributions or the staining of stem cell markers between the N/T and S/I areas of the porcine limbus. However, perhaps this should be expected if it is correct that the limbal trough constitutes the stem cell niche and that this is present around the whole circumference. The limbal trough was observed in both N/T and S/I areas, but it was only in the N/T limbus that the trough seemed to diminish. Yet even when the trough was not apparent, the same pattern of 6C3 staining could be seen, as could the staining patterns of the two limbal specific stem cell markers identified in this investigation. This suggests that the limbal trough is perhaps not the sole location of LESCs/progenitor cells in the porcine cornea. It is uncertain how this could link to the lower colony-forming efficiency demonstrated by limbal epithelial cells taken from the horizontal meridian (Notara *et al.* 2011).

5.4.6 Limitations

One of the limitations of this investigation is the same as others into LESCs – the lack of a specific LESC marker. This was compounded by very few putative stem cell markers being used with porcine tissue. Except for the p63α antibody, which was

chosen as it had been used by Notara *et al.* (2011) with porcine tissue, all other antibodies had to be chosen from selections that did not have confirmed reactivity with porcine tissue. Thus, it cannot be said with certainty that the anti-ABCG2 and anti-K3/K12 antibodies used here were suitably reactive with porcine tissue and potentially different results would be observed with antibodies with more favourable species reactivity.

There is also always the difficulty when examining stem cells in porcine tissue that you cannot look for label-retaining cells as you can in mouse experiments. This cannot be done *in vivo*; yet it has been done *ex vivo* in organ culture, where significantly more label-retaining cells were found in the porcine limbus than the cornea (Seyed-Safi and Daniels 2020). However, after four weeks, there were also some label-retaining cells in the corneal epithelium. Therefore, it is not possible to know exactly where the "true" LESC population may be located in the porcine limbus. The potential for labelling additional cell types outside of the true stem cell population is a recognised drawback to the use of marker molecules currently considered specific for putative stem cells; therefore, the ABCB5- and K19-positive cells identified here may include the LESCs but should not be presumed to all be true LESCs.

5.4.7 Conclusions

In summary, there does appear to be a differential distribution of CS sulphation motifs in the putative porcine limbal stem cell niche, based on the use of anti-CS antibodies with different epitope specificities. 6C3 and 3B3(+) both appear to stain the subepithelial limbal area with 6C3, in particular, associating with invaginations of limbal epithelium that constitute the limbal trough and may be similar to human LCs, and 3B3(+) associated with the nearby stromal cells. As well as HA, the CS sulphation motifs recognised by these antibodies could potentially have roles in stem cell maintenance in the porcine corneal/limbal epithelium. There is also a variation in the localisation of these epitopes across the width of the limbal area, suggesting different sulphation motifs may be contained in separate limbal stem cell niche compartments, as described by Schlötzer-Schrehardt *et al.* (2007). 6C3 staining matches that found at the stem cell niche area of both rabbits and humans,

thus, this is a promising candidate for recognising a CS sulphation motif that maintains the limbal stem cell phenotype across a range of mammalian species.

The porcine limbal trough contains a population of ABCB5- and K19-positive cells that may represent limbal epithelial progenitor cells. Due to staining patterns of the other stem cell and corneal epithelial differentiation markers, it is not possible to define with confidence these cells as true LESCs. Also, due to ABCB5 and K19 labelling posterior to the trough and in N/T areas without an obvious limbal trough, this investigation cannot confirm or refute the exact location of stem/progenitor cells or their niche at the porcine limbus. It may be the case that LESCs are not restricted to just the limbal trough in the porcine eye, like how they are believed to be restricted to the LCs in the human eye.

6 Epithelial-stromal cell interactions in the putative porcine limbal stem cell niche

6.1 Introduction

As mentioned in the introduction, stem cell niches consist of ECM and a range of surrounding cell types. The putative LESCs are in contact or close proximity to multiple cell types in the limbal stroma and also in the epithelia of the cornea, limbus, and conjunctiva. The epithelium is separated from the stroma by its basement membrane, in theory, preventing the cells in these different strata from directly contacting each other. However, it has already been proven that there are discontinuities in the limbal basement membrane that allow stromal and basal epithelial cells to interact.

In both humans and rabbits, SBFSEM has shown breaks in the limbal basement membrane that facilitate interactions between superficial stromal cells and the basal epithelial cells (Dziasko *et al.* 2014; Yamada *et al.* 2015). Stromal cells often extend long processes that approach the basement membrane and then penetrate it to contact the basal epithelium. The basal epithelial cells that are contacted sometimes demonstrate a stem cell-like morphology, raising the possibility of these connections forming part of the stem cell niche.

The nature/phenotype of stromal cell types that are in contact with the epithelium is not entirely certain. They are cells of mesenchymal origin, with keratocytes being derived from the neural crest during development (Zieske 2004). The presence of MSCs has been confirmed in the human limbus (Polisetty *et al.* 2008; Branch *et al.* 2012) and they are believed to form part of the putative limbal stem cell niche. Numerous cell markers have been used to attempt to characterise cells from the limbal stroma, including putative stem markers. Aquaporin-1 (AQP-1), connexin 43, CD73, CD90, CD105, vimentin and α-enolase are just some of those investigated (Polisetty *et al.* 2008; Higa *et al.* 2013; Funderburgh *et al.* 2016) and some of these will be used in the current investigation.

Epithelial-mesenchymal transition (EMT) is also believed to occur in the limbus, involving putative LESCs. Parfitt *et al.* (2015) showed the presence of label-retaining cells in the limbal stroma of mice which could only have come from the epithelium and then migrated into the stroma. Kawakita *et al.* (2005) also demonstrated invasion of the limbal stroma by epithelial cells that had undergone EMT after air-lifting of limbal explants. However, limbal EMT has not been demonstrated *in vivo*, nor has evidence of limbal epithelial cells in the process of EMT been presented.

The presence of these direct cell-cell interactions across the limbal basement membrane has yet to be examined in porcine eyes. In this investigation, the porcine limbal epithelial basement membrane area, subjacent to the limbal trough, will be examined using SBFSEM to determine if these interactions are present here. The areas chosen demonstrate an abundance of stromal cells in very close proximity to the trough, as seen in previous chapters. Immunohistochemical analysis will also be performed to characterise the stromal cell types in close proximity to the epithelial basement membrane to determine which cell types may be involved in these connections.

The hypothesis for this chapter is that direct cell-cell interactions between basal limbal epithelial cells and stromal cells will be observed in the porcine cornea. The other hypothesis is that SBFSEM may be able to be used to identify cells that were possibly undergoing EMT or mesenchymal-epithelial transition at the time of tissue fixation.

6.2 Materials and methods

6.2.1 Serial block-face scanning electron microscopy

6.2.1.1 Preparation of tissue samples

3 porcine eyes were oriented as discussed in section 2.2 and then four limbal segments were manually dissected from each eye; these were taken with their longest axis perpendicular to the limbal tangent (Figure 6.1). The tissue segments were then fixed in 2.5% glutaraldehyde/2% PFA in 0.1 M sodium cacodylate buffer

(pH 7.2) (Appendix 2.6) overnight at 4°C. The segments were washed in 0.1 M sodium cacodylate buffer after this and then stored in buffer at 4°C until the next step in tissue preparation.

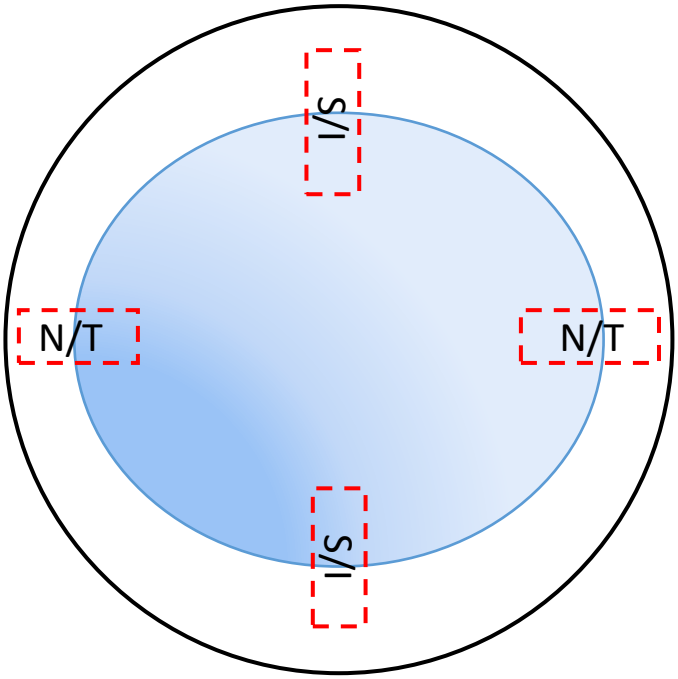

Figure 6.1- An illustration demonstrating how tissue was dissected for this experiment.
Full-thickness sections were taken. Blue area = cornea, white area = sclera. (Not to scale).

Tissue segments were prepared for SBFSEM using a modified "Deerinck" method (Deerinck *et al.* 2010). This staining method allows for the observation of general cell and tissue morphology. All solutions and distilled water were passed through Minisart® syringe filters (Sartorius Stedim Biotech GmbH, Goettingen, Germany) onto the tissue samples. The tissue segments were immersed in 1.5% potassium ferricyanide/1% osmium tetroxide (Appendix 4.1) for 1 hour, followed by 5 x 5 mins washes in distilled water. This was followed by 1 x 30 mins in 1% aqueous thiocarbohydrazide (Appendix 4.1) and then 5 x 5 mins washing in distilled water. The segments were then transferred to 1% aqueous osmium tetroxide (Appendix 2.8) for 1 hour, again, followed by 5 x 5 mins washing in distilled water. Next, the tissue was placed in 1% aqueous UA (Appendix 4.1) (1 x 1 hour), then distilled water (5 x 5 mins). All of these steps were carried out at room temperature.

The tissue segments were then immersed in Walton's lead aspartate (Appendix 4.2) for 1 hour at 60°C. This was followed by 5 x 5 mins washing in distilled water at

room temperature again, then the tissue was dehydrated and embedded in Araldite resin as described in section 2.3.1.

6.2.1.2 Cutting resin blocks

The surfaces of the polymerised blocks were cut away and polished using a Reichert-Jung Ultracut E microtome. Several semi-thin sections of 300 nm were cut first and stained with toluidine blue. These were then assessed on a light microscope to check the quality of tissue processing and select appropriate regions of interest. The blocks were trimmed smaller using razor blades so that only approximately 1 x 2 mm regions of interest, where stromal cells were in close proximity to the epithelial basement membrane of the limbal trough, were sectioned.

6.2.1.3 Image acquisition

The block was then mounted on a Gatan specimen pin (Gatan UK, Oxford, UK), with the polished surface uppermost, using super glue and left to dry for several hours. A silver epoxy resin (TAAB Laboratories, Aldermaston, UK) was then applied to the sides of the specimen block, ensuring it came into contact with the surface of the pin, and left to dry for at least 24 hours. This is applied to remove any charging of the specimen during imaging. The surface to be imaged was then polished further using a diamond knife on the microtome.

The specimen pin was gold coated with approximately 8 nm of gold using a Leica ACE 200 sputter coater (Leica Microsystems, Wetzlar, Germany). The pin was inserted into the Zeiss Sigma VP FEG SEM (Carl Zeiss Ltd, Cambridge, UK) equipped with a Gatan 3View®2 system (Gatan UK, Oxford, UK) within the chamber and imaged at 3.5 KV, a pixel resolution of 5 nm and a dwell time of 8 µs. The Gatan software was set for automated acquisition of serial images, each image alternating with the removal of a 100 nm slice of the block surface by the in-chamber diamond knife. All SBFSEM datasets were recorded at 4096 x 4096 resolution. Imaging was performed by Dr Robert Young at Cardiff University's School of Optometry and Vision Sciences.

6.2.1.4 *Image processing*

For each dataset, 365-549 images were collected. These were then batch converted to TIF format and uploaded to Amira software (FEI, Mérignac, France) for processing and analysis. Due to the complexity and elaborate nature of the structures being examined, the generation of 3D reconstructions of epithelial-stromal cell interactions was performed via manual segmentation and surface generation.

Due to restrictions imposed by the Covid-19 pandemic and subsequent equipment failures, only one S/I sample from one eye was able to be imaged during the thesis timeframe. The results for this sample will be presented below.

6.2.2 Immunohistochemistry

Immunohistochemistry was performed on three porcine eyes as described in Section 2.4. The sections were incubated with the primary antibodies detailed in Table 6.1. The secondary antibodies utilised were a 1:1000 dilution of Alexa Fluor® 594-conjugated goat anti-mouse IgG secondary antibody (Abcam, Cambridge, UK) for sections labelled with MEM-229 and sections labelled with all other antibodies were incubated with a 1:1000 dilution of Alexa Fluor® 594-conjugated goat anti-rabbit IgG secondary antibody (Abcam, Cambridge, UK), all for 1 hour at room temperature.

Antibody (dilution)	Clonality/Isotype	Specificity	Source/Reference
Anti-ALDH3A1 antibody (1:100)	Rabbit polyclonal, IgG	Aldehyde Dehydrogenase 3 Family Member A1 (ALDH3A1)	Abcam, Cambridge, UK
Anti-VE cadherin antibody (1:200)	Rabbit polyclonal, IgG	Vascular endothelial cadherin/cadherin 5/CD144	Abcam, Cambridge, UK (Li *et al.* 2009)
Anti-Aquaporin 1 antibody (1:100)	Rabbit polyclonal, IgG	Aquaporin 1	Abcam, Cambridge, UK (Echevarría *et al.* 2007)
EPR3133 (1:100)	Rabbit monoclonal, IgG	CD90	Abcam, Cambridge, UK (Ramírez *et al.* 2011)
MEM-229 (1:100)	Mouse monoclonal, IgG2a	CD105	Abcam, Cambridge, UK (Singh *et al.* 2012)

Table 6.1- Primary antibodies used in this investigation.

6.3 Results

6.3.1 3D niche reconstruction

Images acquired via SBFSEM were taken from the base of a very prominent section of the limbal trough with many stromal cells close to the basement membrane (Figure 6.2, red box). As was seen with TEM assessment in sections 4.3.1.2 and 4.3.2.2, the basement membrane of the porcine limbal epithelium was very irregular and this was also seen with SBFSEM (Figure 6.3). Many processes and lobed protrusions of the basal epithelial cells extended into the limbal stroma (Figure 6.3, arrowheads). Large stromal cells in the subjacent stroma extended processes of their own that projected towards the basal epithelium (Figure 6.3, arrows).

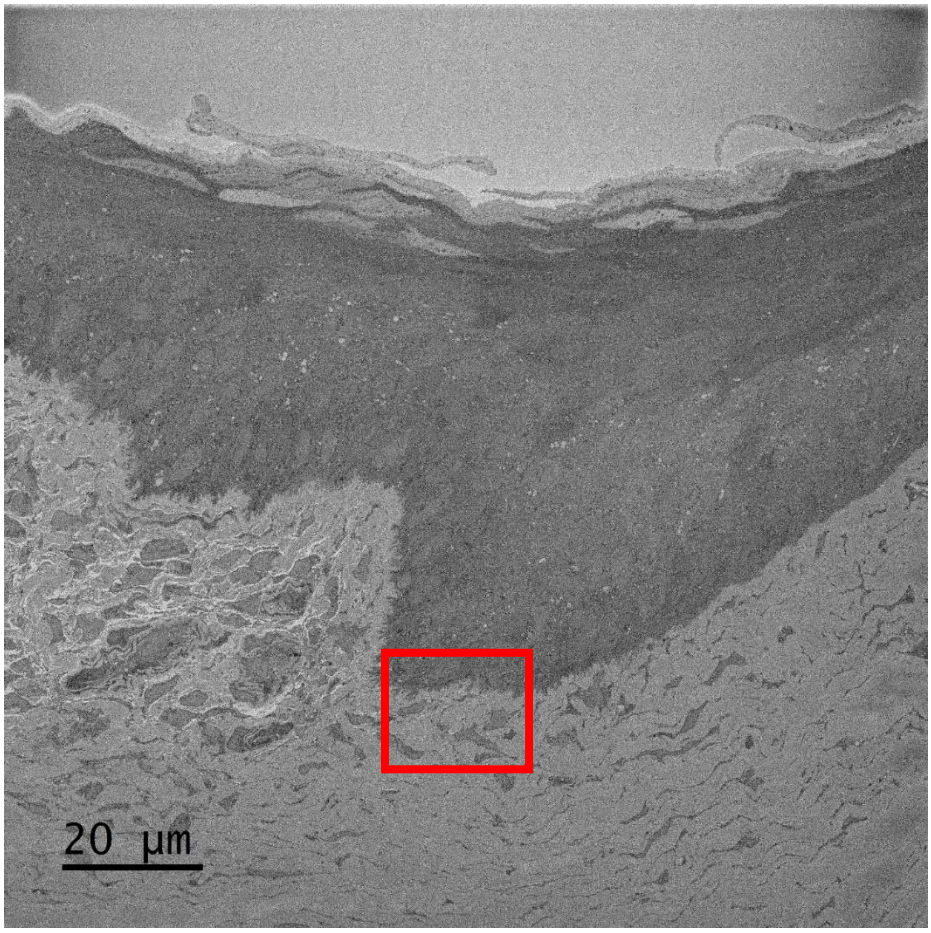

Figure 6.2- A lower magnification serial block-face scanning electron microscopy image demonstrating the area that was used for serial imaging and subsequent 3D reconstructions.
An area was chosen at the very base of the limbal trough where many stromal cells were in the vicinity of the epithelial basement membrane (red box).

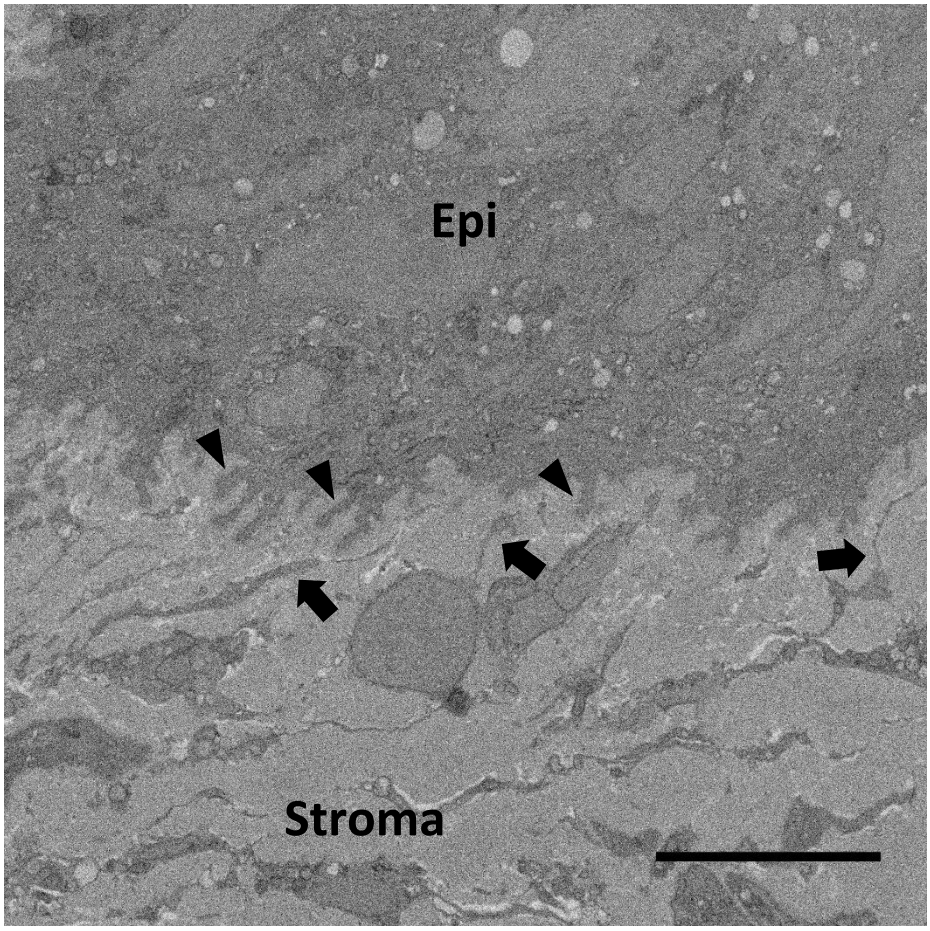

Figure 6.3- A serial block-face scanning electron microscopy image of the epithelial-stromal interface in the porcine limbus.
Many protrusions of the basal epithelial cells (arrowheads) extend into the underlying limbal stroma, whilst stromal cells also extend processes towards the epithelium (arrows). Epi = epithelium. Scale bar = 5 µm.

Some of these stromal cell processes were found to directly contact the basal epithelium (Figure 6.4). Processes would extend towards the epithelial basement membrane and form a focal contact with the basal epithelium, often at one of the projections of the epithelium into the underlying stroma.

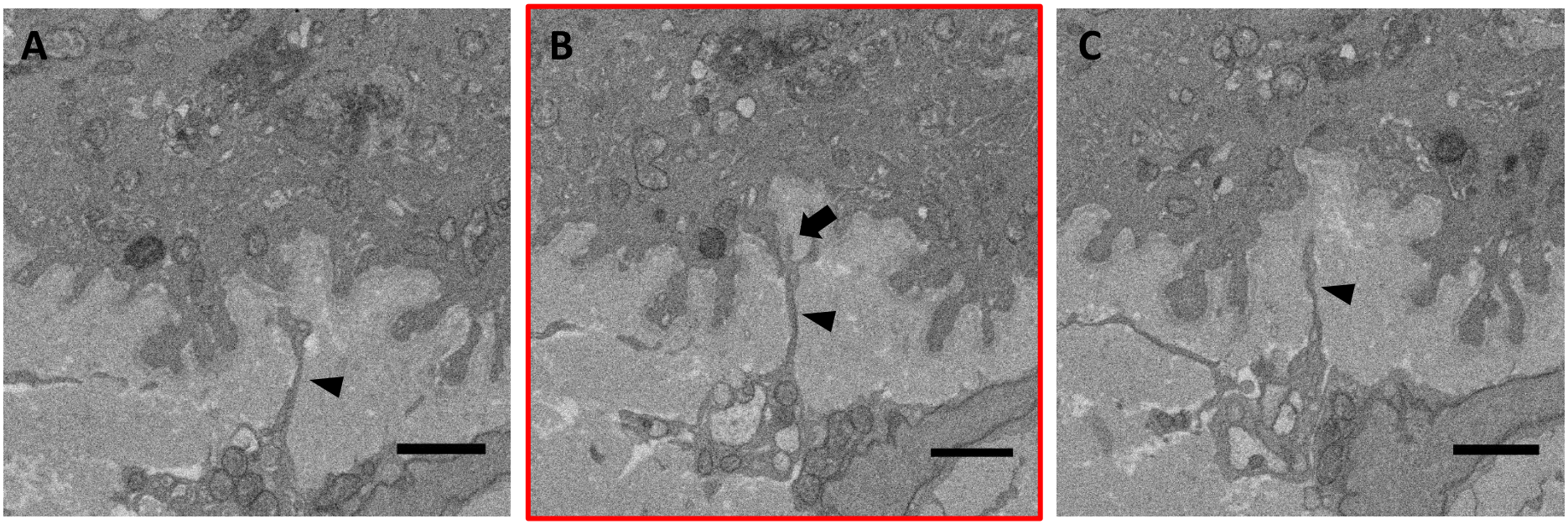

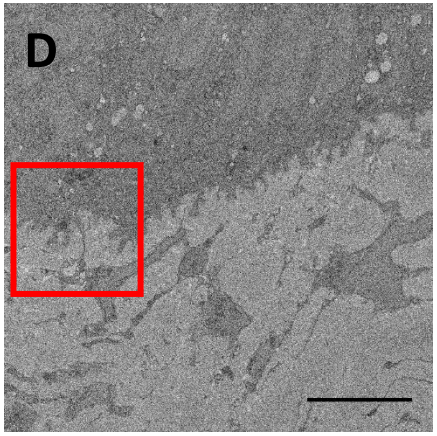

Figure 6.4- Direct contact between a limbal stromal cell and a basal epithelial cell.
Images 400 nm apart demonstrate a process from a stromal cell (arrowheads) extending towards the basal epithelium (A) to then form a focal contact with the epithelial cell (B, arrow). The process then retreats away from the epithelium once more (C). D demonstrates the area of the specimen where this direct contact was observed. Scale bars (A, B, C) = 1 µm, scale bar (D) = 5 µm.

3D reconstructions further demonstrated how irregular the basement membrane profile was (Figure 6.5). These reconstructions also revealed direct cell-cell interaction between limbal stromal cells and basal epithelial cells (Figure 6.6, supplementary video 9). Processes extending from the stromal cells (blue volume) would progress towards the epithelial basement membrane and some of these would form a focal contact with a basal epithelial cell (green volume). Some of these contacts would be at the projections from the epithelial cells themselves but could also be seen at less prominent protrusions as well (Figure 6.7). One stromal cell could make more than one contact with the basal epithelium, as seen in Figure 6.7 and supplementary video 10.

Supplementary video 9: A serial block-face scanning electron microscopy 3D reconstruction of the stromal-epithelial interface in the superior/inferior porcine limbus. The green volume represents the limbal epithelium within the limbal trough and the blue volume represents a limbal stromal cell. The stromal cell extends a process towards the undulating epithelial basement membrane and makes direct contact with an epithelial cell. https://figshare.com/s/f23795c14ce9326c4b11

Supplementary video 10: A serial block-face scanning electron microscopy 3D reconstruction of the stromal-epithelial interface in the superior/inferior porcine limbus. The green volume represents the limbal epithelium within the limbal trough and the blue volume represents a limbal stromal cell. Here, the stromal cell makes more than one contact with the limbal epithelium. https://figshare.com/s/89b446ca41e8b41398d1

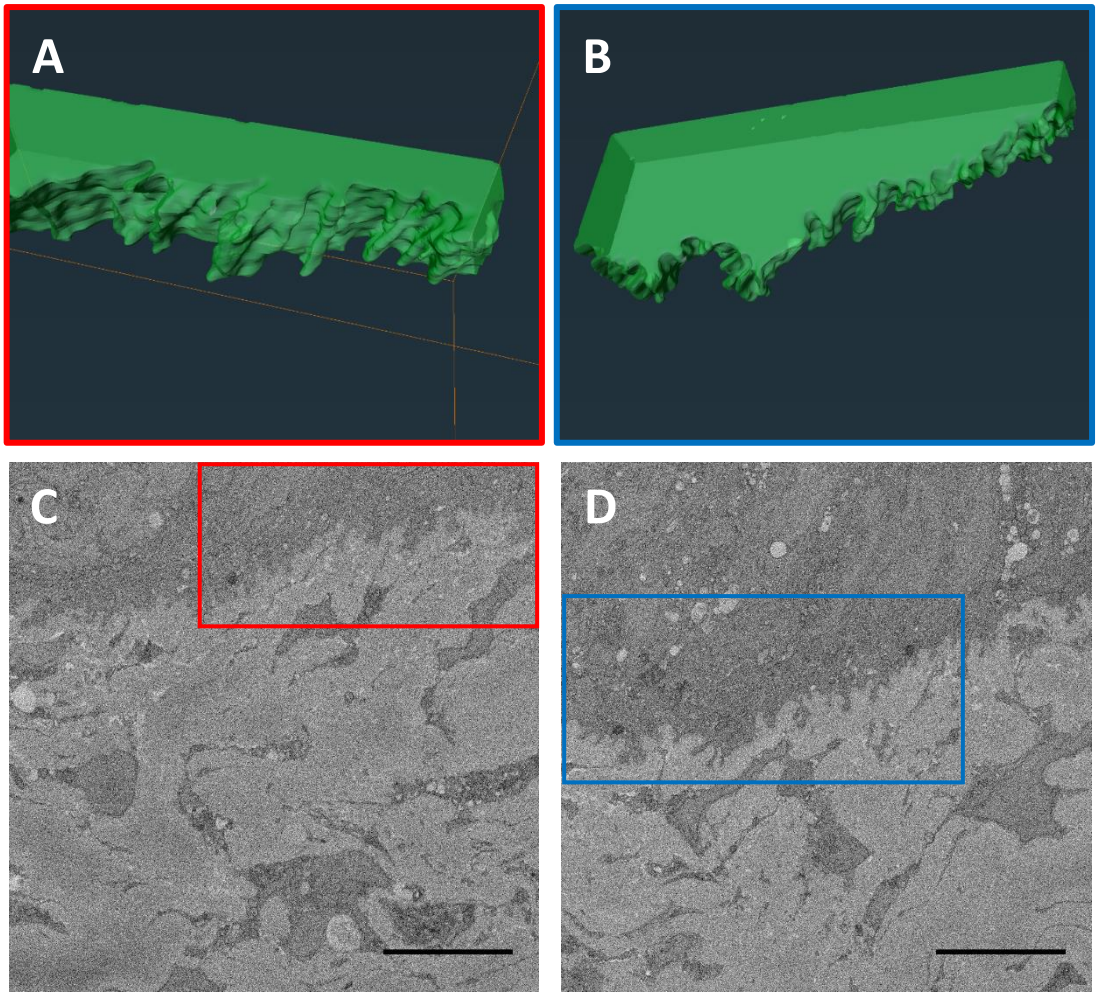

Figure 6.5- 3D reconstructions of a section of porcine limbal epithelium from serial block-face scanning electron microscopy images.

The green volumes (A and B) represent limbal epithelium and the basal surface, at the bottom of the volume, shows a very irregular profile with many protrusions and invaginations. C and D demonstrate where each 3D reconstruction was taken from. Scale bars = 5 µm.

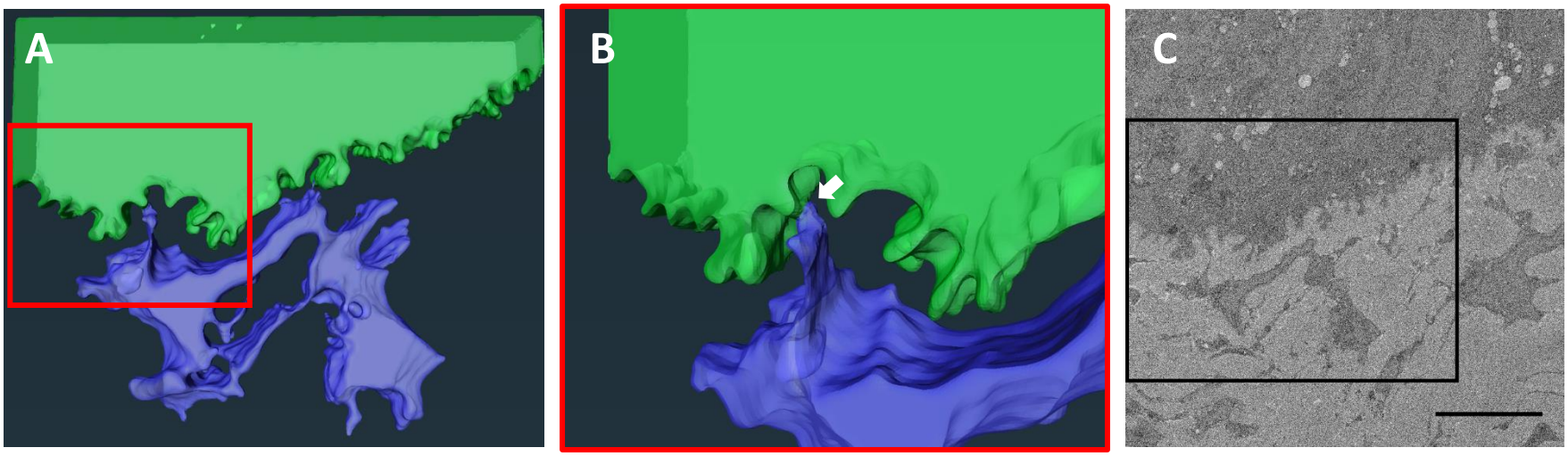

Figure 6.6- A 3D reconstruction of the porcine limbal epithelium demonstrating a direct contact between a stromal cell and the epithelium.
There are large stromal cells (blue volume) in close proximity to the basal limbal epithelium (green volume) (A) and these cells extend processes that then directly contact an epithelial cell (B, arrow). C demonstrates where the 3D reconstruction was taken from. Scale bar = 5 µm.

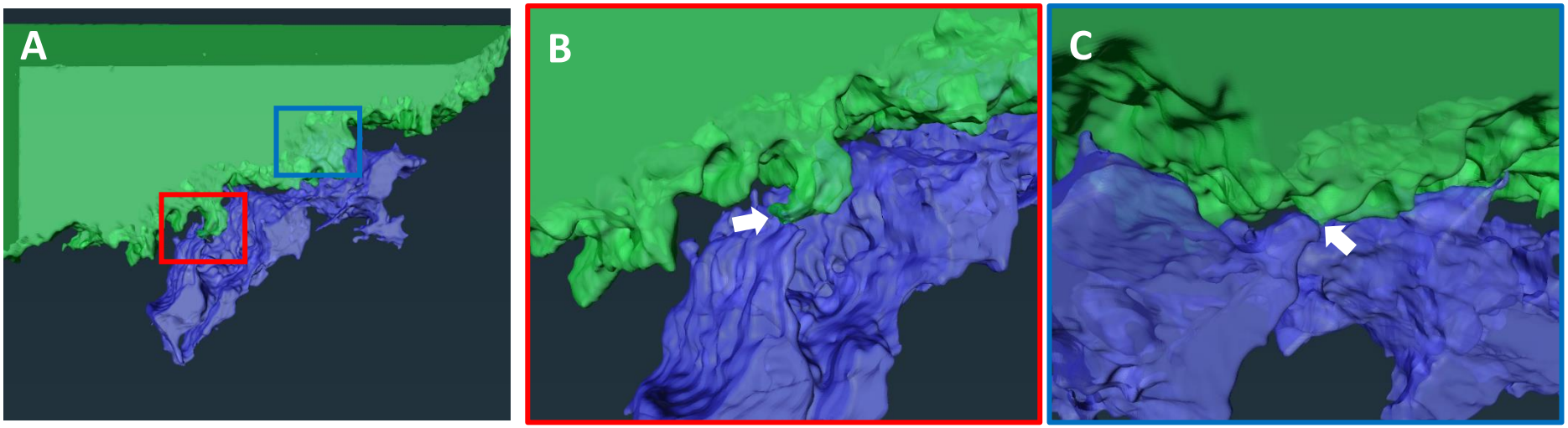

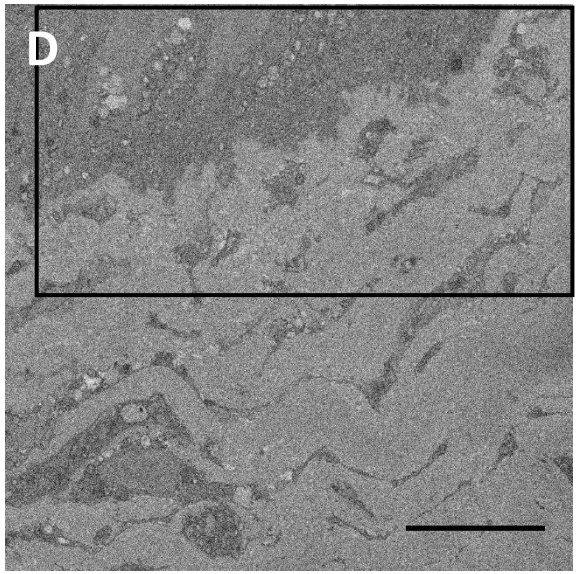

Figure 6.7- A 3D reconstruction demonstrating a stromal cell forming multiple connections with the limbal epithelium.

A large stromal cell (blue volume) close to the epithelial basement membrane forms direct contacts with the epithelium at two points (arrows). In B, the epithelium extends a process to meet the process from the stromal cell. Whereas in C, which is on the back surface of this reconstruction, the stromal process makes contact on a much less prominent protrusion of the epithelium. D demonstrates where the 3D reconstruction was taken from. Scale bar = 5µm.

6.3.2 Immunohistochemistry of stromal cells

6.3.2.1 ALDH3A1 and VE cadherin

Weak ALDH3A1 staining was widespread throughout the limbal stroma, both superficially and deeper (Figure 6.8). Staining was also found throughout the peripheral corneal stroma (Figure 6.10A, B). There was no difference in the distribution between the horizontal and vertical meridians, though staining was weaker in the vertical meridian.

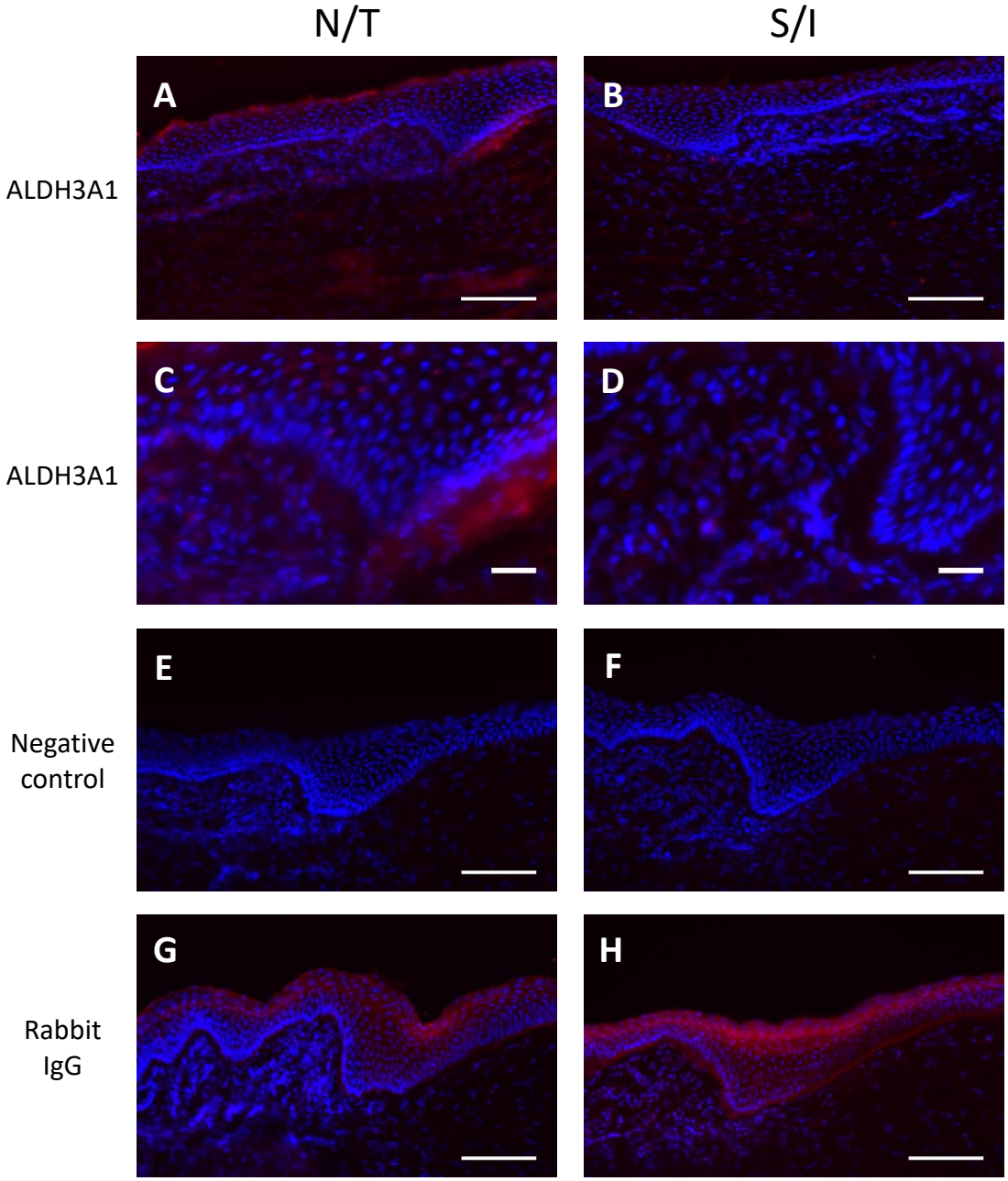

Figure 6.8- Staining of ALDH3A1 within the porcine limbus.
Staining for ALDH3A1 (A-D, red) is found throughout the limbal stroma in both superior/inferior and nasal/temporal areas of the limbus. Scale bars (A, B, E, F, G, H) = 100 µm, (C, D) = 20 µm. DAPI- blue.

VE cadherin was expressed weakly throughout the limbal and peripheral corneal stroma, and also very strongly in the epithelium (Figures 6.9 and 6.10C, D). However, there was some stronger expression of VE cadherin in the superficial limbal stroma, posterior to the limbal trough (Figure 6.9A, B, arrows). Some of these VE cadherin-positive cells were in close proximity to the base of the limbal trough (Figure 6.9C, D, arrowheads). Again, there was no difference between the N/T and S/I limbus.

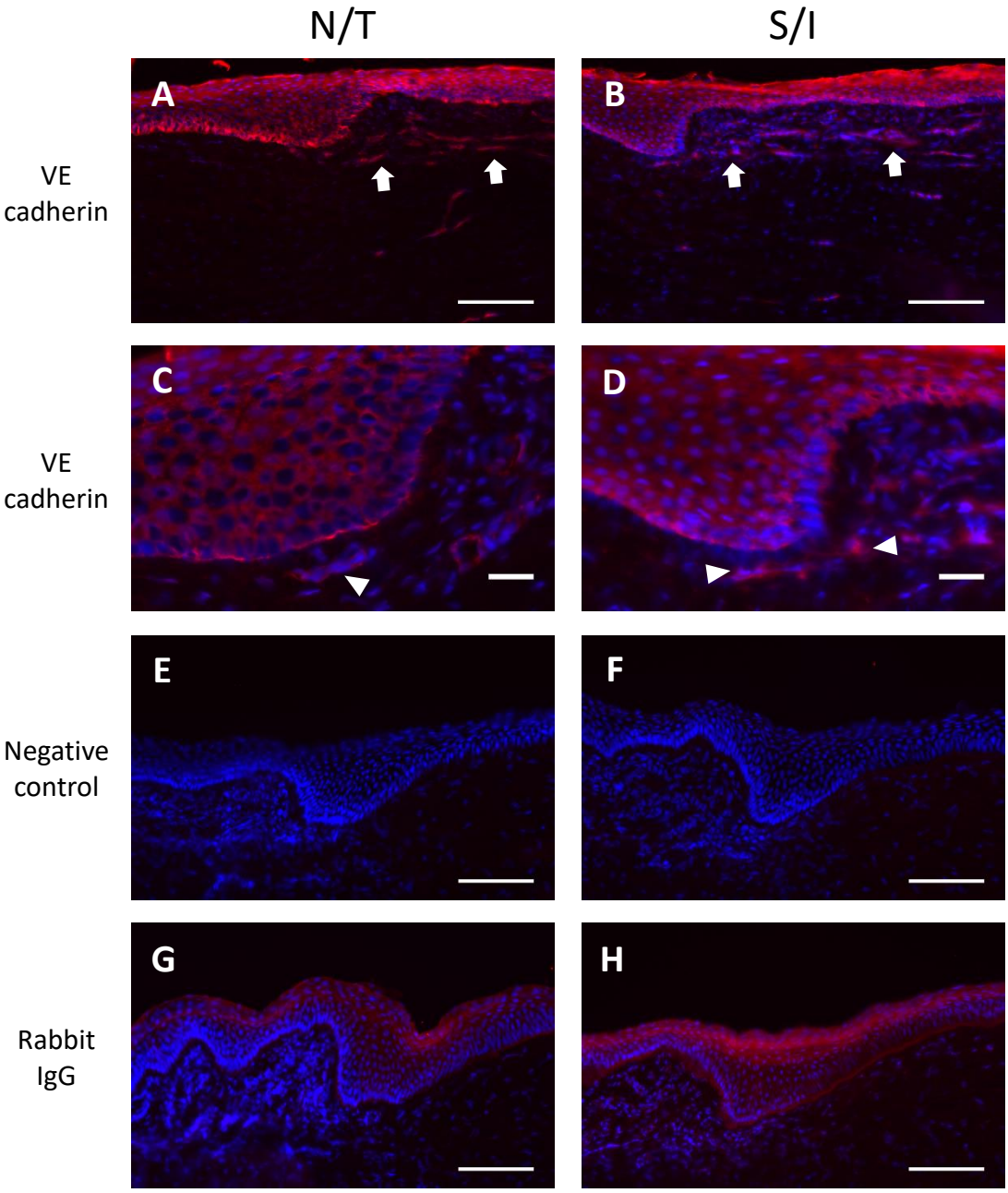

Figure 6.9- Staining of vascular endothelial cadherin within the porcine limbus. *Vascular endothelial cadherin (A-D, red) is expressed throughout the limbal stroma but is especially strong in the subepithelial stroma posterior to the limbal trough (arrows) and some of these cells are close to the epithelial basement membrane (arrowheads). Vascular endothelial cadherin is also expressed by the epithelium, though some of this may be non-specific labelling as demonstrated by the staining with naïve rabbit IgG (G and H, red). Scale bars (A, B, E, F, G, H) = 100 µm, (C, D) = 20 µm. DAPI- blue.*

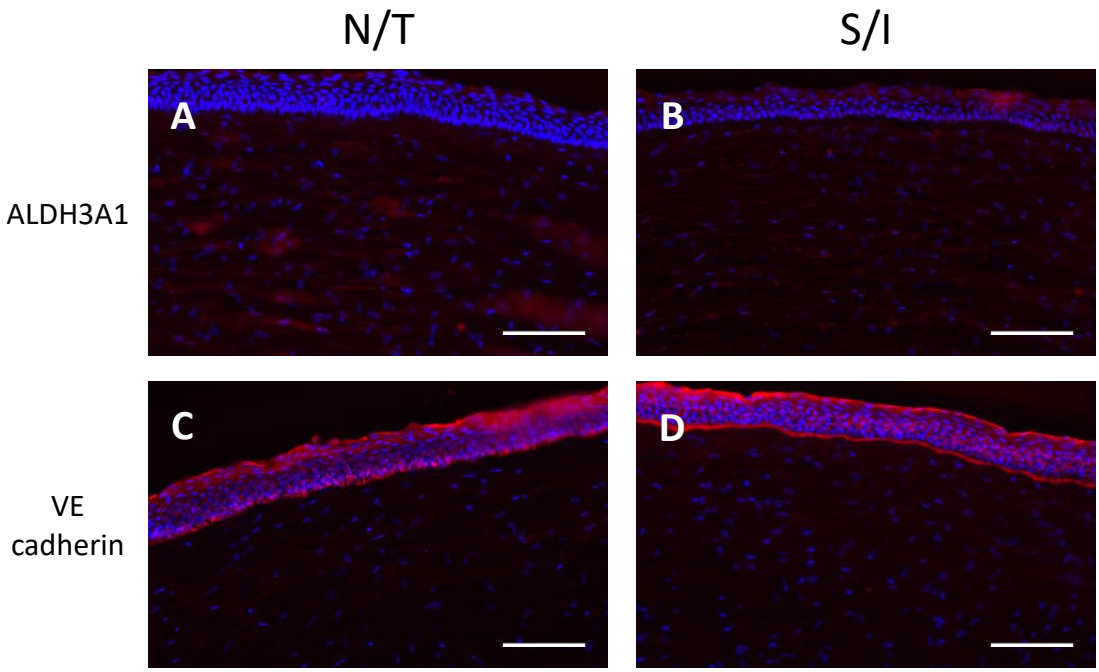

Figure 6.10- Staining of ALDH3A1 and vascular endothelial cadherin within the porcine peripheral cornea.
Both ALDH3A1 (A, B, red) and vascular endothelial cadherin (C, D, red) are expressed within the corneal stroma at a similar level as the limbal stroma. Scale bar = 100 µm. DAPI- blue.

6.3.2.2 AQP1, CD90 and CD105

Weak staining for AQP1 was also observed throughout the limbal stroma in both the N/T and S/I areas (Figure 6.11). However, stronger staining was seen in the subepithelial limbal stroma posterior to the limbal trough (Figure 6.11A, B, arrows), as was seen with VE cadherin. Numerous cells subjacent to the base of the limbal trough demonstrate weak AQP1-positivity (Figure 6.11C, D).

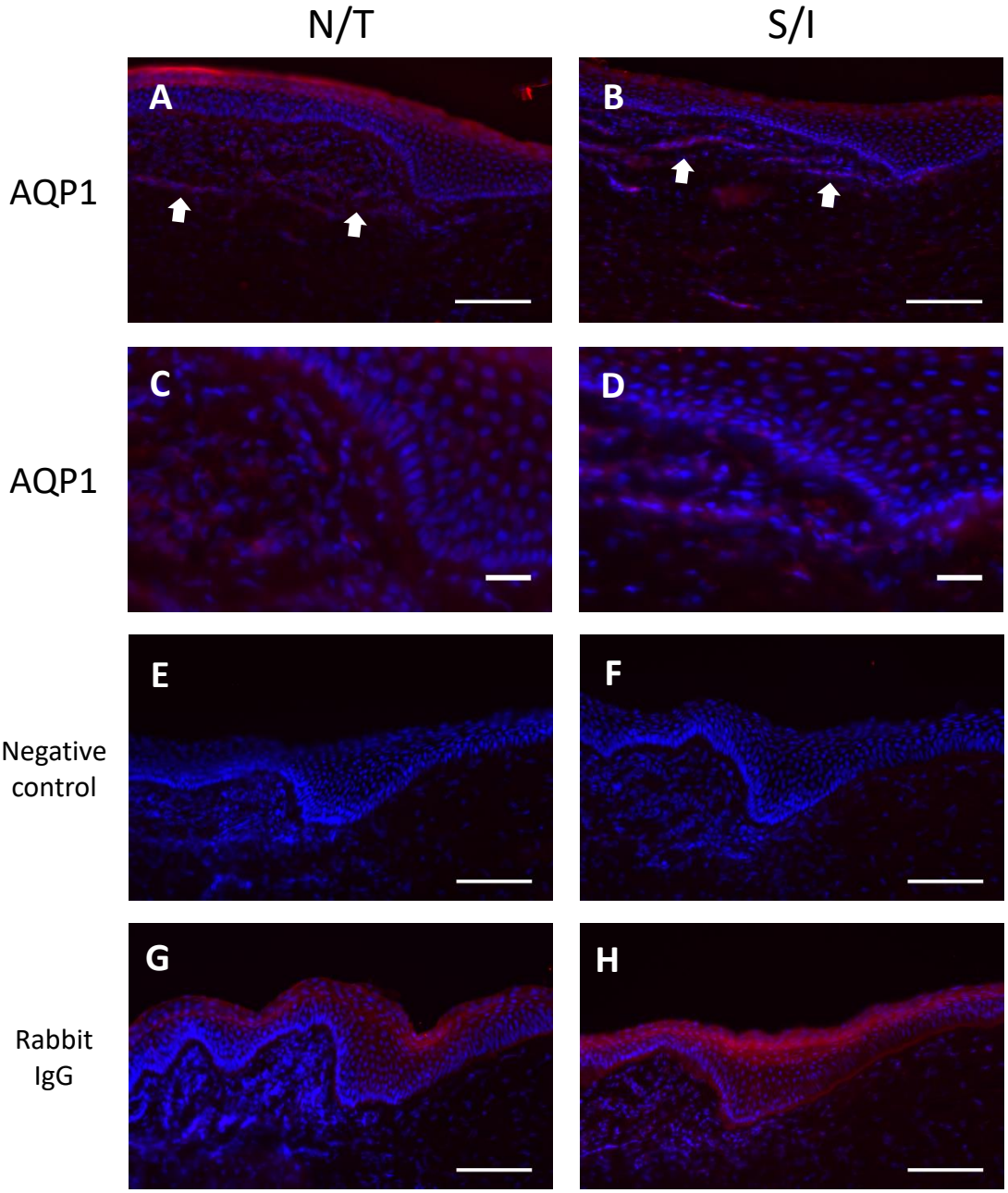

Figure 6.11- Staining of aquaporin 1 within the porcine limbus.
Weak aquaporin 1 (A-D, red) staining is found throughout the limbal stroma with stronger staining visible in the subepithelial stroma posterior to limbal trough (arrows). Scale bars (A, B, E, F, G, H) = 100 µm, (C, D) = 20 µm. DAPI- blue.

No CD90 staining was observed anywhere in the peripheral corneal or limbal stroma (Figure 6.12). Positivity for CD105, however, could be seen weakly in the subepithelial limbal stroma in both the horizontal and vertical meridians (Figure 6.13A, B, arrows), including in stromal cells in close proximity to the basal epithelium of the limbal trough (Figure 6.13C, D, arrowheads). There was no CD105 staining within the peripheral corneal stroma (Figure 6.14).

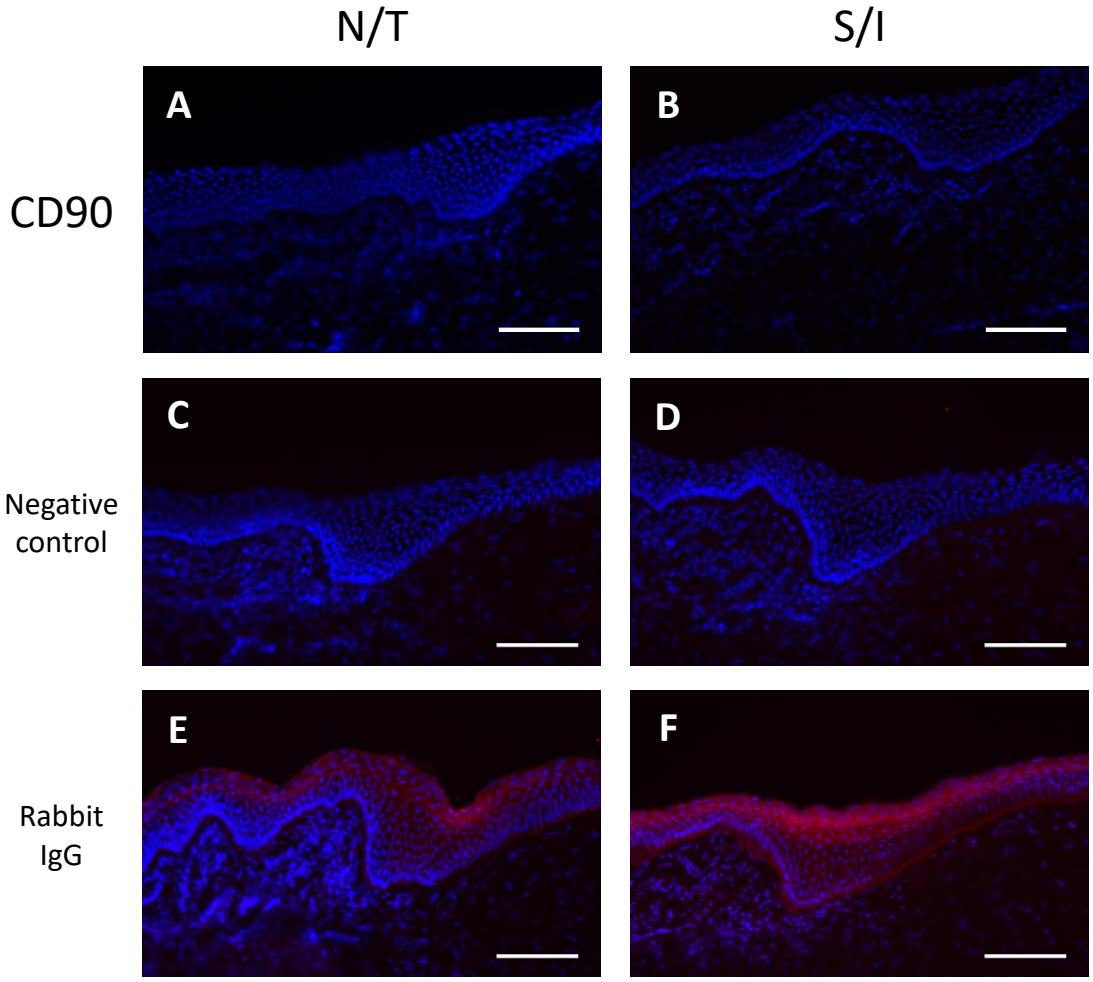

Figure 6.12- Staining of CD90 within the porcine limbus.
No staining for CD90 can be seen anywhere within the porcine limbus. Scale bar = 100 µm. DAPI- blue.

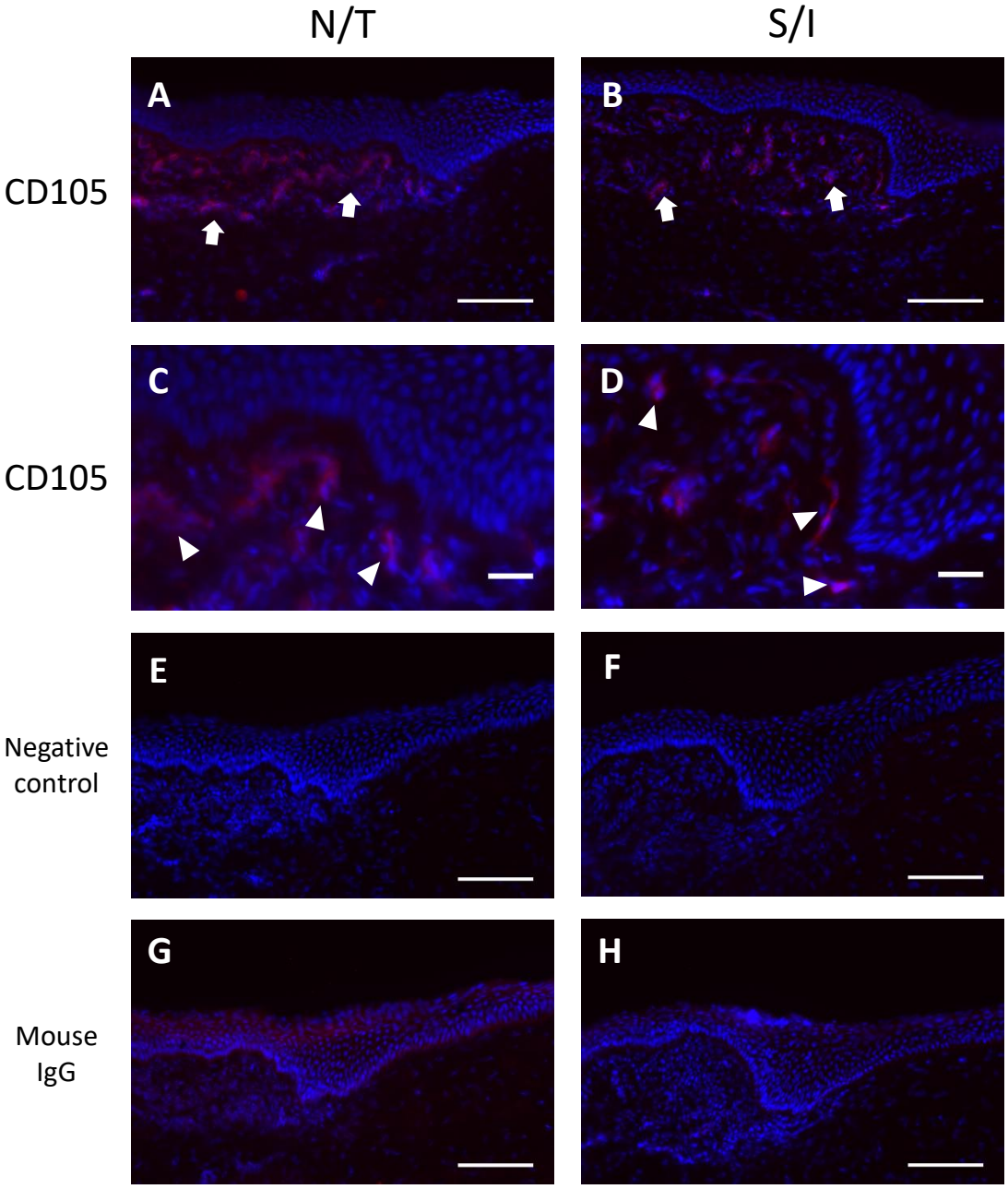

Figure 6.13- Staining of CD105 within the porcine limbus.
CD105 (A-D, red) expression is only seen in the subepithelial limbal stroma, posterior to the limbal trough (arrows). Some of these cells are close to the basal epithelium of the limbal trough (arrowheads), yet there is a distinct cell-free gap between the epithelium and stromal cell populations. Scale bars (A, B, E, F, G, H) = 100 µm, (C, D) = 20 µm. DAPI- blue.

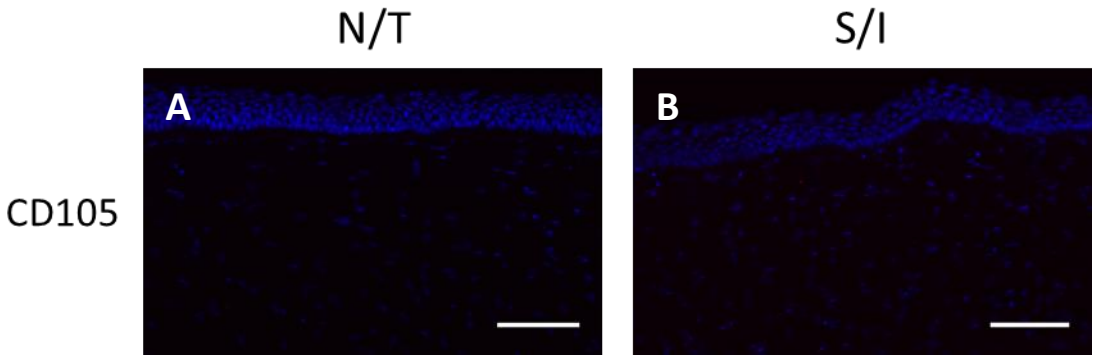

Figure 6.14- Staining of CD105 within the porcine peripheral cornea.
No staining for CD105 is found within the porcine peripheral cornea. Scale bar = 100 µm. DAPI- blue.

6.4 Discussion

6.4.1 Cell-cell interactions in the porcine limbal stem cell niche

It has already been demonstrated that direct interactions between stromal cells and epithelial cells are present in the putative limbal stem cell niches of humans and rabbits (Dziasko *et al.* 2014; Yamada *et al.* 2015), and this investigation shows that they are also present in the porcine limbus. This is now the third mammalian species shown to have this cellular feature at the limbus.

This investigation has also confirmed the observations, seen in chapter 4, of an irregular epithelial basement membrane profile in the porcine limbus. This is very similar to the findings in the rabbit limbus by Yamada *et al.* (2015) where, in the absence of LCs, the basement membrane has this very irregular profile in order to increase the surface area. However, unlike the rabbit limbus, the porcine eye also has larger epithelial protrusions – the limbal trough identified in this project – which also increases surface area here.

The appearance of the stromal processes and the epithelial-stromal cellular connections in porcine tissue are similar to those demonstrated by Yamada *et al.* (2015) and Dziasko *et al.* (2014) in rabbits and humans respectively. The contacts formed in the human limbus were identified at the lateral "walls" of the LCs, whereas the connections observed in the porcine limbus were at the base of the trough. Dziasko and associates demonstrated that the epithelial basement membrane profile is fairly regular in the region of human LCs and, thus, the appearance of the porcine limbus is more similar to that of the rabbit. A large number of stromal cell processes were observed in the porcine limbus and most of these extended towards the epithelial basement membrane, often in very close proximity to it. However, there were only a small number of confirmed direct contacts between these processes and the epithelial cells. It is possible that some of the processes in close proximity to the basement membrane may have formed direct contact, but this feature was removed within the 100 nm serial section taken by the 3View system. This could be improved by reducing the sectioning to 50 nm, allowing greater resolution along the Z-axis.

Both Dziasko and Yamada were able to identify small basal epithelial cells with a high nucleus to cytoplasm ratio. As mentioned in section 1.2.3.1, cells with this morphology are believed to represent the putative LESCs. In humans, it was confirmed that these smaller limbal epithelial cells were involved in the direct contacts with stromal cells. The current investigation has presented images at lower resolution and contrast than the two aforementioned studies, leading to the plasma membranes of epithelial cells being difficult to discern. Thus, it was difficult to discern whether there were any smaller basal epithelial cells with a high nucleus to cytoplasm ratios and whether they were being contacted by the stromal cell processes. The epithelial basement membrane can also be distinguished fully in the human and rabbit investigations, whereas it cannot in the images presented here of the porcine limbus.

As previously stated, the cell types surrounding an adult stem cell population are believed to be key components of the stem cell niche. The presence of direct cell-cell contacts across the epithelial basement membrane in the limbus has raised the notion that these supporting stromal cells directly impact the putative stem cells, as well as via chemical signalling. The important influence of stromal cells on limbal epithelial cells has been demonstrated several times *in vitro*/*ex vivo*. Zhang *et al.* (2010) demonstrated that human limbus-derived mesenchymal cells were as effective as the standard 3T3 fibroblasts as a feeder layer for culturing human limbal epithelial cells, including potentially preserving LESCs. Culturing limbal epithelial progenitor cells with stromal cells of limbal origin has been shown to be better than culturing with those of corneal or scleral origin (Ainscough *et al.* 2011). Chen *et al.* (2011) showed that isolating human LESCs using collagenase also harvests the underlying stromal cells that are in close association with them. It was then shown that culturing these cells together, as opposed to LESCs on their own, helps to maintain the stem cell phenotype (Xie *et al.* 2012; González and Deng 2013).

Melanocytes within the limbal epithelium are another cell type within the putative limbal stem cell niche that forms direct connections with potential LESCs. This has been demonstrated in the human limbus via SBFSEM and melanocytes were found

to be preferentially located in the LCs (Dziasko *et al.* 2014). The melanocytes were closely associated to the apical surface of basal epithelial cells with a stem-like morphology within the LCs. As with stromal cells, limbal melanocytes have also been found to support limbal epithelial cell growth *in vitro* (Dziasko *et al.* 2015). Human limbal melanocytes as a feeder layer appeared to be just as effective as the standard 3T3 feeder cells for the initial expansion of LESCs. Furthermore, culturing the epithelial cells on "real architecture for 3D tissue" (RAFT) tissue equivalents resulted in a stratified, multi-layered epithelium with superficial cells that were terminally differentiated and less differentiated basal cells, when co-cultured with limbal melanocytes. The porcine limbus is quite heavily pigmented, however, no cells that looked similar to limbal melanocytes were seen in the specimen assessed in the current investigation. This is something that requires further investigation as limbal melanocytes are likely to be present in the porcine limbus and may also form close connections to putative LESCs.

It was hoped that evidence of a cell undergoing EMT at the time of tissue processing may be collected via serial block-face imaging. The hypothesis was that if stromal cell-epithelial cell direct contacts were observed and the entirety of the two cells involved could be analysed/reconstructed and only one nucleus was found between the two cells, this would indicate that this could in fact be a single cell undergoing either EMT or mesenchymal-epithelial transition. It would not be possible to distinguish which process was occurring from SBFSEM data alone. However, it was very difficult to reconstruct cells in their entirety, especially stromal cells due to their branched morphology, and the process became unwieldy. It was also the case with the data presented here that a nucleus was detected in every cell, whether stromal or epithelial, that was involved in direct contact and, thus, were not undergoing either transition process. It is also the case that EMT is quite a rare phenomenon under normal, homeostatic conditions and, thus, the chances of observing a cell undergoing this process is rather low. However, this could still be an *ex vivo* method to observe cells in the midst of one of these transitions.

6.4.2 Stromal cell populations in the stem cell niche

Attempts were made in this investigation to identify the cell populations that may be present in the stromal compartment of the limbal stem cell niche. This would then provide an idea of which stromal cells could be forming direct contacts with the basal epithelial cells. It can be seen in most immunofluorescence images that there is a distinct cell nucleus-free gap between the limbal epithelium and the stromal cell populations, part of which will consist of the epithelial basement membrane. Only a few cell nuclei were observed within this gap and these are the cells that are most likely to be in direct contact with the basal epithelium. Despite the presence of stromal cell processes that extend towards the epithelial cells, demonstrated above, the distance between the majority of stromal cells and the basal epithelium suggests that these slightly deeper cells are unlikely to be forming direct connections.

ALDH3A1 and VE cadherin were chosen as markers of fully differentiated keratocytes (Chakravarti *et al.* 2004; Pei *et al.* 2006; Scott *et al.* 2011; Zhang *et al.* 2013); thus, the presence of staining for both of these markers throughout the limbal and corneal stroma is as expected. This suggests that the population of stromal cells within the putative limbal stem cell niche does include fully differentiated keratocytes. Yet, whether these keratocytes have a role in LESC maintenance is uncertain. VE cadherin staining was stronger in the subepithelial limbal stroma. However, this is where limbal blood vessels would be located and – as the name suggests – VE cadherin is found at the endothelial cell junctions of blood vessels (Lampugnani *et al.* 1992) and the increased staining could potentially be related to this. Yet, there were also VE cadherin-positive stromal cells that were in very close proximity to the basal epithelial cells of the limbal trough. Indeed, in this investigation, these were the stromal cells that were observed closest to the epithelium.

The MSC marker expression of putative MSCs taken from the limbal stroma and confirmed bone marrow MSCs has been compared using the markers CD90 and CD105, as well as CD29, CD71 and CD166 by Polisetty *et al.* (2008). The limbal stromal cells were found to express significant amounts of CD90, CD29 and CD166

that were similar to bone marrow MSCs. Limbal MSCs expressed much less CD105 and expressed more CD71 than bone marrow-derived cells. These results are at odds with the current investigation, where no CD90 expression was observed in the porcine limbus but CD105 staining was observed. Isolated limbal stromal cells from humans have been identified that express CD90 and CD105 (Li *et al.* 2012) and stromal cells positive for MSC markers CD90 and CD105 have been observed immediately subjacent to the limbal epithelial basement membrane (Mathews *et al.* 2015). These stromal MSCs were in extremely close proximity to the epithelial cells, but a direct connection was not reported. Dziasko *et al.* (2014) also demonstrated CD90- and CD105-positive cells in the superficial limbal stroma but postulated that they were too deep within the stroma to be the cells making direct contact with the basal epithelium. There do not appear to be any CD105-positive cells within the nucleus-free gap between the epithelial basement membrane and the emergence of superficial stromal cells in the porcine cornea, suggesting these too may not be involved in cell-cell interactions.

Previous investigation of human limbal stromal niche cells revealed direct interactions between a population of stromal cells potentially positive for AQP1 and putative LESCs using TEM (Higa *et al.* 2013). These cells were found to be vimentin-positive but were not melanocytes or vascular/lymphatic endothelial cells. This interaction was suggested to be a calcium-dependent adhesion via N-cadherin. These AQP1-positive cells were noted by Dziasko *et al.*, in their 2014 study, to have a similar morphology and location to the cells that they observed contacting epithelial cells. As in the current investigation, Higa and associates showed that AQP1-positive cells appeared to be widespread throughout the superficial limbal stroma but some, in particular, were in extremely close proximity to basal epithelial cells. No stromal cells were observed in such near proximity in the porcine limbal stem cell niche. AQP1 staining was stronger in the subepithelial stroma, but no cells positive for AQP1 were located close enough to the basal epithelium to suggest being sufficiently near to form direct cell-cell contact.

6.4.3 Limitations

Originally, four limbal sections from three porcine eyes were prepared for this experiment. However, due to shutdowns imposed due to the Covid-19 pandemic and subsequent equipment outages following a return to the lab, only one sample from one eye was able to be imaged. Thus, the sample size is not ideal, yet proof of direct epithelial cell-stromal cell interactions within the porcine limbal stem cell niche has been demonstrated, specifically within the vertical meridian of the limbus. It was hoped that at least one S/I specimen and one N/T specimen could be imaged to determine whether direct cell-cell interactions are present in the putative stem cell niche of both meridians of the porcine limbus. This is something that will need to be explored in future work.

As with the immunofluorescence assessment of putative LESC markers in chapter 5, there was difficulty in finding appropriate antibodies with confirmed reactivity in porcine tissue. Only the anti-CD105 antibody was confirmed to be reactive with porcine tissue and this antibody did provide good results. Based on the results of previous studies, positivity for CD90 in the limbal stroma was expected, but no staining was observed with the antibody used in this investigation. This may be a true result or it could be down to this antibody not being suitable for use with porcine tissue. To investigate this, several antibodies to CD90 should be applied to see if any are reactive with the tissue, as none were found in the initial search for appropriate antibodies.

Another issue when choosing which antibodies to use in this study was the vast array of potential markers that could be investigated (Funderburgh *et al.* 2016). Ultimately, markers that appeared most frequently in the published literature were used. However, these do not represent a definitive identification of putative stromal stem cells and the characterisation of the subepithelial stromal cells of the porcine limbus could be investigated in greater detail by utilising more of the potential markers.

Using SBFSEM, it is not possible to assess immunohistochemical markers that would identify which cell types are involved in the stromal cell-epithelial cell interactions. The sample processing has to be performed *en bloc*, meaning antibodies would not

be able to penetrate very far into the specimen. Higa *et al.* (2013) suggested AQP1-positive stromal cells formed direct contacts with epithelial basal cells via N-cadherin based on separate immunofluorescence images and TEM images, and also in cell culture experiments. However, there was no evidence in the high-resolution TEM images to show that the stromal cells were the AQP1-positive cells. This could be remedied by using immuno correlative light and electron microscopy (Vicidomini *et al.* 2010; Oorschot *et al.* 2014). Under this approach, the same tissue sections in which stromal cells positive for specific markers have been identified via immunofluorescence microscopy could then be assessed with immuno-electron microscopy (Burgoyne *et al.* 2018) to determine whether any of the cells positive for the markers make direct contact with putative LESCs.

6.4.4 Conclusions

The putative limbal stem cell niche of the porcine cornea does include direct cell-cell interactions between stromal cells and the basal epithelial cells, as found in the human and rabbit corneas. The characteristics of these stromal cells are still uncertain. Immunohistochemical data show that stromal cells of the porcine limbus include keratocytes, CD105-positive and AQP1-positive cells, yet further investigation is required to determine which cells are actually in contact with the putative LESCs. Of the stromal cells observed to be in close proximity to the basal epithelium, it was actually VE cadherin-positive cells – suggesting a fully differentiated keratocyte phenotype – that were closest to the epithelial cells.

It is often stated that the limbal stromal ECM composition is one that favours the maintenance of the LESC phenotype and it is within this environment that stromal stem cells are also found (Funderburgh *et al.* 2016). It is then postulated that the presence of these MSCs in the subepithelial stroma constitutes part of the limbal epithelial stem cell niche and their presence helps maintain the epithelial stem cell population (Zhang *et al.* 2010; Chen *et al.* 2011; Xie *et al.* 2012). However, it could be the case that the limbus serves as a niche to both the stromal and epithelial stem cell populations and that the presence of the other stem cell type is mutually beneficial in maintaining stemness. The limbal microenvironment is generally only discussed as being for the benefit of maintaining the LESC population, but it could

equally be there to support stromal stem cells and even the presence of LESCs could be to sustain the stromal stem cell population, as well as vice versa. Studies by Du *et al.* (2009) certainly suggest that the limbal stromal microenvironment is also for the benefit of the stromal stem cell population, with human limbal MSCs differentiating into keratocytes when injected into mouse central corneas.

Direct interaction between the stromal and epithelial cells of the limbus has been clearly demonstrated to be beneficial to the LESC population. Future research now needs to examine how to incorporate this into better treatment of LSCD, particularly when niche reconstruction is needed.

7 Concluding discussion

7.1 Justification for use of a porcine model

At the start of the research described in this thesis, all experimentation was planned to be done on *ex vivo* human tissue. However, these plans had to be abandoned due to supply issues and experimental failures.

The initial source of tissue was human corneoscleral rims provided by collaborators at Kyoto Prefectural University of Medicine. However, the transit time and the fact that these corneas had originally come from US institutions meant that the tissue was in an unusable condition once it arrived in the UK. An attempt to overcome this problem was made when I personally visited and worked for several weeks within Kyoto Prefectural University of Medicine and Baptist Eye Hospital in Kyoto, but still the human tissue was found to be unusable on account of structural degradation, including stromal swelling and loss of outer cell layers.

The next attempt involved using human corneas from UK eye banks. These corneas were transplant-expired and had been stored in organ culture medium for at least 28 days and, again, it was found that once they arrived they were in an unusable condition for the experimentation used in this project.

These tissue sources also led to long wait times for new tissue, thus, it was decided to switch to a porcine model as tissue could be acquired on a weekly basis and in large numbers. As mentioned in sections 1.1.7 and 1.2.2.1, the porcine eye is also already believed to be a suitable model for the human eye due to similarities in size and structure. The main similarity that led to porcine tissue use was the presence of LCs in the porcine limbus, structures that other easily-accessible sources of tissue (mice, rabbits) lack (Grieve *et al.* 2015; Yamada *et al.* 2015).

Notara *et al.* (2011) believe that the porcine limbus can be used as a suitable and accessible model for the human limbal stem cell niche. As well as finding LCs and believing they were distributed in the same way as humans, they also found that de-epithelialised porcine corneas can be used to support the *in vitro* growth of

human limbal epithelial cells and Huang *et al.* (2011) found the same result for supporting rabbit limbal epithelial cell growth. A more recent study compared the protein composition of decellularised corneas of several different species to that in humans, in order to determine the most suitable source of material for xenogeneic grafts, and the porcine cornea was found to be most similar to the human cornea (Sharifi *et al.* 2019). The porcine cornea had a Total Protein Sequence Similarity Score of 91.8%. Thus, these factors led to the decision to use porcine tissue as a model during the investigations in this thesis.

7.2 Conclusions

The results of this thesis both confirm and caution the use of porcine corneas as a model for the human system. The finding of Bowman's layer in the porcine cornea, though it is much thinner and comprises significantly less of the corneal thickness than in the human counterpart, demonstrates that it does consist of the same five layers as found in the human cornea. Additionally, the change in collagen fibril organisation that accompanies the transition of Bowman's layer into the limbal stroma has been demonstrated quantitatively for the first time, confirming its presence. Thus, the porcine cornea is a suitable model tissue system.

Porcine tissue has been used as a model for the limbal epithelial stem cell niche due to its accessibility and the believed presence of LCs analogous to those in humans (Notara *et al.* 2011; Grieve *et al.* 2015). However, this investigation has shown that the limbal epithelial architecture is not as similar to the human cornea as originally thought. It was noticed with all imaging techniques; immunofluorescence images with DAPI nuclear staining, light micrographs of Toluidine blue-stained sections, EM of ultrathin sections, SEM image slices; that a limbal crypt-like structure was present in virtually every image. This prompted the notion of porcine tissue containing one or more continuous, annular limbal crypts that span the entire limbal circumference, which was then demonstrated with microCT. This represents a divergence from human tissue, where multiple, small, discrete LCs are found. As aforementioned, the presence of LCs/Palisades of Vogt noted in previous

investigations of porcine tissue could be accounted for if the Palisades are sufficiently thin that the resolution of the microCT used here could not detect them, or if the imaging plane of the previous studies was at the base of the limbal trough so that small undulations were erroneously taken to represent LCs.

It has also been effectively demonstrated that there are no differences between the horizontal and vertical meridians of the porcine limbus. The distribution of KS and CS/DS PGs, specific CS sulphation motifs, HA, and putative LESC markers did not differ between any of the four quadrants of the porcine limbus. The preferential location of LCs, and thus LESCs, seen in the human eye (Goldberg and Bron 1982; Shortt *et al.* 2007) is not repeated in the porcine cornea. Thus, this significant difference in niche structure must be considered when using a porcine model for the limbal epithelial stem cell niche.

Yet, numerous similarities between the porcine stem cell niche and those of the rabbit and humans have been discovered in this thesis. All three species demonstrate direct cell-cell interaction between basal limbal epithelial cells and stromal niche cells (Dziasko *et al.* 2014; Yamada *et al.* 2015). Pores were identified in the peripheral Bowman's layer that have already been suggested as the channel for corneal nerves (Komai and Ushiki 1991) but could also be openings to allow cellular crosstalk between the two strata. In the process of identifying these cell connections and during TEM assessment, the similarity of the porcine limbal basement membrane profile to the rabbit was demonstrated. It is interesting that the porcine cornea includes the limbal trough, something analogous though not identical to the human limbal crypts, but also includes this very irregular basement membrane as seen in the crypt-less rabbit. The limbal trough would not increase surface area as much as LCs/Palisades of Vogt would. Thus, potentially the porcine limbus has this irregular epithelial basement membrane profile to supplement the limbal trough in increasing the available surface area for interactions between the epithelium and the stromal ECM/cells within the putative stem cell niche.

Cupromeronic blue staining demonstrated the similarity in corneal PG distribution between porcine tissue and human. However, the limbal distribution has not been examined in detail before. Thus, the porcine results presented here are the first to

specifically examine the limbus with cupromeronic blue dye. This did demonstrate differences between the limbus and cornea, though further investigation is required to understand fully which GAGs are involved.

Pigs, rabbits, and humans all demonstrate an abundance of the CS sulphation motif recognised by antibody 6C3 in the subepithelial stroma of the niche (Yamada *et al.* 2015). 3B3(+) is also present in this area in pigs and rabbits (Yamada *et al.* 2015). It has also been shown here that the porcine limbal trough, as well as the limbal epithelium posterior to this, contains a population of epithelial cells that are positive for the putative stem cell markers K19 and ABCB5. The above-mentioned GAGs, as well as HA, coincide with the distribution of these cells suggesting they may have a role in stem cell maintenance – something that has already been proven in the case of HA (Gesteira *et al.* 2017).

The epitope of antibody 6C3 is currently not fully identified, thus, the characteristics of this CS sulphation motif are not known. This is something that requires further investigation to see if it supports the theory of Hayes and associates, which would suggest it is a low sulphated CS oligosaccharide. It is also important to discern where exactly the 6C3 sulphation motif is. It could be matrix-bound, attached to stromal cells in close proximity to the epithelium or, in fact, be a connecting molecule between the two. It could be that the 6C3 epitope is attached specifically to the stromal cells involved in the cell-cell interactions, though the depth of 6C3 staining suggest this may not be the case. The PGs that this epitope is incorporated into also need to be elucidated. The neoepitope recognised by antibody 3B3(+) follows a similar distribution to 6C3 and seems to be closely associated to superficial stromal cells. The full scope of the interactions of ECM, PGs, stromal cells, and epithelial cells is key to understanding how stemness is maintained, and how differentiation and proliferation are induced when leaving the limbal niche area. The fact that the abundance of 6C3 in the subepithelial stroma of the limbal stem cell niche is preserved across three different mammalian species suggests 6C3 could have an important role here.

This thesis has demonstrated that CS and HA are GAGs that form a significant part of the matrix environment of the porcine limbal stem cell niche; something that is

seen in other mammalian species too. These GAGs coincide with potential stem/progenitor cell populations and are promising candidates as regulators of stemness. Indeed, work within the research group has already begun investigating how CS sulphation motifs can impact the development of iPS cells into corneal epithelial cells. Despite the presence of a limbal trough in place of LCs, the presence of direct cell-cell interactions in the porcine LESC niche suggests porcine tissue is still a good model to use and could help in the development of future treatments of limbal stem cell deficiency, including niche reconstruction.

7.3 Future work

As previously mentioned, the epitope recognised by antibody 6C3 is not currently fully identified. This is something that needs to be determined to help elucidate its characteristics, the role it plays in the epithelial stem cell niche and how it does this. Many of the CS antibodies (1B5, 2B6, 3B3, 7D4) produced by the Caterson/Hughes laboratory in Cardiff University's School of Biosciences have more fully understood epitopes (Hayes *et al.* 2008; Caterson 2012), but 6C3 remains to be investigated.

Linked to this is the need to determine exactly where 6C3 is found within the subepithelial stroma. This could be done via immuno-electron microscopy or correlative light and electron microscopy. These high-resolution approaches would allow the distinction of whether this epitope is matrix-bound or cell-bound and give an idea of which cell types it is attached to. Immunofluorescence investigation would also allow for co-localisation studies to determine which PGs and cell types may be associated with the 6C3 epitope.

Further investigation of the cell-cell interactions identified here in the porcine limbus is also required. A greater number of samples needs to be investigated and the nasal/temporal limbus needs to be assessed to determine if cell-cell interactions are also found here. Additionally, it is apparent that there is a large population of stromal cells in close proximity to the epithelial basement membrane posterior to the limbal trough and it should be determined whether these cells are also forming direct contact with basal epithelial cells. Based on the findings in this

thesis that there are no differences between the vertical and horizontal meridians, stromal cell-epithelial cell interactions would be expected in the horizontal meridian. The presence of direct interactions between melanocytes and putative LESCs also needs to be investigated. Preliminary results have shown melanocytes in close association with porcine basal epithelial cells.

Future work should also include examining the impact of including 6C3 in the culturing of limbal epithelial grafts and also incorporating it into LESC niche reconstruction. This could include the use of bioengineered tissue implants to help with the significant shortage of donor corneal tissue and remove the need for autologous limbal explants and would be better for those with bilateral injury.

Appendices

Appendix 1- Solutions and formulations used for X-ray microtomography

Appendix 1.1

4% paraformaldehyde in 0.01 M PBS

Make double strength PBS:

1. Dissolve two PBS tablets (Fisher Scientific UK Ltd, Loughborough, UK) in 200 ml of distilled water.

Make 10% PFA:

1. Add 10 g PFA powder (Agar Scientific Ltd, Stansted, UK) to 100 ml of distilled water
2. Depolymerise PFA by heating to 65°C and periodically swirling
3. Add freshly made 1 M NaOH (0.4 g of sodium hydroxide pellets (Fisher Scientific UK Ltd, Loughborough, UK) in 10 ml distilled water), one drop at a time, and swirl the solution until it becomes clear
4. Cool and then filter through Whatman No. 1 filter paper (Whatman International Ltd, Maidstone, UK).

Mix double strength PBS : 10% PFA : distilled water at a ratio of 5:4:1.

Appendix 1.2

0.5% paraformaldehyde in 0.01 M PBS

1. Make double strength PBS and 10% PFA, as above.
2. Mix double strength PBS : 10% PFA : distilled water at a ratio of 10:1:9.

Appendix 1.3

2% phosphotungstic acid

Dissolve 2 g of phosphotungstic acid powder (Taab Laboratory Equipment Ltd, Aldermaston, UK) in 100 ml of distilled water.

0.6% phosphotungstic acid in 70% ethanol

Mix 30 ml of 2% PTA (made above) with 70 ml of 100% ethanol (Fisher Scientific UK Ltd, Loughborough, UK).

Appendix 1.4

1% osmium tetroxide in 0.01 M PBS

Add 5 ml of stock 2% osmium tetroxide (Agar Scientific Ltd, Stansted, UK) to 5 ml of double strength PBS made above.

Appendix 2- Solutions and formulations used for transmission electron microscopy and scanning electron microscopy

Appendix 2.1

Tris/sodium acetate buffer (without BSA, pH 7.2)

To make double strength Tris/sodium acetate buffer (without BSA, pH 7.2, 50 mM Tris, 60 mM sodium acetate):

1. Add 0.121 g of Tris (Sigma-Aldrich Company Ltd, Gillingham, UK) and 0.0984 g of sodium acetate (Sigma-Aldrich Company Ltd, Gillingham, UK) to 100 ml of distilled water and dissolve
2. Match pH to 7.2

Dilute 1:1 with distilled water to make single strength buffer for rinsing/washing.

4% PFA in Tris/sodium acetate buffer (without BSA, pH 7.2)

1. Make 10% PFA (Appendix 1.1).
2. Mix 50 ml of double strength Tris/sodium acetate buffer (without BSA, pH 7.2), 40 ml of 10% PFA and 10 ml distilled water.

Appendix 2.2

Tris/sodium acetate buffer (with 0.02% BSA, pH 8, 50 mM Tris, 60 mM sodium acetate)

To make double strength Tris/sodium acetate (with BSA, pH 8):

1. Take 50 ml of Tris/sodium acetate buffer made in Appendix 2.1, add 0.02 g of BSA (Sigma-Aldrich Company Ltd, Gillingham, UK)
2. Match pH to 8

Dilute 1:1 with distilled water to make single strength buffer for rinsing/washing.

Appendix 2.3

Chondroitinase ABC 2 units/ml

1. Add 2450 µl of distilled water to vial of chondroitinase ABC from *Proteus vulgaris* 10 units (Sigma-Aldrich Company Ltd, Gillingham, UK) to reconstitute the enzyme
2. Add to the 2450 µl of reconstituted chondroitinase ABC: 2500 µl of double strength Tris/sodium acetate buffer (with BSA, pH 8), 50 µl of protease inhibitor cocktail (Sigma-Aldrich Company Ltd, Gillingham, UK).

Appendix 2.4

25 mM sodium acetate buffer (pH 5.7) containing 0.1 M $MgCl_2$

To make double strength 25 mM sodium acetate buffer (pH 5.7) containing 0.1 M $MgCl_2$:

1. Add 0.41 g of sodium acetate and 4.06 g of magnesium chloride (Fisher Scientific UK Ltd, Loughborough, UK) to 100 ml of distilled water and dissolve
2. Match pH to 5.7.

Dilute 1:1 with distilled water to make single strength buffer for rinsing/washing.

2.5% glutaraldehyde in 25 mM sodium acetate buffer (pH 5.7) containing 0.1 M $MgCl_2$ and 0.05% cupromeronic blue

1. Take 15 ml of double strength sodium acetate buffer made above, add 12 ml of distilled water and 3 ml of 25% glutaraldehyde (Agar Scientific Ltd, Stansted, UK)
2. Add 0.015 g of cupromeronic blue dye (Sigma-Aldrich Company Ltd, Gillingham, UK) and agitate to dissolve.

Appendix 2.5

0.5% Aqueous sodium tungstate

Add 0.05 g of sodium tungstate powder (VWR International Ltd, Luttermouth, UK) to 10 ml of distilled water and dissolve.

0.5% sodium tungstate in 50% ethanol

Add 0.05 g of sodium tungstate powder to 10 ml of 50% ethanol and dissolve.

Appendix 2.6

Araldite resin

1. Pre-warm Araldite monomer CY212 (Agar Scientific Ltd, Stansted, UK) and dodecenylsuccinic anhydride (DDSA) hardener (Agar Scientific Ltd, Stansted, UK) in oven.
2. Measure out 126 ml of Araldite monomer, 144 ml of DDSA and 5.4 ml of BDMA accelerator (Taab Laboratory Equipment Ltd, Aldermaston, UK).
3. Add all components to a pre-warmed conical flask and mix thoroughly by swirling.

Appendix 2.7

0.2 M sodium cacodylate buffer (pH 7.2)

1. Add 4.28 g of sodium cacodylate (Agar Scientific Ltd, Stansted, UK) and 0.044 g of calcium chloride dehydrate (Fisher Scientific UK Ltd, Loughborough, UK) to 50 ml of distilled water and dissolve.
2. Match pH to 7.2.
3. Make volume up to 100 ml with distilled water.

Dilute 1:1 with distilled water to make 0.1 M sodium cacodylate buffer.

2.5% glutaraldehyde/2% PFA in 0.1 M sodium cacodylate buffer (pH 7.2)

Take 50 ml of 0.2 M sodium cacodylate buffer made above and add:

1. 10 ml of stock 25% glutaraldehyde
2. 20 ml of 10% PFA (Appendix 1.1)
3. 20 ml of distilled water.

Appendix 2.8

2% tannic acid

Add 0.2 g of Tannic acid powder (Taab Laboratory Equipment Ltd, Aldermaston, UK) to 10 ml of distilled water and dissolve.

1% aqueous osmium tetroxide

Add 5 ml of stock 2% osmium tetroxide (Agar Scientific Ltd, Stansted, UK) to 5 ml of distilled water.

Appendix 3- Solutions and formulations used for immunofluorescence microscopy

Appendix 3.1

0.01 M Phosphate buffered saline (PBS)

Dissolve one PBS tablet in 200 ml of distilled water.

30% sucrose solution in 0.01 M PBS

1. Weigh out 15 g of sucrose (Alfa Aesar, Heysham, UK) in a 50 ml universal tube
2. Add PBS, made above, up to the 50 ml marker line
3. Mix thoroughly until all the sucrose has dissolved.

Appendix 3.2

0.01 M PBS containing 0.1% Tween 20 and 1% BSA

1. Make 0.01 M PBS as above
2. Add 0.2 ml of Tween 20 (Fisher Scientific UK Ltd, Loughborough, UK)
3. Add 2 g of BSA and agitate vigorously to ensure it dissolves fully.

Appendix 3.3

Chondroitinase ABC 0.1 units/ml

1. Make double strength Tris/sodium acetate buffer (with 0.02% BSA, pH 8, 50 mM Tris, 60 mM sodium acetate) (Appendix 2.2)
2. For 1 ml: add 25 µl of stock 4 units/ml chondroitinase ABC to 500 µl of double strength Tris/sodium acetate buffer (made above) and 475 µl of distilled water.

Appendix 4- Solutions and formulations used for serial block-face scanning electron microscopy

Appendix 4.1

1.5% potassium ferricyanide/1% osmium tetroxide

1. Dissolve 0.15 g of potassium ferricyanide (Fisher Scientific UK Ltd, Loughborough, UK) in 5 ml of distilled water
2. Add 5 ml of stock 2% osmium tetroxide.

1% thiocarbohydrazide

1. Add 0.1 g of thiocarbohydrazide (Sigma-Aldrich Company Ltd, Gillingham, UK) to 10 ml of distilled water
2. Heat in an oven at 60 °C for 1 hour, swirling the solution every 10 mins.

1% aqueous uranyl acetate

Dissolve 0.1 g of uranyl acetate (Agar Scientific Ltd, Stansted, UK) in 10 ml of distilled water.

Appendix 4.2

Stock aspartic acid solution

Dissolve 0.4 g of L-aspartic acid (Sigma-Aldrich Company Ltd, Gillingham, UK) in 100 ml of distilled water.

1N potassium hydroxide

Dissolve 5.6 g of potassium hydroxide (Sigma-Aldrich Company Ltd, Gillingham, UK) in 100 ml of distilled water.

Walton's lead aspartate

1. Dissolve 0.066 g of lead nitrate (Agar Scientific Ltd, Stansted, UK) in 10 ml of stock aspartic acid made above
2. Match pH to 5.5 using 1N potassium hydroxide made above

3. Heat in oven at 60 °C for 30 mins prior to use. If a precipitate forms after heating, the solution will need to be remade.

References

Abhari, S., Eisenback, M., Kaplan, H. J., Walters, E., Prather, R. S. and Scott, P. A. (2018). Anatomic studies of the miniature swine cornea. *The Anatomical Record* 301(11), pp. 1955-1967.

Acloque, H., Adams, M. S., Fishwick, K., Bronner-Fraser, M. and Nieto, M. A. (2009). Epithelial-mesenchymal transitions: The importance of changing cell state in development and disease. *The Journal of Clinical Investigation* 119(6), pp. 1438-1449.

Ahmad, S., Stewart, R., Yung, S., Kolli, S., Armstrong, L., Stojkovic, M., Figueiredo, F. *et al.* (2007). Differentiation of human embryonic stem cells into corneal epithelial-like cells by in vitro replication of the corneal epithelial stem cell niche. *Stem Cells* 25(5), pp. 1145-1155.

Ainscough, S. L., Linn, M. L., Barnard, Z., Schwab, I. R. and Harkin, D. G. (2011). Effects of fibroblast origin and phenotype on the proliferative potential of limbal epithelial progenitor cells. *Experimental Eye Research* 92(1), pp. 10-19.

Alvarado-Villacorta, R., García-Carmona, K. P., Martínez-Pardo, M. E. and Vázquez-Maya, L. (2020). Allogeneic limbal epithelial transplantation modified with solid platelet-rich plasma for bilateral limbal stem cell deficiency. *Cornea* 39(10), pp. 1311-1314.

Amitai-Lange, A., Altshuler, A., Bubley, J., Dbayat, N., Tiosano, B. and Shalom-Feuerstein, R. (2014). Lineage tracing of stem and progenitor cells of the murine corneal epithelium. *Stem Cells* 33(1), pp. 230-239.

Arpitha, P., Prajna, N. V., Srinivasan, M. and Muthukkaruppan, V. (2008). A subset of human limbal epithelial cells with greater nucleus-to-cytoplasm ratio expressing high levels of p63 possesses slow-cycling property. *Cornea* 27(10), pp. 1164-1170.

Ashworth, S., Harrington, J., Hammond, G. M., Bains, K. K., Koudouna, E., Hayes, A. J., Ralphs, J. R. *et al.* (2021). Chondroitin sulfate as a potential modulator of the stem cell niche in cornea. *Frontiers in Cell and Developmental Biology* 8, p. 567358.

Bains, K. K., Fukuoka, H., Hammond, G. M., Sotozono, C. and Quantock, A. J. (2019). Recovering vision in corneal epithelial stem cell deficient eyes. *Contact Lens and Anterior Eye* 42(4), pp. 350-358.

Bao, X., Nishimura, S., Mikami, T., Yamada, S., Itoh, N. and Sugahara, K. (2004). Chondroitin sulfate/dermatan sulfate hybrid chains from embryonic pig brain, which contain a higher proportion of L-iduronic acid than those from adult pig brain, exhibit neuritogenic and growth factor binding activities. *Journal of Biological Chemistry* 279(11), pp. 9765-9776.

Barrandon, Y. and Green, H. (1987). Three clonal types of keratinocyte with different capacities for multiplication. *Proceedings of the National Academy of Sciences of the United States of America* 84(8), pp. 2302-2306.

Basu, S., Sureka, S. P., Shanbhag, S. S., Kethiri, A. R., Singh, V. and Sangwan, V. S. (2016). Simple limbal epithelial transplantation: Long-term clinical outcomes in 125 cases of unilateral chronic ocular surface burns. *Ophthalmology* 123(5), pp. 1000-1010.

Beebe, D. C. and Masters, B. R. (1996). Cell lineage and the differentiation of corneal epithelial cells. *Investigative Ophthalmology & Visual Science* 37(9), pp. 1815-1825.

Behrens, J., Mareel, M. M., Van Roy, F. M. and Birchmeier, W. (1989). Dissecting tumor cell invasion: Epithelial cells acquire invasive properties after the loss of uvomorulin-mediated cell-cell adhesion. *The Journal of Cell Biology* 108(6), pp. 2435-2447.

Benedek, G. B. (1971). Theory of transparency of the eye. *Applied Optics* 10(3), pp. 459-473.

Bettelheim, F. A. and Goetz, D. (1976). Distribution of hexosamines in bovine cornea. *Investigative Ophthalmology & Visual Science* 15(4), pp. 301-304.

Birk, D. E., Fitch, J. M. and Linsenmayer, T. F. (1986). Organization of collagen types I and V in the embryonic chicken cornea. *Investigative Ophthalmology and Visual Science* 27(10), pp. 1470-1477.

Birk, D. E. (2001). Type V collagen: Heterotypic type I/V collagen interactions in the regulation of fibril assembly. *Micron* 32(3), pp. 223-237.

Blazejewska, E. A., Schlötzer-Schrehardt, U., Zenkel, M., Bachmann, B., Chankiewitz, E., Jacobi, C. and Kruse, F. E. (2009). Corneal limbal microenvironment can induce transdifferentiation of hair follicle stem cells into corneal epithelial-like cells. *Stem Cells* 27(3), pp. 642-652.

Bobba, S., Di Girolamo, N., Mills, R., Daniell, M., Chan, E., Harkin, D. G., Cronin, B. G. *et al.* (2017). Nature and incidence of severe limbal stem cell deficiency in Australia and New Zealand. *Clinical & Experimental Ophthalmology* 45(2), pp. 174-181.

Bonanno, J. A. (2012). Molecular mechanisms underlying the corneal endothelial pump. *Experimental Eye Research* 95(1), pp. 2-7.

Boonen, K. J. M., Rosaria-Chak, K. Y., Baaijens, F. P. T., van der Schaft, D. W. J. and Post, M. J. (2009). Essential environmental cues from the satellite cell niche: optimizing proliferation and differentiation. *American Journal of Physiology - Cell Physiology* 296(6), pp. C1338-C1345.

Borcherding, M. S., Blacik, L. J., Sittig, R. A., Bizzell, J. W., Breen, M. and Weinstein, H. G. (1975). Proteoglycans and collagen fibre organization in human corneoscleral tissue. *Experimental Eye Research* 21(1), pp. 59-70.

Boudaoud, A., Burian, A., Borowska-Wykręt, D., Uyttewaal, M., Wrzalik, R., Kwiatkowska, D. and Hamant, O. (2014). FibrilTool, an ImageJ plug-in to quantify fibrillar structures in raw microscopy images. *Nature Protocols* 9, pp. 457-463.

Boulton, M. and Albon, J. (2004). Stem cells in the eye. *The International Journal of Biochemistry and Cell Biology* 36(4), pp. 643-657.

Bourne, W. M., Nelson, L. R. and Hodge, D. O. (1997). Central corneal endothelial cell changes over a ten-year period. *Investigative Ophthalmology & Visual Science* 38(3), pp. 779-782.

Brabletz, T., Jung, A., Hermann, K., Günther, K., Hohenberger, W. and Kirchner, T. (1998). Nuclear overexpression of the oncoprotein β-catenin in colorectal cancer is localized predominantly at the invasion front. *Pathology - Research and Practice* 194(10), pp. 701-704.

Branch, M. J., Hashmani, K., Dhillon, P., Jones, D. R. E., Dua, H. S. and Hopkinson, A. (2012). Mesenchymal stem cells in the human corneal limbal stroma. *Investigative Ophthalmology & Visual Science* 53(9), pp. 5109-5116.

Bron, A. J., Tripathi, R. C. and Tripathi, B. J. (1997). *Wolff's anatomy of the eye and orbit*. 8th ed. ed. London: Chapman & Hall.

Buck, R. C. (1985). Measurement of centripetal migration of normal corneal epithelial cells in the mouse. *Investigative Ophthalmology and Visual Science* 26(9), pp. 1296-1299.

Budak, M. T., Alpdogan, O. S., Zhou, M., Lavker, R. M., Akinci, M. A. M. and Wolosin, J. M. (2005). Ocular surface epithelia contain ABCG2-dependent side population cells exhibiting features associated with stem cells. *Journal of Cell Science* 118(Pt 8), pp. 1715-1724.

Bueno, J. M., Gualda, E. J. and Artal, P. (2011). Analysis of corneal stroma organization with wavefront optimized nonlinear microscopy. *Cornea* 30(6), pp. 692-701.

Burdsal, C. A., Damsky, C. H. and Pedersen, R. A. (1993). The role of E-cadherin and integrins in mesoderm differentiation and migration at the mammalian primitive streak. *Development* 118(3), pp. 829-844.

Burgoyne, T., Lane, A., Laughlin, W. E., Cheetham, M. E. and Futter, C. E. (2018). Correlative light and immuno-electron microscopy of retinal tissue cryostat sections. *PloS ONE* 13(1), p. e0191048.

Calonge, M., Pérez, I., Galindo, S., Nieto-Miguel, T., López-Paniagua, M., Fernández, I., Alberca, M. *et al.* (2019). A proof-of-concept clinical trial using mesenchymal stem cells for the treatment of corneal epithelial stem cell deficiency. *Translational Research* 206, pp. 18-40.

Castro-Muñozledo, F. (2013). Review: Corneal epithelial stem cells, their niche and wound healing. *Molecular Vision* 19, pp. 1600-1613.

Caterson, B., Mahmoodian, F., Sorrell, J. M., Hardingham, T. E., Bayliss, M. T., Carney, S. L., Ratcliffe, A. *et al.* (1990). Modulation of native chondroitin sulphate structure in tissue development and in disease. *Journal of Cell Science* 97(3), pp. 411-417.

Caterson, B. (2012). Fell-Muir Lecture: Chondroitin sulphate glycosaminoglycans: fun for some and confusion for others. *International Journal of Experimental Pathology* 93(1), pp. 1-10.

Chakravarti, S., Magnuson, T., Lass, J. H., Jepsen, K. J., LaMantia, C. and Carroll, H. (1998). Lumican regulates collagen fibril assembly: Skin fragility and corneal opacity in the absence of lumican. *The Journal of Cell Biology* 141(5), pp. 1277-1286.

Chakravarti, S., Wu, F., Vij, N., Roberts, L. and Joyce, S. (2004). Microarray studies reveal macrophage-like function of stromal keratocytes in the cornea. *Investigative Ophthalmology & Visual Science* 45(10), pp. 3475-3484.

Chan, C. C. and Holland, E. J. (2013). Severe limbal stem cell deficiency from contact lens wear: Patient clinical features. *American Journal of Ophthalmology* 155(3), pp. 544-549.

Chapman, J. A. (1974). The staining pattern of collagen fibrils: I. An analysis of electron micrographs. *Connective Tissue Research* 2(2), pp. 137-150.

Chapman, J. A., Tzaphlidou, M., Meek, K. M. and Kadler, K. E. (1990). The collagen fibril—A model system for studying the staining and fixation of a protein. *Electron Microscopy Reviews* 3(1), pp. 143-182.

Chen, J. J. and Tseng, S. C. (1990). Corneal epithelial wound healing in partial limbal deficiency. *Investigative Ophthalmology & Visual Science* 31(7), pp. 1301-1314.

Chen, S.-Y., Han, B., Zhu, Y.-T., Mahabole, M., Huang, J., Beebe, D. C. and Tseng, S. C. G. (2015). HC-HA/PTX3 purified from amniotic membrane promotes BMP signaling in limbal niche cells to maintain quiescence of limbal epithelial progenitor/stem cells. *Stem Cells* 33(11), pp. 3341-3355.

Chen, S. Y., Hayashida, Y., Chen, M. Y., Xie, H. T. and Tseng, S. C. G. (2011). A new isolation method of human limbal progenitor cells by maintaining close association with their niche cells. *Tissue Engineering. Part C, Methods* 17(5), pp. 537-548.

Chen, W. Y. W., Mui, M. M., Kao, W. W. Y., Liu, C. Y. and Tseng, S. C. G. (1994). Conjunctival epithelial cells do not transdifferentiate in organotypic cultures: expression of K12 keratin is restricted to corneal epithelium. *Current Eye Research* 13(10), pp. 765-778.

Chen, Z., de Paiva, C. S., Luo, L., Kretzer, F. L., Pflugfelder, S. C. and Li, D. Q. (2004). Characterization of putative stem cell phenotype in human limbal epithelia. *Stem Cells* 22(3), pp. 355-366.

Cheng, C., Lee, Y. H., Lin, S. P., HuangFu, W. C. and Liu, I. H. (2014). Cell-autonomous heparanase modulates self-renewal and migration in bone marrow-derived mesenchymal stem cells. *Journal of Biomedical Science* 21(1), p. 21.

Commo, S., Gaillard, O. and Bernard, B. A. (2004). Human hair greying is linked to a specific depletion of hair follicle melanocytes affecting both the bulb and the outer root sheath. *British Journal of Dermatology* 150(3), pp. 435-443.

Connon, C. J., Martins Gouveia, R., Paterson, C., Lepert, G., Mohan, R. R. and Gupta, S. (2017). The mechanical properties of the human corneal limbus and its influence on epithelial stem cell phenotype. *Investigative Ophthalmology & Visual Science* 58(8), p. 4243.

Cornelison, D. D. W., Filla, M. S., Stanley, H. M., Rapraeger, A. C. and Olwin, B. B. (2001). Syndecan-3 and syndecan-4 specifically mark skeletal muscle satellite cells and are implicated in satellite cell maintenance and muscle regeneration. *Developmental Biology* 239(1), pp. 79-94.

Cotsarelis, G., Cheng, S. Z., Dong, G., Sun, T.-T. and Lavker, R. M. (1989). Existence of slow-cycling limbal epithelial basal cells that can be preferentially stimulated to proliferate: Implications on epithelial stem cells. *Cell* 57(2), pp. 201-209.

Coudrillier, B., Geraldes, D. M., Vo, N. T., Atwood, R., Reinhard, C., Campbell, I. C., Raji, Y. *et al.* (2016). Phase-contrast micro-computed tomography measurements of the intraocular pressure-induced deformation of the porcine lamina cribrosa. *IEEE Transactions on Medical Imaging* 35(4), pp. 988-999.

Cummings, R. D. (2009). The repertoire of glycan determinants in the human glycome. *Molecular BioSystems* 5(10), pp. 1087-1104.

Danielson, K. G., Baribault, H., Holmes, D. F., Graham, H., Kadler, K. E. and Iozzo, R. V. (1997). Targeted disruption of decorin leads to abnormal collagen fibril morphology and skin fragility. *The Journal of Cell Biology* 136(3), pp. 729-743.

Davanger, M. and Evensen, A. (1971). Role of the pericorneal papillary structure in renewal of corneal epithelium. *Nature* 229(5286), pp. 560-561.

Dawson, D., Ubels, J. and Edelhauser, H. (2011). Cornea and sclera. In: Levin, L. and Nilsson, S. and Ver Hoeve, J. and Wu, S. and Alm, A. and Kaufman, P. eds. *Adler's physiology of the eye*. 11th ed. Saunders Elsevier, pp. 71-130.

Deerinck, T. J., Bushong, E. A., Thor, A. and Ellisman, M. H. (2010). *NCMIR methods for 3D EM: A new protocol for preparation of biological specimens for serial block face scanning electron microscopy*. Available at: http://ncmir.ucsd.edu/sbfsem-protocol.pdf. [Accessed: 20/08/2019].

Dellagi, K., Vainchenker, W., Vinci, G., Paulin, D. and Brouet, J. C. (1983). Alteration of vimentin intermediate filament expression during differentiation of human hemopoietic cells. *The EMBO Journal* 2(9), pp. 1509-1514.

DelMonte, D. W. and Kim, T. (2011). Anatomy and physiology of the cornea. *Journal of Cataract and Refractive Surgery* 37(3), pp. 588-598.

Denk, W. and Horstmann, H. (2004). Serial block-face scanning electron microscopy to reconstruct three-dimensional tissue nanostructure. *PLoS biology* 2(11), p. e329.

Dennis, J. E., Merriam, A., Awadallah, A., Yoo, J. U., Johnstone, B. and Caplan, A. I. (1999). A quadripotential mesenchymal progenitor cell isolated from the marrow of an adult mouse. *Journal of Bone and Mineral Research* 14(5), pp. 700-709.

Di Girolamo, N. (2011). Stem cells of the human cornea. *British Medical Bulletin* 100, pp. 191-207.

Di Iorio, E., Barbaro, V., Ruzza, A., Ponzin, D., Pellegrini, G. and De Luca, M. (2005). Isoforms of ΔNp63 and the migration of ocular limbal cells in human corneal regeneration. *Proceedings of the National Academy of Sciences of the United States of America* 102(27), pp. 9523-9528.

Dravida, S., Pal, R., Khanna, A., Tipnis, S. P., Ravindran, G. and Khan, F. (2005). The transdifferentiation potential of limbal fibroblast-like cells. *Developmental Brain Research* 160(2), pp. 239-251.

Du, L., Wu, X., Pang, K. and Yang, Y. (2011). Histological evaluation and biomechanical characterisation of an acellular porcine cornea scaffold. *British Journal of Ophthalmology* 95(3), pp. 410-414.

Du, Y., Carlson, E. C., Funderburgh, M. L., Birk, D. E., Pearlman, E., Guo, N., Kao, W. W. Y. *et al.* (2009). Stem cell therapy restores transparency to defective murine corneas. *Stem Cells* 27(7), pp. 1635-1642.

Dua, H. S. (1998). The conjunctiva in corneal epithelial wound healing. *British Journal of Ophthalmology* 82(12), pp. 1407-1411.

Dua, H. S., Shanmuganathan, V. A., Powell-Richards, A. O., Tighe, P. J. and Joseph, A. (2005). Limbal epithelial crypts: a novel anatomical structure and a putative limbal stem cell niche. *British Journal of Ophthalmology* 89(5), pp. 529-532.

Dua, H. S., Faraj, L. A., Said, D. G., Gray, T. and Lowe, J. (2013). Human corneal anatomy redefined. *Ophthalmology* 120(9), pp. 1778-1785.

Dupont, S., Morsut, L., Aragona, M., Enzo, E., Giulitti, S., Cordenonsi, M., Zanconato, F. *et al.* (2011). Role of YAP/TAZ in mechanotransduction. *Nature* 474, pp. 179-183.

Dziasko, M. A., Armer, H. E., Levis, H. J., Shortt, A. J., Tuft, S. and Daniels, J. T. (2014). Localisation of epithelial cells capable of holoclone formation in vitro and direct interaction with stromal cells in the native human limbal crypt. *PloS ONE* 9(4), p. e94283.

Dziasko, M. A., Tuft, S. J. and Daniels, J. T. (2015). Limbal melanocytes support limbal epithelial stem cells in 2D and 3D microenvironments. *Experimental Eye Research* 138, pp. 70-79.

Ebato, B., Friend, J. and Thoft, R. A. (1987). Comparison of central and peripheral human corneal epithelium in tissue culture. *Investigative Ophthalmology and Visual Science* 28(9), pp. 1450-1456.

Ebato, B., Friend, J. and Thoft, R. A. (1988). Comparison of limbal and peripheral human corneal epithelium in tissue culture. *Investigative Ophthalmology and Visual Science* 29(10), pp. 1533-1537.

Echevarría, M., Muñoz-Cabello, A. M., Sánchez-Silva, R., Toledo-Aral, J. J. and López-Barneo, J. (2007). Development of cytosolic hypoxia and hypoxia-inducible factor stabilization are facilitated by aquaporin-1 expression. *Journal of Biological Chemistry* 282(41), pp. 30207-30215.

Echevarria, T. J., Chow, S., Watson, S., Wakefield, D. and Di Girolamo, N. (2011). Vitronectin: A matrix support factor for human limbal epithelial progenitor cells. *Investigative Ophthalmology & Visual Science* 52(11), pp. 8138-8147.

Enders, C., Braig, E.-M., Scherer, K., Werner, J. U., Lang, G. K., Lang, G. E., Pfeiffer, F. *et al.* (2017). Advanced non-destructive ocular visualization methods by improved X-ray imaging techniques. *PloS ONE* 12(1), p. e0170633.

Engler, A. J., Sen, S., Sweeney, H. L. and Discher, D. E. (2006). Matrix elasticity directs stem cell lineage specification. *Cell* 126(4), pp. 677-689.

Espana, E. M., Grueterich, M., Romano, A. C., Touhami, A. and Tseng, S. C. G. (2002). Idiopathic limbal stem cell deficiency. *Ophthalmology* 109(11), pp. 2004-2010.

Espana, E. M., Kawakita, T., Romano, A., Di Pascuale, M., Smiddy, R., Liu, C. Y. and Tseng, S. C. G. (2003). Stromal niche controls the plasticity of limbal and corneal epithelial differentiation in a rabbit model of recombined tissue. *Investigative Ophthalmology & Visual Science* 44(12), pp. 5130-5135.

Espandar, L., Steele, J. F. and Lathrop, K. L. (2017). Optical coherence tomography imaging of the palisades of Vogt to assist clinical evaluation and surgical planning in a case of limbal stem-cell deficiency. *Eye & Contact Lens* 43(5), pp. e19-e21.

Evans, M. J. and Kaufman, M. H. (1981). Establishment in culture of pluripotential cells from mouse embryos. *Nature* 292, pp. 154-156.

Faber, C., Scherfig, E., Prause, J. U. and Sørensen, K. E. (2008). Corneal thickness in pigs measured by ultrasound pachymetry in vivo. *Scandinavian Journal of Laboratory Animal Science* 35(1), pp. 39-43.

Feneck, E. M., Lewis, P. N., Ralphs, J. and Meek, K. M. (2018). A comparative study of the elastic fibre system within the mouse and human cornea. *Experimental Eye Research* 177, pp. 35-44.

Feng, Y. and Simpson, T. L. (2008). Corneal, limbal, and conjunctival epithelial thickness from optical coherence tomography. *Optometry and Vision Science* 85(9), pp. E880-E883.

Ferraris, C., Chevalier, G., Favier, B., Jahoda, C. A. and Dhouailly, D. (2000). Adult corneal epithelium basal cells possess the capacity to activate epidermal, pilosebaceous and sweat gland genetic programs in response to embryonic dermal stimuli. *Development* 127(24), pp. 5487-5495.

Figueira, E. C., Di Girolamo, N., Coroneo, M. T. and Wakefield, D. (2007). The phenotype of limbal epithelial stem cells. *Investigative Ophthalmology & Visual Science* 48(1), pp. 144-156.

Fitch, J. M., Birk, D. E., Linsenmayer, C. and Linsenmayer, T. F. (1990). The spatial organization of Descemet's membrane-associated type IV collagen in the avian cornea. *Journal of Cell Biology* 110(4), pp. 1457-1468.

Fléchon, J.-E., Degrouard, J. and Fléchon, B. (2004). Gastrulation events in the prestreak pig embryo: Ultrastructure and cell markers. *Genesis* 38(1), pp. 13-25.

Foster, J. W., Jones, R. R., Bippes, C. A., Gouveia, R. M. and Connon, C. J. (2014). Differential nuclear expression of Yap in basal epithelial cells across the cornea and substrates of differing stiffness. *Experimental Eye Research* 127, pp. 37-41.

Frank, N. Y., Pendse, S. S., Lapchak, P. H., Margaryan, A., Shlain, D., Doeing, C., Sayegh, M. H. *et al.* (2003). Regulation of progenitor cell fusion by ABCB5 P-glycoprotein, a novel human ATP-binding cassette transporter. *Journal of Biological Chemistry* 278(47), pp. 47156-47165.

Fuchs, E. and Raghavan, S. (2002). Getting under the skin of epidermal morphogenesis. *Nature Reviews Genetics* 3(3), pp. 199-209.

Fullwood, N. J. and Meek, K. M. (1993). A synchrotron X-ray study of the changes occurring in the corneal stroma during processing for electron microscopy. *Journal of Microscopy* 169(1), pp. 53-60.

Funderburgh, J. L., Funderburgh, M. L. and Du, Y. (2016). Stem cells in the limbal stroma. *The Ocular Surface* 14(2), pp. 113-120.

Galindo, S., Herreras, J. M., López-Paniagua, M., Rey, E., de la Mata, A., Plata-Cordero, M., Calonge, M. *et al.* (2017). Therapeutic effect of human adipose tissue-derived mesenchymal stem cells in experimental corneal failure due to limbal stem cell niche damage. *Stem Cells* 35(10), pp. 2160-2174.

Garcion, E., Halilagic, A., Faissner, A. and ffrench-Constant, C. (2004). Generation of an environmental niche for neural stem cell development by the extracellular matrix molecule tenascin C. *Development* 131(14), pp. 3423-3432.

Geroski, D. H., Matsuda, M., Yee, R. W. and Edelhauser, H. F. (1985). Pump function of the human corneal endothelium. *Ophthalmology* 92(6), pp. 759-763.

Gesteira, T. F., Sun, M., Coulson-Thomas, Y. M., Yamaguchi, Y., Yeh, L. K., Hascall, V. and Coulson-Thomas, V. J. (2017). Hyaluronan rich microenvironment in the limbal stem cell niche regulates limbal stem cell differentiation. *Investigative Ophthalmology & Visual Science* 58(11), pp. 4407-4421.

Gilbert, P. M., Havenstrite, K. L., Magnusson, K. E. G., Sacco, A., Leonardi, N. A., Kraft, P., Nguyen, N. K. *et al.* (2010). Substrate elasticity regulates skeletal muscle stem cell self-renewal in culture. *Science* 329(5995), pp. 1078-1081.

Gipson, I. K. (1989). The epithelial basement membrane zone of the limbus. *Eye* 3, pp. 132-140.

Gitay-Goren, H., Soker, S., Vlodavsky, I. and Neufeld, G. (1992). The binding of vascular endothelial growth factor to its receptors is dependent on cell surface-associated heparin-like molecules. *Journal of Biological Chemistry* 267(9), pp. 6093-6098.

Goldberg, M. F. and Bron, A. J. (1982). Limbal palisades of Vogt. *Transactions of the American Ophthalmological Society* 80, pp. 155-171.

Gonzalez, G., Sasamoto, Y., Ksander, B. R., Frank, M. H. and Frank, N. Y. (2018). Limbal stem cells: identity, developmental origin, and therapeutic potential. *Wiley Interdisciplinary Reviews: Developmental Biology* 7(2), p. e303.

González, S. and Deng, S. X. (2013). Presence of native limbal stromal cells increases the expansion efficiency of limbal stem/progenitor cells in culture. *Experimental Eye Research* 116, pp. 169-176.

Gouveia, R. M., Vajda, F., Wibowo, J. A., Figueiredo, F. and Connon, C. J. (2019). YAP, ΔNp63, and β-catenin signaling pathways are involved in the modulation of corneal epithelial stem cell phenotype induced by substrate stiffness. *Cells* 8(4), p. 347.

Green, S. J., Tarone, G. and Underhill, C. B. (1988). Aggregation of macrophages and fibroblasts is inhibited by a monoclonal antibody to the hyaluronate receptor. *Experimental Cell Research* 178(2), pp. 224-232.

Grieve, K., Ghoubay, D., Georgeon, C., Thouvenin, O., Bouheraoua, N., Paques, M. and Borderie, V. M. (2015). Three-dimensional structure of the mammalian limbal stem cell niche. *Experimental Eye Research* 140, pp. 75-84.

Gupta, P., Oegema, T. R., Brazil, J. J., Dudek, A. Z., Slungaard, A. and Verfaillie, C. M. (1998). Structurally specific heparan sulfates support primitive human hematopoiesis by formation of a multimolecular stem cell niche. *Blood* 92(12), pp. 4641-4651.

Haddad, A. and Faria-e-Sousa, S. J. (2014). Maintenance of the corneal epithelium is carried out by germinative cells of its basal stratum and not by presumed stem cells of the limbus. *Brazilian Journal of Medical and Biological Research* 47(6), pp. 470-477.

Hall, C. E., Jakus, M. A. and Schmitt, F. O. (1945). The structure of certain muscle fibrils as revealed by the use of electron stains. *Journal of Applied Physics* 16(8), pp. 459-465.

Hammond, G. M., Young, R. D., Muir, D. D. and Quantock, A. J. (2020). The microanatomy of Bowman's layer in the cornea of the pig: Changes in collagen fibril architecture at the corneoscleral limbus. *European Journal of Anatomy* 24(5), pp. 399-406.

Hann, C. R., Bentley, M. D., Vercnocke, A., Ritman, E. L. and Fautsch, M. P. (2011). Imaging the aqueous humor outflow pathway in human eyes by three-dimensional micro-computed tomography (3D micro-CT). *Experimental Eye Research* 92(2), pp. 104-111.

Harkin, D. G., Foyn, L., Bray, L. J., Sutherland, A. J., Li, F. J. and Cronin, B. G. (2015). Concise reviews: Can mesenchymal stromal cells differentiate into corneal cells? A systematic review of published data. *Stem Cells* 33(3), pp. 785-791.

Hart, R. W. and Farrell, R. A. (1969). Light scattering in the cornea. *Journal of the Optical Society of America* 59(6), pp. 766-774.

Hascall, V. C., Heinegård, D. K. and Wight, T. N. (1991). Proteoglycans: metabolism and pathology. In: Hay, E.D. ed. *Cell biology of extracellular matrix*. 2nd ed. New York: Plenum Press, pp. 149-175.

Hassell, J. R. and Birk, D. E. (2010). The molecular basis of corneal transparency. *Experimental Eye Research* 91(3), pp. 326-335.

Hatch, K. M. and Dana, R. (2009). The structure and function of the limbal stem cell and the disease states associated with limbal stem cell deficiency. *International Ophthalmology Clinics* 49(1), pp. 43-52.

Hayashi, R., Yamato, M., Sugiyama, H., Sumide, T., Yang, J., Okano, T., Tano, Y. *et al.* (2007). N-Cadherin is expressed by putative stem/progenitor cells and melanocytes in the human limbal epithelial stem cell niche. *Stem Cells* 25(2), pp. 289-296.

Hayashi, S., Osawa, T. and Tohyama, K. (2002). Comparative observations on corneas, with special reference to bowman's layer and descemet's membrane in mammals and amphibians. *Journal of Morphology* 254(3), pp. 247-258.

Hayes, A. J., Tudor, D., Nowell, M. A., Caterson, B. and Hughes, C. E. (2008). Chondroitin sulfate sulfation motifs as putative biomarkers for isolation of articular

cartilage progenitor cells. *Journal of Histochemistry and Cytochemistry* 56(2), pp. 125-138.

Hayes, A. J., Hughes, C. E., Ralphs, J. R. and Caterson, B. (2011). Chondroitin sulphate sulphation motif expression in the ontogeny of the intervertebral disc. *European Cells and Materials* 21, pp. 1-14.

Hayes, A. J., Hughes, C. E., Smith, S. M., Caterson, B., Little, C. B. and Melrose, J. (2016). The CS sulfation motifs 4C3, 7D4, 3B3[−]; and perlecan identify stem cell populations and their niches, activated progenitor cells and transitional areas of tissue development in the fetal human elbow. *Stem Cells and Development* 25(11), pp. 836-847.

Hayes, S., Boote, C., Lewis, J., Sheppard, J., Abahussin, M., Quantock, A. J., Purslow, C. *et al.* (2007). Comparative study of fibrillar collagen arrangement in the corneas of primates and other mammals. *The Anatomical Record* 290(12), pp. 1542-1550.

Hedbys, B. O. (1961). The role of polysaccharides in corneal swelling. *Experimental Eye Research* 1(1), pp. 81-91.

Higa, K., Shimmura, S., Miyashita, H., Shimazaki, J. and Tsubota, K. (2005). Melanocytes in the corneal limbus interact with K19-positive basal epithelial cells. *Experimental Eye Research* 81(2), pp. 218-223.

Higa, K., Kato, N., Yoshida, S., Ogawa, Y., Shimazaki, J., Tsubota, K. and Shimmura, S. (2013). Aquaporin 1-positive stromal niche-like cells directly interact with N-cadherin-positive clusters in the basal limbal epithelium. *Stem Cell Research* 10(2), pp. 147-155.

Higashiyama, S., Abraham, J. A. and Klagsbrun, M. (1993). Heparin-binding EGF-like growth factor stimulation of smooth muscle cell migration: dependence on interactions with cell surface heparan sulfate. *The Journal of Cell Biology* 122(4), pp. 933-940.

Ho, L. T. Y., Harris, A. M., Tanioka, H., Yagi, N., Kinoshita, S., Caterson, B., Quantock, A. J. *et al.* (2014). A comparison of glycosaminoglycan distributions, keratan sulphate sulphation patterns and collagen fibril architecture from central to peripheral regions of the bovine cornea. *Matrix Biology* 38, pp. 59-68.

Holan, V., Trosan, P., Cejka, C., Javorkova, E., Zajicova, A., Hermankova, B., Chudickova, M. *et al.* (2015). A comparative study of the therapeutic potential of

mesenchymal stem cells and limbal epithelial stem cells for ocular surface reconstruction. *STEM CELLS Translational Medicine* 4(9), pp. 1052-1063.

Holdsworth, D. W. and Thornton, M. M. (2002). Micro-CT in small animal and specimen imaging. *Trends in Biotechnology* 20(8), pp. S34-S39.

Holland, E. J. and Schwartz, G. S. (1997). Iatrogenic limbal stem cell deficiency. *Transactions of the American Ophthalmological Society* 95, pp. 95-110.

Hollingsworth, J. O., Perez-Gomez, I., Mutalib, H. A. and Efron, N. (2001). A population study of the normal cornea using an in vivo, slit-scanning confocal microscope. *Optometry and Vision Science* 78(10), pp. 706-711.

Holst, M.-C. and Powley, T. L. (1995). Cuprolinic Blue (quinolinic phthalocyanine) counterstaining of enteric neurons for peroxidase immunocytochemistry. *Journal of Neuroscience Methods* 62(1), pp. 121-127.

Huang, A. J. and Tseng, S. C. (1991). Corneal epithelial wound healing in the absence of limbal epithelium. *Investigative Ophthalmology & Visual Science* 32(1), pp. 96-105.

Huang, M. H., Li, N. Y., Wu, Z., Wan, P. X., Liang, X. W., Zhang, W., Wang, X. R. *et al.* (2011). Using acellular porcine limbal stroma for rabbit limbal stem cell microenvironment reconstruction. *Biomaterials* 32(31), pp. 7812-7821.

Ida, M., Shuo, T., Hirano, K., Tokita, Y., Nakanishi, K., Matsui, F., Aono, S. *et al.* (2006). Identification and functions of chondroitin sulfate in the milieu of neural stem cells. *Journal of Biological Chemistry* 281(9), pp. 5982-5991.

Iozzo, R. (1998). Matrix proteoglycans: From molecular design to cellular function. *Annual Review of Biochemistry* 67, pp. 609-652.

Iozzo, R. (2000). *Proteoglycans*. New York: Marcel Dekker, Inc.

Islam, M. M., Buznyk, O., Reddy, J. C., Pasyechnikova, N., Alarcon, E. I., Hayes, S., Lewis, P. *et al.* (2018). Biomaterials-enabled cornea regeneration in patients at high risk for rejection of donor tissue transplantation. *npj Regenerative Medicine* 3(1), p. 2.

Ito, M., Yang, Z., Andl, T., Cui, C., Kim, N., Millar, S. E. and Cotsarelis, G. (2007). Wnt-dependent de novo hair follicle regeneration in adult mouse skin after wounding. *Nature* 447(7142), pp. 316-320.

Ivanishko, Y., Bravin, A., Kovalev, S., Lisutina, P., Lotoshnikov, M., Mittone, A., Tkachev, S. *et al.* (2017). Feasibility study of the 3D visualization at high resolution of intra-cranial rabbit eyes with X-ray CT phase-contrast imaging. *Investigative Ophthalmology & Visual Science* 58(13), pp. 5941-5948.

Ivaska, J., Pallari, H., Nevo, J. and Eriksson, J. E. (2007). Novel functions of vimentin in cell adhesion, migration, and signaling. *Experimental Cell Research* 313(10), pp. 2050-2062.

Izumikawa, T., Sato, B. and Kitagawa, H. (2014). Chondroitin sulfate is indispensable for pluripotency and differentiation of mouse embryonic stem cells. *Scientific Reports* 4, p. 3701.

Jakus, M. A. (1956). Studies on the cornea. II. The fine structure of Descemet's membrane. *The Journal of Biophysical and Biochemical Cytology* 2(4), pp. 243-252.

Jay, L., Brocas, A., Singh, K., Kieffer, J. C., Brunette, I. and Ozaki, T. (2008). Determination of porcine corneal layers with high spatial resolution by simultaneous second and third harmonic generation microscopy. *Optics Express* 16(21), pp. 16284-16293.

Jester, J. V. (2008). Corneal crystallins and the development of cellular transparency. *Seminars in Cell & Developmental Biology* 19(2), pp. 82-93.

Jester, J. V., Murphy, C. J., Winkler, M., Bergmanson, J. P. G., Brown, D., Steinert, R. F. and Mannis, M. J. (2013). Lessons in corneal structure and mechanics to guide the corneal surgeon. *Ophthalmology* 120(9), pp. 1715-1717.

Johansson, U. E., Eftekhari, S. and Warfvinge, K. (2010). A battery of cell- and structure-specific markers for the adult porcine retina. *Journal of Histochemistry & Cytochemistry* 58(4), pp. 377-389.

Jones, R. R., Hamley, I. W. and Connon, C. J. (2012). Ex vivo expansion of limbal stem cells is affected by substrate properties. *Stem Cell Research* 8(3), pp. 403-409.

Kaji, Y. (2002). Anatomy of the cornea, limbus and sclera. In: Agarwal, S. and Agarwal, A. and Apple, D. and Buratto, L. and Ali ó, J. and Pandey, S. and Agarwal, A.

eds. *Textbook of ophthalmology: volume 1*. New Delhi: Jaypee Brothers Medical Publishers, pp. 939-944.

Kalluri, R. (2009). EMT: When epithelial cells decide to become mesenchymal-like cells. *The Journal of Clinical Investigation* 119(6), pp. 1417-1419.

Kalluri, R. and Weinberg, R. A. (2009). The basics of epithelial-mesenchymal transition. *The Journal of Clinical Investigation* 119(6), pp. 1420-1428.

Kamma-Lorger, C. S., Boote, C., Hayes, S., Moger, J., Burghammer, M., Knupp, C., Quantock, A. J. *et al.* (2010). Collagen and mature elastic fibre organisation as a function of depth in the human cornea and limbus. *Journal of Structural Biology* 169(3), pp. 424-430.

Kapoor, R., Bornstein, P. and Sage, E. H. (1986). Type VIII collagen from bovine Descemet's membrane: structural characterization of a triple-helical domain. *Biochemistry* 25(13), pp. 3930-3937.

Karus, M., Samtleben, S., Busse, C., Tsai, T., Dietzel, I. D., Faissner, A. and Wiese, S. (2012). Normal sulfation levels regulate spinal cord neural precursor cell proliferation and differentiation. *Neural Development* 7, p. 20.

Kasper, M., Moll, R., Stosiek, P. and Karsten, U. (1988). Patterns of cytokeratin and vimentin expression in the human eye. *Histochemistry* 89(4), pp. 369-377.

Kato, M., Saunders, S., Nguyen, H. and Bernfield, M. (1995). Loss of cell surface syndecan-1 causes epithelia to transform into anchorage-independent mesenchyme-like cells. *Molecular Biology of the Cell* 6(5), pp. 559-576.

Kato, N., Shimmura, S., Kawakita, T., Miyashita, H., Ogawa, Y., Yoshida, S., Higa, K. *et al.* (2007). β-catenin activation and epithelial-mesenchymal transition in the pathogenesis of pterygium. *Investigative Ophthalmology & Visual Science* 48(4), pp. 1511-1517.

Kawakita, T., Espana, E. M., He, H., Li, W., Liu, C. and Tseng, S. C. G. (2005). Intrastromal invasion by limbal epithelial cells is mediated by epithelial-mesenchymal transition activated by air exposure. *The American Journal of Pathology* 167(2), pp. 381-393.

Kawashima, H., Atarashi, K., Hirose, M., Hirose, J., Yamada, S., Sugahara, K. and Miyasaka, M. (2002). Oversulfated chondroitin/dermatan sulfates containing

GlcAβ1/IdoAα1–3GalNAc(4,6-O-disulfate) interact with L- and P-selectin and chemokines. *Journal of Biological Chemistry* 277(15), pp. 12921-12930.

Kawashima, M., Kawakita, T., Higa, K., Satake, Y., Omoto, M., Tsubota, K., Shimmura, S. *et al.* (2010). Subepithelial corneal fibrosis partially due to epithelial-mesenchymal transition of ocular surface epithelium. *Molecular Vision* 16, pp. 2727-2732.

Kenyon, K. R. and Tseng, S. C. G. (1989). Limbal autograft transplantation for ocular surface disorders. *Ophthalmology* 96(5), pp. 709-723.

Kethiri, A. R., Basu, S., Shukla, S., Sangwan, V. S. and Singh, V. (2017). Optimizing the role of limbal explant size and source in determining the outcomes of limbal transplantation: An in vitro study. *PloS ONE* 12(9), pp. e0185623-e0185623.

Kim, J. C. and Tseng, S. C. G. (1995). Transplantation of preserved human amniotic membrane for surface reconstruction in severely damaged rabbit corneas. *Cornea* 14(5), pp. 473-484.

Kinoshita, S., Friend, J. and Thoft, R. A. (1981). Sex chromatin of donor corneal epithelium in rabbits. *Investigative Ophthalmology and Visual Science* 21(3), pp. 434-441.

Komai, Y. and Ushiki, T. (1991). The three-dimensional organization of collagen fibrils in the human cornea and sclera. *Investigative Ophthalmology & Visual Science* 32(8), pp. 2244-2258.

Kraushaar, D. C., Dalton, S. and Wang, L. (2013). Heparan sulfate: a key regulator of embryonic stem cell fate. *Biological Chemistry* 394(6), pp. 741-751.

Kruse, F. E., Chen, J. J., Tsai, R. J. and Tseng, S. C. (1990). Conjunctival transdifferentiation is due to the incomplete removal of limbal basal epithelium. *Investigative Ophthalmology & Visual Science* 31(9), pp. 1903-1913.

Ksander, B. R., Kolovou, P. E., Wilson, B. J., Saab, K. R., Guo, Q., Ma, J., McGuire, S. P. *et al.* (2014). ABCB5 is a limbal stem cell gene required for corneal development and repair. *Nature* 511(7509), pp. 353-357.

Kureshi, A. K., Dziasko, M., Funderburgh, J. L. and Daniels, J. T. (2015). Human corneal stromal stem cells support limbal epithelial cells cultured on RAFT tissue equivalents. *Scientific Reports* 5, p. 16186.

Lagali, N., Edén, U., Utheim, T. P., Chen, X., Riise, R., Dellby, A. and Fagerholm, P. (2013). In vivo morphology of the limbal palisades of Vogt correlates with progressive stem cell deficiency in aniridia-related keratopathy. *Investigative Ophthalmology and Visual Science* 54(8), pp. 5333-5342.

Lampugnani, M. G., Resnati, M., Raiteri, M., Pigott, R., Pisacane, A., Houen, G., Ruco, L. P. *et al.* (1992). A novel endothelial-specific membrane protein is a marker of cell-cell contacts. *Journal of Cell Biology* 118(6), pp. 1511-1522.

Lange, W., Debbage, P. L., Basting, C. and Gabius, H. J. (1989). Neoglycoprotein binding distinguishes distinct zones in the epithelia of the porcine eye. *Journal of anatomy* 166, pp. 243-252.

Langley, T. and Ledford, J. (2008). The cornea. In: Lens, A. and Nemeth, S. and Ledford, J. eds. *Ocular anatomy and physiology*. 2nd ed. Thorofare: Slack Incorporated, pp. 57-66.

Latta, L., Viestenz, A., Stachon, T., Colanesi, S., Szentmáry, N., Seitz, B. and Käsmann-Kellner, B. (2018). Human aniridia limbal epithelial cells lack expression of keratins K3 and K12. *Experimental Eye Research* 167, pp. 100-109.

Lauweryns, B., van den Oord, J. J., De Vos, R. and Missotten, L. (1993). A new epithelial cell type in the human cornea. *Investigative Ophthalmology & Visual Science* 34(6), pp. 1983-1990.

Lazopoulos, K. A. and Stamenović, D. (2008). Durotaxis as an elastic stability phenomenon. *Journal of Biomechanics* 41(6), pp. 1289-1294.

Lee, J. M., Dedhar, S., Kalluri, R. and Thompson, E. W. (2006). The epithelial–mesenchymal transition: new insights in signaling, development, and disease. *The Journal of Cell Biology* 172(7), pp. 973-981.

Lee, S., Chung, M., Lee, S.-R. and Jeon, N. L. (2020). 3D brain angiogenesis model to reconstitute functional human blood–brain barrier in vitro. *Biotechnology and Bioengineering* 117(3), pp. 748-762.

Lehrer, M. S., Sun, T. T. and Lavker, R. M. (1998). Strategies of epithelial repair: modulation of stem cell and transit amplifying cell proliferation. *Journal of Cell Science* 111(19), pp. 2867-2875.

Lepert, G., Gouveia, R. M., Connon, C. J. and Paterson, C. (2016). Assessing corneal biomechanics with Brillouin spectro-microscopy. *Faraday Discussions* 187, pp. 415-428.

Leszczyński, B., Sojka-Leszczyńska, P., Wojtysiak, D., Wróbel, A. and Pędrys, R. (2018). Visualization of porcine eye anatomy by X-ray microtomography. *Experimental Eye Research* 167, pp. 51-55.

Levis, H. J., Massie, I., Dziasko, M. A., Kaasi, A. and Daniels, J. T. (2013). Rapid tissue engineering of biomimetic human corneal limbal crypts with 3D niche architecture. *Biomaterials* 34(35), pp. 8860-8868.

Lewis, P. N., Pinali, C., Young, R. D., Meek, K. M., Quantock, A. J. and Knupp, C. (2010). Structural interactions between collagen and proteoglycans are elucidated by three-dimensional electron tomography of bovine cornea. *Structure* 18(2), pp. 239-245.

Lewis, P. N., White, T. L., Young, R. D., Bell, J. S., Winlove, C. P. and Meek, K. M. (2016). Three-dimensional arrangement of elastic fibers in the human corneal stroma. *Experimental Eye Research* 146, pp. 43-53.

Li, D. Q., Chen, Z., Song, X. J., de Paiva, C. S., Kim, H. and Pflugfelder, S. C. (2005). Partial enrichment of a population of human limbal epithelial cells with putative stem cell properties based on collagen type IV adhesiveness. *Experimental Eye Research* 80(4), pp. 581-590.

Li, G., Zhu, Y.-T., Xie, H., Chen, S. and Tseng, S. C. G. (2012). Mesenchymal stem cells derived from human limbal niche cells. *Investigative Ophthalmology & Visual Science* 53(9), pp. 5686-5697.

Li, Y., Yang, Y., Yang, L., Zeng, Y., Gao, X. and Xu, H. (2017). Poly(ethylene glycol)-modified silk fibroin membrane as a carrier for limbal epithelial stem cell transplantation in a rabbit LSCD model. *Stem Cell Research & Therapy* 8(1), pp. 256-256.

Li, Z., Wilson, K. D., Smith, B., Kraft, D. L., Jia, F., Huang, M., Xie, X. *et al.* (2009). Functional and transcriptional characterization of human embryonic stem cell-derived endothelial cells for treatment of myocardial infarction. *PloS ONE* 4(12), p. e8443.

Lie, D., Colamarino, S. A., Song, H., Desire, L., Mira, H., Consiglio, A., Lein, E. S. *et al.* (2005). Wnt signalling regulates adult hippocampal neurogenesis. *Nature* 437(7063), pp. 1370-1375.

Lin, C. W., Sherman, B., Moore, L. A., Laethem, C. L., Lu, D., Pattabiraman, P. P., Rao, P. V. *et al.* (2018). Discovery and preclinical development of Netarsudil, a novel ocular hypotensive agent for the treatment of glaucoma. *Journal of Ocular Pharmacology and Therapeutics* 34(1-2), pp. 40-51.

Lindberg, K., Brown, M. E., Chaves, H. V., Kenyon, K. R. and Rheinwald, J. G. (1993). In vitro propagation of human ocular surface epithelial cells for transplantation. *Investigative Ophthalmology & Visual Science* 34(9), pp. 2672-2679.

Liu, C.-Y., Birk, D. E., Hassell, J. R., Kane, B. and Kao, W. W. Y. (2003). Keratocan-deficient mice display alterations in corneal structure. *Journal of Biological Chemistry* 278(24), pp. 21672-21677.

Liu, C. Y., Zhu, G., Westerhausen-larson, A., Converse, R., Candace, W. C. K., Sun, T. and Winston, W. Y. K. (1993). Cornea-specific expression of K12 keratin during mouse development. *Current Eye Research* 12(11), pp. 963-974.

Liu, W., Deng, C., McLaughlin, C. R., Fagerholm, P., Lagali, N. S., Heyne, B., Scaiano, J. C. *et al.* (2009). Collagen–phosphorylcholine interpenetrating network hydrogels as corneal substitutes. *Biomaterials* 30(8), pp. 1551-1559.

Liu, X.-H., Yin, H.-X., Zhu, H., Wang, Z.-T., Zhao, P.-F., Lv, H., Ding, H.-Y. *et al.* (2018). Three-dimensional visualization of rat retina by X-ray differential phase contrast tomographic microscopy. *Microscopy Research and Technique* 81(6), pp. 655-662.

Ljubimov, A. V., Burgeson, R. E., Butkowski, R. J., Michael, A. F., Sun, T. T. and Kenney, M. C. (1995). Human corneal basement membrane heterogeneity: Topographical differences in the expression of type IV collagen and laminin isoforms. *Laboratory Investigation* 72(4), pp. 461-473.

Lo, C. M., Wang, H., Dembo, M. and Wang, Y. (2000). Cell movement is guided by the rigidity of the substrate. *Biophysical Journal* 79(1), pp. 144-152.

Lobo, E. P., Delic, N. C., Richardson, A., Raviraj, V., Halliday, G. M., Di Girolamo, N., Myerscough, M. R. *et al.* (2016). Self-organized centripetal movement of corneal epithelium in the absence of external cues. *Nature communications* 7, p. 12388.

Majo, F., Rochat, A., Nicolas, M., Abou Jaoude, G. and Barrandon, Y. (2008). Oligopotent stem cells are distributed throughout the mammalian ocular surface. *Nature* 456(7219), pp. 250-254.

Marshall, G. E., Konstas, A. G. and Lee, W. R. (1991a). Immunogold fine structural localization of extracellular matrix components in aged human cornea II. Collagen types V and VI. *Graefe's Archive for Clinical and Experimental Ophthalmology* 229(2), pp. 164-171.

Marshall, G. E., Konstas, A. G. and Lee, W. R. (1991b). Immunogold fine structural localization of extracellular matrix components in aged human cornea. I. Collagen types I–IV and laminin. *Graefe's Archive for Clinical and Experimental Ophthalmology* 229(2), pp. 157-163.

Mathews, S., Chidambaram, J. D., Lanjewar, S., Mascarenhas, J., Prajna, N. V., Muthukkaruppan, V. and Chidambaranathan, G. P. (2015). In vivo confocal microscopic analysis of normal human anterior limbal stroma. *Cornea* 34(4), pp. 464-470.

Matic, M., Petrov, I. N., Chen, S., Wang, C., Wolosin, J. M. and Dimitrijevich, S. D. (1997). Stem cells of the corneal epithelium lack connexins and metabolite transfer capacity. *Differentiation* 61(4), pp. 251-260.

Maurice, D. M. (1957). The structure and transparency of the cornea. *Journal of Physiology* 136(2), pp. 263-286.

Maurice, D. M. (1962). Clinical physiology of the cornea. *International Ophthalmology Clinics* 2(3), pp. 562-572.

McKee, H. D., Irion, L. C. D., Carley, F. M., Brahma, A. K., Jafarinasab, M. R., Rahmati-Kamel, M., Kanavi, M. R. *et al.* (2014). Re: Dua et al.: Human corneal anatomy redefined: a novel pre-Descemet layer (Dua's layer) (Ophthalmology 2013;120:1778–85). *Ophthalmology* 121(5), pp. e24-e25.

Medici, D., Hay, E. D. and Goodenough, D. A. (2006). Cooperation between Snail and LEF-1 transcription factors is essential for TGF-β1-induced epithelial-mesenchymal transition. *Molecular Biology of the Cell* 17(4), pp. 1871-1879.

Meek, K. M., Blamires, T., Elliott, G. F., Gyi, T. J. and Nave, C. (1987). The organisation of collagen fibrils in the human corneal stroma: A synchrotron X-ray diffraction study. *Current Eye Research* 6(7), pp. 841-846.

Meek, K. M., Quantock, A. J., Elliott, G. F., Ridgway, A. E. A., Tullo, A. B., Bron, A. J. and Thonar, E. J. M. A. (1989). Macular corneal dystrophy: The macromolecular structure of the stroma observed using electron microscopy and synchrotron X-ray diffraction. *Experimental Eye Research* 49(6), pp. 941-958.

Meek, K. M., Quantock, A. J., Boote, C., Liu, C. Y. and Kao, W. W. Y. (2003). An X-ray scattering investigation of corneal structure in keratocan-deficient mice. *Matrix Biology* 22(6), pp. 467-475.

Meek, K. M. and Boote, C. (2004). The organization of collagen in the corneal stroma. *Experimental Eye Research* 78(3), pp. 503-512.

Meek, K. M. and Knupp, C. (2015). Corneal structure and transparency. *Progress in Retinal and Eye Research* 49, pp. 1-16.

Melrose, J., Isaacs, M. D., Smith, S. M., Hughes, C. E., Little, C. B., Caterson, B. and Hayes, A. J. (2012). Chondroitin sulphate and heparan sulphate sulphation motifs and their proteoglycans are involved in articular cartilage formation during human foetal knee joint development. *Histochemistry and Cell Biology* 138(3), pp. 461-475.

Merindano, M. D., Costa, J., Canals, M., Potau, J. M. and Ruano, D. (2002). A comparative study of Bowman's layer in some mammals: Relationships with other constituent corneal structures. *European Journal of Anatomy* 6(3), pp. 133-139.

Mertsch, S., Hasenzahl, M., Reichl, S., Geerling, G. and Schrader, S. (2020). Decellularized human corneal stromal cell sheet as a novel matrix for ocular surface reconstruction. *Journal of Tissue Engineering and Regenerative Medicine* 14(9), pp. 1318-1332.

Michel, M., Torok, N., Godbout, M. J., Lussier, M., Gaudreau, P., Royal, A. and Germain, L. (1996). Keratin 19 as a biochemical marker of skin stem cells in vivo and in vitro: Keratin 19 expressing cells are differentially localized in function of anatomic sites, and their number varies with donor age and culture stage. *Journal of Cell Science* 109(5), pp. 1017-1028.

Mittone, A., Ivanishko, Y., Kovalev, S., Lisutina, P., Lotoshnikov, M., Tkachev, S., Tkacheva, M. *et al.* (2018). High resolution hard X-ray 3D mapping of a Macaca fascicularis eye: A feasibility study without contrast agents. *Physica Medica* 51, pp. 7-12.

Morrison, S. J. and Spradling, A. C. (2008). Stem cells and niches: Mechanisms that promote stem cell maintenance throughout life. *Cell* 132(4), pp. 598-611.

Müller, L. J., Pels, E., Schurmans, L. R. H. M. and Vrensen, G. F. J. M. (2004). A new three-dimensional model of the organization of proteoglycans and collagen fibrils in the human corneal stroma. *Experimental Eye Research* 78(3), pp. 493-501.

Najjam, S., Gibbs, R. V., Gordon, M. Y. and Rider, C. C. (1997). Characterization of human recombinant interleukin 2 binding to heparin and heparan sulfate using an ELISA approach. *Cytokine* 9(12), pp. 1013-1022.

Nakatsu, M. N., González, S., Mei, H. and Deng, S. X. (2014). Human limbal mesenchymal cells support the growth of human corneal epithelial stem/progenitor cells. *Investigative Ophthalmology & Visual Science* 55(10), pp. 6953-6959.

Nautscher, N., Bauer, A., Steffl, M. and Amselgruber, W. M. (2016). Comparative morphological evaluation of domestic animal cornea. *Veterinary Ophthalmology* 19(4), pp. 297-304.

Newton, R. H. and Meek, K. M. (1998). Circumcorneal annulus of collagen fibrils in the human limbus. *Investigative Ophthalmology & Visual Science* 39(7), pp. 1125-1134.

Nishida, K., Kinoshita, S., Ohashi, Y., Kuwayama, Y. and Yamamoto, S. (1995). Ocular surface abnormalities in aniridia. *American Journal of Ophthalmology* 120(3), pp. 368-375.

Noisa, P., Ramasamy, T. S., Lamont, F. R., Yu, J. S. L., Sheldon, M. J., Russell, A., Jin, X. *et al.* (2012). Identification and characterisation of the early differentiating cells in neural differentiation of human embryonic stem cells. *PloS ONE* 7(5), p. e37129.

Notara, M., Schrader, S. and Daniels, J. T. (2011). The porcine limbal epithelial stem cell niche as a new model for the study of transplanted tissue-engineered human limbal epithelial cells. *Tissue Engineering Part A* 17(5-6), pp. 741-750.

Okada, H., Danoff, T. M., Kalluri, R. and Neilson, E. G. (1997). Early role of Fsp1 in epithelial-mesenchymal transformation. *American Journal of Physiology-Renal Physiology* 273(4), pp. F563-F574.

Omoto, M., Katikireddy, K. R., Rezazadeh, A., Dohlman, T. H. and Chauhan, S. K. (2014). Mesenchymal stem cells home to inflamed ocular surface and suppress allosensitization in corneal transplantation. *Investigative Ophthalmology & Visual Science* 55(10), pp. 6631-6638.

Oorschot, V. M. J., Sztal, T. E., Bryson-Richardson, R. J. and Ramm, G. (2014). Chapter 11 - Immuno correlative light and electron microscopy on Tokuyasu cryosections. In: Müller-Reichert, T. and Verkade, P. eds. *Methods in Cell Biology*. Vol. 124. Academic Press, pp. 241-258.

Ordonez, P. and Di Girolamo, N. (2012). Limbal epithelial stem cells: Role of the niche microenvironment. *Stem Cells* 30(2), pp. 100-107.

Palma, V., Lim, D. A., Dahmane, N., Sánchez, P., Brionne, T. C., Herzberg, C. D., Gitton, Y. *et al.* (2004). Sonic hedgehog controls stem cell behavior in the postnatal and adult brain. *Development* 132(2), pp. 335-344.

Parfitt, G. J., Pinali, C., Young, R. D., Quantock, A. J. and Knupp, C. (2010). Three-dimensional reconstruction of collagen–proteoglycan interactions in the mouse corneal stroma by electron tomography. *Journal of Structural Biology* 170(2), pp. 392-397.

Parfitt, G. J., Kavianpour, B., Wu, K. L., Xie, Y., Brown, D. J. and Jester, J. V. (2015). Immunofluorescence tomography of mouse ocular surface epithelial stem cells and their niche microenvironment. *Investigative Ophthalmology & Visual Science* 56(12), pp. 7338-7344.

Park, C. Y., Lee, J. K., Zhang, C. and Chuck, R. S. (2015). New details of the human corneal limbus revealed with second harmonic generation imaging. *Investigative Ophthalmology & Visual Science* 56(10), pp. 6058-6066.

Park, M., Richardson, A., Pandzic, E., Lobo, E. P., Lyons, J. G. and Di Girolamo, N. (2019). Peripheral (not central) corneal epithelia contribute to the closure of an annular debridement injury. *Proceedings of the National Academy of Sciences of the United States of America* 116(52), pp. 26633-26643.

Pathak, M., Cholidis, S., Haug, K., Shahdadfar, A., Moe, M. C., Nicolaissen, B. and Drolsum, L. (2013). Clinical transplantation of ex vivo expanded autologous limbal epithelial cells using a culture medium with human serum as single supplement: A retrospective case series. *Acta Ophthalmologica* 91(8), pp. 769-775.

Patruno, M., Perazzi, A., Martinello, T., Blaseotto, A., Di Iorio, E. and Iacopetti, I. (2017). Morphological description of limbal epithelium: searching for stem cells crypts in the dog, cat, pig, cow, sheep and horse. *Veterinary Research Communications* 41(2), pp. 169-173.

Pauklin, M., Thomasen, H., Pester, A., Steuhl, K. P. and Meller, D. (2011). Expression of pluripotency and multipotency factors in human ocular surface tissues. *Current Eye Research* 36(12), pp. 1086-1097.

Pei, Y., Reins, R. Y. and McDermott, A. M. (2006). Aldehyde dehydrogenase (ALDH) 3A1 expression by the human keratocyte and its repair phenotypes. *Experimental Eye Research* 83(5), pp. 1063-1073.

Pelham, R. J. and Wang, Y. l. (1997). Cell locomotion and focal adhesions are regulated by substrate flexibility. *Proceedings of the National Academy of Sciences* 94(25), pp. 13661-13665.

Pellegrini, G., Traverso, C. E., Franzi, A. T., Zingirian, M., Cancedda, R. and De Luca, M. (1997). Long-term restoration of damaged corneal surfaces with autologous cultivated corneal epithelium. *The Lancet* 349(9057), pp. 990-993.

Pellegrini, G., Golisano, O., Paterna, P., Lambiase, A., Bonini, S., Rama, P. and De Luca, M. (1999). Location and clonal analysis of stem cells and their differentiated progeny in the human ocular surface. *The Journal of Cell Biology* 145(4), pp. 769-782.

Pellegrini, G., Dellambra, E., Golisano, O., Martinelli, E., Fantozzi, I., Bondanza, S., Ponzin, D. *et al.* (2001). p63 identifies keratinocyte stem cells. *Proceedings of the National Academy of Sciences* 98(6), pp. 3156-3161.

Persson, A., Vorontsov, E., Larson, G. and Nilsson, J. (2020). Glycosaminoglycan domain mapping of cellular chondroitin/dermatan sulfates. *Scientific Reports* 10(1), p. 3506.

Poli, M., Burillon, C., Auxenfans, C., Rovere, M.-R. and Damour, O. (2015). Immunocytochemical diagnosis of limbal stem cell deficiency: Comparative asnalysis of current corneal and conjunctival biomarkers. *Cornea* 34(7), pp. 817-823.

Polisetti, N., Zenkel, M., Menzel-Severing, J., Kruse, F. E. and Schlötzer-Schrehardt, U. (2016). Cell adhesion molecules and stem cell-niche-interactions in the limbal stem cell niche. *Stem Cells* 34(1), pp. 203-219.

Polisetty, N., Fatima, A., Madhira, S. L., Sangwan, V. S. and Vemuganti, G. K. (2008). Mesenchymal cells from limbal stroma of human eye. *Molecular Vision* 14, pp. 431-442.

Quantock, A. J. and Meek, K. M. (1988). Axial electron density of human scleral collagen. Location of proteoglycans by x-ray diffraction. *Biophysical Journal* 54(1), pp. 159-164.

Quantock, A. J., Meek, K. M. and Chakravarti, S. (2001). An X-ray diffraction investigation of corneal structure in lumican-deficient mice. *Investigative Ophthalmology & Visual Science* 42(8), pp. 1750-1756.

Rada, J. A., Cornuet, P. K. and Hassell, J. R. (1993). Regulation of corneal collagen fibrillogenesis in vitro by corneal proteoglycan (lumican and decorin) core proteins. *Experimental Eye Research* 56(6), pp. 635-648.

Rama, P., Matuska, S., Paganoni, G., Spinelli, A., De Luca, M. and Pellegrini, G. (2010). Limbal stem-cell therapy and long-term corneal regeneration. *New England Journal of Medicine* 363(2), pp. 147-155.

Ramaesh, K., Ramaesh, T., Dutton, G. N. and Dhillon, B. (2005). Evolving concepts on the pathogenic mechanisms of aniridia related keratopathy. *The International Journal of Biochemistry and Cell Biology* 37(3), pp. 547-557.

Ramirez-Miranda, A., Nakatsu, M. N., Zarei-Ghanavati, S., Nguyen, C. V. and Deng, S. X. (2011). Keratin 13 is a more specific marker of conjunctival epithelium than keratin 19. *Molecular Vision* 17, pp. 1652-1661.

Ramírez, G., Hagood, J. S., Sanders, Y., Ramírez, R., Becerril, C., Segura, L., Barrera, L. *et al.* (2011). Absence of Thy-1 results in TGF-β induced MMP-9 expression and confers a profibrotic phenotype to human lung fibroblasts. *Laboratory Investigation* 91(8), pp. 1206-1218.

Ramos, T., Scott, D. and Ahmad, S. (2015). An update on ocular surface epithelial stem cells: cornea and conjunctiva. *Stem Cells International* 2015, p. 601731.

Regal, S., O'Connor, D., Brige, P., Delattre, R., Djenizian, T. and Ramuz, M. (2019). Determination of optical parameters of the porcine eye and development of a simulated model. *Journal of Biophotonics* 0(0), p. e201800398.

Remington, L. A. (2012). *Clinical anatomy and physiology of the visual system*. 3rd ed. St. Louis: Elsevier Butterworth Heinemann.

Reya, T., Morrison, S. J., Clarke, M. F. and Weissman, I. L. (2001). Stem cells, cancer, and cancer stem cells. *Nature* 414, pp. 105-111.

Riemersma, J. C. (1968). Osmium tetroxide fixation of lipids for electron microscopy a possible reaction mechanism. *Biochimica et Biophysica Acta (BBA) - Lipids and Lipid Metabolism* 152(4), pp. 718-727.

Rohaina, C. M., Then, K. Y., Ng, A. M. H., Wan Abdul Halim, W. H., Zahidin, A. Z. M., Saim, A. and Idrus, R. B. H. (2014). Reconstruction of limbal stem cell deficient corneal surface with induced human bone marrow mesenchymal stem cells on amniotic membrane. *Translational Research* 163(3), pp. 200-210.

Romano, A. C., Espana, E. M., Yoo, S. H., Budak, M. T., Wolosin, J. M. and Tseng, S. C. G. (2003). Different cell sizes in human limbal and central corneal basal epithelia measured by confocal microscopy and flow cytometry. *Investigative Ophthalmology & Visual Science* 44(12), pp. 5125-5129.

Rønning, S. B., Pedersen, M. E., Andersen, P. V. and Hollung, K. (2013). The combination of glycosaminoglycans and fibrous proteins improves cell proliferation and early differentiation of bovine primary skeletal muscle cells. *Differentiation* 86(1), pp. 13-22.

Ruiz-Ederra, J., García, M., Hernández, M., Urcola, H., Hernández-Barbáchano, E., Araiz, J. and Vecino, E. (2005). The pig eye as a novel model of glaucoma. *Experimental Eye Research* 81(5), pp. 561-569.

Sado, Y., Kagawa, M., Kishiro, Y., Sugihara, K., Naito, I., Seyer, J. M., Sugimoto, M. *et al.* (1995). Establishment by the rat lymph node method of epitope-defined monoclonal antibodies recognizing the six different α chains of human type IV collagen. *Histochemistry and Cell Biology* 104(4), pp. 267-275.

Sánchez-Abarca, L. I., Hernández-Galilea, E., Lorenzo, R., Herrero, C., Velasco, A., Carrancio, S., Caballero-Velázquez, T. *et al.* (2015). Human bone marrow stromal cells differentiate into corneal tissue and prevent ocular graft-versus-host disease in mice. *Cell Transplantation* 24(12), pp. 2423-2433.

Sanchez, I., Martin, R., Ussa, F. and Fernandez-Bueno, I. (2011). The parameters of the porcine eyeball. *Graefe's Archive for Clinical and Experimental Ophthalmology* 249(4), pp. 475-482.

Sangwan, V. S., Basu, S., MacNeil, S. and Balasubramanian, D. (2012). Simple limbal epithelial transplantation (SLET): A novel surgical technique for the treatment of unilateral limbal stem cell deficiency. *British Journal of Ophthalmology* 96(7), pp. 931-934.

Sarrió, D., Rodriguez-Pinilla, S. M., Hardisson, D., Cano, A., Moreno-Bueno, G. and Palacios, J. (2008). Epithelial-mesenchymal transition in breast cancer relates to the basal-like phenotype. *Cancer Research* 68(4), pp. 989-997.

Sartaj, R., Zhang, C., Wan, P., Pasha, Z., Guaiquil, V., Liu, A., Liu, J. *et al.* (2017). Characterization of slow cycling corneal limbal epithelial cells identifies putative stem cell markers. *Scientific Reports* 7(1), p. 3793.

Saunders, S. and Bernfield, M. (1988). Cell surface proteoglycan binds mouse mammary epithelial cells to fibronectin and behaves as a receptor for interstitial matrix. *The Journal of Cell Biology* 106(2), pp. 423-430.

Sawaguchi, S., Yue, B. Y., Chang, I., Sugar, J. and Robin, J. (1991). Proteoglycan molecules in keratoconus corneas. *Investigative Ophthalmology and Visual Science* 32(6), pp. 1846-1853.

Scadden, D. T. (2006). The stem-cell niche as an entity of action. *Nature* 441(7097), pp. 1075-1079.

Schermer, A., Galvin, S. and Sun, T. T. (1986). Differentiation-related expression of a major 64K corneal keratin in vivo and in culture suggests limbal location of corneal epithelial stem cells. *The Journal of Cell Biology* 103(1), pp. 49-62.

Schlötzer-Schrehardt, U. and Kruse, F. E. (2005). Identification and characterization of limbal stem cells. *Experimental Eye Research* 81(3), pp. 247-264.

Schlötzer-Schrehardt, U., Dietrich, T., Saito, K., Sorokin, L., Sasaki, T., Paulsson, M. and Kruse, F. E. (2007). Characterization of extracellular matrix components in the limbal epithelial stem cell compartment. *Experimental Eye Research* 85(6), pp. 845-860.

Schlötzer-Schrehardt, U., Bachmann, B. O., Tourtas, T., Torricelli, A. A. M., Singh, A., González, S., Mei, H. *et al.* (2015). Ultrastructure of the posterior corneal stroma. *Ophthalmology* 122(4), pp. 693-699.

Schofield, R. (1978). The relationship between the spleen colony-forming cell and the haemopoietic stem cell. *Blood cells* 4(1-2), pp. 7-25.

Schofield, R. (1983). The stem cell system. *Biomedicine & Pharmacotherapy* 37(8), pp. 375-380.

Schwartz, G. S. and Holland, E. J. (1998). Iatrogenic limbal stem cell deficiency. *Cornea* 17(1), pp. 31-37.

Scott, J. E. (1972). Histochemistry of Alcian blue: III. The molecular biological basis of staining by Alcian blue 8GX and analogous phthalocyanins. *Histochemie* 32(3), pp. 191-212.

Scott, J. E. (1980). Collagen-proteoglycan interactions. Localization of proteoglycans in tendon by electron microscopy. *Biochemical Journal* 187(3), pp. 887-891.

Scott, J. E. (1985). Proteoglycan histochemistry — a valuable tool for connective tissue biochemists. *Collagen and Related Research* 5(6), pp. 541-575.

Scott, J. E. and Haigh, M. (1985). 'Small'-proteoglycan: collagen interactions: Keratan sulphate proteoglycan associates with rabbit corneal collagen fibrils at the 'a' and 'c' bands *Bioscience Reports* 5(9), pp. 765-774.

Scott, J. E. and Haigh, M. (1988a). Identification of specific binding sites for keratan sulphate proteoglycans and chondroitin-dermatan sulphate proteoglycans on collagen fibrils in cornea by the use of cupromeronic blue in 'critical-electrolyte-concentration' techniques. *Biochemical Journal* 253(2), pp. 607-610.

Scott, J. E. and Haigh, M. (1988b). Keratan sulphate and the ultrastructure of cornea and cartilage: a 'stand-in' for chondroitin sulphate in conditions of oxygen lack? *Journal of anatomy* 158, pp. 95-108.

Scott, S.-G., Jun, A. S. and Chakravarti, S. (2011). Sphere formation from corneal keratocytes and phenotype specific markers. *Experimental Eye Research* 93(6), pp. 898-905.

Seeram, E. (2016). *Computed tomography: Physical principles, clinical applications, and quality control*. 4th ed. St. Louis: Elsevier.

Seligman, A. M., Wasserkrug, H. L. and Hanker, J. S. (1966). A new staining method (OTO) for enhancing contrast of lipid-containing membranes and droplets in osmium tetroxide-fixed tissue with osmiophilic thiocarbohydrazide (TCH). *The Journal of Cell Biology* 30(2), pp. 424-432.

Seyed-Safi, A. G. and Daniels, J. T. (2020). A validated porcine corneal organ culture model to study the limbal response to corneal epithelial injury. *Experimental Eye Research* 197, p. 108063.

Shanmuganathan, V. A., Foster, T., Kulkarni, B. B., Hopkinson, A., Gray, T., Powe, D. G., Lowe, J. *et al.* (2007). Morphological characteristics of the limbal epithelial crypt. *British Journal of Ophthalmology* 91(4), pp. 514-519.

Shapiro, M. S., Friend, J. and Thoft, R. A. (1981). Corneal re-epithelialization from the conjunctiva. *Investigative Ophthalmology & Visual Science* 21(1), pp. 135-142.

Sharifi, R., Yang, Y., Adibnia, Y., Dohlman, C. H., Chodosh, J. and Gonzalez-Andrades, M. (2019). Finding an optimal corneal xenograft using comparative analysis of corneal matrix proteins across species. *Scientific Reports* 9(1), p. 1876.

Shortt, A. J., Secker, G. A., Munro, P. M., Khaw, P. T., Tuft, S. J. and Daniels, J. T. (2007). Characterization of the limbal epithelial stem cell niche: Novel imaging techniques permit in vivo observation and targeted biopsy of limbal epithelial stem cells. *Stem Cells* 25(6), pp. 1402-1409.

Shu, C., Hughes, C., Smith, S. M., Smith, M. M., Hayes, A., Caterson, B., Little, C. B. *et al.* (2013). The ovine newborn and human foetal intervertebral disc contain perlecan and aggrecan variably substituted with native 7D4 CS sulphation motif: spatiotemporal immunolocalisation and co-distribution with Notch-1 in the human foetal disc. *Glycoconjugate Journal* 30(7), pp. 717-725.

Silverman, L. and Glick, D. (1969). The reactivity and staining of tissue proteins with phosphotungstic acid. *Journal of Cell Biology* 40(3), pp. 761-767.

Singh, S., Kloss, F. R., Brunauer, R., Schimke, M., Jamnig, A., Greiderer-Kleinlercher, B., Klima, G. *et al.* (2012). Mesenchymal stem cells show radioresistance in vivo. *Journal of Cellular and Molecular Medicine* 16(4), pp. 877-887.

Sirko, S., von Holst, A., Wizenmann, A., Götz, M. and Faissner, A. (2007). Chondroitin sulfate glycosaminoglycans control proliferation, radial glia cell differentiation and neurogenesis in neural stem/progenitor cells. *Development* 134(15), pp. 2727-2738.

Smith, J. W. (1969). The transparency of the corneal stroma. *Vision Research* 9(3), pp. 393-396.

Sorrell, J. M., Mahmoodian, F. and Caterson, B. (1988). Immunochemical and biochemical comparisons between embryonic chick bone marrow and epiphyseal cartilage chondroitin/dermatan sulphate proteoglycans. *Journal of Cell Science* 91(1), pp. 81-90.

Sorrell, J. M., Mahmoodian, F., Schafer, I. A., Davis, B. and Caterson, B. (1990). Identification of monoclonal antibodies that recognize novel epitopes in native chondroitin/dermatan sulfate glycosaminoglycan chains: their use in mapping functionally distinct domains of human skin. *Journal of Histochemistry & Cytochemistry* 38(3), pp. 393-402.

Sorrell, J. M., Carrino, D. A. and Caplan, A. I. (1993). Structural domains in chondroitin sulfate identified by anti-chondroitin sulfate monoclonal antibodies. Immunosequencing of chondroitin sulfates. *Matrix* 13(5), pp. 351-361.

Spradling, A., Drummond-Barbosa, D. and Kai, T. (2001). Stem cells find their niche. *Nature* 414(6859), pp. 98-104.

Stepp, M. A. and Zieske, J. D. (2005). The corneal epithelial stem cell niche. *The Ocular Surface* 3(1), pp. 15-26.

Sun, T., Tseng, S. C. and Lavker, R. M. (2010). Location of corneal epithelial stem cells. *Nature* 463, pp. E10-E11.

Svaldenienė, E., Babauskienė, V. and Paunksnienė, M. (2003). Structural features of the cornea: Light and electron microscopy. *Veterinarija ir Zootechnika* 24(46), pp. 50-55.

Takahashi, K. and Yamanaka, S. (2006). Induction of pluripotent stem cells from mouse embryonic and adult fibroblast cultures by defined factors. *Cell* 126(4), pp. 663-676.

Takashima, S., Mkrtchyan, M., Younossi-Hartenstein, A., Merriam, J. R. and Hartenstein, V. (2008). The behaviour of Drosophila adult hindgut stem cells is controlled by Wnt and Hh signalling. *Nature* 454(7204), pp. 651-655.

Tateishi, K., He, J., Taranova, O., Liang, G., D'Alessio, A. C. and Zhang, Y. (2008). Generation of insulin-secreting islet-like clusters from human skin fibroblasts. *Journal of Biological Chemistry* 283(46), pp. 31601-31607.

Thoft, R. A. (1977). Conjunctival transplantation. *Archives of Ophthalmology* 95(8), pp. 1425-1427.

Thoft, R. A. and Friend, J. (1983). The X, Y, Z hypothesis of corneal epithelial maintenance. *Investigative Ophthalmology & Visual Science* 24(10), pp. 1442-1443.

Tiedemann, K., Olander, B., Eklund, E., Todorova, L., Bengtsson, M., Maccarana, M., Westergren-Thorsson, G. *et al.* (2005). Regulation of the chondroitin/dermatan fine structure by transforming growth factor-β1 through effects on polymer-modifying enzymes. *Glycobiology* 15(12), pp. 1277-1285.

Tiwari, A., Loughner, C. L., Swamynathan, S. and Swamynathan, S. K. (2017). KLF4 plays an essential role in corneal epithelial homeostasis by promoting epithelial cell fate and suppressing epithelial–mesenchymal transition. *Investigative Ophthalmology & Visual Science* 58(5), pp. 2785-2795.

Toole, B. (1991). Proteoglycans and hyaluronan in morphogenesis and differentiation. In: Hay, E.D. ed. *Cell biology of extracellular matrix*. 2nd ed. New York: Plenum Press, pp. 305-341.

Townsend, W. M. (1991). The limbal palisades of Vogt. *Transactions of the American Ophthalmological Society* 89, pp. 721-756.

Tsai, R. J., Sun, T. and Tseng, S. C. G. (1990). Comparison of limbal and conjunctival autograft transplantation in corneal surface reconstruction in rabbits. *Ophthalmology* 97(4), pp. 446-455.

Tsai, R. J., Li, L. and Chen, J. (2000). Reconstruction of damaged corneas by transplantation of autologous limbal epithelial cells. *New England Journal of Medicine* 343(2), pp. 86-93.

Tseng, S. G., Prabhasawat, P., Barton, K., Gray, T. and Meller, D. (1998). Amniotic membrane transplantation with or without limbal allografts for corneal surface reconstruction in patients with limbal stem cell deficiency. *Archives of Ophthalmology* 116(4), pp. 431-441.

Urciuolo, A., Quarta, M., Morbidoni, V., Gattazzo, F., Molon, S., Grumati, P., Montemurro, F. *et al.* (2013). Collagen VI regulates satellite cell self-renewal and muscle regeneration. *Nature communications* 4, p. 1964.

Van Buskirk, E. M. (1989). The anatomy of the limbus. *Eye* 3, p. 101.

Varghese, S., Hwang, N. S., Canver, A. C., Theprungsirikul, P., Lin, D. W. and Elisseeff, J. (2008). Chondroitin sulfate based niches for chondrogenic differentiation of mesenchymal stem cells. *Matrix Biology* 27(1), pp. 12-21.

Vicidomini, G., Gagliani, M. C., Cortese, K., Krieger, J., Buescher, P., Bianchini, P., Boccacci, P. *et al.* (2010). A novel approach for correlative light electron microscopy analysis. *Microscopy Research and Technique* 73(3), pp. 215-224.

Vleminckx, K., Vakaet, L., Mareel, M., Fiers, W. and Van Roy, F. (1991). Genetic manipulation of E-cadherin expression by epithelial tumor cells reveals an invasion suppressor role. *Cell* 66(1), pp. 107-119.

Wang, C., Wang, T., Young, T., Lai, Y. and Yen, M. (2013). The critical role of ECM proteins within the human MSC niche in endothelial differentiation. *Biomaterials* 34(17), pp. 4223-4234.

Wang, Y., Wang, G., Luo, X., Qiu, J. and Tang, C. (2012). Substrate stiffness regulates the proliferation, migration, and differentiation of epidermal cells. *Burns* 38(3), pp. 414-420.

Watanabe, K., Nishida, K., Yamato, M., Umemoto, T., Sumide, T., Yamamoto, K., Maeda, N. *et al.* (2004). Human limbal epithelium contains side population cells expressing the ATP-binding cassette transporter ABCG2. *FEBS Letters* 565(1-3), pp. 6-10.

Watson, M. L. (1958). Staining of tissue sections for electron microscopy with heavy metals. *Journal of Biophysical and Biochemical Cytology* 4(4), pp. 475-478.

West, J. D., Dorà, N. J. and Collinson, J. M. (2015). Evaluating alternative stem cell hypotheses for adult corneal epithelial maintenance. *World Journal of Stem Cells* 7(2), pp. 281-299.

Wight, T. N., Heinegård, D. K. and Hascall, V. C. (1991). Proteoglycans: structure and function. In: Hay, E.D. ed. *Cell biology of extracellular matrix*. 2nd ed. New York: Plenum Press, pp. 45-78.

Willen, M. D., Sorrell, J. M., Lekan, C. C., Davis, B. R. and Caplan, A. I. (1991). Patterns of glycosaminoglycan/proteoglycan immunostaining in human skin during aging. *Journal of Investigative Dermatology* 96(6), pp. 968-974.

Williams, J. T., Southerland, S. S., Souza, J., Calcutt, A. F. and Cartledge, R. G. (1999). Cells isolated from adult human skeletal muscle capable of differentiating into multiple mesodermal phenotypes. *The American Surgeon* 65(1), pp. 22-26.

Wilson, R. S. and Roper-Hall, M. J. (1982). Effect of age on the endothelial cell count in the normal eye. *The British Journal of Ophthalmology* 66(8), pp. 513-515.

Wilson, S. E. and Hong, J. (2000). Bowman's layer structure and function: Critical or dispensable to corneal function? A hypothesis. *Cornea* 19(4), pp. 417-420.

Witzgall, R., Brown, D., Schwarz, C. and Bonventre, J. V. (1994). Localization of proliferating cell nuclear antigen, vimentin, c-Fos, and clusterin in the postischemic kidney. Evidence for a heterogenous genetic response among nephron segments, and a large pool of mitotically active and dedifferentiated cells. *Journal of Clinical Investigation* 93(5), pp. 2175-2188.

Wu, R., Zhu, G., Galvin, S., Xu, C., Haseba, T., Chaloin-Dufau, C., Dhouailly, D. *et al.* (1994). Lineage-specific and differentiation-dependent expression of K12 keratin in rabbit corneal/limbal epithelial cells: cDNA cloning and Northern blot analysis. *Differentiation* 55(2), pp. 137-144.

Xie, H., Chen, S., Li, G. and Tseng, S. C. G. (2012). Isolation and expansion of human limbal stromal niche cells. *Investigative Ophthalmology & Visual Science* 53(1), pp. 279-286.

Xie, T. and Spradling, A. C. (1998). *decapentaplegic* is essential for the maintenance and d ivision of germline stem cells in the Drosophila ovary. *Cell* 94(2), pp. 251-260.

Xue, C., Plieth, D., Venkov, C., Xu, C. and Neilson, E. G. (2003). The gatekeeper effect of epithelial-mesenchymal transition regulates the frequency of breast cancer metastasis. *Cancer Research* 63(12), pp. 3386-3394.

Yamada, K., Young, R. D., Lewis, P. N., Shinomiya, K., Meek, K. M., Kinoshita, S., Caterson, B. *et al.* (2015). Mesenchymal–epithelial cell interactions and proteoglycan matrix composition in the presumptive stem cell niche of the rabbit corneal limbus. *Molecular Vision* 21, pp. 1328-1339.

Yan, D. and Lin, X. (2009). Shaping Morphogen Gradients by Proteoglycans. *Cold Spring Harbor Perspectives in Biology* 1(3), p. a002493.

Yang, J., Mani, S. A., Donaher, J. L., Ramaswamy, S., Itzykson, R. A., Come, C., Savagner, P. *et al.* (2004). Twist, a master regulator of morphogenesis, plays an essential role in tumor metastasis. *Cell* 117(7), pp. 927-939.

Young, R. D. (1985). The ultrastructural organization of proteoglycans and collagen in human and rabbit scleral matrix. *Journal of Cell Science* 74(1), pp. 95-104.

Young, R. D., Tudor, D., Hayes, A. J., Kerr, B., Hayashida, Y., Nishida, K., Meek, K. M. *et al.* (2005). Atypical composition and ultrastructure of proteoglycans in the mouse corneal stroma. *Investigative Ophthalmology and Visual Science* 46(6), pp. 1973-1978.

Zeisberg, M. and Neilson, E. G. (2009). Biomarkers for epithelial-mesenchymal transitions. *The Journal of Clinical Investigation* 119(6), pp. 1429-1437.

Zhang, G., Chen, S., Goldoni, S., Calder, B. W., Simpson, H. C., Owens, R. T., McQuillan, D. J. *et al.* (2009). Genetic evidence for the coordinated regulation of collagen fibrillogenesis in the cornea by decorin and biglycan. *Journal of Biological Chemistry* 284(13), pp. 8888-8897.

Zhang, K., Ren, X.-X., Li, P., Pang, K.-P. and Wang, H. (2019). Construction of a full-thickness human corneal substitute from anterior acellular porcine corneal matrix and human corneal cells. *International Journal of Ophthalmology* 12(3), pp. 351-362.

Zhang, S., Espandar, L., Imhof, K. M. P. and Bunnell, B. A. (2013). Differentiation of human adipose-derived stem cells along the keratocyte lineage In vitro. *Journal of Clinical & Experimental Ophthalmology* 4(270), p. 11435.

Zhang, X., Sun, H., Li, X., Yuan, X., Zhang, L. and Zhao, S. (2010). Utilization of human limbal mesenchymal cells as feeder layers for human limbal stem cells cultured on amniotic membrane. *Journal of Tissue Engineering and Regenerative Medicine* 4(1), pp. 38-44.

Zhao, J., Mo, V. and Nagasaki, T. (2008a). Distribution of label-retaining cells in the limbal epithelium of a mouse eye. *Journal of Histochemistry & Cytochemistry* 57(2), pp. 177-185.

Zhao, X., Das, A. V., Thoreson, W. B., James, J., Wattnem, T. E., Rodriguez-Sierra, J. and Ahmad, I. (2002). Adult corneal limbal epithelium: A model for studying neural potential of non-neural stem cells/progenitors. *Developmental Biology* 250(2), pp. 317-331.

Zhao, X., Das, A. V., Bhattacharya, S., Thoreson, W. B., Sierra, J. R., Mallya, K. B. and Ahmad, I. (2008b). Derivation of neurons with functional properties from adult limbal epithelium: Implications in autologous cell therapy for photoreceptor degeneration. *Stem Cells* 26(4), pp. 939-949.

Zhou, S., Schuetz, J. D., Bunting, K. D., Colapietro, A., Sampath, J., Morris, J. J., Lagutina, I. *et al.* (2001). The ABC transporter Bcrp1/ABCG2 is expressed in a wide variety of stem cells and is a molecular determinant of the side-population phenotype. *Nature Medicine* 7(9), pp. 1028-1034.

Zieske, J. D. (2004). Corneal development associated with eyelid opening. *International Journal of Developmental Biology* 48, pp. 903-911.

Zuk, P. A., Zhu, M., Mizuno, H., Huang, J., Futrell, J. W., Katz, A. J., Benhaim, P. *et al.* (2001). Multilineage cells from human adipose tissue: Implications for cell-based therapies. *Tissue Engineering* 7(2), pp. 211-228.